UNIVERSITAT DE BARCELONA

Membrane Trafficking of TGF-β and Transcriptome Analysis in Marfan Syndrome

Anna-Maria Elisa Siegert

Membrane Trafficking of TGF-β and Transcriptome Analysis in Marfan Syndrome

Doctoral degree of Biomedicine at the

University of Barcelona

Submitted by:

Anna-Maria Elisa Siegert

This work was performed at the Department of Biomedical Sciences in the Faculty of Medicine of the University of Barcelona under the supervision of Dr. Gustavo Egea Guri.

Anna-Maria Elisa Siegert Dr. Gustavo Egea Guri

Programa de Doctorat de Biomedicina

A mi familia

A mis amigos

A todos los que me acompañaron: Mil gracias!

Pluck any atom from your body

and it is no more alive than is a grain of sand.

It is only when they come together within the nurturing refuge of a cell that these diverse materials can take a part in the amazing dance that we call life.

Bill Bryson "A Short History of Nearly Everything"

Acknowledgements

Well..I really don´t even quite know where to start! I am so thankful for all of the support, love, and motivation that I have received throughout the past four years! In so many ways it´s been about the most emotional time possibly imaginable and it was marked by very high highs and very low lows. I know that all of you who have accompanied me and have been there for me have also suffered and laughed and celebrated just as much as I have. That´s why the following pages are dedicated to all of you! Although I think that it´s going to be very, very difficult to really express my gratitude, I am simply going to give it a try..just bear with me, it´s going to make sense in the end, I promise!

Als allererstes möchte ich mich bei den Protagonisten dieser dramaturgischen Höchstleistung bedanken: Meine Eltern und mein Bruder. Ganz davon abgesehen, dass ich gerade "dramaturgisch" und dessen Schreibweise im Duden nachlesen musste, ist Euch natürlich der grösste Teil dieser Arbeit zu verdanken! Vielen Dank für die Diskussionen, Telefonate und Ermunterungen während dieser langen Zeit der Selbstzweifel. Vielen Dank, dass Ihr da wart und nie an mir gezweifelt habt. Simon, auch du wirst sehen, wie alle kleinen Puzzleteilchen in ihren Platz fallen. Irgendwie, irgendwo, irgendwann und es wäre natürlich besser, wenn es jetzt und sofort passieren würde, aber mit Geduld und ehrlicher Arbeit kommt man dann doch ans Ziel. So irgendwie, irgendwo, irgendwann dann. Und natürlich hätte ich diesen Weg, der dann doch wohl etwas holpriger war als er hätte sein müssen, nie gewählt, wäre es nicht für all die Stärke und Willenskraft gewesen, die Ihr mir mitgeben habt. Vielen Dank, dass Ihr mich habt machen lassen, es hat mich glücklich gemacht!

Next in this series of emotional outbursts is you, Jack! You know that I often ask myself how I could possible ever thank you, how I could possibly ever do the same for you as you did for me. Well, I guess the answer is: I can´t. I can only tell you that what you have lived through with me during the past years is simply incredible and has given me the strength, joy and courage to go on. You have laughed with me, you have cried with me, you have picked me up and carried me a few steps, you have comforted me and you have talked to me. Many times, you have opened my eyes and you have shown me a different perspective. You have given me confidence and you have done everything in your power to make me feel good at all times. Although it might not have seemed like it at times: your efforts have not gone unnoticed! You have been such an important part throughout this whole time that it truly was not only my journey, but ours. I am looking forward to the many more adventures that are to come!

Además, quiero dar las gracias a mi director de tesis, a Gustavo Egea. Gracias por darme la oportunidad de realizar le tesis en este laboratorio, por permitirme crecer tanto como investigadora y como persona, gracias también por dejarme realizar mis propias ideas y compartir tus opiniones conmigo.

Acknowledgements

Sobre todo, muchas gracias por dejarme presentar la primera tesis en la nueva línea de investigación del Síndrome de Marfan lo cual sin duda es especial para nosotros dos.

Por el otro lado, quiero dar las gracias a toda la gente que ha estado en el laboratorio conmigo durante estos años. En primer lugar, quiero decir mil gracias a ti, Carla, mi grande! Tú me has apoyado, ayudado y aconsejado tanto, que dudo que un día te pueda devolver este favor enorme! Has estado siempre tanto como brillante científica como amiga espectacular. Gracias por confiar en mi, gracias por dejarme formar parte de tu vínculo gracienc y gracias por hacerme sentir siempre apreciada, estimada y acogida! Es muy especial esto para una guiri como yo! Has bebido muchas cervezas conmigo y me has animado tantas veces ... ya no se pueden contar! Has formado (y sigues formando) una parte muy importante de esta etapa y espero que formarás una parte muy importante de la siguiente también! Disfruta del flamenco, de la rumba, de la cerveza y de la vida! Ya ves que me cuesta un poco expresar bien mis agradecimientos ... pero creo que me entiendes! Siempre me entiendes!

Muchas gracias al resto del grupo de los Gustavos! A Dasha, que ya eres mamá! Que increíble! Muchas gracias por tu ayuda y tu apoyo, he aprendido mucho de ti en tantos sentidos! Me alegro mucho por ti y por tu familia, os deseo todo lo mejor del mundo para el futuro! Muchas gracias a ti, Thayna, y el tiempo que hemos estado juntas en el lab! Tu alegría brasileña acoplada con tu serenidad ha sido un placer. Espero que te encontrarás con muchas inspiraciones, mucha creatividad, y aún más felicidad en tu camino! Muchas gracias también a ti, Laura! Eres un sol y especialmente en la última etapa de mi tesis me has apoyado mucho con tu alegría y tu esfuerzo. Te lo agradezco mucho y estoy a la vez muy orgullosa de ti! Muchas gracias a ti, Júlia! Que tu última etapa sea leve y que también lo disfrutes un poco! Es igual de bonito que duro! Mucha suerte también para ti Fabio, que tus proyectos tiren y que te vaya bien en tu camino.

Durante este tiempo he tenido la suerte de conocer a muchos amigos en mi alrededor, que me han dado alegría cada día! Vamos por orden de mesas para que no me lie ... porque he pensado tanto en escribir estas palabras, pero ahora que ha llegado el momento me quedo literalmente sin palabras. Sara (la tocaya de mi proteína favorita) Tu eres un sol, una alegría, una querida! Muchas gracias por tantas conversaciones y risas sobre cosas varias, de estrés continuo hasta moda y yoga! Que alegría verte cada día! Que alegría eres tú! Nunca cambies y no dudes de ti! Gerardo: Eres genial! Te debo mil gracias por haberme enseñado tantas cosas increíblemente interesantes, pero también por muchas cervezas, muchos ánimos y mucha amistad! Sigue contándonos cosas interesantes de todos los campos científicos (y no-científicos) y no te pelees demasiado con los muebles del Ikea … al final siempre sobra un tornillo, es normal! Laureta: Aunque ya no estás sentada en tu silla sigues en mi corazón! Muchas gracias por ser una amiga muy buena durante todo este tiempo que hemos

compartido. Muchas gracias por tus ánimos y tu locura! Te agradezco tus sonrisas y tus abrazos, y que me has dejado formar parte de tu propia aventura "tesis" también! Te extraño mucho! Vuelve a Barcelona cuando puedas, siempre habrá sitio para ti! Maite: Que haríamos sin ti? Siempre estas, siempre nos ayudas, siempre nos animas! Haces tantas cosas para nosotros! Gracias por animarme también en épocas difíciles y gracias por compartir tu experiencia conmigo, me ha ayudado mucho! Eres un sol! Elena: La bonita Helen! Me pongo a llorar pensando que ya no nos vamos a ver cada día y que ya no estarás sentada de mi lado! Hemos compartido una época muy importante para las dos, y te agradezco que has estado y que has conversado y que has celebrado conmigo! Pero aunque quizás ya no nos veremos cada día voy a estar para ti hasta el final y te daré tantos ánimos como los que me diste tú también! Ahora vamos al minilab, el famoso minilab! George: Suuuuuch a haaaaaaandsome man! Be a good boy George! Muchas gracias a ti de hecho por muchas cosas. Por un lado tu compañía, tu ánimo y tu mente brillante científica! Por el otro lado también muchas gracias por haber tenido tanta paciencia conmigo, la guiri del lab! Yo sé que he sido agobiante en momentos, pero siempre me has hecho sentir bienvenida y que formo parte también de vuestro minilab! Muchas gracias! Marta: Eres lo máximo! Pienso que eres una persona estupenda con tus comentarios inesperados e hiper graciosos y tu corazón enorme! Me encanta tu humor! Siempre has tenido tiempo para ayudar y para hacer una broma y te lo agradezco muchísimo! Sé que tu camino te será leve porque eres una crack! Rafa: Eres una persona muy especial con un karma tan bueno, que tu reencarnación será un unicornio. Muchas gracias por tu ayuda, tus bromas, tu manera de ser, tu sonrisa y tu ánimo incansable! Que te vaya excelente en tu siguiente etapa! Gloria: Pues amor, ya eres mami también! Como me alegro por ti! Leyendo estas frases no lo puedes saber pero de hecho ahora mismo que escribo todo esto aún no ha nacido la Vera y estamos todos nerviosos! Te doy mil gracias pero sobre todo te agradezco los ánimos que me diste! You´re mi spirit guide! Eres tan graciosa y relajada, me encantaba verte y tu sonrisa cada día! Me ayudaste mucho y sobretodo en los últimos pasos. Muchas gracias por estar y hacerlo todo mas leve! Que tu siguiente etapa sea estupenda y que estés muy feliz con tu Verita! Y la siguiente mamá: Ana! Muchas gracias a ti, Ana, por todo el tiempo que hemos compartido, por ayudarme en tantos sentidos y todo esto con tanta energía! Eres fenomenal! Viéndote a ti parece todo muy fácil..no sé cómo lo haces! Espero que un día yo también voy a tener la fuerza de llevar todo con tanta facilidad como lo haces tú! Raquel: Muchas gracias a ti, Raquel! La verdad que no me puedo imaginar que dentro de poco ya no estarás más en el lab..de hecho me parece que siempre has estado! No me puedo imaginar que solo ha sido un poco más que un año! Muchas gracias por tus sonrisas y tus historias realmente flipantes! Las disfruté mucho! Que tengas mucha suerte en tu camino y que te vaya todo excelente, tú puedes hacer lo que quieras! Muchas gracias también a Ened! Eres tan brillante y siempre llevas una sonrisa! Ha sido realmente un placer conocerte! Muchas gracias por

muchas charlas y bromas, y que te vaya todo excelente porque eres excelente! Andrés (y por defecto la hermosa Claudia que nos ha dado tanta alegría): Eres genial! Como llevas todo y como vives la vida! Y este estilo de moda! Wow! Muchas gracias por haber compartido estos años conmigo y muchas gracias por consejos varios! Eres una alegría de persona! Mercé: Hemos compartido muchas conversaciones muy interesantes y hemos compartido muchas ideas! Te agradezco el tiempo que hemos estado juntas y tus ánimos y tu preocupación. Has sido un apoyo realmente grande, además en el ultimo año! Muchas gracias por todo esto! Phil: Gosh golly, you´re a funny man! Thanks Phil for a lot of whimsical jokes and a lot of (life) advice that truly came from the heart! I am going to go totally overboard her and describe some of your t-shirt designs as ludicrously silly! I hope that you can feel my appreciation for your hilarity, especially in the midst of my confusingly complex last year! Muchas gracias también a las secres Núria, Carme y Mercé! Lo que vosotras hacéis para nosotros es increíble y os debo mucho! Me habéis arreglado tantos problemas y dudas, y todo esto siempre con mucha calma y una sonrisa! Quizás no os dais cuenta, pero en momentos de pleno pánico (entro mucho en pleno pánico) vuestra manera de solucionar los problemas como si no fuera nada me ha ayudado mucho! Por lo tanto, os quiero agradecer todo lo que habéis hecho por mi durante los últimos años! También quiero dar las gracias a los jefes de grupo Esther, Silvia, Jordi y Pep por generar un ambiente agradable en todos los momentos en que nos hemos encontrado!

Ahora tomamos un café y hacemos una pausa y enseguida nos vamos a la tercera planta. Aaah, la tercera planta! Siempre me ha gustado pasar por vuestro lab! Y ahora puedo decir las gracias a una persona que realmente ha hecho posible lo imposible: Inés! Eres la reina! La reina de todo de hecho..de escribir tu tesis de la velocidad de la luz, de hacer millones de actividades extracurriculares (lo cual en si mismo en un concepto confuso para mi), de hacer baile tradicional en Nepal y mucho mas! Creo que no me es de todo posible expresar bien cuanto me has ayudado en los últimos años! Tu amistad ha sido una luz cada día y tu sonrisa una alegría! Muchas gracias por llevarme al cross-fit y por “sacar los demonios”, muchas gracias por todos los mensajes que me enviaste desde Nepal y que me animaron tanto! Mucha gracias por ser un ejemplo tan genial y por enseñarnos que se puede con esta tesis! Que te vaya excelente durante los últimos meses en Nepal y que vuelves con inspiración, motivación y la misma sonrisa que llevaste cuando te fuiste! Seguimos con sonrisas porque en la tercera planta sonríen mucho..así son las chicas esas..Georgina: Eres genial! Eres un sol! Eres tan graciosa! Y además eres un apoyo increíble! Muchas gracias por exactamente estas cosas, por tu genialidad, tus bromas realmente fantásticas, tu apoyo y tu compañía! Te prometo que no voy a faltar en la siguiente calcotada! O barbacoa..o lo que sea que vosotros montáis en este barrio animado! La siguiente sonrisa es para Ana: Muchas gracias Ana, no solamente por tu experiencia y tus consejos que nos han ayudado mucho en el día a día aquí arriba en la quinta planta, pero también para tu

compañía y tus ánimos, tu manera de ser que es tan positiva y tu apoyo! Otra sonrisa siempre viene de Mireia: Muchas gracias por reírte de mis bromas, muchas gracias por dar tu apoyo, muchas gracias por ser una chica super amable y abierta y curiosa! Además, muchas gracias a Andrea: Que te sea leve el resto de tu trayecto! Muchas gracias por tus ánimos y tu conocimiento en especial del CAST..muchas veces que nos hemos quedado colgados aquí arriba y nos salvaste! Y muchas gracias a Cristina! Tu me sorprendiste mucho y muchas veces porque eres tan joven y tan sabia a la vez! Creo que para ti todo saldrá excelente en la vida y me alegro de verte feliz! Lo que me alegra aún más es que te veo muy animada y motivada! Sigue así! Ya me repito mucho…debe ser un aburrimiento muy grande leer mis agradecimientos pero es verdad! Sois tan increíbles! Aunque igual no me expreso suficientemente bien pero "sois increíbles y agradezco muchísimo lo que habéis hecho durante los últimos años" es el punto esencial.

Vamos al Cellex ahora! El Cellex es este lugar mágico donde no tengo acceso. Por esto, las chicas del Cellex siempre me tenían que abrir las puertas..que agobiante..jejeje! Núria!!!!! Muchas gracias a ti Núria! Muchas veces, cuando estaba dudando una decisión, tu siempre me hiciste sentir segura y me diste confianza! Muchas gracias por tus sonrisas y tus cotilleos! He disfrutado mucho de tu amistad!!!! Muchas gracias por muchas noches en el ascot con las neuronas fritas después de un día largo de lab! No cambies y sigues con tu ritmo científico brillante! Laura: Eres una chica super maja! Te veo trabajando como una loca y veo que te salen las cosas muy bien! Puedes estar muy orgullosa de ti misma! Muchas gracias por tus sonrisas y de que siempre te ríes de mis bromas (que a veces son bastante malas)! Espero que te vaya genial en tu camino y que sigues haciendo buena investigación con todo el ánimo que ya tienes! Annika: Ein Vergnügen dich kennenzulernen und auf einmal festzustellen, dass wir ja sozusagend aus der selben Ecke kommen! Auch wenn man den Bämbel ab und zu vermisst, bist du ja viel eingebürgerter hier als ich! Lass es dir gutgehen und mach weiter so! Du bist auf jeden Fall auf dem richtigen Weg, vor allem mit den guten Leuten, die dir hier zur Seite stehen! Vero: Un placer de haber compartido muchas sonrisas y de que siempre me contaste cosas interesantes de Argentina! Quizás un día tendré la oportunidad de irme por allá y verlo todo!

Nos quedamos un momento en el Cellex aunque nos vamos a una planta diferente a un lab que no tiene nada que ver con nuestra unidad y llamamos a la puerta de Marlies y su lab! Marlies!!!!!!! Mi querida Marlies! Hemos compartido tantos años juntas ahora que se me hace impensable que un día no estaremos cada día en el mismo sitio, contándonos nuestras penas y alegrías! Te amo de verdad! Has estado durante el master (que hicimos – obviamente – excelente!) y durante una época muy difícil para mi y luego durante una época muy alegre, caótica, llena de vida y emociones! He tenido la suerte de conocer mucho de tu vida: Amigos de Chile que vinieron a visitarte, tu madre hermosa, tu gente de aquí..He tenido la suerte de acompañarte durante tu tesis tanto como tú me acompañaste a mí!

Tu alegría chilena y tu manera de pensar me han roto un poco la rigidez alemana que llevo dentro. Tus consejos y tus ideas me han ayudado a resolver situaciones difíciles tanto que tu jovialidad me llena el corazón! Prepara ya una habitación de invitados en Chile que yo me compro el billete en seguida! Muchas, muchas y muchísimas gracias por todo! También quiero dar las gracias a la gente de tu lab ya que durante estos años he tenido la suerte de conocerlos! Muchas gracias a Oriol, Laura, Esther y Marie-Carmen! Mucha suerte para todos vosotros! Sois geniales!

Ahora nos pasamos a un lugar, donde nunca puse pie pero sé que existe: La sala blanca! Gracias a la normas estrictas de la sala blanca, las trabajadoras vienen al nuestro lab a tomarse el café y he tenido el placer absoluto de conocerlas. Raquel: Te debo muchas gracias! Muchas gracias por darme ánimo, motivación, por escucharme y por aconsejarme. Muchas gracias por el cross-fit! Que bien lo pasé contigo y con Inés! Volveré tan pronto me sea posible! Cris: Eres una persona hiper positiva! Y esto es contagioso. Muchas gracias por exactamente esto! Muchas bromas, muchas risas y mucha coreografía de baile (que jamás aprendí bien..intentaré hacerlo mejor la siguiente vez!) Gemma: Un mega hiper placer de conocerte! Un mega hiper placer de hacer bromas contigo y contarnos de nuestras vidas! Muchas gracias por conversaciones realmente surrealistas, por muchas risas y mucho ánimo!

Además, quiero dar las gracias a Cris, Nahir, Anna, Sara, Sandra y Marga! Con vosotras he compartido mi primer año aquí en Barcelona y me habéis enseñado muchas cosas, del castellano hasta Inmunología. Y no solamente esto, pero también durante los últimos años habéis estado y me habéis dado mucha alegría y mucha comida japonesa! Aún algunas de vosotras ya estáis en otros sitios y otras posiblemente si irán, sé que siempre vais a estar y os agradezco vuestra amistad!

Muchas gracias también a Elisenda, María y Anna del confocal! Muchas gracias por ayudarme con dudas y enseñarme con mucha paciencia la parte técnica de la microscopia confocal. Muchas gracias también a Anna Alsina y Esther Trench de la administración del programa de doctorado por siempre contestar a dudas y ayudarme con cualquier trámite o documento.

I do sincerely hope that I was able to express my gratitude and let you all know how much fun I´ve had with you in the past years just as much as I appreciate the empathy and reassurance during hard times. However, some people are still missing on my list of acknowledgements. I do prefer the Spanish “agradecimientos” because I feel like acknowledging something is not the same as being really and truly grateful. And that´s how I feel in many ways.

I would like to thank all of my friends who have been there for me, who have listened to my complaints, who have shed a tear or two with me and who have put up with raging mood swings. Thank you, Joe, for letting me write “the beast” (and other tiny beasts) at your place. I truly enjoyed

my time at your dining room table and you popping in and out, sometimes hilariously singing along to admittingly very good tunes. You deserve a big shout! I probably wouldn´t have been able to write as much, as fast, and as concentrated if it hadn´t been for your generosity, friendship and hilarity! Many thanks to Peeg! Peeg, you have been a fabulously great friend throughout this whole journey and you have (knowingly or unknowingly) always distracted me from feeling sorry for myself with truly hilarious and bizarre consequences! Adam! You fine specimen of manhood, you deserve one of the biggest shouts for your kindness and friendship and awesomeness! You have always told me "Annie, Annie (The double "Annie" is very important here): You can be upset now but we all know you´re gonna do it" and every time I have really appreciated it and, most importantly, I have listened to you! That does not happen often.. In fact, I have to thank the two of you, Peeg and Adam, together because you seem to have used the same strategy over the years which was basically telling me that I am not going to give up anyway so I might as well sit down, shut up, and have a beer. Thanks for believing in me! Thanks to Rose! Oh, lovely Rose! Thank you so much, Rose, for the endless support, for sitting through relentlessly boring practice presentations, and for listening to stories that in hindsight made very little sense. I know you´ll have a great time in Madrid with your new job and your new adventure! And we always have a place for you! Thanks to the neighbours: Jen, Sam, Aidan and Domi! Knowing you around the corner was blissful! Knowing that on a moment's notice my pals are going to hang out with me, distract my dazzled mind, and are always there for me is everything I could have wished for. I hope to have you guys around (the corner) for much longer and for much more shenanigans! You´re awesome! Mateo: Many many thanks for all of your support, especially in the past months! You´ve taken lots of time out of your day to help me out and you´ve really made a difference. Many many thanks for being a really good friend (and a naughty one), for chatting with me, for doing outrageously fun trips with us, for being understanding, for just simply being great! Many thanks to Elena, a wonderfully scientific, joyful and positive addition to my Barcelona life! Muchísimas gracias a ti por tranquilizarme, contarme de tu propia experiencia del doctorado y reírte conmigo del surrealismo laboral diario y de las emociones bizarras que se siente durante esta época! Thanks to Giuli and Mike! Thanks so much for lovely times on your terrace, for going camping, skiing, for being patient, for listening to my nonsense, for being there and being really good friends! It always felt simply great and relaxed being with you and spending time with you. I wish you all the best in your new house with new adventures and lots of joy! Muchas gracias a Marta, Toni, Carlos y Pepe! Sois fantásticos! Hemos pasado muchos tiempos muy buenos juntos y vosotros realmente habéis estado para mi durante épocas duras. Sois los reyes y os agradezco todo lo que habéis hecho para mí y todos los tiempos que hemos pasado juntos. Muchas gracias! Muchas gracias también a Karen! Karen, me has dado muchos ánimos durante estos años! Empezábamos juntas en el T-system y aquí seguimos! Muchas gracias por

ser una muy buena amiga, por muchas noches en el cine, por mucha comida mexicana y muchas sonrisas!!! Muchas gracias por escuchar y aconsejar, por cotilleos y alegría! Thank you Bee! You have been with me for so long now, you have always believed in me and you have always had such wonderful things to say! You´ve inspired me endlessly and I want to thank you for all of the good times and the difficult ones that you have lived with me. I am more than grateful for you! Thanks to Ted, Roisin and Clidna! You wonderful, heart-warming, joyful beauties! I am so thankful for you, all the time we´ve spent together, and all of the support you´ve given me, especially from far away! Many wonderful and sincere talks, many hilarious situations, and a lot of merriment! Thanks for the bond between us and thanks for the efforts you have gone through to be with me. Let us continue especially the merriment and the wondrous adventures that might await us.

Dann möcht ich doch bitte auch nochmal kurz einen Schwenker machen in chronologischer Reihenfolge. Es fehlen noch ein paar Schauspieler in diesem Theater frei nach “last but not least”: Ganz tief aus meinem Herzen heraus spriesst der Dank für die sogenannten “Juchemer” Linda, Toni, Katha, Charlotte, und Isi und die “Heiner” Sandy, Stephie, Marie, Ina, Käthe, Laura und Elli. Immer da, immer parat. Immer für einen Kaffee zu haben. Immer für einen Wein zu haben. Diese ganzen langen Jahre über seid ihr immer wieder bei mir gewesen, habt mich besucht wo auch immer ich war, seid sofort angedüst gekommen wenn ich mal wieder an Ort und Stelle war, habt mich eingeladen zu Hochzeiten, Geburtstagen und anderen Feierlichkeiten. Und darum will ich mich bei euch für eure Freundschaft bedanken. Wenn ich so darüber nachdenke, bekommt man ja nicht so oft die Gelegenheit so eine lange Danksagunsliste zu schreiben, die dann Leute auch noch lesen müssen und sich wahrscheinlich bis über beide Ohren langweilen. Aber ich habe jetzt das Glück in die Hände gelegt bekommen genau so etwas machen zu dürfen. Und alle müssen höflich weiterlesen. Ich finde es schon besonders, dass wir alle uns noch so nacheinader sehnen und so für einander da sind und dafür will ich euch ganz offiziell Danke sagen! Ihr seid grossartig!

Und mir fehlen da noch ein paar Personen, die in den letzten Jahren sehr wichtig waren: Vielen Dank an Viola, Nora und Frank! Die Zeit in Amsterdam liegt so fern in der Vergangenheit aber ist gleichzeitig so greifbar wie die Gegenwart. Amsterdam hat einen ganz wichtigen Platz in meinem Herzen und das euretwegen! Vielen Dank, dass es jedesmal wieder so ist, als hätten wir uns erst gestern das letzte Mal gesehen. Vielen Dank, dass ich weiss, dass Ihr da seid. Vielen Dank für Eure Freundschaft und vielen Dank für die äusserst unterhaltsame Zeit mit euch (so mal ganz förmlich ausgedrückt).

Every reader is probably a bit exhausted by now from all of these emotions and names and things. So, I think it´s time to come to an end: “With every call of life, the heart must part and start again, in

courage and joy" (Stufen, Hermann Hesse). I hope I was able to express my gratitude to all of you who so patiently have been with me, have inspired and encouraged me. Thank you, a thousand times!

Resumen

El síndrome de Marfan (MFS, del inglés *Marfan Syndrome*) es una enfermedad que afecta al tejido conjuntivo de herencia autosómico dominante. MFS fue descrito en 1896 por Antoine Marfan y afecta aproximadamente entre 1.5 y 17.2 personas de cada 100,000. El gen mutado causante de la enfermedad es *FBN1* que codifica para una glicoproteína de 350 kDa llamada Fibrillina-1 (FBN1). FBN1 constituye un elemento esencial de la matriz extracelular (ECM, del inglés *extracellular matrix*) por su capacidad de ensamblarse en estructuras complejas conocidas como microfibrillas, las cuáles, junto con la elastina, forman las fibras elásticas del tejido conjuntivo. En el MFS, las mutaciones en el gen *FBN1* causan la disrupción de las fibras elásticas causando síntomas variados en el sistema esquelético, ocular y cardiovascular. La complicación más grave la constituye el aneurisma de la aorta ascendente que tiene origen en la túnica media, la cual se compone de células musculares lisas (VSCM, del inglés *vascular smooth muscle cells*) y de fibras elásticas. Estos aneurismas afectan 75-80% de los pacientes y conllevan un alto riesgo de disección. Las únicas medidas terapéuticas disponibles son la evaluación y el control de la progresión del aneurisma, el uso de antagonistas de receptores β-adrenérgicos y la cirugía reparativa.

Las mutaciones de la FBN1 son multiples y se pueden encontrar a lo largo de todo el gen. La recurrencia de mutaciones puntuales es excepcionalmente baja y se han descrito cerca de 3000 mutaciones diferentes. La predicción de los órganos involucrados y el riesgo cardiovascular a partir de la mutación especifica es difícil debido a la baja correlación genotipo-fenotipo. Las mutaciones se clasifican en dos categorías definidas por los efectos que se producen al nivel proteico. Mutaciones sin sentido (*nonsense*), debidas al desplazamiento del marco de lectura (*frameshift*), del sitio de empalme (*splice site*) o la deleción (*gene deletion*) inducen un fenotipo haploinsuficiente como consecuencia de la reducción de la cantidad de FBN1 total. Mutaciones con cambio de sentido (*missense*) inducen un fenotipo dominante negativo lo cual conlleva defectos cualitativos de la proteína que afectan sus funciones como por ejemplo su plegamiento o las interacciones proteína-proteína resultando en una matriz frágil y desorganizada. Conceptualmente las mutaciones dominante negativas deberían inducir un fenotipo más heterogéneo que las mutaciones haploinsuficientes debido a que mutaciones en sitios discretos suelen tener efectos distintos mientras que el fenotipo en la haploinsuficiencia debería ser más constante.

La FBN1 no solamente es importante para el soporte estructural de la ECM, sino que también juega un papel crucial en la regulación del factor de crecimiento transformador-β (TGF-β, del inglés *transforming growth factor-β*). El TGF-β es importante para el desarrollo, el equilibrio célula-ECM y la homeostasis celular. Su desregulación está relacionada con varias enfermedades fibroticas, autoinmunes y en cáncer. Por sus dominios característicos de 8 cisteínas, la FBN1 se une de una manera específica a la proteína de unión a TGF-β latente (LTBP, del inglés *latent TGF-β binding protein*)

que por otro lado forma un complejo con el TGF-β maduro. De este modo, la FBN1 regula la disponibilidad del TGF-β en el ambiente extracelular. Se ha demostrado que debido a la fragmentación de las fibras elásticas los niveles del TGF-β en pacientes con MFS están aumentados y correlacionan con el riesgo de desarrollar aneurismas aórticos.

El TGF-β puede ser activado tanto por factores solubles del medio extracelular como por integrinas, las cuales están incluidas en la ECM y actúan como presentadoras del TGF-β a sus receptores. El aumento de la expresión de integrinas se ha demostrado en varias enfermedades en las cuales la señalización de la TGF-β induce cambios fisiológicos. Por lo tanto, se han considerado factores importantes en el control de la señalización del TGF-β al nivel extracelular. La activación del TGF-β facilita la unión del ligando a su receptor II (TBRII) lo cual cambia su afinidad para el receptor I (TBRI) frente a la unión del ligando induciendo su transfosforilación y la endocitosis del complejo. La endocitosis del complejo puede tener lugar en dos dominios membranales distintos: por la vía clatrina-dependiente o caveolina-1 (CAV-1)-dependiente, esta última situada en las balsas lipídicas. Dependiendo de la vía de la internalización, la cascada de señalización del TGF-β tendrá efectos opuestos. Los complejos internalizados por la vía de la clatrina están asociados con la señalización mediante proteínas especificas llamadas SARA y SMAD2. Los receptores internalizados por la vía de la clatrina siguen la ruta de los endosomas tempranos, dónde SARA se unirá al complejo induciendo el reclutamiento de SMAD2, que será fosforilado y seguidamente translocado al núcleo por el co-factor SMAD4. La unión del complejo SMAD2/SMAD4 al ADN induce una multitud de cambios en la expresión de varios centenares de genes reguladores de la remodelación de la ECM. Por el contrario, la internalización por la vía CAV-1-dependiente se ha asociado con la atenuación de la señal mediante la unión de SAMD7, que inhibe la unión de mediadores de la señalización y a la vez facilita la unión de ligasas de la ubiquitina que inducen la degradación del complejo por la vía del proteasoma. Por lo tanto, se ha propuesto que la compartimentación de los receptores es un mecanismo regulador de la célula para la señalización de la TGF-β.

Debido al papel regulador de las dos vías de la internalización, en este estudio hemos investigado si la compartimentación de los complejos TGF-β-receptor internalizados por cada una de las vías contribuye al aumento de señalización por TGF-β en el MFS. Hemos visto que en el estado basal los mediadores de la señalización SARA y SMAD2 están más enriquecidos en la fracción de membrana en las VSMC de pacientes con MFS. Además, hemos visto que estos mediadores también interactúan más con el TBRII en las células MFS que las controles y finalmente hemos observado que la colocalización de SARA con el marcador endosomal EEA1 está aumentada. Esto nos indica que en MFS existe una mayor disponibilidad para transducir la señalización activadora por TGF-β. Asimismo, hemos demostrado un aumento en la colocalización entre EEA1, SARA y TGF-β. El aumento de la co-

localización de estas tres proteínas podría deberse a un incremento en la transcripción de RAB5 y su localización preferente en endomembranas en individuos con MFS, considerando que RAB5 induce el reclutamiento de SARA en los endosomas tempranos. Por lo tanto, concluimos que una disfuncionalidad en la proteína RAB5 induce una mayor eficiencia de la señalización por TGF-β en los endosomas tempranos debido a un incremento en el reclutamiento de SARA a las membranas donde inducirá la fosforilación de SMAD2 e iniciará la cascada de señalización. Por otro lado, hemos visto que en las VSMC las dos vías clatrina- y CAV-1-dependiente no son entidades separadas, sino que en parte convergen y forman vesículas doblemente positivas para EEA1 y CAV-1. Curiosamente, estudios anteriores sugieren que estas vesículas doble-positivas podrían estar involucradas en la atenuación de la señalización del TGF-β por la vía lisosomal. Además, hemos visto que la localización del TGF-β en estas vesículas doble-positivas se veía disminuida en las VSCM de pacientes, lo cual nos indica que este mecanismo atenuador de la señalización podría estar afectado en MFS. En conclusión, nuestros estudios demuestran que la señalización aumentada asociada a la vía endosomal se debe a un aumento de reclutamiento de SARA en los endosomas tempranos mediado por RAB5, favoreciendo la unión de SMAD2 al receptor. El incremento de la señalización está facilitado por un menor tránsito de TGF-β hacia estructuras endociticas doble-positivas para EEA1 y CAV-1, asociadas a la atenuación de la señalización.

En este estudio también nos hemos interesado por el papel de las integrinas como activadoras del TGF-β a nivel de la ECM. Hemos visto que a nivel transcripcional todas las integrinas analizadas estaban disminuidas en tejido aórtico procedente de pacientes con MFS. A nivel proteico hemos visto que la integrina β1 (ITGB1) en particular se encuentra menos activa en tejido aórtico de pacientes MFS. Esto es particularmente interesante considerando que esta misma integrina es diana directa de un micro ARN (miRNA, del inglés *micro RNA*) llamado *miR29b* que a su vez se encuentra aumentado en MFS. A la vez, *miR29b* también se une a *FBN1* induciendo su degradación o dirigiéndole hacia regiones subcelulares para su procesamiento. Una posible explicación para la disminución de las integrinas podría ser uniones indiscriminadas dependientes de *miR29b*. Por el otro lado, *miR29b* se podría ver aumentado para restablecer la homeostasis intracelular, la cual estaría afectada por las mutaciones en la *FBN1*. Otra posible explicación de la disminución de las integrinas podría ser un mecanismo compensatorio a nivel extracelular para controlar la señalización aumentada de TGF-β.

Una complicación tanto en el diagnóstico como en el tratamiento del MFS es la heterogeneidad de las mutaciones de la *FBN1.* Un problema adicional es que los métodos de secuenciación convencionales solamente analizan los exones más comúnmente afectados, lo cual conlleva en sí mismo un sesgo que evita la exploración de las regiones menos susceptibles a presentar mutaciones. Estudios a gran escala han intentado correlacionar el fenotipo de pacientes con el tipo de mutación, bien sea

haploinsuficiencia o dominancia negativa. A pesar de esta clasificación, dichos estudios no han podido relacionar de manera concluyente el riesgo de implicaciones aorticas y la necesidad de intervenciones clínicas a raíz del tipo de mutación. Por lo tanto, decidimos secuenciar el mARN de VSMC de la parte dilatada y no-dilatada de 5 pacientes MFS con aneurisma intervenidos cirurgicamente. Hemos detectado una heterogeneidad amplia de mutaciones entre todos los pacientes. Sin embargo, dos mutaciones en dos pacientes diferentes eran del mismo tipo (mutación con cambio de sentido, prediciendo un fenotipo dominante negativo). Los dos pacientes no compartieron ninguna alteración en vías clasificadas como significativas por el análisis de enriquecimiento ontológico de genes, indicándonos que estos pacientes no comparten ningún perfil genético. Esto fue sorprendente ya que este tipo de mutación es uno de las más comunes e investigados en el MFS. No obstante, encontramos una segunda mutación que no solamente era del mismo tipo, sino que era exactamente idéntica entre dos pacientes. Esta mutación se encuentra en la 3´UTR, la cual es una región poca investigada en MFS, pero altamente relacionada con otras enfermedades tanto cardiovasculares como del tejido conjuntivo. Aún más interesante fue que los dos pacientes mostraban genes expresados diferencialmente en la zona no-dilatada. El análisis de enriquecimiento identificó que estos genes estaban altamente involucrados en la respuesta a proteínas desplegadas (UPR, del inglés *unfolded protein response*) y el estrés del retículo endoplasmático (ER stress, del inglés *endoplasmic reticulum stress*). La UPR es una respuesta adaptativa para restablecer la homeostasis celular, pero causa cambios patofisiológicos si no se resuelve a lo largo del tiempo. Aunque la 3´UTR no se traduce a proteína, se ha visto que mutaciones en esta región pueden ser la causa de la UPR y de fenotipos concretos debido a la multitud de funciones reguladoras de la 3´UTR. Sorprendentemente encontramos expresiones diferenciales en los genes y su asociación con ER stress solamente en mARN derivado de VSMC de la zona aortica no-dilatada, sugiriendo en acuerdo con resultados previos en un modelo ratón de fibrosis cardiaca, que la UPR y el ER stress son transitorios y aparecen previamente a los efectos perjudiciales en el tejido aórtico. Las consecuencias patológicas del ER stress se pueden atribuir a la implicación simultanea de los mediadores principales del ER stress en la estabilización de la señalización del TGF-β. Por ejemplo, genes codificantes para proteínas de choque térmico se veían alteradas en la zona no-dilatada de pacientes. A la vez, estas proteínas están asociadas con la estabilización de la señal TGF-β-dependiente por SMAD2 debido a su interacción directa con el complejo del receptor y su capacidad de aumentar la unión de mediadores de la señalización con el complejo. Además, 3´UTR son dianas principales para miRNAs y mutaciones en estas regiones pueden generar la pérdida de un sitio de unión para miRNAs. Esto puede causar la insuficiente degradación de *FBN1*, su acumulación en el ER y, como consecuencia, ER stress.

En resumen, podemos decir que en VSMC procedentes de aneurismas ascendentes de pacientes MFS la señalización está desregulada debido a alteraciones en el reclutamiento de mediadores de la señalización hacia endosomas tempranos. Además, concluimos que a nivel extracelular las integrinas como activadoras del TGF-β están disminuidas posiblemente como un mecanismo compensatorio de la señalización incrementada. Adicionalmente hemos definido un nuevo subgrupo de pacientes MFS con una mutación desconocida que induce un perfil de ER stress transitorio manifestándose en el fenotipo aórtico.

Abbreviations

ANG II	Angiotensin II
BMP	Bone morphogenic protein
BP	Biological Processes
b-TGF-β	Biotinylated TGF-β
CAV-1	Caveolin-1
cbEGF-like	Calcium-binding EGF-like
CC	Cellular compartments
CLTC	Clathrin
Co-SMAD	Common-mediator SMAD
CTGF	Connective tissue growth factor
DEG	Differentially expressed genes
ECM	Extracellular matrix
EEA1	Early endosome associated protein-1
EGF	Epidermal growth factor
EL	Ectopia lentis
ER	Endoplasmic reticulum
ER stress	Endoplasmic reticulum stress
ERAD	ER-associated degradation
ESCRT	Endosomal sorting complex required for transport
FBN1	Fibrillin-1
FKBP12	12 KDa FK506-Binding Protein
GDF	Growth/differentiation factor
GF	Growth factor
GFR	Growth factor receptor
GO	Gene ontology
I-SMAD	Inhibitory SMAD
ITGB1	Integrin β1
KEGG	Kyoto encyclopaedia of genes and genomes
LAP	Latency-associated peptide
LFC	Log fold change
LLC	Large latent complex
LTBP	Latent TGF-β-binding protein
MF	Molecular Functions
MFS	Marfan Syndrome

Abbreviations

MFSd	MFS dilated aortic zone
MFSnd	MFS non-dilated aortic zone
miRNA	Micro RNA
MMP	Matrix metalloproteinase
MVB	Multivesicular bodies
OSA	Obstructive sleep apnea
PCA	Principal Component Analysis
PIKC1	Protein that interacts with kinase C
PTC	Premature truncation codon
Ptdlns(3)P	Phohsphatidylinositol 3-phosphate
ROS	Reactive ocygen species
R-SMAD	Receptor regulated SMAD
SARA	SMAD anchor for receptor activation
SBD	SMAD-binding domain
SBE	SMAD binding element
SLC	Small latent complex
SPIA	Signalling Pathway Analysis
TB/8-Cys	TGF-β-binding protein like containing 8 cysteine
TBRI	TGF-β receptor 1
TBRII	TGF-β receptor 2
TGF-β	Transforming growth factor-β
TGN	Trans-golgi network
TSP-1	Thrombospondin-1
UPR	Unfolded protein response
VSMC	Vascular smooth muscle cell

Contents

Contents

Introduction

1. Introduction

1.1. Marfan Syndrome

Marfan Syndrome (MFS) is a multisystemic connective tissue disorder with autosomal dominant inheritance that affects between 1.5 and 17.2 in 100,000 live births (1). It is named after its discoverer Antoine Marfan, who defined MFS in 1896. The multisystemic disease is characterised mainly by skeletal, ocular and cardiovascular manifestations. MFS is caused by a mutation of the gene encoding the extracellular matrix (ECM) protein Fibrillin-1 (FBN1) (2). FBN1 is a structural glycoprotein belonging to the family of fibrillins and forms the principal component of microfibrils. Together with elastin, microfibrils constitute the elastic fibres of the ECM in connective tissues throughout the body. Close to 3000 different *FBN1* mutations with variable and unknown dysfunctionality have been identified to date, however, the progress of the disease is difficult to predict through its mutation (3–5).

1.1.1. Cardiovascular manifestations

The most severe complications in MFS are of cardiovascular nature. Progressive aortic root enlargement and ascending aortic aneurysms with the risk of dissection, regurgitation and rupture are the primary cause of death in MFS and affect around 77% of patients (6–8). The only measures available to treat aortic complications are regular imaging to evaluate aortic dilatation progression, β-adrenergic receptor antagonist and prophylactic or acute surgical repair (6,9). Even though aortic surgical repair has increased the life span of MFS patients significantly, many have to undergo subsequent surgeries, often at other sites of the aorta than the one of initial dilatation or rupture (10). Other cardiovascular complications include mitral valve prolapse, which is the most prevalent valvular abnormality occurring in 35%-54% of patients, mitral valve regurgitation and aortic insufficiency (6–8).

1.1.2. Skeletal and muscle system

The musculoskeletal phenotype in MFS patients is the most readily visible characteristic associated with the disease. Most commonly associated features are Pectus excavatum and Pectus carinatum (carved-in and protruding chest appearance; **Fig. 1.1.A**) as well as a decrease in bone mass, dolichostenomelia (unusually long limbs) and arachnodactyly (abnormally long fingers and toes; **Fig. 1.1.B**) (6,11,12). A further feature of MFS are spine deformities such as scoliosis (abnormal lateral curvature of the spine) and kyphosis (unnatural curvature of the upper back; **Fig. 1.1.C**) whose progression is associated with increased pain in the spine area (13). In addition, Marfan patients suffer from muscle myopathies and failure to regenerate skeletal muscle after injury or assault (14).

1.1.3. Ocular and other systems

Ectopia lentis (EL) is the dislocation of the eye lens and occurs in approximately 50% of Marfan patients, affecting either one or both eyes at the same time (8). Ocular pathologies in MFS are attributed to stretching of the tunica scleralis which leads to zonular fibre rupture and lens dislocation (6,15). Furthermore, MFS patients have been reported to suffer spontaneous pneumothorax, which is the uncoupling of the lung from the chest wall through the collection of air in the pleural space (16). Spontaneous pneumothorax can cause shortness of breath, chest pain, lack of oxygen and a rapid heart rate. Even though a small spontaneous pneumothorax usually only requires monitoring, MFS patients with recurring and even contralateral pneumothorax requiring surgery have been reported (17). A further clinical feature is the occurrence of obstructive sleep apnea (OSA) which occurs in approximately 34% of MFS patients (18). OSA is caused by craniofacial abnormalities as well as upper airway problems and is reported to accelerate the onset of aortic events (18,19).

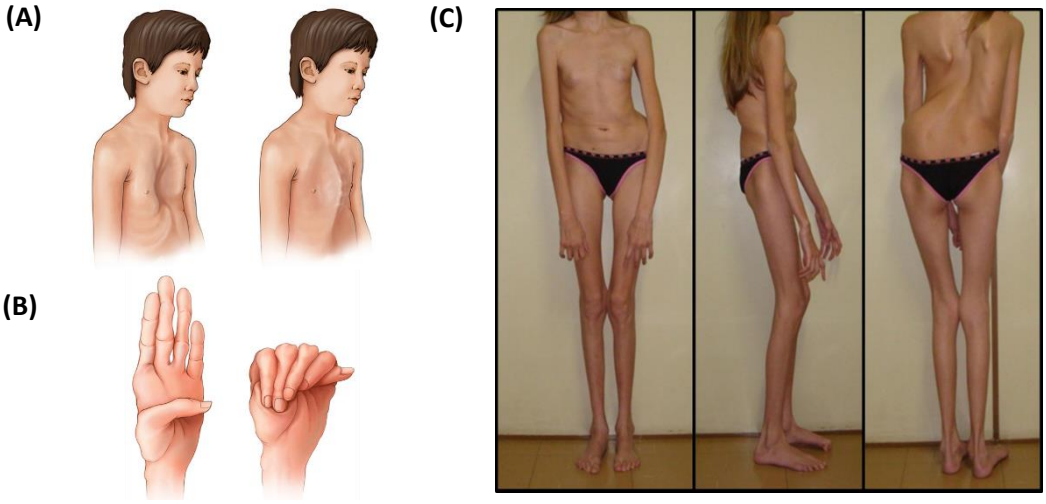

Fig 1.1. Skeletal features of Marfan Syndrome. (A) *Indented and Protruding breastbone (Pectus excavatum and Pectus carniatum).* ***(B)*** *Arachnodactyly and the thumb sign where the thumb tip extends the length of the palm. Modified from the Mayo Foundation for Medical Education and Research.* ***(C)*** *Severe scoliosis and kyphosis in a young female patient. Modified from* (20).

1.2. Differential diagnosis

Due to the multisystemic nature of the disease, diagnosis requires more than a single test, but a scoring system named “Ghent nosology” which takes multiple factors into account. The scoring system

includes cardinal features as well as less specific manifestations which a MFS patient must display. The two most important cardinal features are the size of the aorta/aortic risk of dissection calculated by its Z-score (AoZ≥2) and the occurrence of EL. All other cardiovascular and ocular manifestations as well as other organs affected contribute to a systemic score that facilitates the correct diagnosis in the absence of genetic testing or, in some cases, in the absence of *FBN1* mutation **(Table 1.1.)**. The combination of symptoms as well as family history assist in the differential diagnosis of MFS (12). However, diagnosing patients remains challenging due to the lack of a medical reference standard and the accuracy and specificity of diagnostic criteria (1).

Box 1. Revised diagnostic criteria
In the absene of family history: 1) Ao (Z≥2) AND EL 2) Ao (Z≥2) AND *FBN1* mutation 3) Ao (Z≥2) AND systemic score of ≥7 points 4) EL AND *FBN1* mutation identified in patient with aortic aneurysm **In the presence of family history** 1) EL 2) Systemic score of ≥7 points 3) Ao (Z≥2 above 20 years of age, Z≥3 below 20 years of age)
Box 2. Scoring of systemic features
1 point: Skeletal features such as chest asymmetry, scoliosis, reduced elbow extension, distinctive facial features 2 points: Pneumothorax, dural ectasia, pectus carniatum deformity 3 points: Wrist and thumb sign *A total of 20 points can be scored and ≥7 points indicates systemic involvement*
Box 3. Criteria for causal *FBN1* mutation
1) *FBN1* mutation previously shown in family history 2) De novo mutation of one of the following: - Nonsense - Inframe or out of frame deletion/insertion - Splice Site mutation affecting splicing on mRNA/cDNA level - Missense mutation affecting a critical FBN1 domain

Table 1.1. Scoring system for the differential diagnosis of MFS. Box 1*. Revised criteria for diagnosing a patient with MFS in the absence and presence of family history.* ***Box 2.*** *Table of scoring system for non-cardinal features with a score of ≥7 indicating MFS.* ***Box 3.*** *Type of FBN1 mutation considered causative for the diagnosis of MFS. Modified from* (12)*.*

1.3. Fibrillin-1

MFS is caused by various possible mutation variants of the 11,756 base pairs large *FBN1* gene on chromosome 15q21.1, which encodes the 350 kDa heavy ECM glycoprotein FBN1 (2,21). FBN1 is a vital element of microfibrils, which are 10-20 nm extracellular structural components that are ubiquitous in both elastic and non-elastic connective tissues throughout the body (22,23). These fibrillin abundant microfibrils can associate with a variety of ECM components such as elastin to form elastic fibres. The spatial arrangement of these elastic fibres is tissue specific and ranges from parallel bundles of microfibrils in the lens to ordered concentric rings of elastic fibres attached by microfibrils in the tunica media of the aorta (22).

1.3.1. Structure of Fibrillin-1

The glycoprotein FBN1 consists primarily of 47 epidermal growth factor (EGF)-like domains, interspersed with seven characteristic domains of each eight cysteines (TB/8-Cys) **(Fig. 1.2.)**. The EGF-like domains contain six highly conserved cysteine residues that form intramodule disulphide bonds and induce β-sheet formation of the protein. In addition, 43 of the 47 EGF-like domains contain calcium binding consensus sequences (cbEGF) (22,24).

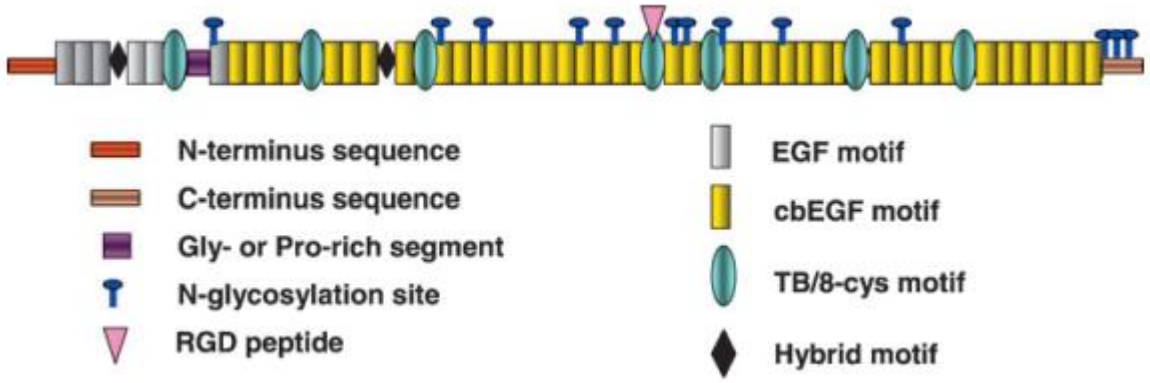

Fig.1.2. Structure of the large glycoprotein FBN1. *Schematic illustration of FBN1: (cb)-EGF-like domains are interspersed with TB/8-Cys motifs. The RGD motif indicated by pink arrow is a versatile binding domain. Disulphide bonds are formed between EGF-like domains. The cb-EGF motifs displayed in yellow are calcium binding. Modified from* (22).

Depending on the adjacent domains, cbEGF domains bind calcium with varying affinities between 300 nM to 350 µM (21,25,26). Under physiological conditions, the saturation of calcium binding sites

restricts the flexibility of FBN1, forcing it into a rod-like shape (27). Calcium binding is therefore mainly important for the structural integrity of FBN1, however, calcium saturation also stabilizes the protein against proteolytic degradation and facilitates protein-protein interactions (24,26). Multiple sets of cb-EGF domains are separated from one another by interspersing TB/8-Cys domains. These highly unique domains are organized into 6 anti-parallel β-strands and 2 α-helices which are held together by disulphide bonds and hydrophobic interactions (28,29). The TB/8-Cys domains determine some of the most important binding characteristics of FBN1 as they contain a unique sequence which is solely shared with the latent TGF-β binding protein (LTBP) (22,28). An RGD motif found in the TB/8-Cys4 module is a versatile binding partner for proteins ranging from integrins to bone morphogenic proteins (BMPs) (30–32).

1.3.2. Synthesis

The 350 kDa FBN1 is initially synthesized as profibrillin-1 which interacts with endoplasmic reticulum (ER) chaperone proteins BiP/HSP70 and GRP94/HSP90. These chaperone proteins protect the pro-protein from cleavage whilst being transported through trans-golgi network (TGN) (33). After secretion from the TGN, pro-fibrillin-1 is C-terminally cleaved between amino acids 2731 and 2732 and converted into the 20 kDa smaller fibrillin-1 by pro-protein convertases of the PACE/Furin family (34). The correct cleavage is fundamental for the appropriate incorporation of FBN1 into the ECM and is independent of synthesis status (35). Mutations immediately adjacent to the consensus sequence have been reported in MFS patients, which lead to reduced proteolytical cleavage and deposition into the ECM despite normal FBN1 secretion levels (34).

1.4. FBN1 mutation

Mutations in *FBN1* are manifold and found throughout the entire length of the gene. Of all reported *FBN1* mutations only 12% are recurrent and the actual number of mutations might be significantly higher due to failure to report mutations or correctly diagnose MFS in patients (4,5). Adding to the genetic variability seen in MFS, 25% of all *FBN1* mutations are spontaneous without exhibiting any family history (5). Furthermore, a significant portion of cases remains genetically unresolved which is due to the labour intensity of mutant testing and the omission of non-exonic *FBN1* regions as disease causing variants (36,37). The variable clinical features seen in MFS are attributed to the distinct underlying genetic mechanisms. Different types of mutations may produce a dominant negative or a haploinsufficient genotype. In dominant negative mutations, one mutated gene product acts antagonistically to the wild-type product, which in MFS is particularly pathogenic due to the polymeric structure of FBN1 in the formation of microfibrils (38). Haploinsufficent genotypes on the other hand

have only one functioning allele which produces insufficient gene product and therefore less FBN1 at the ECM level (39). These two mutation types lead to diverse outcomes of FBN1 functionality, FBN1 tissue distribution, and eventually clinical manifestation (8). In addition, mutations in *FBN1* have been associated with phenotypes other than classic MFS such as isolated aortic aneurysms, isolated ectopia lentis and Weill-Marchesani Syndrome, a connective tissue disease that, contrary to MFS, is characterized by small stature and unusually short fingers and toes (5). The disparate clinical features of conditions caused by *FBN1* mutations underscore the importance of cell context and FBN1 microfibril incorporation in the clinical variability and lack of genotype-phenotype correlation (5,8)

1.4.1. Missense mutations

About two thirds of all known *FBN1* mutations are classified as missense, which are single nucleotide changes resulting in a codon change and a different amino acid. The majority of these affects one of the 43 cbEGF domains (21). The most common cbEGF domain missense mutation produces a substitution of cysteine residues and disrupts the disulphide bond formation between them. Disulphide bond disruption leads to misfolding of the protein, disorganization of a given module and global loss of structural integrity (8,40,41). The second most common missense mutation affects the calcium binding residues of the cbEGF domains. This produces a lower affinity for calcium binding and increased risk of proteolytic degradation (24,42). However, cysteine substitutions have been found to show confined localized effects depending on the affected cbEGF domain. Structural consequences can vary from intracellular FBN1 retention to increased proteolytic degradation, which stresses the functional heterogeneity of mutations clustered into the same category (41,43,44). Clinical phenotypes associated with *FBN1* missense mutations range from mild phenotypes lacking cardiovascular manifestations to severe neonatal phenotypes exhibiting deleterious aortic events and cardiac failure (8,21,45). Missense mutations in exons 24-32 have emerged as the most consistent indicator of aortic risk. Mutations in this middle region of *FBN1* have been found in all cases of lethal neonatal MFS and define a high risk group of severe cardiovascular manifestations including aortic aneurysms (8).

1.4.2. Premature truncation and codon mutations

Around 10-20% of all recorded MFS mutations include insertions, deletions and frameshifts leading to a premature truncation codon (PTC). PTCs produce nonsense-mediated decay and reduced mRNA concentration (5,21). The reduced mRNA concentration leads to approximately halved synthesis of normal sized FBN1 and disproportionately decreased matrix deposition, creating structurally inferior connective tissue (46). In MFS, PTC mutations are largely associated with characteristic skeletal

phenotypes, however, the occurrence of aortic dilatation and dissection has been reported (47). Even more so, aortic events occur at a younger age in patients with a truncation mutation than in patients with missense mutation involving a cysteine substitutions (8,47). On the other hand, a lower incidence of ectopia lentis has been reported in patients with PTC mutation as opposed to cysteine substitution (48). Yet, in spite of mutation type clustering, most mutations remain unique to individual affected families (49).

1.4.3. Splice Site Mutations

Some 10-15% of all mutations found in in MFS consist of various splicing errors such as in-frame exon skipping and activation of cryptic splicing sites. Exon skipping may cause the deletion of one or more entire cbEGF domain, leading to reduced FBN1 synthesis and matrix deposition (5,50). Cases of whole gene deletion have been reported in MFS, however, rarely (51). Some of the most severe types of MFS are caused by splice site mutations and aortic events appear at an earlier age in MFS patients with splice site mutations than missense mutations (47,52). Exon skipping produces these severe phenotypes as it omits multiples of three nucleotides and preserves the reading frame. The result are shortened fibrillin monomers that are able to take part in the microfibril assembly but interfere with the polymerization process and lead to severe microfibril disruption (52).

1.5. FBN1 mediates TGF-β activation

Apart from its structural role, the second main physiological function of FBN1 is the regulation of Transforming Growth Factor-β (TGF-β) (53,54). TGF-β is secreted into the extracellular environment as a large latent complex (LLC) which is covalently attached to the latent TGF-β-binding protein (LTBP). LTBPs interact with FBN1 through their characteristic 8-Cys module uniquely shared between the two proteins (54–56). TGF-β plays a vital part in a number of processes throughout development and is crucial for the maintenance of balance between cells and ECM and, therefore, tissue homeostasis. Its deregulation is implicated in a variety of diseases ranging from fibrosis and cancer to autoimmune and vascular diseases (55,57). In this way, FBN1, being a vital component of the ECM, contributes to the temporal and spatial regulation of the versatile TGF-β **(Fig. 1.3.)**.

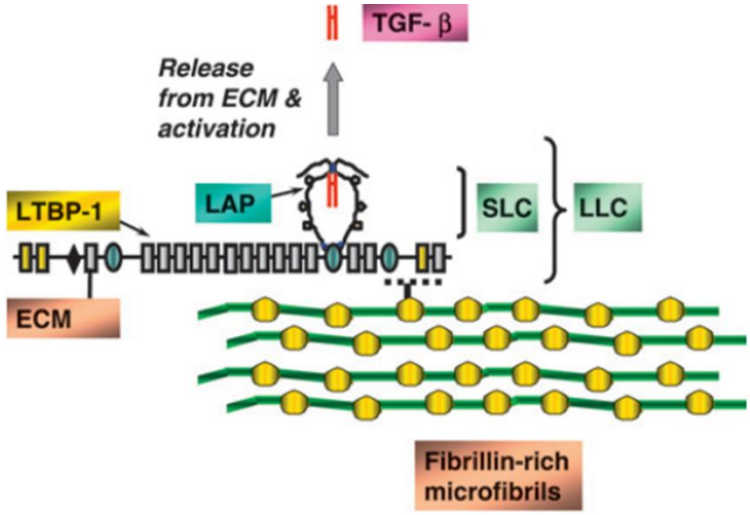

Fig. 1.3. Mature TGF-β is matrix-bound and controlled by FBN1 through the interaction with LTBP. *Shown are the components of the small and large latent TGF-β complexes (SLC and LLC respectively) and its interaction with ECM and microfibrils. Modified from* (22).

1.5.1. Clinical features of TGF-β

TGF-β is the principal regulator of fibrosis, wound healing and tissue repair. TGF-β is found in all tissues and released by the majority of cells including infiltrating lymphocytes, macrophages/monocytes and platelets (58). During wound healing, myofibroblasts become activated and migrate towards the site of injury. The release and activation of TGF-β stimulates the synthesis of extracellular matrix proteins and simultaneously inhibits their degradation (59,60). Amongst the proteins induced by TGF-β are type I collagen, fibronectin and connective tissue growth factor (CTGF), all of which enhance a contractile cellular phenotype and prolong the induction of ECM (61). Antagonist of TGF-β induced matrix deposition at the site of wound repair are macrophage induced Tumor Necrosis Factor α (TNF-α) and Interferon-γ (INF- γ) which is a pleiotropic cytokine produced by T and Natural Killer (NK) cells (61–63). Under normal conditions, the balance between profibrotic and antifibrotic factors enables the correct wound repair and tissue restoration. However, the excess of TGF- β leads to pathologic tissue fibrosis and compromises organ structure as well as its function. At the same time, the deficiency or absence of TGF β leads to severely impaired wound repair, tissue necrosis, organ failure and death, emphasizing the importance of TGF-β homeostasis (64,65).

1.5.2. TGF-β in aortic aneurysms

Under physiological conditions, TGF-β is maintained in an inactive state by controlled binding of LTBP to FBN1. In MFS, the fragmentation of microfibrils caused by insufficient or dysfunctional FBN1 leads to the reduced binding capacity of LTBP and increased active TGF-β in the extracellular environment **(Fig.1.4.)** (54,55). As such, TGF-β has emerged as an important molecular factor of aneurysm progression. TGF-β neutralizing antibodies as well as the inhibition of TGF-β expression through cross-activating pathways have been shown to decrease aneurysm formation in an animal model of MFS (66–68). In MFS patients, higher levels of circulating TGF-β were shown to positively correlate with aortic root diameter and have therefore been proposed as biomarker for aortic risk (69). Increased levels of TGF-β in the environment of aortic vascular smooth muscle cells (VSMC) have been directly linked to intracellular changes leading to impaired tissue repair, muted immune responses and limited angiogenesis (70). The dysregulation of TGF-β in MFS challenges the view of structural deficiencies being the sole cause of aneurysm formation and provide an opportunity for targeted therapy (55,71).

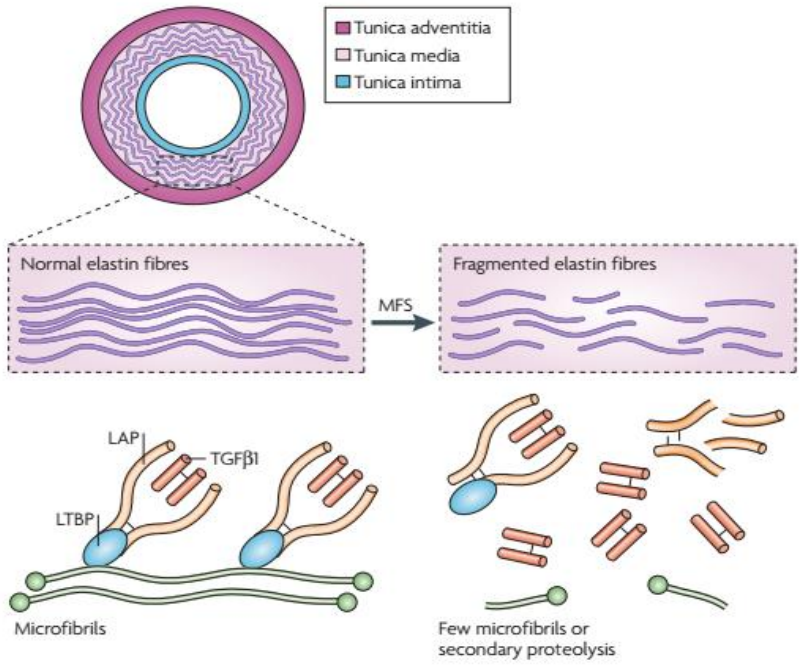

Fig.1.4. The fragmentation of fibrillin microfibrils leads to increased TGF-β in the extracellular environment. *Fragmentation of the elastic fibres of the aortic tunica media, which is rich in smooth muscle cells, elastic fibres and collagens, is associated with excessive release of the LLC from the ECM and increased active TGF-β. Modified from* (55).

1.6. TGF-β secretion and ECM incorporation

TGF-β belongs to the TGF-β superfamily which includes nearly 30 proteins in mammals. Amongst these are TGF-β, inhibins, activins, bone morphogenic proteins (BMPs) and growth/differentiation factors (GDFs). Three different TGF-β isoforms have been identified in mammals: TGF-β1, TGF-β2 and TGF-β3. All three isoforms share 75-80% homology between each other and have paracrine and autocrine profibrotic effects (55,72,73). TGF-β is initially synthesized as a pre-pro-protein which is proteolytically processed at its N-terminal in the rough endoplasmic reticulum. Two monomers each dimerize through disulphide bridges to form pro-TGF-β. Furin convertases cleave the pro-dimer and convert it into the small latent TGF-β complex (SLC). The SLC consists of the latency-associated peptide (LAP) and the mature TGF-β, which are held together by covalent bonds. To attach the SLC to the ECM, the 8-Cys3 domain of LTBP covalently binds the SLC (74), resulting in the formation of the large latent TGF-β complex (LLC) **(Fig. 1.5.A-C)**. LTBP is crucial for linkage of the complex to the ECM. The N-terminal LTBP hinge region binds to fibronectin and other ECM components. The C-terminal LTBP region on the other hand interacts with the N-terminal region of FBN1 **(Fig.1.5.D)**. In this way LTBPs and FBN1 offer crucial support in targeting TGF-β to specific sites and controlling its activation (55,56,75).

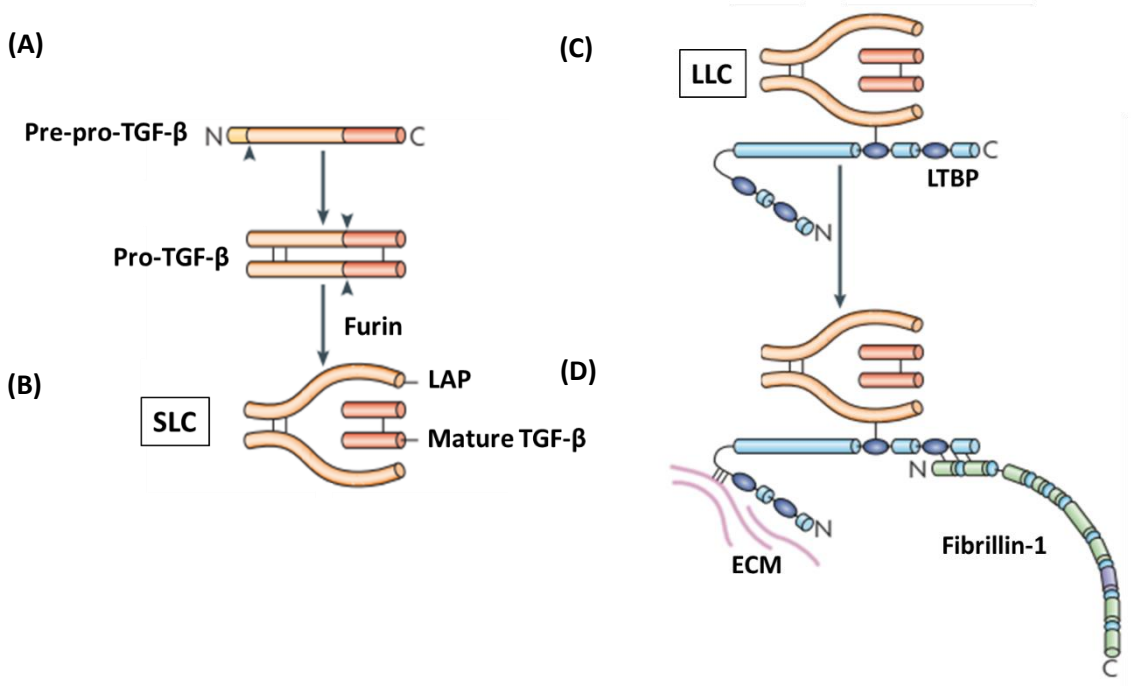

Fig. 1.5. Secretion and ECM incorporation of TGF-β. *The nascent pre-pro- TGF-β undergoes a series of cleavage* ***(A)*** *and conversion* ***(B)*** *processes until the covalent interaction with LTBP* ***(C)*** *allows its ECM incorporation and FBN1- microfibrils controlled regulation* ***(D)****. Modified from* (55).

1.6.1. TGF-β release from the ECM

For TGF-β to bind to its receptor and initiate signalling, the LLC containing the mature protein must be released from FBN1 microfibrils as well as the ECM. LLC release can be initiated by LTBP displacement from FBN1. Microfibrils are degraded by elastase, an inflammatory proteolytic enzyme, which induces the release of FBN1 fragments. These fragments themselves are able to compete with LTBP for binding at their own N-terminal, therefore displacing the LTBP (54,55). To release the LLC from the ECM, proteases such as plasmin and thrombin cleave the LTBP hinge region which frees the LLC whilst the LTBP N-terminal fragment remains bound to the ECM **(Fig.1.6.)** (55,76). Furthermore, BMPs have also recently been identified as additional key elements for LLC release by cleaving the LTBP hinge region at two specific sites resulting in a free LLC complex (77).

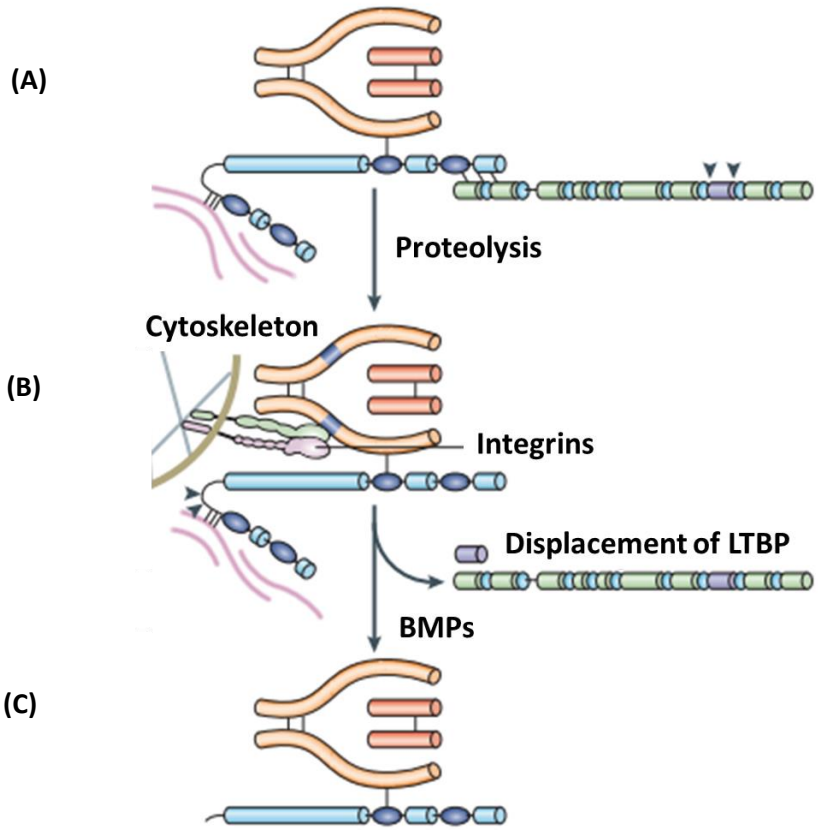

Fig.1.6. TGF-β release from the ECM. *TGF-β can be released from microfibrils through cleavage processes such as those involving inflammatory proteolytic enzymes* ***(A)*** *which induce a process that displaces LTBP from microfibrils. Integrins can mechanically release the mature cytokine directly from LAP* ***(B).*** *Proteases and BMPs then release the LLC from the ECM for further processing* ***(C).*** *Modified from* (55).

1.7. TGF-β activation and receptor binding

For TGF-β to become activated, the mature active cytokine must be cleaved from the LAP complex to induce receptor binding and signalling. This process can be integrin-independent after the LLC is released from the ECM, or integrin-associated at various stages of the extracellular release. However, under all circumstances, it is the LAP complex that is directly targeted (55,76). A widely accepted integrin-independent mechanism is the cleavage of LAP by matrix metalloproteinases (MMPs) to release active mature TGF-β (78). MMPs are extremely pleiotropic and can perform more than one function. They have been shown to also be directly involved in wound healing responses, ECM degradation and remodelling. The degradation of ECM may sustain the lack of TGF-β targeting to the ECM and the increased TGF β activation. In turn, TGF-β has been suggested to transcriptionally control the activation of MMPs, therefore sustaining a positive feedback loop between TGF-β and MMPs (61,79,80). Changes in the pH can furthermore activate TGF-β independently of integrins. Extremely acidic environments induce the disintegration of LAP which releases active TGF-β (81). Another TGF-β activating mechanism are reactive oxygen species (ROS), which are induced by NAD(P)H oxidase and mitochondria. ROS have been shown to alter the confirmation of LAP and expose active TGF-β. On the other hand, TGF-β signalling induces the production of ROS by activating NAD(P)H oxidase, interfering with mitochondrial function, and suppressing antioxidant enzymes. This leads to a vicious cycle of a global redox imbalance favouring TGF-β induced tissue fibrosis under non-homeostatic conditions (82,83). However, one of the most significant activators of TGF-β is thrombospondin-1 (TSP-1). TSP-1 is a large homotrimeric glycoprotein that interacts with LAP through the TSP-1 sequence KRFK and the LAP sequence LSKL. The binding induces a conformational modification of LAP which subsequently exposes mature and active TGF-β (84–86). TSP-1 has furthermore been associated with increased fibrosis and the development of vascular inflammation which, in turn, might activate dormant TGF-β (87,88). TSP-1 is frequently expressed at sites of wound healing and inflammation. The interference with the activating process of TGF-β by TSP-1 has been shown to improve the generation of fibrosis and ECM deposition in a murine model of inflammatory renal disease (87). Considering the multifunctionality of TGF-β, targeting TSP-1 has been proposed as a viable therapeutic approach for local TGF-β overactivation (87,88).

1.7.1. Integrin-mediated TGF-β activation

Integrins are incorporated components of the ECM and crucial for cell adhesion to ECM components. They interact directly with growth factors (GF) and control their storage at the ECM as well as their activation (89). Integrins are transmembrane proteins consisting of an α and a β subunit. 18 α and 8 β subunits are known which can form 24 specific and non-redundant integrin heterodimers that are not

constitutively active, but rather are mostly found in an inactive conformation on cell membranes (90). Some integrins directly bind to the ECM incorporated FBN1 which triggers downstream activation, cell spreading and focal contact adhesion (91). The cross-talk between GF receptors (GFR) and integrins is extensive and especially interactions between TGF-β and integrins have been thoroughly studied. TGF-β is an exceptional GF as, in its latent forms, it is part of the ECM and binding target for integrins (92). TGF-β signalling has been shown to alter the confirmation of integrins, inducing a shift to a high affinity binding state in and inside-out fashion. In particular the integrins α1, α2, α3, α4 and β1 are upregulated by TGF-β at mRNA, protein and cell surface expression levels (93,94). On the other hand, activated integrins have the capacity to activate latent TGF-β. Some integrins have been shown to bind LAP of latent, matrix associated TGF-β through their shared RGD sequence **(Fig.1.7.)**. In contrast to soluble factors that cleave the latent TGF-β complex and release mature TGF-β, integrins use shear forces to distort LAP and present mature TGF-β in a proximity-dependent manner to its receptor (76,95). These shear forces are generated through pulling by the actin cytoskeleton which is connected to the cytoplasmic tail of integrins and involves the Rho associated kinase/ROCK signalling pathway. The pulling force is only effective if the ECM is mechano-resistant and able to bind LTBP in an efficient way (96). The cross-talk between TGF-β, the ECM, and integrins has been proposed to be a major player in fibrosis through the enhanced ECM deposition and the resulting tissue stiffness. It has been hypothesized that the increased contractility seen in fibrotic diseases enhances the activation of matrix bound latent TGF-β by increasing the shear forces applied by integrins (95). Indeed, it has been shown that the increase in integrin-dependent TGF-β activation is associated with increased fibrosis and that in particular the integrin subunit β1 (ITGB1) plays a crucial part in this activation. Integrin β1 has been shown to respond rapidly to and become upregulated by TGF-β treatment in a myofibroblast model of fibrosis (97). Furthermore, inhibiting ITGB1 has been shown to have antifibrotic effects in contractile cells due to decreased integrin dependent TGF-β activation (98).

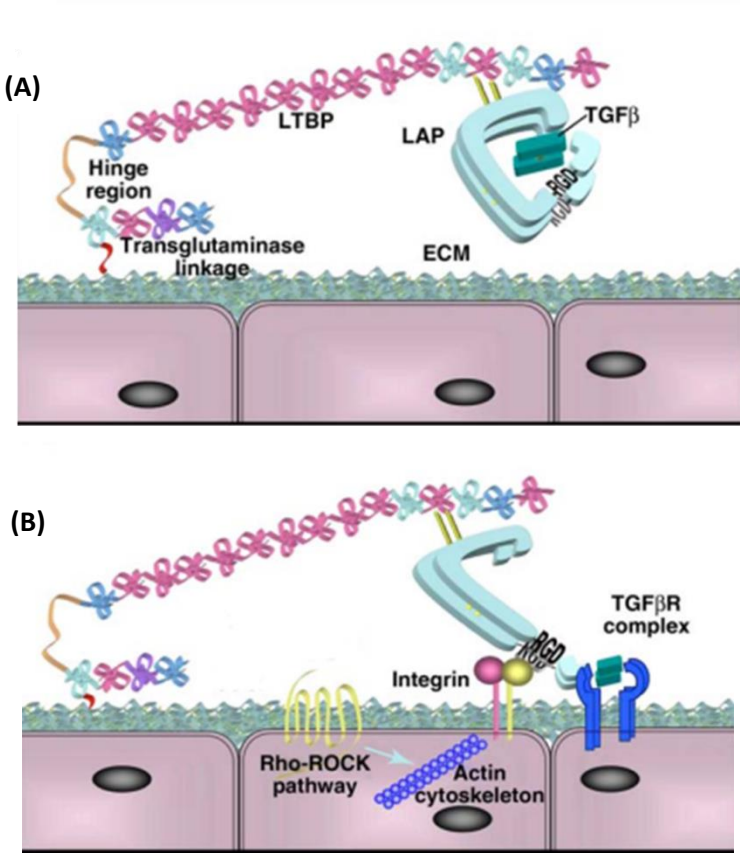

Fig. 1.7. Latent TGF-β activation by integrins. (A) *Mature TGF-β is bound to the ECM on the cell surface by interaction of LAP with LTBP.* ***(B)*** *Binding of integrins is predicted to cause a conformational change of LAP and present TGF-β to its receptors. The process relies on an intact ECM and may be facilitated by the cell contraction enhancing Rho-ROCK signalling pathway. Modified from* (95).

1.7.2. TGF-β receptor binding

TGF-β signals through a heterodimeric receptor complex belonging to the serine/threonine kinase family which comprises 12 members: 7 type I receptors and 5 type II receptors, all of which are dedicated to signalling by the TGF-β superfamily. The transmembrane TGF-β superfamily receptors consist of about 500 amino acids organized into a Cys-rich extracellular N-terminal ligand binding domain, a transmembrane domain, and a C-terminal serine/threonine kinase domain (99,100). TGF-β (amongst which are the three isoforms TGF-β1, TGF-β2, and TGF-β3) signals through a heterocomplex consisting of the TGF-β type II (TBRII) and either of the TGF-β type I receptors (TBRI; also known as ALK5, which induces the classical canonical SMAD2-dependent signalling or ALK1 which induces SMAD1/5 phosphorylation), whilst other members of the TGF-β superfamily signal through other combinations of specialised type I and type II receptors **(Fig.1.8.)**. The TBRI contains a characteristic

SGSGSG sequence which is termed the GS domain. This domain is found N-terminal of the intracellular kinase domain and the successful activation of TBRI requires transphosphorylation of its GS domain by TBRII upon ligand binding (73,100,101). A third type of auxiliary TGF-β receptor (TBRIII; amongst which are endoglin and betaglycan) may assist the low affinity TGF-β2 isoform to bind TBRII (102). TGF-β does not interact with the isolated TBRI but shows a high affinity for TBRII and binds to its ectodomain. The recruitment of TBRI allows for correct complex assembly and subsequent receptor phosphorylation. However, the heterocomplex formation consists in fact of not only one TGF-β ligand but a ligand dimer and four receptor molecules, whilst each receptor only binds one ligand at a time and the TBRI and TBRII bind TGF-β at adjacent positions on the ligand surface (100,103). It is not clear why TGF-β changes its affinity for the TBRI once it is bound to TBRII. A hypothetical model suggests a conformational change of TGF-β, exposing a TBRI binding site once it is bound to TBRII (103). Whichever the process, the binding of the dimeric ligand to TBRII and the incorporation of TBRI in the complex brings the receptors close enough to each other to enable transphosphorylation of TBRI by TBRII. Whilst TBRI needs to be phosphorylated, TBRII kinase is assumed to be constitutively active, although the regulatory process remains elusive (100). The GS region of TBRI is not only a crucial phosphorylation sequence, but also serves to prevent phosphorylation and therefore activation of the receptor complex. Proteins like 12 KDa FK506-Binding Protein (FKBP12) can bind to the unphosphorylated GS region and inhibit phosphorylation of TBRI by TBRII, thereby controlling TGF-β signalling at the receptor level (57,104).

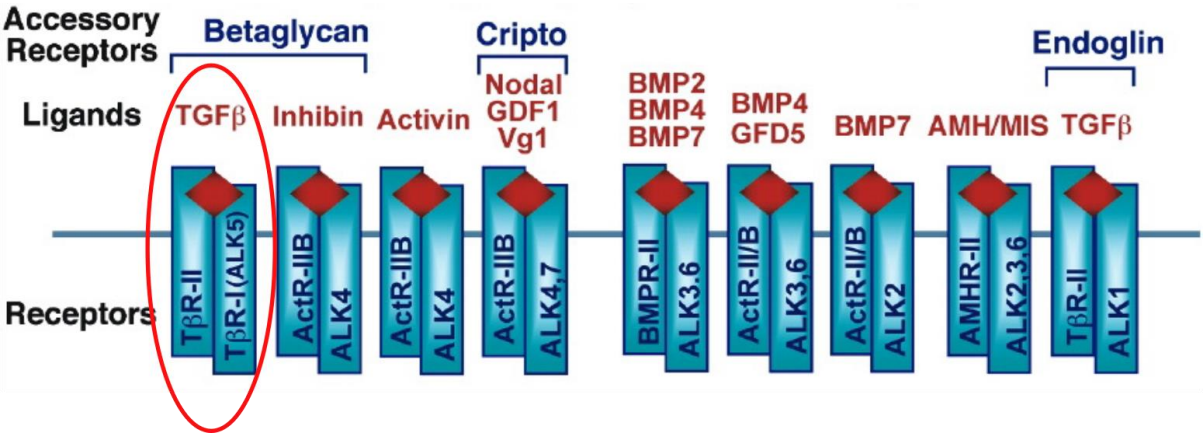

Fig.1.8. TGF-β superfamily receptors, ligands, accessory receptors and their relationship. *Receptors can arrange in various combinations and transduce signals in a ligand-specific manner. The same receptor combination can also accept various ligands such as in the case of receptor heterocomplex BMPRII and ALK3.6, which binds three different BMP ligands. Here, we focus on the heterocomplex TBRI/ALK5 and TBRII and its associated signalling pathways as indicated by the red circle. Modified from* (100).

1.8. TGF-β receptor complex endocytosis

Once TGF-β has bound to TBRII and TBRI has been recruited and phosphorylated, TGF-β receptor complex endocytosis takes place through two different pathways: the clathrin-dependent pathway and the caveolin-1/lipid-raft-dependent pathway. These two pathways have been shown to have opposite effects on signal transduction (101). Whereas TGF-β receptors internalised through clathrin-coated pits are associated with the transduction of TGF-β signal and receptor recycling, the internalisation through lipid raft-associated caveolae is involved in the signal abrogation and proteasome receptor degradation (101,105). In this way, the membrane trafficking of TGF-β receptors is suggested to play a crucial role in the control over the signalling response and therefore to be a regulatory mechanism of signal transduction.

1.8.1. Clathrin-dependent endocytosis

During clathrin-dependent endocytosis, the plasma membrane invaginates to form vesicles containing cargo such as receptor-ligand complexes. Cytoplasmic clathrin triskelia polymerize into hexagons and pentagons and assemble a clathrin coat around the vesicles, which then bud off the plasma membrane and enter the intracellular space. Clathrin forms a protective coat around the cargo containing vesicles, however, it does not directly bind neither the plasma membrane nor the vesicle cargo and therefore relies on adaptor and accessory proteins (106,107). Once the cargo is taken up into the cell, the clathrin coat is released and the uncoated vesicle fuses into early endosomes. The receptor cargo undergoes either recycling to the plasma membrane or passes through to more mature endosomes such as multivesicular bodies (MVB) and lysosomes for lysosomal degradation (106,108). In this way, the TGF-β receptor complex internalises through clathrin-coated vesicles and may undergo either fate. TGF-β receptor signalling associated with clathrin-dependent endocytosis takes place at early endosomes. The signalling mediators of all TGF-β family members in vertebrates were discovered in 1996 and are called SMADs; a portmanteau of the drosophila protein homologue “MAD” and the Caenorhabditis elegans homologue “SMA” (109–111). Three classes of SMAD mediators with different functionalities exist (100,112) :

1) The receptor regulated SMADs (R-SMADs) including SMAD1, SMAD2, SMAD3, SMAD5, and SMAD8/9
2) The common-mediator SMAD (co-SMAD) SMAD4 which interacts directly with R-SMADs
3) The inhibitory SMADs (I-SMADs) including SMAD6 and SMAD7 which inhibit the activation of R-SMADs and co-SMADs.

SMAD signalling is specific but not exclusive for either of the TGF-β family members in that TBRI and TBRII signalling is executed through the recruitment and phosphorylation of a SMAD2 and SMAD3 complex and the subsequent recruitment of SMAD4. As a controlling mechanism, the receptor activation can be blocked by SMAD7 (100,112). The specificity of either R-SMAD for each TGF-β receptor family member is ensured by matching amino acid sequences termed the L45 Loop and the L3 Loop, which are found adjacent of the TBRI kinase domain and the carboxy-terminal of R-SMADs respectively (113,114). However, R-SMAD binding to TBRI must be facilitated by SARA (Smad anchor for receptor activation), a FYVE domain containing auxiliary protein that recruits SMAD2 to TBRI and controls SMAD2 subcellular localization by targeting it to the membrane of early endosomes (115,116). Furthermore, SARA has been shown to be a crucial downstream mediator of Rab5-mediated endosomal trafficking and might serve as the key player in TGF-β signal regulation by orchestrating the spatial endosomal localisation and recruitment of signalling mediators (117). The interaction of SARA with TBRI allows therefore for a more efficient recruitment and phosphorylation of signalling mediators. SMAD2/3 become directly phosphorylated by TBRI which at the same time destabilizes their interaction with SARA, allows complex dissociation, and increases their affinity for SMAD4. The SMAD2/3 complex recruits and binds through their C-terminal pSer-X-pSer motifs to the surface pocket of the SMAD4 MH2 domain and the complex subsequently translocates to the nucleus to regulate target gene transcription **(Fig.1.9.)** (118–120). The binding of the SMAD complex occurs in a sequence specific manner identified as a short 5′-AGAC-3′ binding domain termed minimal Smad binding element (SBE) (121,122). The DNA binding of the SMAD complex immediately enables a multitude of changes in the expression of several hundreds of genes amongst which are critical regulators of ECM remodelling such as collagen, elastin and MMPs (123–125). In MFS, increased TGF-β dependent pSMAD2/SMAD4 nuclear translocation has been associated with aortic aneurysms due to collagen deposition and elastin fragmentation at the ECM level (126,127). Once the R-SMADs have become phosphorylated and have exerted their effect on a multitude of possible targets, TBRI and TBRII themselves either undergo lysosomal degradation or recycle back to the plasma membrane to restart the cycle. The recycling mechanism for TGF-β receptors has been shown to depend on the Rab11 machinery and to be constitutive as it may be ligand-dependent or -independent (128). The lysosomal degradation however has been associated with a molecule called Dapper, which preferentially associates with TBRI in Rab7 positive late endosomes facilitating the cargo transport form early to late endosomes (129).

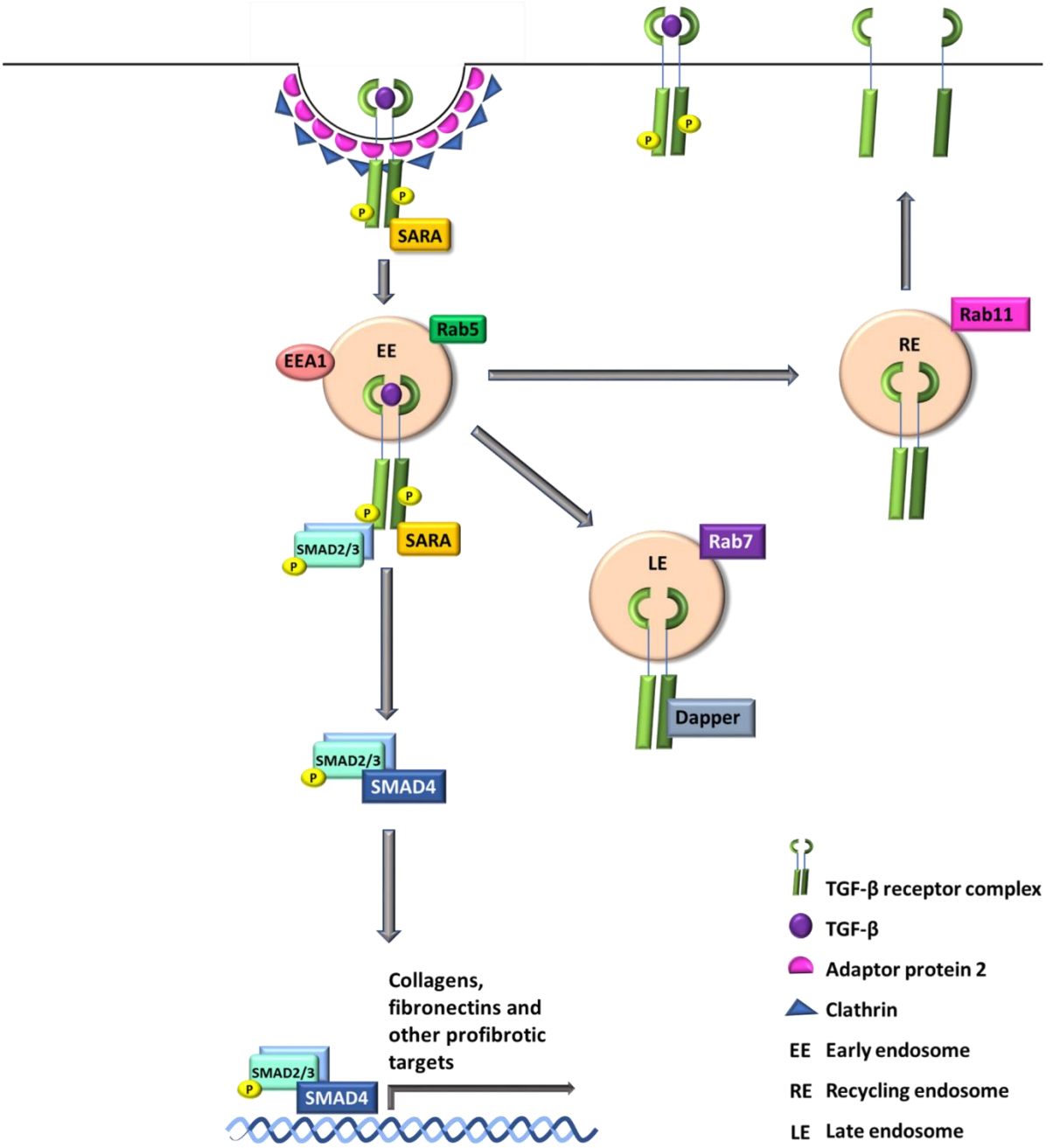

Fig.1.9. TGF-β receptor endocytosis through the clathrin-dependent pathway. *Receptor dimer and ligand complexes form on the cell surface and internalise through clathrin coated vesicles. Cargo vesicles fuse into EEA1-positive early endosomes where SARA binds and recruits SMAD2/3 under the regulation of Rab5. The SMAD2/3 complex becomes phosphorylated by TBRI and detaches from the receptor complex, at the same time forming a heterocomplex with SMAD4 which translocates to the nucleus inducing gene transcription. The receptor complex may either undergo Rab7-mediated transport to late lysosomes or Rab11-mediated recycling.*

1.8.2. Caveolin-dependent endocytosis

Caveolae form smooth invaginations of the plasma membrane which are characterized by the presence of caveolin-1 (CAV-1). These invaginations are located within glycolipid rafts which are detergent-insoluble, low-density membrane fractions rich in sphingolipids and cholesterol (130). Caveolae are highly immobile structures and CAV-1 is a stable component of the membrane without showing any lateral diffusion (131). Caveolae and their associated lipid rafts mediate the internalisation of sphingolipids, sphingolipid binding toxins, GTP-anchored proteins and tyrosine kinase receptors as well as TGF-β receptors (101,132). Unlike clathrin, Cav-1 does not dissociate from the membrane during endocytosis, even after invagination and vesicles formation (131,133). Whilst the mechanisms of the CAV-1-dependent pathway have been less well characterized than their clathrin-dependent counterpart, TGF-β receptor endocytosis through caveolae has been demonstrated and linked to TGF-β signal attenuation through proteasome receptor degradation (101,134). TGF-β receptor internalisation through caveolae is associated with the binding of the inhibitory SMAD7 to TBRI. SMAD7 exerts its antagonistic function by competing with R-SMADs for receptor binding, thereby preventing SMAD2/3 phosphorylation (135). SMAD7 transcriptional expression is rapidly induced by TGF-β itself to ensure a controlled feedback loop of TGF-β signalling (136). SMAD7 binding recruits the E3 ubiquitin ligase SMURF2 which poly-ubiquitinates the receptor and induces proteasome degradation of the tagged receptor complex **(Fig.1.10.)** (101,137). Although CAV-1-dependent endocytosis was long believed not to be involved in constitutive membrane trafficking, it has been shown to be important in the regulation and of TGF-β signalling (101,131).

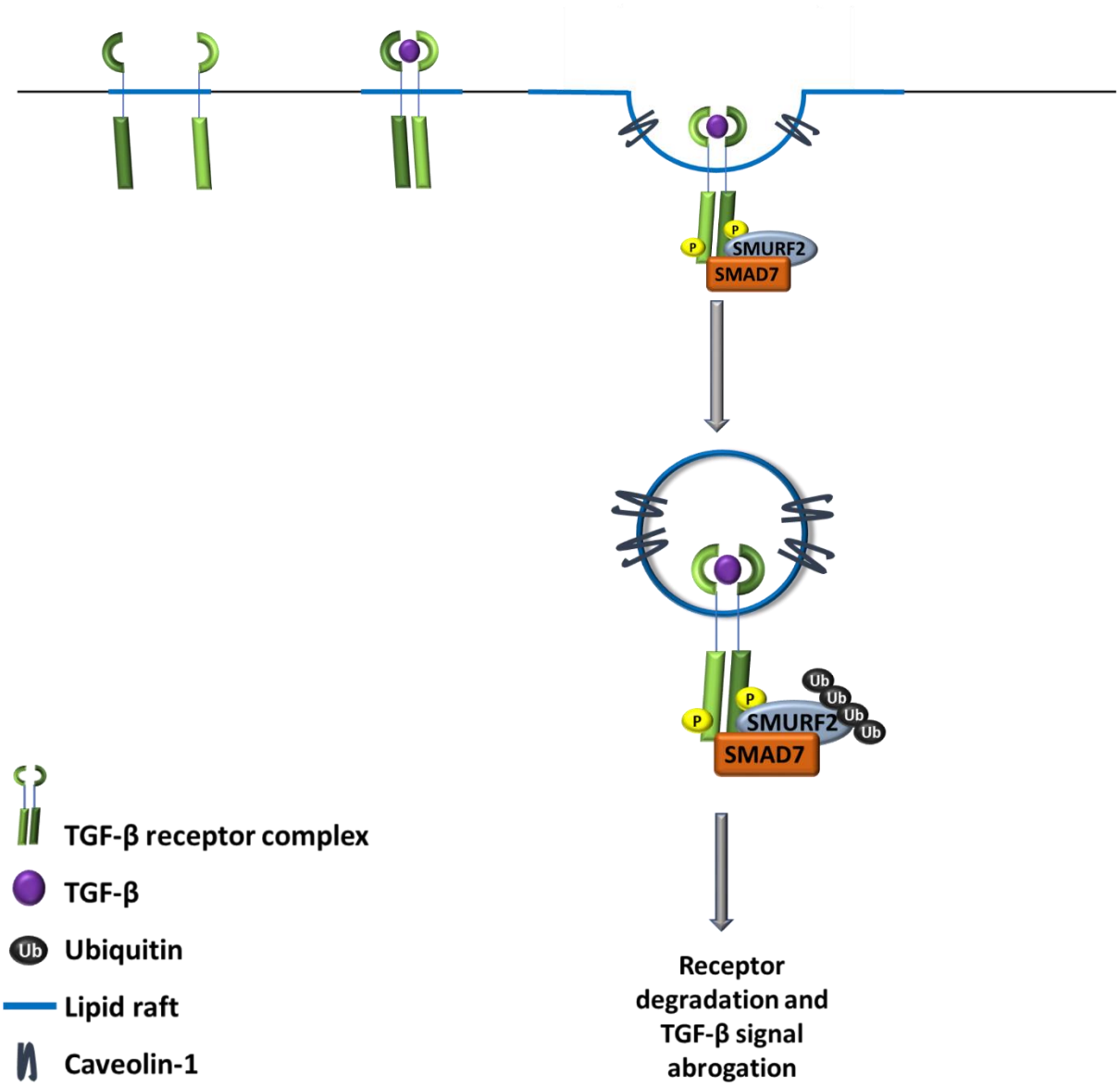

Fig.1.10. TGF-β receptor endocytosis through the caveolin-dependent pathway. *Receptor dimer and ligand complex formation associated with lipid rafts internalises through the CAV-1-dependent pathway. The inhibitory SMAD7 binds to the receptor complex and blocks R-SMAD recruitment, phosphorylation and signal propagation. The ubiquitin ligase SMURF2 poly-ubiquitinates the receptor complex and targets it for degradation.*

1.8.3. Induction of receptor compartmentalisation

The compartmentalisation of TGF-β receptors is an elegant way for the cell to control TGF-β signalling and might be an important mechanism to control receptor turnover as well as the duration, magnitude and nature of the signalling event (132). Many proteins such as TGF-β co-receptors help to orchestrate the process of organising the receptors into different compartments. The TGF-β co-receptor CD109 for example is a GPI-anchored protein that directly associates with CAV-1 and increases TGF-β binding to its receptors. CD109 facilitates the TGF-β-receptor complex internalisation via caveolae and is therefore a crucial inducer of TGF-β receptor degradation (134,138). Protein that interacts with kinase C (PIKC1) is a scaffold protein that directly interacts with the TBRI C-terminus to enhance the interaction between TBRI and CAV-1, thereby promoting TGF-β receptor complex endocytosis through caveolae (105). CD44 and its ligand hyaluronic acid (or hyaluronan; HA) have been shown to induce a shift from non-lipid raft residing receptors towards lipid rafts under the control of MAP kinases. HA binding to its receptor is the driving force behind lipid-raft associated TGF-β receptor turnover (139,140). Interleukin-6 (IL-6) on the other hand, which is a master regulator of inflammatory processes, has been shown to induce an enhanced transcriptional TGF-β response and increased compartmentalisation into non-lipid rafts. Even though the exact mechanisms of how IL-6 induces partitioning into non-lipid raft remains unclear, it is believed to depend on IL-6 binding to its cognate receptor (141). A disintegrin and metalloproteinase 12 (ADAM12), a glycoprotein with furthermore integrin binding activity, has also been identified as a TGF-β signal enhancer. It does so by accumulating TBRII at early endosomal membranes and stabilises the receptor by blocking SMAD7 binding sites (142). The vast majority of co-proteins induce a transition from non-raft domains towards raft compartments, thereby inhibiting TGF-β signalling. This is due to the fact that TGF-β receptors preferentially associate with non-lipid rafts unless a stimulus induces the transition towards lipid rafts (139). In this way, clathrin-dependent endosomal endocytosis may be seen as the default setting of TGF-β receptor endocytosis whilst the cell controls for TGF-β overstimulation through receptor transition into lipid-raft compartments.

1.8.4. Clathrin- and caveolin-dependent endocytic pathway merge into double positive multifunctional sorting centres

Even though the TGF-β receptor compartmentalization has been shown to play a crucial role in signal transduction, abrogation and receptor turnover (101), a strict implementation of pathway segregation is arduous. Especially, the role of SMAD7 challenges the compartmentalisation rule as SMAD7 has been shown to be involved in both pathways through its direct interaction with R-SMADs and inhibition of their complex formation with SMAD4 (143). At the DNA level, SMAD7 may compete with

the R-SMAD-SMAD4 complex for DNA binding, therefore controlling directly the R-SMAD driven transcriptional response (144). In addition, it has been shown that the clathrin-dependent and the CAV-1-dependent pathways can in fact merge to form vesicles containing cargo internalised through both pathways. Caveolar vesicles may follow a RAB5-dependent pathway which leads to their fusion with early endosomes within which the low pH allows the caveolar vesicle cargo to diffuse into the surrounding membrane whilst remaining trapped within the endosomal limiting membrane (133). Thus, unlike cyclic assembly and disassembly of coat proteins in vesicular transport, caveolar vesicles transiently and stably interact with endosomes to form subdomains and release cargo. Furthermore, TGF-β receptors have been shown to internalise into CAV-1/EEA1 double positive multi-component organelles which are positive for signalling mediators of both pathways and suggested to be multifunctional sorting centres **(Fig.1.11)** (145). Furthermore, TBRII was demonstrated to internalise into CAV-1- and EEA1-double positive vesicular structures corresponding to MVB, targeting the receptor for degradation (146). MVBs contain the Endosomal Sorting Complexes Required for Transport (ESCRT) which recognise and bind ubiquitinated cargo and subsequently initiate the transport of those proteins to late endosomes (146,147). These data imply that besides playing a central role in the promotion of TGF-β signalling, early endosomes may also be involved in signal abrogation and by decreasing receptor availability, CAV-1/EEA1 double positive endosomes could help to attenuate TGF-β signalling. The exact mechanisms by which endocytosis controls signal transduction and receptor turnover is under controversial debate, supporting the unquestionably complex nature of TGF-β receptor endocytosis and its downstream effect.

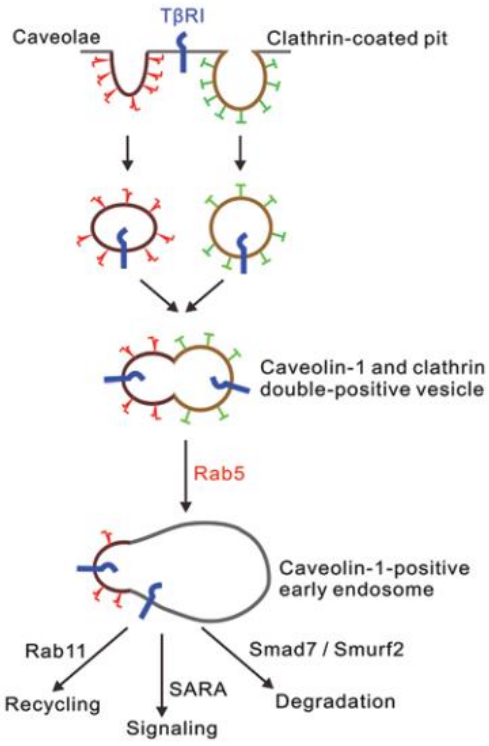

Fig.1.11. TGF-β receptors internalised through the clathrin- and caveolin-dependent pathway merge into multifunctional sorting vesicles. *During TGF-β endocytosis, EEA1- and CAV-1-positive vesicles can merge into double-positive structures containing multiple signalling mediators of both pathways. The multi-component organelles may be an important sorting mechanism for cargo internalised through the endosomal pathway and destined for degradation. Modified from* (145).

1.8.5. Non-canonical signalling

Apart from the canonical and SMAD-dependent signalling pathway, TGF-β exerts its pathophysiological effects through the so-called non-canonical, SMAD-independent pathway (148). Through this pathway, TBRI phosphorylates ShcA proteins which induces their association with Grb2 and Sos. The complex formation initiates Erk1/Erk2 MAP kinase signalling, which is an important regulator of cell differentiation, proliferation and apoptosis (149,150). This pathway in particular has been shown to be involved in the formation of aortic aneurysms in a mouse model of MFS, and might be an interesting target similar to canonical TGF-β signalling (151). Another apoptosis inducing pathway that TGF-β ligand binding activates, is the JNK and p38 MAP kinase pathway. The MAP kinase response is facilitated by the TRAF6 ubiquitin ligase which serves as a scaffolding protein to help mediate kinase assembly and activation (152). However, MAP kinase pathways and SMAD signalling pathways have also been demonstrated to interact with each other through the target of rapamycin complex 2 (mTORC2). The activation of mTORC2 controls the state of SMAD2/3 phosphorylation and targets them for ubiquitination and subsequent degradation (153,154). However, due to conflicting data on the two signalling pathways, it is unclear which pathway plays a more important role in TGF-β signalling (148).

1.8.6. TGF-β-independent SMAD activation

TGF-β induced SMAD signalling and its ability to bind DNA and control the transcription of numerous genes is a critical regulator of ECM integrity, cardiac and vascular remodelling as well as risk of aortic aneurysm. However, TGF-β-independent activators also induce SMAD signalling and its pathological consequences. In cardiovascular remodelling, Angiotensin II (Ang II) is a crucial regulator of fibrosis, inflammation and contributor to vascular damage which, like TGF-β, employs the SMAD-dependent signalling pathway (155). However, Ang II and TGF-β have been shown to not act completely independently of each other but to form a signalling network in cardiac remodelling events. Ang II directly induces the expression of TGF-β, therefore favouring further TGF-β signalling (156). On the other hand, TGF-β promotes Ang II induced cardiovascular events which are reverted by TGF-β inhibition (157). The suggested causal relationship between TGF-β and Ang II implies a functional link between the two signalling pathways and indicates that TGF-β acts downstream of Ang II. Interestingly, the molecular mechanism by which Ang II induces mRNA expression of TGF-β is by PKC induced p38 MAP kinase signalling under the control of NAD(P)H oxidase (158,159). As mentioned before, a reciprocal relationship between TGF-β and NAD(P)H oxidase exists. NAD(P)H oxidase has been shown to not only induce TGF-β signalling but also to be induced by TGF-β in a feed forward

manner which suggests a TGF-β amplification loop that sustains itself and, in addition, is fed into by interrelated signalling pathways (160,161).

Hypothesis and objectives

2. Hypothesis and objectives

Due to its role in vascular remodelling, TGF-β has been suggested as a molecular link between *FBN1* mutation and disease development. TGF-β has emerged as a promising therapeutic target assisting in the prediction of aneurysm formation and development. Yet, the involvement of TGF-β in aneurysm development remains a controversial topic based on increased SMAD2 signalling in patients affected with loss of function mutations of TGF-β receptors, alternative TGF-β signalling pathways and possible compensatory mechanisms (162). Nevertheless, previous work in our lab has identified a pathogenic TGF-β induced vascular smooth muscle cell phenotypic switch in MFS (127). Furthermore, the TGF-β receptor compartmentalisation has been associated with opposing signalling outcome. Clathrin-dependent TGF-β endocytosis induces signalling whereas Caveolin-1-dependent endocytosis abrogates the signal and leads to receptor degradation (101). Therefore, we hypothesised an imbalance of the TGF-β receptor compartmentalisation in a way that favours the R-SMAD-dependent signalling cascade in vascular smooth muscle cells (VSMC) from MFS patients. Additionally, we considered alterations of integrin-dependent TGF-β activation, which might facilitate the increased signalling at the extracellular level. Furthermore, due to the low correlation between genotype-phenotype in MFS, we were interested in genetic alterations specific to the formation of ascending aortic aneurysms. The significant heterogeneity of phenotypes that was found in MFS patients with mutations of the same type (8) suggests thus far unidentified factors, possibly induced by the *FBN1* mutation itself, that define the phenotype. Therefore, we hypothesised that *FBN1* mutations cause a myriad of transcriptional alterations, which, at least in part, could help to explain the aortic phenotype in MFS.

Therefore, the objectives of this work were:

1) To establish whether increased TGF-β signalling in VSMC is contributed to by alterations in the cellular endocytic compartmentalisation of TGF-β receptors and to evaluate whether key targets of the TGF-β trafficking and signalling cascade show alterations in VSMC from MFS patients.
2) To explore the differential expression of TGF-β-activating FBN1-binding integrins in human aortic tissue from MFS patients.
3) To determine alterations at the transcriptomic level and assess gene ontology enrichment in VSMC derived mRNA from MFS patients.

Material and Methods

3. Material and Methods

3.1. Material

3.1.1. Antibodies

Primary Antibody	Host species	Dilution ICC/IHC	Dilution WB	Manufacturer
SARA	Rabbit	**1:100**	**1:1,000**	Santa Cruz, CA, USA sc-9135
RhoGDI	Rabbit	-	**1:1,000**	Santa Cruz, CA, USA sc-359
RAB5	Rabbit	-	**1:1,000**	Santa Cruz, CA, USA sc-309
SMAD7	Mouse	**1:100**	**1:1,000**	Santa Cruz, CA, USA Sc-101152
TBRII	Goat	-	**1:500**	R&D Systems MN, USA AF-241-NA
SMAD2	Mouse	-	**1:1,000**	Cell Signaling MA, USA 3103S
pSMAD3 (Ser423/425)	Rabbit	**1:100**	-	Cell Signaling MA, USA 9520
EEA1	Mouse	**1:200**	**1:1,000**	BD Biosciences NJ, USA 610456
TrfR	Mouse	-	**1:3,000**	Invitrogen CA, USA 13-6800
CD29/ITGβ1	Rabbit	**1:100**	**-**	Absolute antibody Oxford, UK Ab0021-23.1
Active CD29/ITGβ1	Rat	**1:100**	**-**	BD Biosciences NJ, USA 550531

Secondary Antibody	Target species	Dilution ICC	Dilution WB	Manufacturer
HRP	Rabbit	**-**	**1:3,000**	Promega WI, USA W401B
HRP	Mouse	**-**	**1:3,000**	Promega WI, USA W402B
HRP	Goat	**-**	**1:2,000**	Promega WI, USA V805A
Alexa488	Rabbit	**1:250**	**-**	Invitrogen CA, USA A-11070

Secondary Antibody	Target species	Dilution ICC	Dilution WB	Manufacturer
Alexa647	Rabbit	**1:250**	-	Invitrogen CA, USA A21245
Cy3	Mouse	**1:250**	-	Jackson Research PA, USA 115.167.003
Cy3	Rat	**1:250**	-	Jackson Research PA, USA 712.165.150

3.1.2. Reagents and kits

Reagent	Description	Concentration	Manufacturer
Recombinant Human-TGF- β1	Recombinant human TGF-β1 expressed in CHO cells	2ng/µl	Merck Millipore Darmstadt, Germany
Human TGF-β 1 Biotinylated Fluorokine Flow Cytometry Kit	Biotinylated rhTGF- β1 and fluorescein-conjugated avidin	Following manufactures instructions	R&D Systems MN, USA
Dynabeads® Protein A	Magnetic beads for immunoprecipitation	25µl	Invitrogen CA, USA
***DC*™ protein assay**	Detergent compatible colorimetric protein quantification	Following manufactures instructions	Bio-Rad CA, USA
Western Blotting Luminol Agent	ECL light emitting system for protein detection	-	Santa Cruz CA, USA
RNeasy Mini Kit	Purification of total RNA	-	Qiagen Hilden, Germany
TRIzol® Reagent	Total RNA extraction reagent	1 ml per 2x2 mm aortic tissue	Thermo Fisher MA, USA
TaqMan® MicroRNA Reverse Transcription Kit	Quantitative conversion of miRNA to cDNA	Following manufactures instructions	Applied Biosystem CA, USA
High Capacity cDNA Reverse Transcription kit	Quantitative conversion of RNA to cDNA	Following manufactures instructions	Applied Biosystem CA, USA

Reagent	Description	Concentration	Manufacturer
SYBR®Green JumpStart™ *Taq* ReadyMix™	Master mix for quantitative gene expression	3.125µl/reaction	Sigma-Aldrich, MO, USA
TaqMan® MicroRNA assay has-miR-29b	Assay for the detection and quantification of non-coding RNAs	Following manufactures instructions	Applied Biosystem CA, USA
TaqMan® Universal Master Mix II, with UNG	Probe-based master mix for quantitative gene expression	Following manufactures instructions	Applied Biosystem CA, USA

3.2. Methods

3.2.1. Tissue collection and ethics statements

Normal ascending aortic tissue was collected from heart donors through the organ donation organization at Hospital Clínic I Provincial (Barcelona, Spain). The age and gender of heart donors was unknown, due to Spanish legal protection of organ donor privacy. Ascending aortic samples were collected from MFS patients undergoing reparatory aortic aneurysm surgery. All patients fulfilled diagnostic criteria according to Ghent nosology (163), however, no genetic information on FBN1 mutations was available. The aortic samples were stored in Dulbecco's Modified Eagle's Medium for transport. Human tissues were collected with the required approval from the Institutional Clinical Review Board of the clinical centres (Hospital Clínic I Provincial and the Marfan Unit at the Hospital 12 de Octubre in Madrid) and the patient's written consent conformed to the ethical guidelines of the 1975 Declaration of Helsinki.

3.2.2. Human vascular smooth muscle cell culture

Human VSMC were isolated from healthy ascending aortae, the non-dilated and the dilated region of Marfan patient ascending aortae. The dilated region was identified as the zone of aortic aneurysm formation, whereas the non-dilated region was the non-aneurysmal, adjacent tissue zone. Aortic tissue was cleaned and the tunica media was separated from the innermost intima and the external adventitia layers. The tunica media was then cut into 1-2 mm cubes, which were transferred to 100 mm culture plates. After their adhesion at 37°C for 45 min in a cell culture incubator, the tissue cubes were gently covered with 4 ml of 231 culture medium, supplemented with 25 ml of Smooth Muscle Growth Supplement (SMGS) (both by Gibco, CA, USA), 100 mg/mL streptomycin and 100 U/mL

penicillin. Cell cultures were maintained at 37°C in a humidified 5% CO_2 atmosphere. Explants were left undisturbed for 4 days to prevent detachment. VSMC migrated from the explant within 1-2 weeks. After removing the explants from the flask surface, cells were trypsinized and used as routinely subcultured P1 stage cells. Primary cell cultures have limited expansion and were used for experiments between passages P1 and P7 and half the medium was replaced every 4 days. The validation of cultured cells as VSMC was carried out as indicated previously (127).

3.2.3. Western Blotting

For Western Blotting experiments, immunoprecipitates or 20 µg of subcellular fractions were analysed on SDS-PAGE and transferred to nitrocellulose membranes for 90 min at 100 V. Membranes were blocked in 5% BSA/Tris Buffered Saline (TBS) (20 mM Tris-HCl, pH 7.5, 150 mM NaCl) for 1 hr. Antibodies to TBRII, SMAD2, SMAD7, SARA, RhoGDI and transferrin receptor were diluted in 1% BSA/TBS containing 0.02% sodium azide and incubated overnight at 4°C. Membranes were rinsed 3 times and incubated with secondary peroxidase-conjugated IgG in 1% BSA/TBS for 1 h. Membranes were rinsed again and developed at room temperature with Western Blotting Luminol Reagent using Hyperfilm (Amersham Pharmacia Biotech, Uppsala, Sweden). Band intensities were measured by densitometry scanning using ImageJ software (National Institute of Health, Bethesda, MD).

3.2.4. Membrane and cytosol fractionation of VSMC

VSMC were grown on 100 mm cell culture plates until confluent. Cells were rinsed twice in PBS and scraped into lysis buffer (250 mM saccharose, 10 mM HEPES, 1 mM EDTA, pH 7.5) supplemented with protease inhibitors. Extracts were mechanically lysed with 30 strokes of a 30G syringe, and subjected to 90 min of ultracentrifugation at 45,000 rpm using an S140-AT rotor (Thermo Fisher Scientific, Waltham, USA) at 4°C. The resulting supernatant was the cytosolic fraction. The membrane fraction containing pellet was resuspended in 100 µl radioimmunoprecipitation assay buffer (10 mM Tris-HCl, pH 7.5, 1 mM EDTA, 0.5 mM EGTA, 1% Triton X-100, 0.1% sodium deoxycholate, 0.1% SDS 140 mM NaCl) supplemented with protease inhibitors. Twenty µg of each subcellular fraction were analysed by 12% (v/v) SDS-PAGE and blotted as described above. Cytosol and membrane protein bands were quantified and relativized against their respective fraction markers RhoGDI and transferrin receptor (TrfR). Membrane enrichment was calculated by normalization with the corresponding cytosolic fraction, and membrane enrichment in Marfan patients was normalized against controls. Statistical analysis was performed by one-sample t-test or Wilcoxon signed-rank test. The immunoblots shown are representative of at least four independent experiments.

3.2.5. Immunoprecipitation of TBRII

Membrane fractions were obtained as described above and protein concentrations were adjusted using immunoprecipitation buffer (10 mM Tris-HCl, pH 7.5, 50 mM NaCl, 1% Triton X-100, 5 mM EDTA), supplemented with protease inhibitors. Equal amounts of membrane fractions (100 µg) were incubated overnight at 4°C with 30 µg of goat anti-TBRII or goat IgG. The following day, lysate and antibody were precipitated with 25 µl of magnetic beads conjugated with protein A for 1 h at 4°C. The beads were rinsed 4 times with immunoprecipitation buffer and immunoprecipitates were eluted by adding 20 µl of loading buffer 5X containing 10% β-mercaptoethanol. Samples were analysed by 7.5-9% (v/v) SDS-PAGE and blotted as described above. Western blot bands were quantified relative to the precipitated TRBII, and Marfan relative band intensities were normalized against controls. Statistical analysis was performed by one-sample t-test or Wilcoxon signed-rank test. The immunoblots shown are representative of at least three independent experiments.

3.2.6. Immunofluorescence in VSMC

VSMC were grown on coverslips to 70-80% confluency and starved in serum-free 231 culture medium for 18 h. Signalling was induced by adding 2 ng/µl of recombinant human TGF-β to the cell medium and allowing its internalisation for 30 min at 37°C. Cells were rinsed with PBS, fixed in 4% paraformaldehyde in PBS for 15 min at room temperature, rinsed three times with PBS and incubated for 20 min with 50 mM ammonium chloride/PBS pH 7.4. Cells were permeabilised for 10 min with 0.1% saponin, 1% BSA in PBS. Antibody combinations of SARA/EEA1 and SMAD7/CAV-1 were incubated for 1 h at room temperature, followed by 45 min of secondary antibody incubation (Alexa Fluor 488-conjugated goat anti-rabbit, Cy3-conjugated goat anti-mouse IgG). Coverslips were mounted onto microscope slides using DAPI-Fluoromount water soluble mounting agent. Images were taken using a Leica TSC SL confocal microscope with a 63x oil objective, and analysed using CellProfiler automated image analysis software (Carpenter Lab, Broad Institute of Harvard and MIT). Statistical analysis was performed using two-tailed paired t-tests. The images shown are representative of four independent experiments.

For pSMAD3 nuclear translocation experiments, VSMC were grown on coverslips to 70-80% confluency and starved in serum-free 231 culture medium for 18 h. VSMCs were either washed and fixed in 4% paraformaldehyde in PBS for 15 min or signalling was induced by incubating cells for 30 min with recombinant TGF-β or b-TGF-β at 37°C. Immunostaining of pSMAD3 followed by Alexa488 was performed as indicated above. Images were taken using an Olympus BX60 fluorescence microscope with a 60x oil objective, and analysed using CellProfiler image analysis software. The

translocation index (TI) was defined as the ratio of the pSMAD3 mean fluorescence intensity in the nucleus in comparison with the pSMAD3 mean fluorescence intensity in the cytosol, relativised by the area of each separate cell. Statistical analysis was performed using repeated measures ANOVA, followed by uncorrected Fisher´s LSD multiple comparison. The images shown are representative of three independent experiments.

3.2.7. Immunofluorescence in human aortic tissue

Aortic explants from the dilated zone of MFS patients and control donors were embedded in cryomolds using Tissue Tek® O.C.T. Compound (Sakura, Leiden, NL) and immediately frozen and stored at -80°C. Aortic explants were cryostat sectioned at 5µm and fixed on microscope slides with a series of 5 min acetone/ acetone and choloroform/acetone incubations at -20°. Tissue sections were left O/N at room temperature, washed with PBS and blocked with 1% BSA/PBS for 1 h at room temperature. Samples were rinsed 3 times with PBS and incubated with the primary antibody combination specific to ITGβ1 and active ITGβ1 for 1 h at room temperature. After 3 washes with PBS, samples were incubated with the secondary antibody combination Cy3/Alex488 and stained with DAPI. Cover slides were mounted using Mowiol and left to dry in the dark overnight (O/N) at room temperature. Images were taken using a Leica TSC SP5 confocal microscope at 40x objective and analysed using a custom-made ImageJ plugin. The percentage of active ITGβ1 relative to total ITGβ1 was calculated. Statistical analysis was performed using unpaired t-test. The images shown are representative of six independent experiments.

3.2.8. Biotinylated-TGF-β endocytic transport

VSMC were grown on coverslips to 70-80% confluency and starved in serum-free 231 culture medium for 18 h. Internalisation experiments were performed as follows: starved cells were incubated with b-TGF-β for 60 min at 4°C, followed by incubation of avidin-fluorescein for 2 h at 4°C, according to the manufacturer’s instructions. Cells were either rinsed with cold PBS (0 min) and fixed in 4% paraformaldehyde in PBS for 15 min, or the b-TGF-β/avidin-fluorescein complex was allowed to internalise for 30 minutes at 37°C and cells were subsequently fixed. Immunostainings of primary antibodies EEA1, SARA, CAV-1 and secondary Cy3 and Alexa 647 conjugates were performed as indicated above. Coverslips were mounted onto microscope slides using DAPI-Fluoromount water soluble mounting agent. Images were taken using a Leica TSC SP5 confocal microscope with a 63x oil objective, and analysed using CellProfiler image analysis software. Large EEA1-positive ring-like structures were defined by the Euler number where $e \leq 0.5$ was considered a ring-like structure. The

ratio of a colocalizing large ring-like structure relative to a non-colocalizing ring-like structure, relative to the entire EEA1 positive pool was calculated as follows:

$$Ratio\ of\ colocalization = \left(\frac{Colocalization\ X}{Total\ large\ structures}\right) * \left(\frac{Total\ large\ structures}{Total\ EEA1}\right)$$

Statistical analysis was performed using repeated measures ANOVA followed by uncorrected Fisher´s LSD multiple comparison. The images shown are representative of at least four independent experiments.

3.2.9. Gene expression in VSCM

RNeasy Mini Kit was used for total RNA isolation. Reverse transcription (RT) was carried out using High Capacity Reverse Transcriptase kit. One µg of total RNA from each sample was used for cDNA synthesis. Expression levels were determined in triplicate in a C1000 Thermal Cycler CFX384 Real-Time System (BioRad, Hercules, CA, USA) using SYBR® Green JumpStart™ Taq ReadyMix™ (Sigma-Aldrich, St. Louis, MO) and primers as stated in **Table 2.1**. The expression of RPS28 was used as a house-keeping control. Transcriptional expression of Marfan patients was normalized to controls. Statistical analysis was performed using one-sample t-test or Wilcoxon signed-rank test.

3.2.10. Gene expression in human aortic tissue

Aortic explants were homogenized using a bullet blender, ⌀ 0.9-2 and 3 mm stainless steel beads (Next Advance, NY, USA) and 1ml TRIzol®. Samples were incubated on ice for 30 min, beads were removed and RNA was precipitated as per manufactures instructions. RNA was resuspended in 20 µl RNase free water and quantified by nanodrop. One µg of total RNA from each sample was used for complementary DNA synthesis. Expression levels were determined as stated above. The expression of RPS28 was used as a house-keeping control. Transcriptional expression of Marfan patients was normalized to controls. Statistical analysis was performed using one-sample t-test or Wilcoxon signed-rank test.

3.2.11. miR-29b expression in human aortic tissue

Aortic explants were homogenized as stated above and total RNA was precipitated using TRIzol®. Micro RNA was reverse transcribed using TaqMan® MicroRNA Reverse Transcription Kit. Expression levels were determined in triplicate in a C1000 Thermal Cycler CFX384 Real-Time System (BioRad, Hercules, CA, USA) using TaqMan® MicroRNA assay has-miR-29b and TaqMan® Universal Master Mix II, with UNG. The expression of GAPDH was used as a house-keeping control. Transcriptional

expression of Marfan patients was normalized to controls. Statistical analysis was performed using one-sample t-test.

Table 2.1. Real-time PCR primer sets used for gene expression experiments

	Primer sequences (5´-3´)	
Gene	**Sense**	**Antisense**
CLTC	CTTTCCAAAGAAGGCAGTGG	TCAAGAACACCACATCATGC
CAV1	GCGACCCTAAACACCTCAAC	GTGAAGCTGGCCTTCCAAAT
AP2B1	CAGATGGGAGCAGTGGATCT	AGGTGAAGGAGCAAAGGTTG
SMURF2	TCCTCGGCTGTCTGCTAACT	TCAGGCATTCTGTGTCATCA
SARA	CTGTGTCACACGACCCAGTC	TTCCAACAGGACTTCCAACC
RAB5A	CAAGGCCGACCTAGCAAATA	TGTTTTAGCGGATGTCTCCA
RAB5C	CCAACATCGTCATTGCACTC	AGCAAACTGTTGTCGTCTGC
ITGB1	TCCCTGAAAGTCCCAAGTGT	TGTGCTGCATTCACAATGTC
ITGB5	GGGGGCTTTGATGCAGTA	ATGTGGGGCACATCATCTGT
ITGA5	CAGGCCAGTTCCATCTATGA	GGCACACCAGCAACAAAGT
RPS28	GCTCGTGTCGTCCATGAAT	CCGTGTGCAGCCTATCAAG

3.2.12. Stranded mRNA library preparation and sequencing

VSMC from 4 male Control donors, and 5 male MFS patients were grown to confluency. Of MFS patients, VSMC from the dilated as well as non-dilated zone were used. Confluent VSMC were collected in sterile PBS and RNA was extracted using RNeasy® Mini Kit (Quiagen, Hilden, Germany). Total RNA was assayed for quantity and quality using Qubit® RNA HS Assay (Life Technologies) and RNA 6000 Nano Assay on a Bioanalyzer 2100. The RNASeq libraries were prepared from total RNA using the TruSeq®Stranded mRNA LT Sample Prep Kit. Briefly, 500ng of total RNA was used as the input material and was enriched for the mRNA fraction using oligo-dT magnetic beads. The mRNA was fragmented in the presence of divalent metal cations and at high temperature (resulting RNA fragment size was 80-250nt, with the major peak at 130nt). The second strand cDNA synthesis was performed

in the presence of dUTP instead of dTTP, facilitating strand specificity. The blunt-ended double stranded cDNA was 3´adenylated and Illumina indexed adapters were ligated. The ligation product was enriched with 15 PCR cycles and the final library was validated on an Agilent 2100 Bioanalyzer with the DNA 7500 assay. The libraries were sequenced on HiSeq2000 (Illumina, Inc) in paired-end mode with a read length of 2x76bp using TruSeq SBS Kit v4. For each sample over 30 million paired-end reads were generated in a fraction of a sequencing v4 flow cell lane, following the manufacturer's protocol. Image analysis, base calling and quality scoring of the run were processed using the manufacturer's software Real Time Analysis (RTA 1.18.66.3) and followed by generation of FASTQ sequence files by CASAVA.

3.2.13. Bioinformatic analysis

Raw sequences (FASTQ format) were processed through the Rsubread/align (164) instruction and aligned to the GRCh38 Genome Reference Consortium Human Reference 38 (hg38) human genome assembly to obtain binary summarized files (Bam). Bam files of RNA readings were processed using the Rsubread package in the R environment and summarized to features of the hg38 version of the human genome with the function "featureCounts" (165). Summarized readings by gene were then normalized using voom normalization (166) to fit the count matrix into linear modelling with the package limma (167) in which we divided the samples into six groups: MFS 3´UTR (M031and M054), MFS no mutation (M035 and M052) and MFS cysteine substitution (M054 and M057), further subdivided into dilated and non-dilated region origin, and extracted the contrasts to the control group. Using the group matrix, a linear fit model algorithm was used to obtain differentially expressed genes (DEGs) that complied with $p < 0.05$ and fold change >2. DEGs. Normalized whole read counts were used to cluster samples with package hcluster using standard hierarchical cluster with average linkage. Heatmap visualization and clustering of DEGs was done with R package "hcluster". Genecodis (168) tools were used to obtain Gene Ontology and Kyoto Encyclopedia of Genes and Genomes (KEGG) pathway terms enrichment using the adjusted p value <0.05 after a hypergeometric test. Finally, Signaling Pathway Impact Analysis (SPIA) was performed in R using the "spia" package (169) with the normalized fold change values for the comparisons obtained earlier.

Results

4. Results

4.1. TGF-β endocytic pathway compartmentalisation in MFS

TGF-β receptor internalization takes place through both clathrin-coated pits and lipid raft-associated caveolin-1 (CAV-1)-positive vesicles which have opposite effects on TGF-β signal transduction (101). The ligand binds the constitutively active TGF-β receptor II (TBRII) which leads to TGF-β receptor I (TBRI; also named ALK5) recruitment and phosphorylation (100). Receptor/ligand complexes internalized through clathrin-coated pits are targeted to early endosome associated protein-1 (EEA1) positive early endosomes, and initiate SMAD2/3 phosphorylation and signalling. In contrast to clathrin-dependent endocytosis, receptor internalization through caveolae destines receptors for proteasome degradation by binding of SMAD7 and E3 ubiquitin ligase poly-ubiquitination, which terminates the signalling cascade (101,143). The role of TGF-β in MFS has thus far mostly been investigated in murine models. To date, the importance of TGF-β in MFS is supported by the beneficial effects of TGF-β-receptor blockers and neutralizing TGF-β antibodies on the progress of aortic aneurysms in murine models (127,170) as well as increased pSMAD2 signalling (171). However, increased signalling has been largely attributed to alterations at the epigenetic level (171). Whether TGF-β subcellular compartmentalization and signal activating mechanisms contribute to the increased profibrotic signalling in MFS remains to be elucidated. Here we examine the significance of TGF-β signal regulation by its endocytic compartmentalization at endogenous levels in primary human VSMC from aneurysmal aortic tissue of Marfan patients.

4.1.1. TGF-β signalling mediators SARA and SMAD2 are enriched at cell membrane fractions and show increased receptor interaction in human Marfan VSMC

As described before, the clathrin- and CAV-1-dependent internalization pathways are each associated with the signalling mediators SARA/SMAD2 and SMAD7 respectively. To study the contribution of these TGF-β signalling mediators at basal levels, we analysed their membrane to cytosol ratio in VSMCs cultured from aneurysmal MFS patient aortae and Control donors. If not further specified, VSMCs used in the following experiments originated from the dilated region of patient aortae. SMAD2, SARA and SMAD7 were analysed by Western Blot in VSMC membrane and cytosol fractions. Cytosol and membrane protein bands were quantified and relativized against their respective fraction markers (RhoGDI/cytosol and the Transferrin receptor/membrane). Membrane enrichment was calculated by normalization against the corresponding cytosolic fraction. Results showed an increase of SMAD2 and its anchoring factor SARA at cell membranes (**Fig. 4.1.A**). Smad7 levels remained unaltered (**Fig. 4.1.B**),

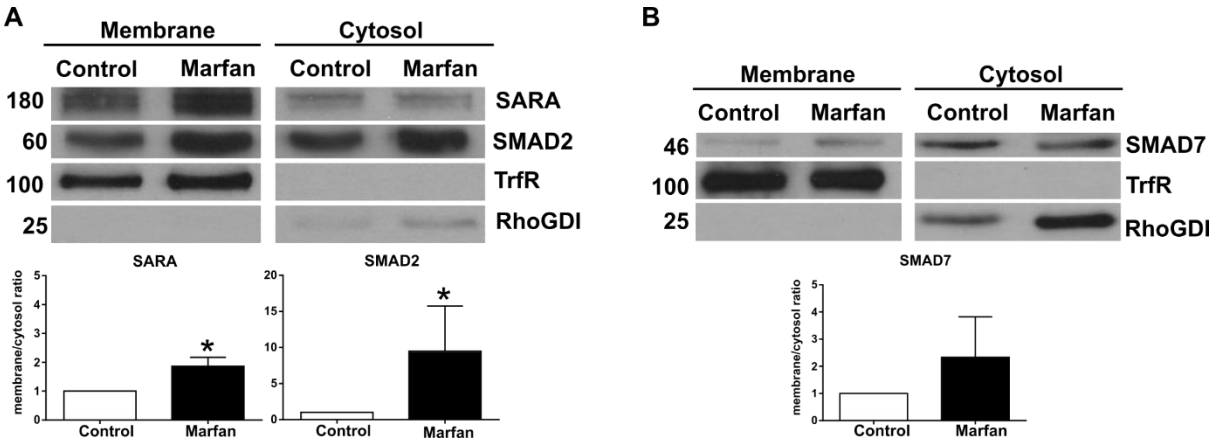

Figure 4.1. SARA and SMAD2 are enriched in membrane fractions of Marfan VSMC. *Membrane enrichment analysis of* ***(A)*** *SARA (N=7, *p<0.05) and SMAD2 (N=7, *p<0.05) and* ***(B)*** *Smad7 (N=4, p=0.4392). VSMC from Marfan and controls were lysed, membrane and cytosol were fractionated and analysed by Western blot. Cytosol and membrane protein bands were quantified and relativized against their respective fraction markers RhoGDI and transferrin receptor (TrfR). Membrane enrichment was calculated by normalization with the corresponding cytosolic fraction, and membrane enrichment in Marfan patients was normalized against controls. Results are represented as mean ± SEM.*

Next, we assessed the interaction of the TGF-β receptor II (TBRII) with downstream signalling molecules associated with the clathrin- and CAV-1-dependent internalization pathway at basal levels. As indicated above, cultured VSMC from Marfan and control samples were lysed and the respective membrane fractions were isolated. TBRII was immunoprecipitated from membrane fractions and the receptor interaction with SARA, SMAD2, and SMAD7 was analysed by Western blot. Interaction of SMAD2 and SARA with endogenous TBRII was significantly higher in Marfan VSMC membranes than in control cells **(Fig. 4.2.A)**. No alterations were observed for SMAD7 **(Fig. 4.2.B)**.

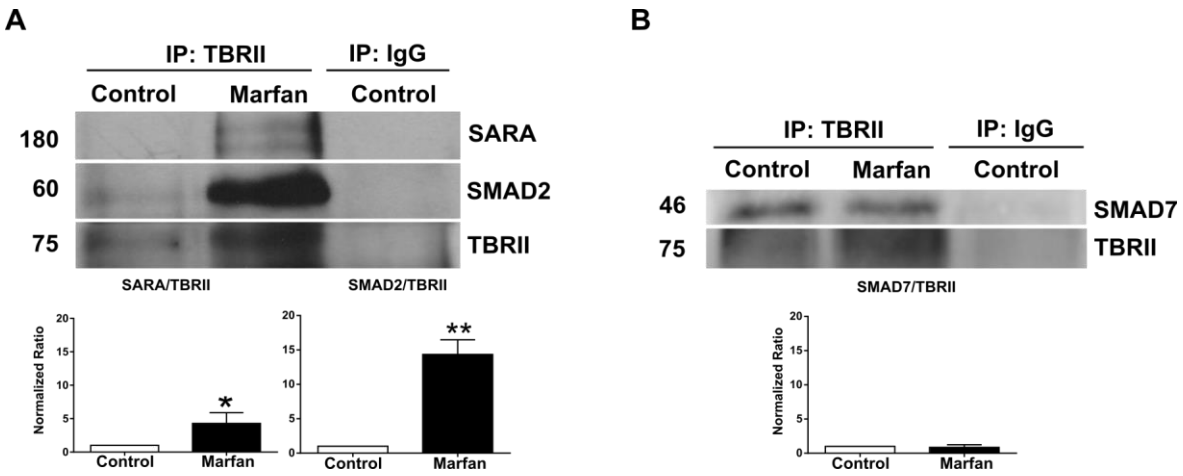

Figure 4.2. SARA and SMAD2 show increased interaction with TGF-β receptor II in Marfan VSMC. *VSMC from Marfan and controls were lysed and membrane and cytosol fractions were obtained. TBRII was immunoprecipitated from the membrane fraction only. Immunoprecipitates were subjected to Western blotting, and receptor interaction of* ***(A)*** *SARA (N=7, *p<0.05) and SMAD2 (N=4, **p<0.01), and* ***(B)*** *SMAD7 (N=3, p=0.7514) was analysed by quantifying protein bands relative to the precipitated TRBII. Marfan relative band intensities were normalized against controls. Results are represented as mean ± SEM.*

4.1.2. TGF-β induces increased SARA recruitment to early endosomes in MFS VSMC

To further address the pathway association of TGF-β signalling mediators in aortic VSCM in MFS, colocalization experiments of SARA/EEA1 and SMAD7/CAV-1 were performed. SARA is a crucial player in the control of TGF-β receptor complex signal promotion through its phosphatidylinositol 3-phosphate (Ptdlns(3)P) binding FYVE domain that directly recruits SMAD2 to the receptor complex at early endosomal membranes (115,116,172). Cultured Marfan and control VSMC were starved overnight and treated with recombinant TGF-β for 30 min. Cells were co-stained with either anti-SARA/anti-EEA1 or anti-SMAD7/anti-CAV-1 antibodies. After TGF-β internalization, Marfan cells showed increased colocalization of SARA with EEA1 **(Fig. 4.3.A)**, indicating that more SARA is recruited to early endosomes in MFS. In accordance with our previous experiments, the CAV-1-associated signalling mediator SMAD7 colocalization with CAV-1 remained unaltered **(Fig. 4.3.B)**.

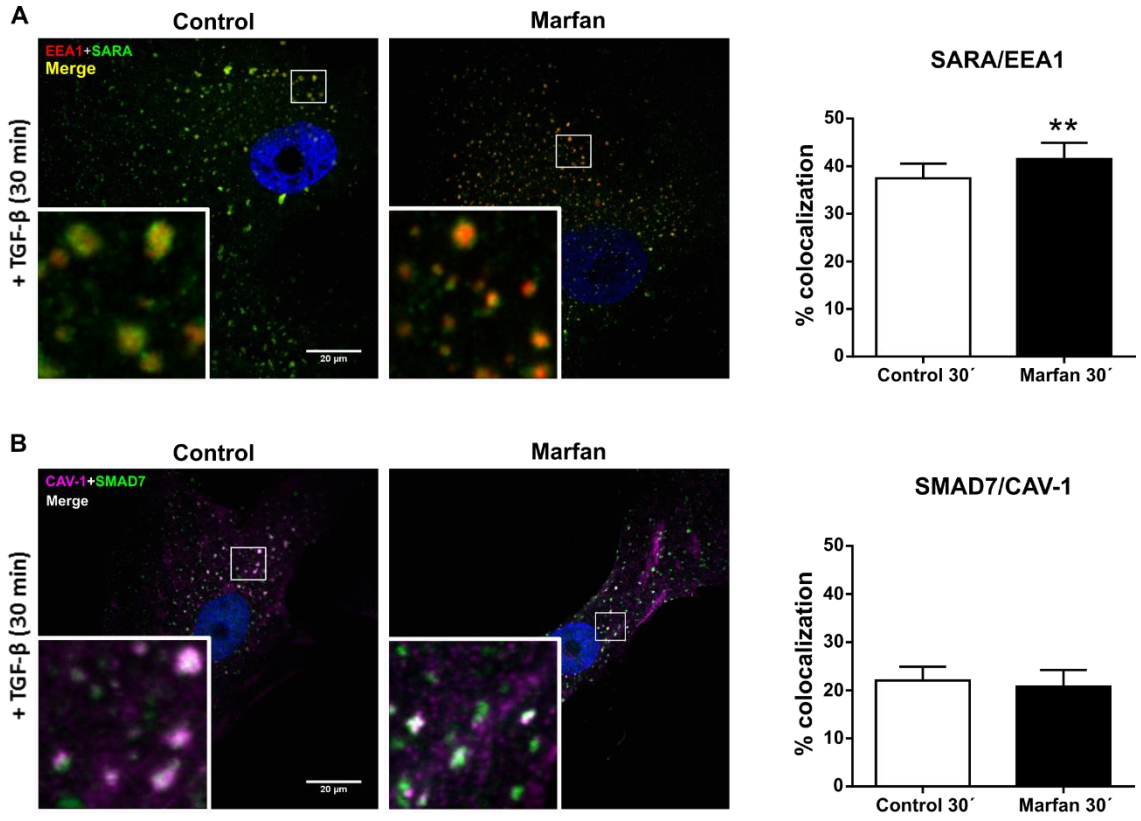

Figure 4.3. SARA localizes more to early endosomes in TGF-β stimulated Marfan VSMC. *Cultured VSMC were starved and treated with recombinant TGF-β for 30 min and subsequently fixed and immunolabeled. Colocalization of* ***(A)*** *SARA with EEA1 (N=4, **p<0.01) and* ***(B)*** *SMAD7 with CAV-1 (N=4, p=0.5179) was analysed. The percentage of colocalization was calculated relative to non-colocalizing SARA and SMAD7, respectively. Results are represented as mean ± SEM. Bar, 20 µm.*

4.1.3. Characterization of signal induction by b-TGF-β

To examine the clathrin- and CAV-1-dependent endocytic pathways, a biotinylated TGF-β (b-TGF-β) was used. Biotinylated TGF-β was added to its receptor complex in starved VSMC and allowed to internalise. The biotinylated TGF-β was subsequently visualized with FITC-conjugated streptavidin. Its bioactivity was validated by assessing its ability to induce the nuclear translocation of pSMAD3. For comparative purposes, non-biotinylated TGF-β was used in parallel. Results showed that b-TGF-β induced pSMAD3 nuclear translocation at equal levels as recombinant TGF-β, and both induced significantly higher translocation than seen in untreated cells **(Fig. 4.4.)**, validating b-TGF-β as a representative molecular tool to explore the internalization routes of TGF-β at endogenous levels in VSMC.

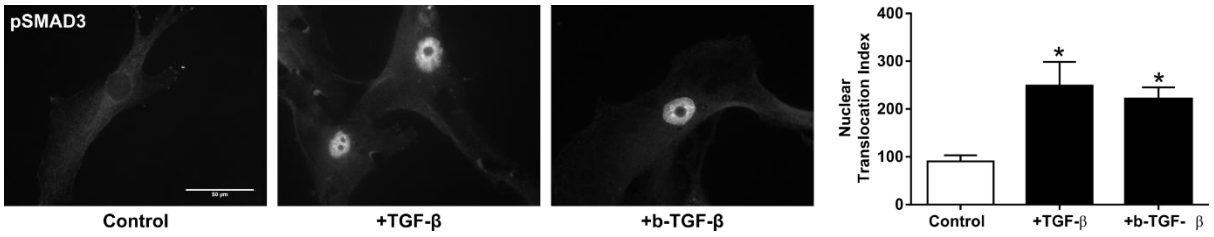

Figure 4.4. Biotin-tagged TGF-β is bioactive. *VSMC were starved and either fixed or TGF-β and b-TGF-β were allowed to internalize for 30 min. Nuclear translocation of pSMAD3 was analysed (N=3, RM ANOVA *p<0.05, LSD Control vs. +TGF-β *p<0.05, Control vs. +b-TGF-β *p<0.05). Results are represented as mean ± SEM. Bar, 50 µm.*

4.1.4. TGF-β internalizes equally through the clathrin- and CAV-1-dependent endocytic pathways in Marfan VSMC compared to control VSMC

To examine whether the increased clathrin pathway-associated TGF-β signalling in MFS is due to an altered endocytic pathway compartmentalization, VSMC were treated with b-TGF-β and immunostainings were performed using specific antibodies to EEA1 as a marker of the clathrin-dependent pathway, and to CAV-1 to reveal the lipid raft/caveolin-1-dependent route. Cells were treated with b-TGF-β, either immediately fixed or allowed to internalize for 30 min prior to fixation, and co-stained with either anti-EEA1 or anti-CAV-1 antibodies. The percentage of colocalizing b-TGF-β with the respective endocytic markers for either pathway was evaluated. As expected, 30 min after internalization of b-TGF-β, both control and Marfan VSMC showed a significant increase in colocalization of b-TGF-β in EEA1- or CAV-1-positive endomembrane structures **(Fig. 4.5.A and 4.5.B, respectively)**. However, no differences were found between control and Marfan cells for either endocytic pathway.

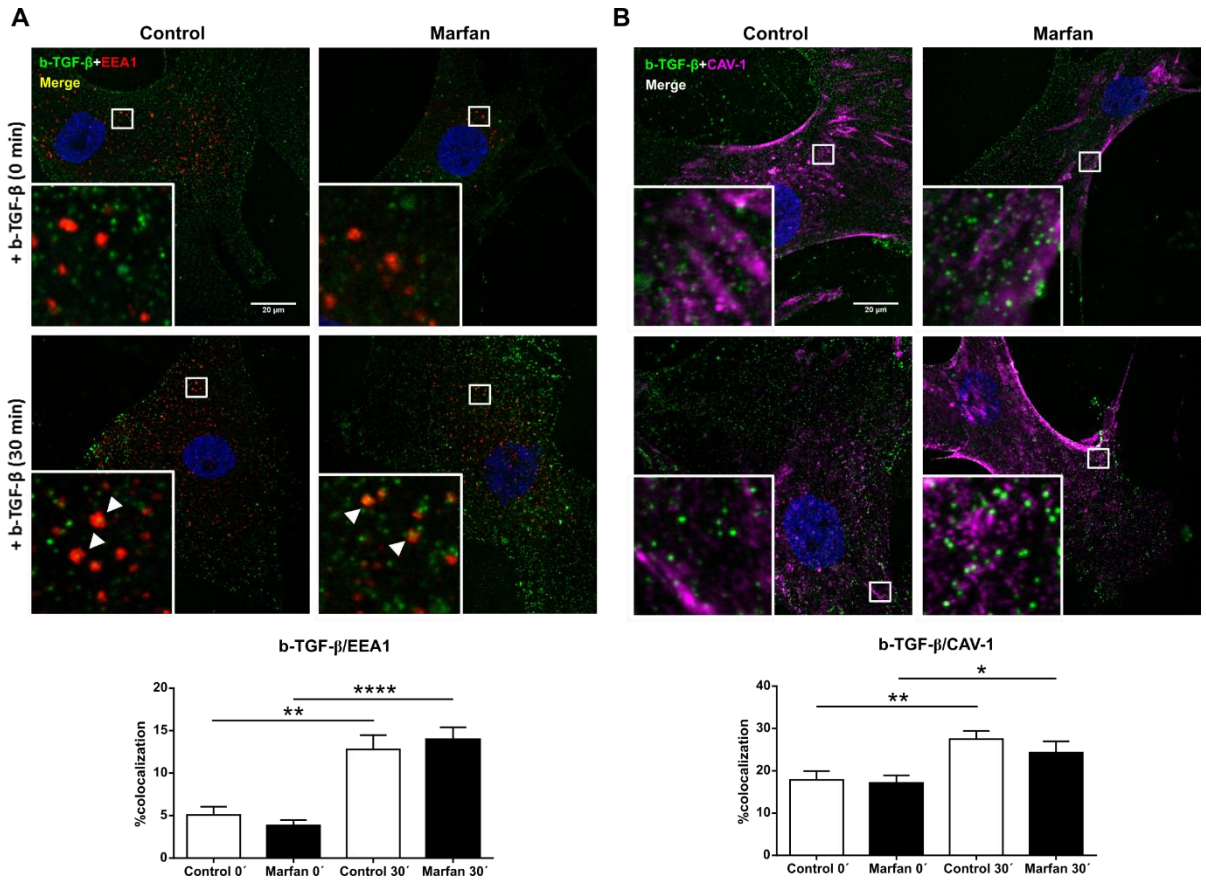

Figure 4.5. The clathrin- and CAV-1-dependent endocytic pathways are unaltered in VSMC from MFS patients. *VSMC were starved and incubated with b-TGF-β followed by fluorescein-conjugated avidin. The complex was internalized for 0 or 30 min. Colocalization of b-TGF-β with* ***(A)*** *EEA1 (N=9, RM ANOVA ****p<0.0001, LSD Control 0 min vs. Marfan 0 min p=0.1949; Control 30 min vs. Marfan 30 min p=0.5157) or* ***(B)*** *CAV-1 (N=5, RM ANOVA **p<0.01, LSD Control 0 min vs. Marfan 0 min p= 0.5279; Control 30 min vs. Marfan 30 min p=0.1795) was analysed. The percentage of colocalization was calculated relative to non-colocalizing b-TGF-β. Results are represented as mean ± SEM. White arrows in (A) show colocalization of b-TGF-β (green) with EEA1 (red) in endocytic vesicular structures. Bar, 20 µm.*

Furthermore, we examined key molecules involved in the two internalization pathways by quantitative RT-PCR. For the clathrin-dependent pathway we assessed transcriptional expression levels of clathrin (CLTC) and the catalytic subunit of its adaptor protein (AP2B1). CAV-1-pathway associated genes were caveolin-1 (CAV-1) and the E3 ubiquitin protein ligase which tags the receptor for degradation (SMURF2). In line with the previous results, we did not observe any changes at the transcriptional level in any of the aforementioned genes **(Fig. 4.6.)**.

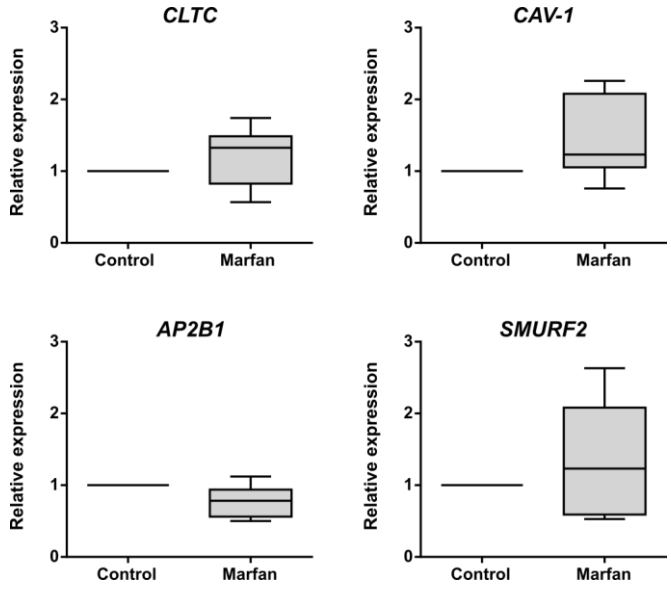

Figure 4.6. Clathrin- and caveolin-1-dependent downstream effectors are not transcriptionally altered in Marfan VSMC. *RNA from VSMC was extracted and transcriptional expression of CLTC (Clathrin; N=6, p=0.2624), CAV-1 (Caveolin-1; N=6, p=0.118), AP2B1 (Clathrin-adaptor protein complex 2 subunit B1; N=6, p=0.0598) and SMURF2 (SMAD Ubiquitination Regulatory Factor 2; N=6, p=0.3532) was analysed. Expression results in Marfan patients were normalized to Control. Results are represented as box and whiskers from min to max.*

4.1.5. SARA is increased at TGF-β containing early endosomes in human Marfan VSMC

The ambiguously increased TGF-β signalling despite unaltered clathrin-pathway associated internalization suggests further intracellular mechanisms that facilitate the TGF-β signalling cascade by increasing the efficiency of signal mediator recruitment to early endosomes. Having established that TGF-β does not internalise more through the clathrin-dependent pathway but that the clathrin-associated signalling is increased in MFS, we assessed whether TGF-β-dependent signal mediation is altered at early endosomes. We performed b-TGF-β internalization studies as aforementioned and co-stained with both EEA1 and SARA. Colocalization of both markers with b-TGF-β was significantly higher after internalization in both Marfan and control VSMC. Importantly, after internalization, Marfan cells showed higher colocalization of SARA with b-TGF-β and EEA1 compared to control cells indicating increased efficiency of signalling at early endosomes in Marfan VSMC **(Fig. 4.7.A)**.

4.1.6. TGF-β is targeted less to EEA1 and CAV-1 double-positive endosomes

Experimental evidence shows that the clathrin- and the CAV-1-associated endocytic pathways are not entirely separate entities, but that both pathways merge to form multifunctional signalling organelles that are associated with cargo sorting and degradation (145,146). Therefore, we performed b-TGF-β internalization studies and co-stained VSMC with EEA1 and CAV-1. An increase in triple-colocalization was observed after b-TGF-β internalization in both Marfan and control VSMC. In addition, triple-colocalization was significantly lower in Marfan than in control cells after ligand internalization, demonstrating decreased trafficking of TGF-β into these endocytic multifunctional sorting stations **(Fig. 4.7.B)**.

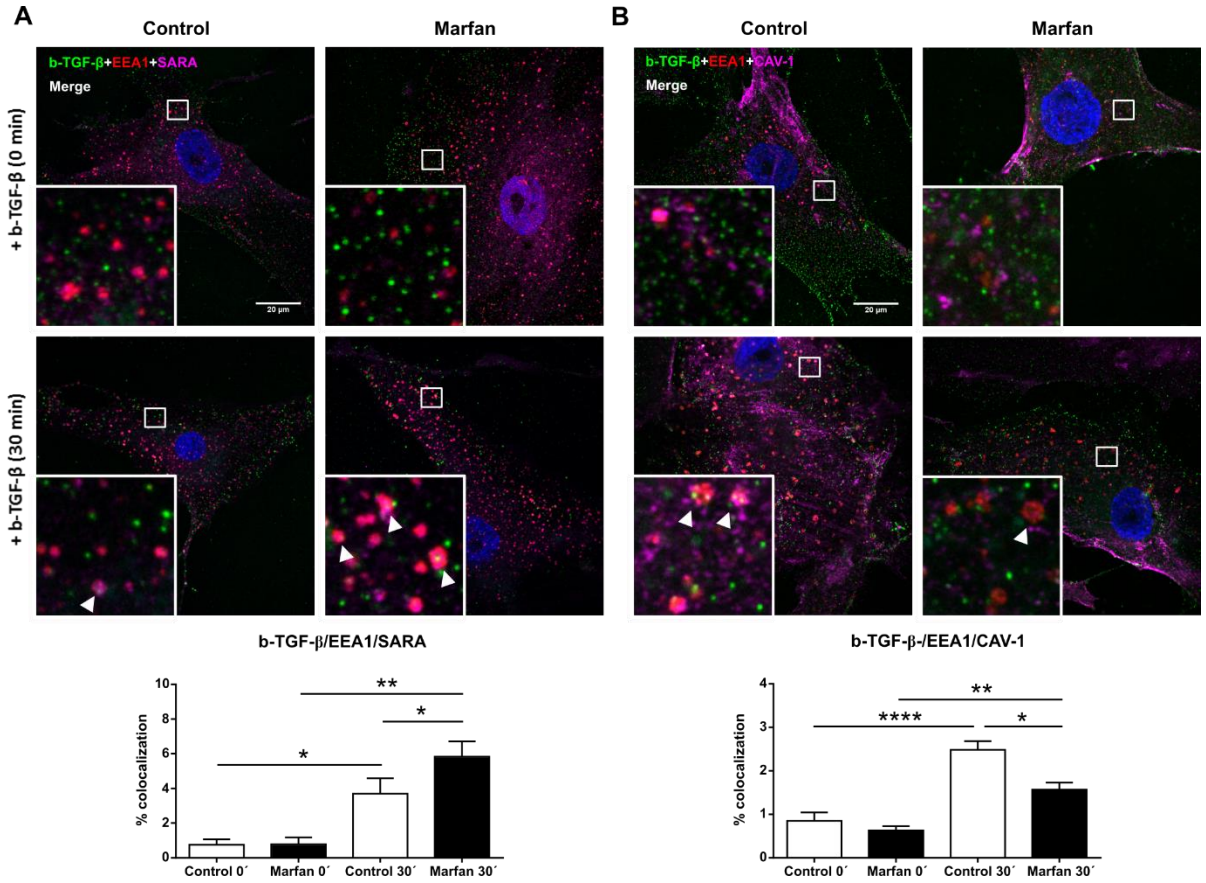

Figure 4.7. TGF-β internalizes more into SARA/EEA1- and less into EEA1/CAV-1-positive early endosomes in Marfan VSCM. *VSMC were starved and incubated with b-TGF-β followed by fluorescein-conjugated avidin. The complex was internalized for 0 and 30 min. Colocalization of b-TGF-β with* ***(A)*** *EEA1/SARA (N=4, RM ANOVA **p<0.01, LSD Control 0 min vs Marfan 0 min p=0.8486; LSD Control 30 min vs Marfan 30 min *p<0.05) and* ***(B)*** *EEA1/CAV-1 (N=5, RM ANOVA **p<0.01, LSD Control 0 min vs. Marfan 0 min, p=0.3899; Control 30 min vs. Marfan 30 min, *p<0.05) was analysed. The percentage of colocalization was calculated relative to non-colocalizing b-TGF-β. Results are represented as mean ± SEM. White arrows show triple colocalization of internalized b-TGF-β with EEA1/SARA or EEA1/CAV-1 in endocytic vesicular structures, respectively. Bar, 20 µm.*

Furthermore, these EEA1/CAV-1 double-positive endosomes have been shown to be enlarged structures described to be MVBs, which are responsible for sorting of receptors destined for degradation (146). We indeed observed large, ring-like EEA1-positive structures in VSMC, and quantitative analysis showed a significant increase in both Marfan and control VSMC after b-TGF-β internalization (**Fig. 4.8.A)**. The colocalization of b-TGF-β with CAV-1 and these large, ring-like EEA1-positive structures was then assessed, which significantly increased after b-TGF-β internalization in control VSMC only. In addition, less colocalization was seen in Marfan than in control cells after b-TGF-β internalization, which indicates a decreased trafficking of TGF-β into EEA1/CAV-1-double positive forming MVBs **(Fig. 4.8.B)**.

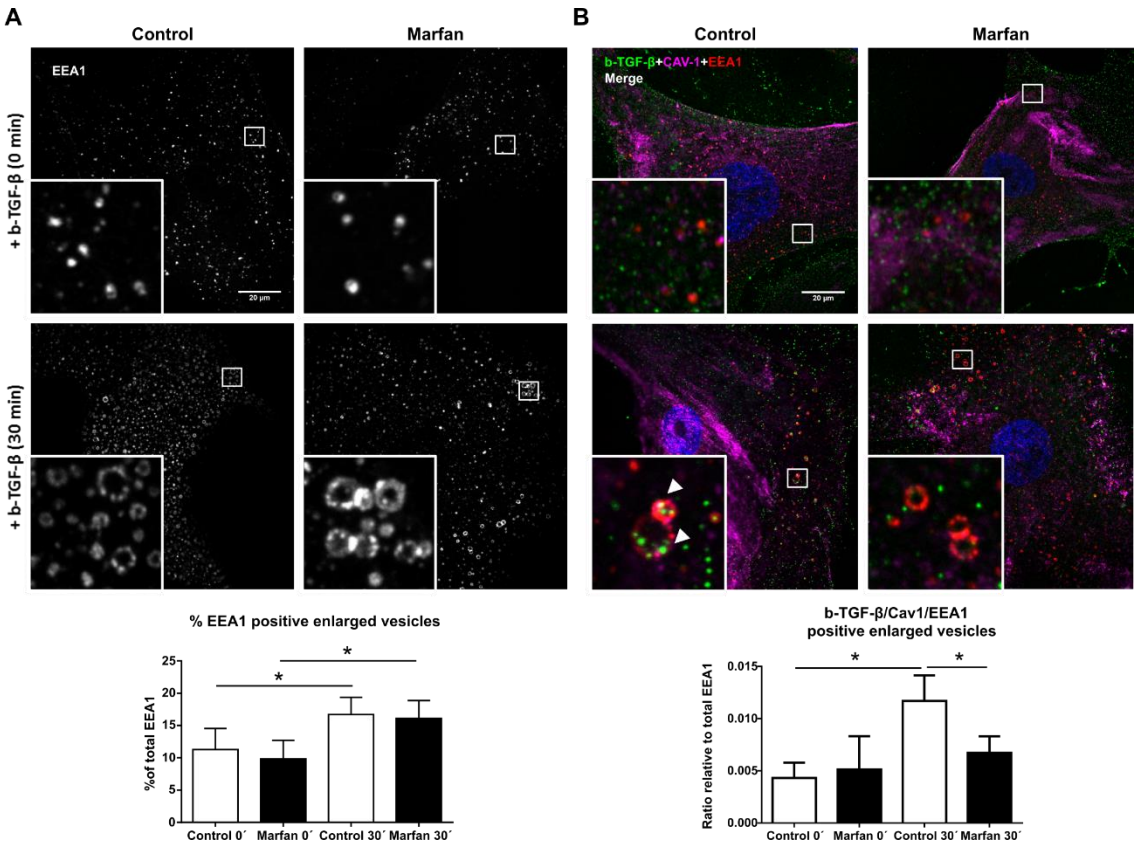

Figure 4.8. Internalized b-TGF-β is destined less to EEA1/CAV-1 positive enlarged vesicles. *VSMC were starved and incubated with b-TGF-β and the complex was internalized for 0 or 30 min.* ***(A)*** *The percentage of EEA1-positive large ring-like cytoplasmic vesicular structures was analysed relative to total EEA1-positive structures (N=5, RM ANOVA *p<0.05, LSD C 0 min vs. C 30 min, *p<0.05, Marfan 0 min vs. Marfan 30 min, *p<0.05).* ***(B)*** *Colocalization of b-TGF-β with CAV-1- and EEA1-positive large ring-like structures was analysed (N=5, RM ANOVA p=0.0977, LSD Control 0 min vs. Marfan 0 min, p=0.7343; Control 30 min vs. Marfan 30 min, *p<0.05). The ratio of colocalizing large ring-like endosomal structures to non-colocalizing ones was calculated relative to total EEA1 positive endosomes. Results are represented as mean ± SEM. White arrows show colocalization of internalized b-TGF-β with double-positive large ring-like early endosomes. Bar, 20 µm.*

4.1.7. The small GTPase RAB5 is overexpressed in human Marfan VSMC

SARA is a key molecule in the signalling cascade as it directly recruits SMAD2 to the receptor complex and thus enhances TGF-β signalling (115). Just the same as EEA1, SARA is recruited to early endosomes through its FYVE domain by the small GTPase RAB5 and hence acts as its effector (117). RAB proteins play a vital role in vesicular trafficking and are essential regulators of compartmentalization through their cyclical activation and inactivation by GTP binding at membranes and GDP binding in the cytosol (173). We therefore assessed the transcriptional level of *SARA, RAB5A* and *RAB5C* in Marfan and control VSMC. Marfan cells showed an upregulation of *RAB5A* and *RAB5C*, but not *SARA* **(Fig. 4.9.A)**. Furthermore, we assessed the ratio of active membrane bound RAB5 to inactive cytosolic RAB5 by membrane cytosol fractionation as described above. In Marfan VSMC, RAB5 was significantly enriched in membrane fractions **(Fig. 4.9.B)**. These results strongly suggest that in Marfan VSMC the increased localization of SARA at endomembranes is mediated by higher expression levels of RAB5.

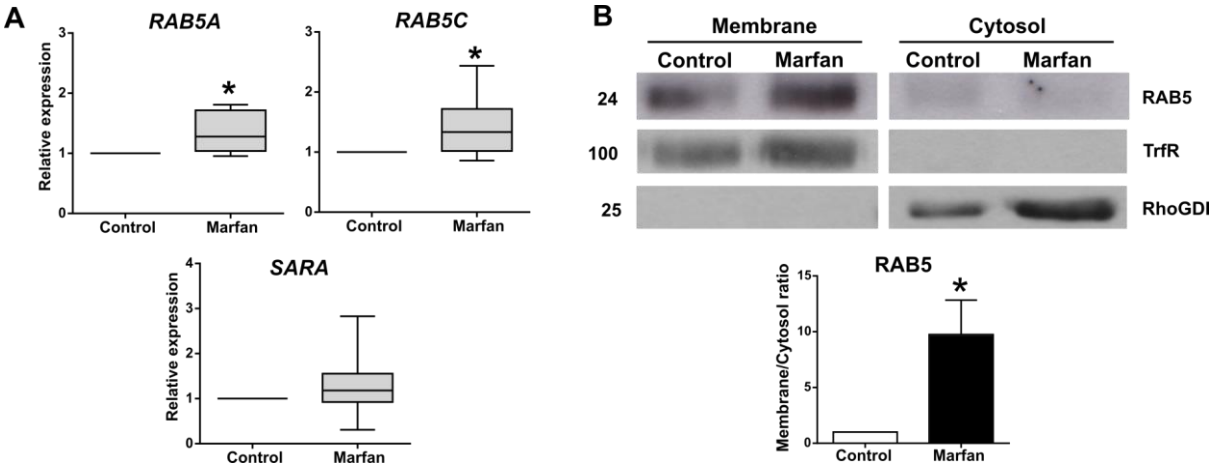

Figure 4.9. RAB5 is upregulated and recruited more to cell membranes in Marfan VSMC. (A) *RNA from VSMC was extracted and transcriptional expression of RAB5A (Control N=6; Marfan N=8, *p<0.05), RAB5C (N=7, *p<0.05) and SARA (Control N=6; Marfan N=8, p=0.3125) was assessed. Gene expression in Marfan patients was normalized to controls. Results are represented as box and whiskers from min to max.* ***(B)*** *Membrane enrichment analysis by Western blotting of RAB5 (N=5, *p<0.05). Membrane and cytosol fractions from Marfan and control VSMC were obtained and analysed by Western blot. Membrane and cytosol bands were relativized against their respective fraction marker, and membrane fractions were normalized against their corresponding cytosolic fraction. Marfan membrane bands were normalized against controls. Results are represented as mean ± SEM.*

4.2. Differential integrin expression

Integrins are important signal transmitters between the ECM and the cell through their mechanical linkage to the ECM and their TGF-β regulation. The TB/8-Cys4 module within FBN1 contains an RGD (Arg-Gly-Asp) motif which binds integrins with varying affinity (91). This interaction controls the integrin localization within the ECM and allows integrin proximity to the LTBP which contains TGF-β. As mentioned before, some integrins have the capacity to bind TGF-β, mechanically distort LAP, and present the mature TGF-β to its receptors, thereby controlling TGF-β signal propagation (95). Integrins form non-redundant heterodimers with varying functionality. Integrins β1, β5 and α5 are molecules that in a heterodimer formation bind both TGF-β and FBN1 and their upregulation has been associated with TGF-β signalling (89,91). Moreover, involvement of the β1 subunit has been associated with fibrosis and increased TGF-β activation (98). As integrins are by default inactive, the activating force is the binding of the β subunit to its α counterpart, inducing an activating shift in the heterodimer (174). The role of integrin expression in MFS has thus far been scarcely studied, yet integrins could be a significant contributor to aneurysm development. We here assessed expression levels of TGF-β and FBN1-binding integrins in aortic tissue from MFS patients.

4.2.1. TGF-β-regulating integrins are downregulated in aortic tissue from Marfan patients

Due to the modularity of FBN1 as extracellular matrix protein, we assessed the expression of TGF-β-binding integrins in aortic tissue of MFS patients. Aortic tissue was preferred in the experimental design as VSMCs in culture are removed from their interaction with the tissular extracellular matrix and therefore may not maintain their original interaction with their extracellular matrix as it occurs in intact tissue. We assessed the transcriptional expression of the subunits β1 and β5 and α5 by quantitative real time PCR and found a downregulation of all three transcripts in aortic medial tissue from MFS patients (**Fig. 4.10.A**). Furthermore, these three subunits have been described as direct or indirect targets of *miR-29b*, a micro RNA (miRNA) which has recently become the focus of attention due to its *FBN1* binding site and mRNA quality control (175–177). To examine whether the downregulation of the integrin subunits coincided with *miR-29b* expression, we assessed *miR-29b* expression in aortic tissue from MFS patients as well as controls and found a compelling upregulation of the miRNA (**Fig. 4.10.A**). Furthermore, we assessed whether the downregulation of *ITGB1* is also reflected at the protein level. Cryosections of aortic tissue from MFS patients and Control donors were stained with anti-ITGB1 and an antibody specific to only the active β1 subunit conformation. Quantitative analysis of immunofluorescence intensity showed no changes between Control and MFS aortae with respect to total anti-β1 fluorescence. Compellingly, a significant decrease in intensity of the ITGB1 active conformation was observed in MFS sections (**Figure 4.10.B**).

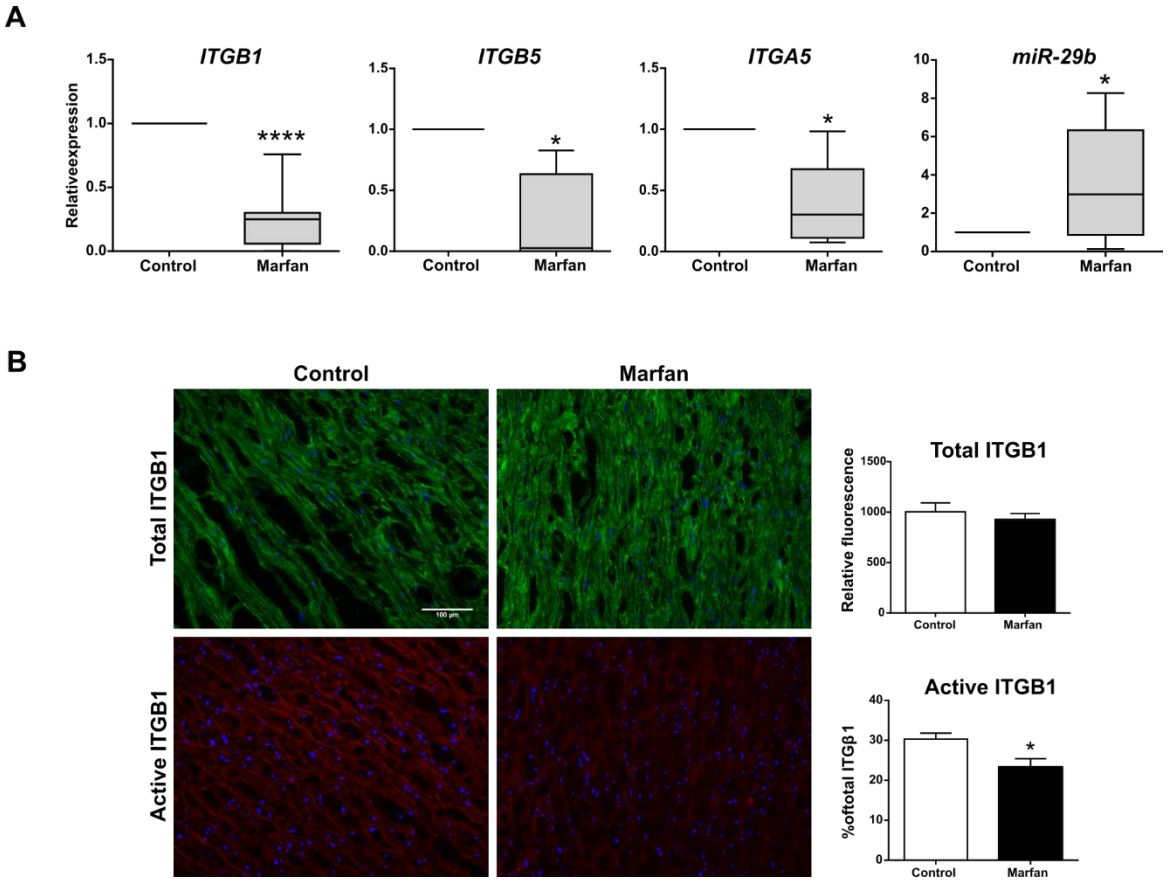

Figure 4.10. Integrin subunits B1, B5 and A5 are downregulated in MFS whilst miR29b is upregulated. (A) *RNA was extracted from Control and Marfan patient aortic tissue and levels of ITGB1 (Control N= 9; Marfan N=11; ****p<0.0001), ITGB5 (Control N=3; Marfan N=4; *p<0.05), ITGA5 (Control N=3; Marfan N=5; *p<0.05) and miR29b (N=10; *p<0.05) were assessed. Expression levels of Marfan patients were normalised to Controls. Results are represented as box and whiskers from min to max.* ***(B)*** *Aortic tissue from Controls and patients was cryo-sectioned and stained for total ITGβ1 (Control N=7; Marfan N=5; p=0.4983) and active ITGβ1 (Control N=7; Marfan N=5; *p<0.05). Results are represented as mean ± SEM. Bar, 100 μm.*

4.3. Gene ontological pathway analysis based on transcriptome sequencing in MFS

One of the most critical factors in the diagnosis and treatment of MFS is the poor correlation between variant of gene mutation and phenotype. Mutations clustered into the same group may have convergent outcomes depending on the locus where the mutation is found (8). Even identical mutations do not necessarily cause the same clinical phenotype despite affected individuals being related (178). Large-scale studies have addressed the association between *FBN1* mutation type and severity of disease as well as the specificity of organ involvement in relation to mutation type (4,8). However, the large variability of variant mutations is not easily interpreted and variant databases my

contain confounding information, not last due to the limitations of conventional exonic testing (37). Such is the challenge of gene testing, that in a case study of an entire affected family, patients had remained negative for a *FBN1* mutation even after substantial genomic testing. Only linkage analysis and cDNA sequencing revealed a deep intronic mutation generating a new splice site and nonsense-mediated mRNA decay (36). It is suggested, that about 10% of causative *FBN1* mutations are being missed by standard methods and require whole-genome sequencing in order to appropriately correlate gene mutation with disease outcome. Furthermore, the significant heterogeneity of phenotypes, even when clustered by mutation type, indicates that the mutated *FBN1* induces a whole network of intracellular alterations which might not necessarily correlate with mutation type but rather with thus far unidentified factors. Therefore, we performed RNA sequencing on RNA obtained from control and MFS VSMC. To gain insight into processes that may lead up to the development of aortic aneurysms, we obtained RNA from de dilated and non-dilated zone of the medial aortic layer.

4.3.1. FBN1 mutation types are extremely heterogeneous between MFS patients with aortic events

VSMC from five male MFS patients and four male control donors were extracted and cultured from the dilated (d) and non-dilated (nd) zone of aortic medial explants. All patients had suffered aortic dilatation and had undergone surgical repair. RNA was extracted and mRNA was sequenced by poly-A selection. In total, four different FBN1 mutations were found in MFS patients of which one mutation was identical in patients M031d/nd and M054d/nd (**Table 4.1.**). Two further MFS patients did not have any mutation in the FBN1 gene despite showing a clinical MFS phenotype. Patients M057d/nd and M054d/nd both had a predicted missense variant on chr15 48446711 and chr15 48456714 respectively. The mutation on chr15 48446711 belongs to the most common group of mutations found in MFS which substitutes a cysteine in the FBN1 calcium-binding EGF-like domain 32 (48). The second missense variant of patient M054d/nd on chr15 48456714 is predicted to cause yet another cysteine substitution at amino acid position 1782. However, this particular protein position has been described to show little cardiac effect (179). Furthermore, a second mutation was identified in patient M057d/nd on chr15 48416186. Interestingly, this mutation is an intron variant at rs76155368 SNP site as annotated (National Institute of Biotechnology Information, Available at: www.ncbi.nlm.nih.gov/SNP/) but has not been previously associated with MFS. A second mutation was furthermore identified in patient M054d/nd at chr15 48409001. Interestingly, we found the exact same mutation in patient and M031d/nd. Given that of all reported FBN1 mutations only 12% are recurrent, two out of five patients sharing the exact same mutation is an intriguing finding (49). The mutation is located at the SNP site rs56194244 within the 3´UTR of FBN1 and has been mentioned in

relation with a sole case of MFS, however, has never been described or cited (National Institute of Biotechnology Information, Available at: www.ncbi.nlm.nih.gov/variation/view/).

FBN1 mutation VSMC extracted from the dilated aortic medial zone								
		Mutation type		**M031d**	**M035d**	**M052d**	**M054d**	**M057d**
chr15	48409001	3´UTR	G>A	DP2=2,49	DP2=51,0	DP2=191,0	DP2=66,60	DP2=129,0
chr15	48416186	intron	C>T	DP2=9,0	DP2=8,0	DP2=8,0	DP2=7,0	DP2=9,12
chr15	48446711	missense	C>T	DP2=1422,0	DP2=1091,0	DP2=4060,1	DP2=3455,1	DP2=2025,1467
chr15	48456714	missense	C>T	DP2=721,0	DP2=546,0	DP2=1994,0	DP2=807,845	DP2=1693,1

FBN1 mutation VSMC extracted from the non-dilated aortic medial zone								
		Mutation type		**M031**	**M035**	**M052**	**M054**	**M057**
chr15	48409001	3´UTR	G>A	DP2=4,21	DP2=73,0	DP2=73,0	DP2=36,39	DP2=58,0
chr15	48416186	intron	C>T	DP2=2,0	DP2=15,0	DP2=10,0	DP2=8,0	DP2=8,3
chr15	48446711	missense	C>T	DP2=1140,0	DP2=1691,1	DP2=1805,0	DP2=1818,0	DP2=817,694
chr15	48456714	missense	C>T	DP2=551,0	DP2=796,0	DP2=843,0	DP2=496,503	DP2=839,0

Table 4.1. FBN1 mutations of MFS patients. *FBN1 was screened for mutations in all five male MFS diagnosed patients. In total four different mutations were found of which one was identical in two patients (chr15 48409001). Cysteine substitutions (chr15 48446711 and 48456714) were both predicted to cause missense mutations of the gene. One novel intronic mutation (chr15 48416186) with unknown outcome was found in one patient. Upper panel: mutation type and chromosomal location identified in VSMC from the dilated aortic medial zone. Lower panel: mutation type and chromosomal location identified in VSMC from the non-dilated aortic medial zone. Red boxes indicate the number of an alternative allele to the reference sequence e.g. a FBN1 variant different from the unmutated allele.*

4.3.2. Principal Component Analysis and Clustering of patients

Raw counts were log transformed and Principal Component Analysis (PCA) was performed on all samples (**Fig. 4.11.A**). Due to the high variability within the MFSd and MFSnd groups and the heterogeneity of mutation types, principal components 1 to 3 accounted for a low cumulative amount of the variance in our samples (**Fig. 4.11.B**). As a result of the high heterogeneity of the mutations in our samples and the low genotype to phenotype relation in MFS (8), patients were clustered by mutation type for further analysis to control for molecular consequences that could be mutation type-dependent. Six groups were obtained from the Marfan diagnosed patients: MFS 3´UTR (M031 and M054), MFS no mutation (M035 and M052) and MFS cysteine substitution (M054 and M057); the

groups further divided into dilated and non-dilated zone samples. Based on his *FBN1* mutation profile, patient M054 was clustered into both 3´UTR and cysteine substitution group for analysis.

A

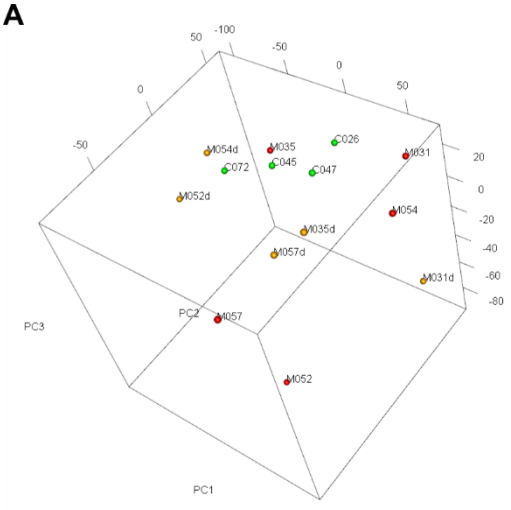

B

	PC1	PC2	PC3
Standard deviation	53.47	40.29	35.24
Proportion of Variance	0.29	0.16	0.12
Cumulative Proportion	0.29	0.45	0.58

Figure 4.11. Principal Component Analysis of DE genes. *Raw counts were normalized and log transformed and Principal Component Analysis (PCA) was performed on all samples.* ***(A)*** *Linear combination of components 1 to 3 are shown. Control samples are shown in green, the non-dilated aortic zone of MFS patients in red and the dilated zone in yellow.* ***(B)*** *Standard deviation, Proportion of variance and cumulative proportion of principal components 1 to 3.*

4.3.3. The non-dilated zone from MFS patients with 3´UTR mutation shows a differentially expressed gene profile

For each clustered group, expression levels of the dilated zone and the non-dilated zone were compared with control expression levels. Differentially expressed genes were selected based on the following criteria: adjusted p-value < 0.05 with Benjamini-Hochberg correction, and LFC > 2. Neither MFS patients with cysteine mutation nor MFS patients without *FBN1* mutation showed any changes in gene expression in either zone. However, 21 genes were differentially expressed in the non-dilated zone of MFS patients with the identical 3´UTR mutation, of which 20 were upregulated and 1 was downregulated in comparison with control levels (**Table 4.2. and Fig. 4.12.**).

Differentially expressed genes MFS non-dilated zone 3´UTR mutation vs. Control						
Ensembl_ID	Chr	P.Value	**adj.P.Val**	Entrez_ID	Gene_Symbol	**logFC**
ENSG00000145050	3	1.51E-07	**0.000881447**	7873	MANF	**2.218700236**
ENSG00000203914	1	2.26E-07	**0.000881447**	343477	HSP90B3P	**1.401730176**
ENSG00000259706	15	2.66E-07	**0.000881447**	7190	HSP90B2P	**1.512506073**
ENSG00000184164	22	1.90E-06	**0.00308846**	79174	CRELD2	**2.106644862**
ENSG00000090520	3	2.04E-06	**0.00308846**	51726	DNAJB11	**1.809949117**
ENSG00000102580	13	2.17E-06	**0.00308846**	5611	DNAJC3	**1.477015156**
ENSG00000149428	11	2.07E-06	**0.00308846**	10525	HYOU1	**2.271583263**
ENSG00000215895	1	1.42E-05	**0.014096289**	400750	AL354702.7	**2.101273797**
ENSG00000128228	22	4.88E-06	**0.00606918**	23753	SDF2L1	**2.452464154**
ENSG00000142188	21	2.21E-05	**0.018290602**	757	TMEM50B	**1.413483265**
ENSG00000166598	12	9.41E-06	**0.010390831**	7184	HSP90B1	**1.447354609**
ENSG00000167797	11	3.81E-05	**0.027051472**	10263	CDK2AP2	**1.472378972**
ENSG00000108389	17	4.59E-05	**0.03040555**	9110	MTMR4	**1.117620691**
ENSG00000154734	21	1.94E-05	**0.017550027**	9510	ADAMTS1	**-2.405840232**
ENSG00000250746	4	6.38E-05	**0.036255719**	100288073	RP11-39C10.1	**1.920543762**
ENSG00000071537	14	5.47E-05	**0.033970467**	6400	SEL1L	**1.313808596**
ENSG00000044574	9	3.80E-05	**0.027051472**	3309	HSPA5	**1.990675005**
ENSG00000063241	19	8.97E-05	**0.044360615**	79763	ISOC2	**1.046034128**
ENSG00000128590	7	0.000103118	**0.044578343**	4189	DNAJB9	**1.738096843**
ENSG00000143870	2	9.37E-05	**0.044360615**	10130	PDIA6	**1.044457326**
ENSG00000155660	7	9.82E-05	**0.044364931**	9601	PDIA4	**1.91095168**

Table 4.2. Differentially expressed genes identified in FBN1 MFSnd 3'UTR mutation vs Control. *21 genes were identified to be differentially expressed in VSMC from the non-dilated zone of MFS patients with 3´UTR mutation in FBN1. All genes but ADAMTS1 were upregulated in comparison with controls. Ensembl ID, adjusted p-values and logFC are shown in bold.*

Interestingly, no differences in gene expression were observed in the dilated zone from the same patients in comparison to control levels. Amongst the upregulated targets were transcripts for proteins involved in the endoplasmic reticulum stress response (ER stress) to unfolded protein such as *SEL1L*, *MANF* and *CRELD2*. Furthermore, the transcripts for molecular chaperones *HSP90B1, HSPA5, HSP90B3P, HSP90B2P, SDF2L1* and the hypoxia-induced *HYOU1* were also found to be upregulated, of which *HSP90B2P* is incidentally located on the same chromosome as FBN1. Further differentially expressed chaperones were DnaJ Heat Shock Protein Family Member B11, C3 and B9 (*DNAJB11, DNAJC3, DNAJB9*). Other targets resident in the ER and associated with protein processing were the Protein Disulfide Isomerase Family A members *PDIA4* and *PDIA6*. Given the increased TGF-β release from the ECM, an interesting finding is the upregulation of TGF-β signal inhibitor *MTMR4* and the

downregulation of the TGF-β activator *ADAMTS1*. Further upregulations were observed for the novel protein coding sequence *ISOC2*, the multi-pass transmembrane protein *TMTM50B*, the Cyclin-dependent-Kinase associated protein *CDK2AP2* and the two pseudogenes *AL354702.7* and *RP11-39C10.1*.

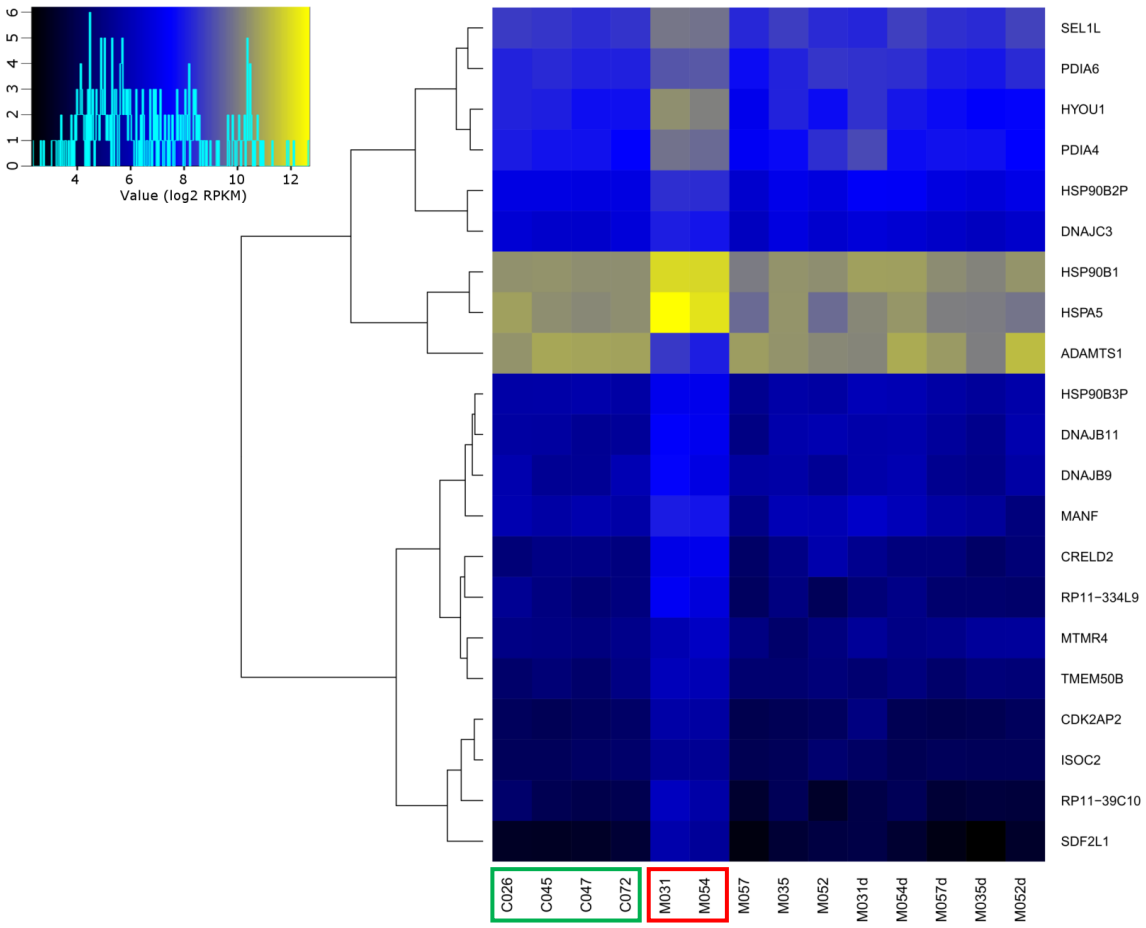

***Figure 4.12. Genes from the non-dilated aortic zone of 3´UTR FBN1 mutations are differentially expressed**. A heat map of the 21 differentially expressed genes is shown. MFSnd 3´UTR (red box) expression levels were compared with control (green box) expression levels. Differentially expressed genes were selected based on the following criteria: adjusted p-value < 0.05 with Benjamini-Hochberg correction, and LFC > 2. Colour codes are representative for log2 RPKM (reads per kilobase million). Counts range from low (black) to high (yellow).*

4.3.4. 3´UTR FBN1 mutation induces a transcriptomic profile of ER stress and ERAD associated degradation in response to glycoprotein misfolding

Gene ontological analysis was performed using the GeneCodis tool for modular and singular enrichment analysis (168,180,181). Out of the 21 differentially expressed genes, 4 genes did not show any annotations: *HSP90B3P, HSP90B2P, AL354702* and *RP11-39C10*. Enrichment analysis clearly identified a specific cluster of Biological Processes (BP) associated with the catabolic cellular mechanisms involved with glycoprotein misfolding in the ER. Amongst the most significant processes were *protein folding* (GO: 0006457), *ER-associated protein catabolic processes* (GO: 0030433) and *glycerol ether metabolic processes* (GO: 0006662) (**Fig. 4.13.A)**. The upregulated genes associated with these, amongst others, belonged to the family of molecular chaperones such as *HSP90B1, HSPA5*, the *DNAJ* members and the ER resident *PDIA6* and *PDIA4*. The elemental activities as defined by Molecular Functions (MF) of the gene products were found to be *misfolded protein binding* (GO: 0051787) and *unfolded protein binding* (GO: 0051082) as well as *heat shock protein binding* (GO: 0031072) *chaperone binding* (GO: 0051087) and *protein disulphide isomerase* and *oxireductase activity* (GO: 003756 and GO: 0015035 respectively) (**Fig. 4.13.B**). In line with the previous results, enrichment analysis identified the *endoplasmic reticulum* (GO: 005783), the *endoplasmic reticulum-Golgi intermediate compartment* (GO: 005793) and the *melanosome* (GO: 0042470) as cellular compartments (CC) of gene product activity (**Fig. 4.13.C**). Apart from the members of the chaperone molecule family and the protein isomerases, gene products of *SDF2L1, SEL1L, TMEM50B, MANF, HYOU1* and *CRELD2* were associated with the CC identified. In addition, the Kyoto Encyclopedia of Genes and Genomes (KEGG) pathway maps identified genes involved in *protein processing in the endoplasmic reticulum* as a molecular network (**Fig. 4.14.A**). We then performed Signalling Pathway Impact Analysis (SPIA) to identify the most relevant altered cellular pathways due to 3´UTR FBN1 mutation. We found a significant alteration of *protein processing at the endoplasmic reticulum* (**Fig. 4.14.B**). More specifically, our identified differentially expressed genes were shown to be involved in protein recognition by luminal chaperones and protein targeting of terminally misfolded and accumulated proteins leading to ER-associated degradation (ERAD) of ubiquitin tagged proteins by the proteasome.

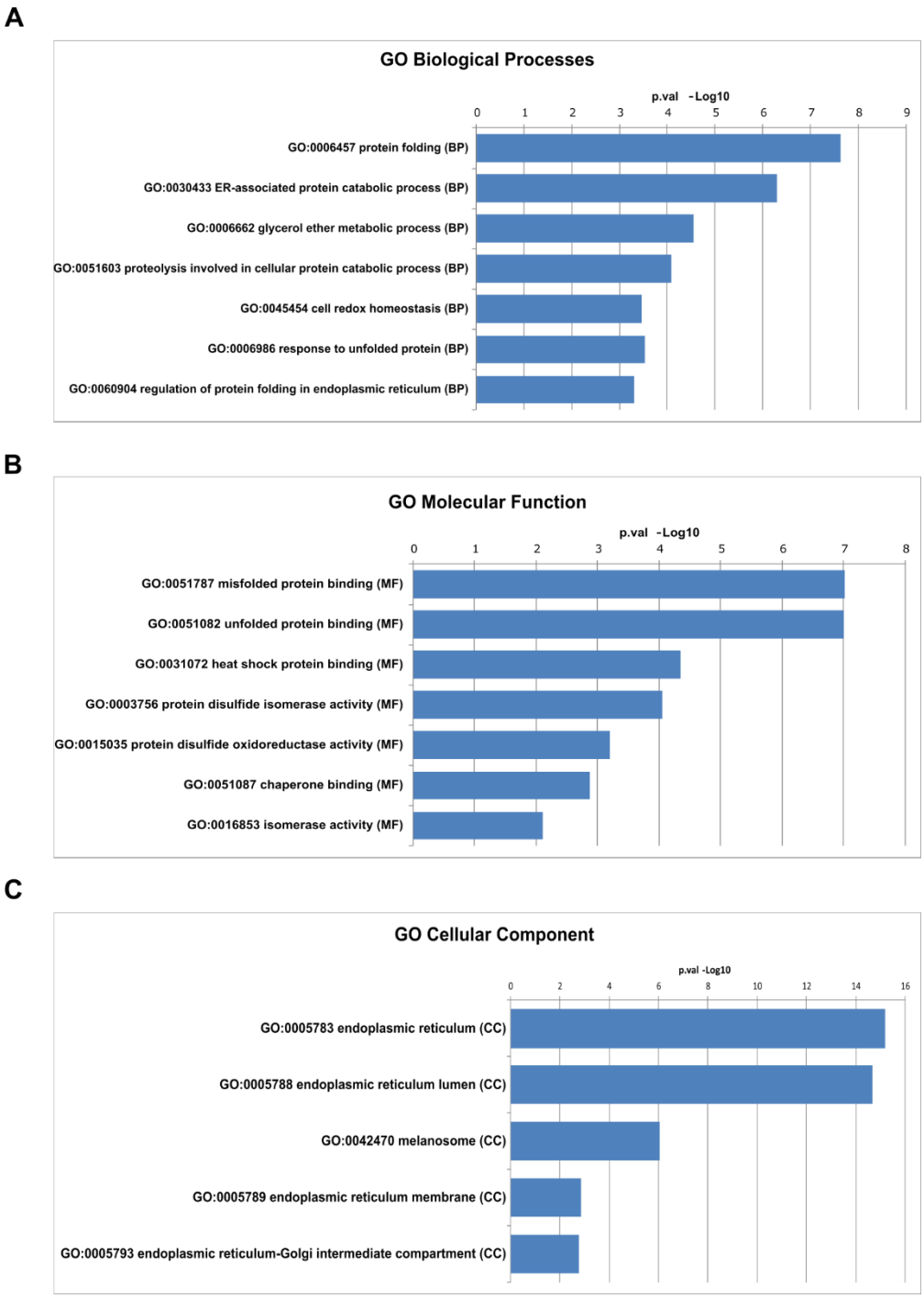

Figure 4.13. Gene ontology enrichment analysis of VSMC from the non-dilated aortic zone of MFS patients vs controls*. GO was identified by GeneCodis.* ***(A)*** *GO Biological Processes identified a distinct profile of ER-associated processes in response to protein misfolding.* ***(B)*** *The Molecular Functions associated with the differentially expressed genes were grouped into unfolded protein binding.* ***(C)*** *The Cellular Components involved in the misfolded protein binding processes were shown to be the ER and the ER-Golgi intermediates.*

A

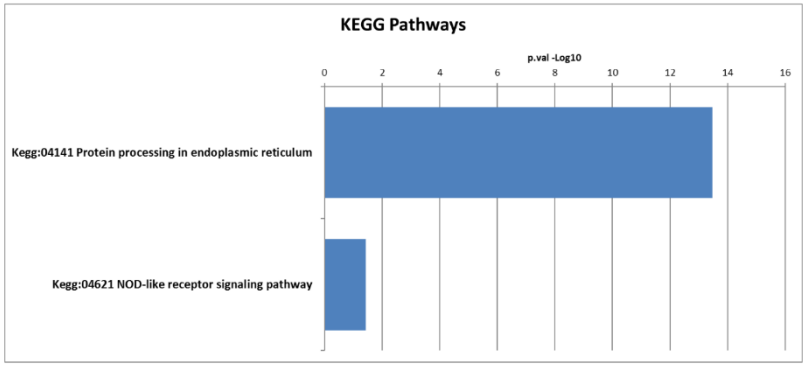

B

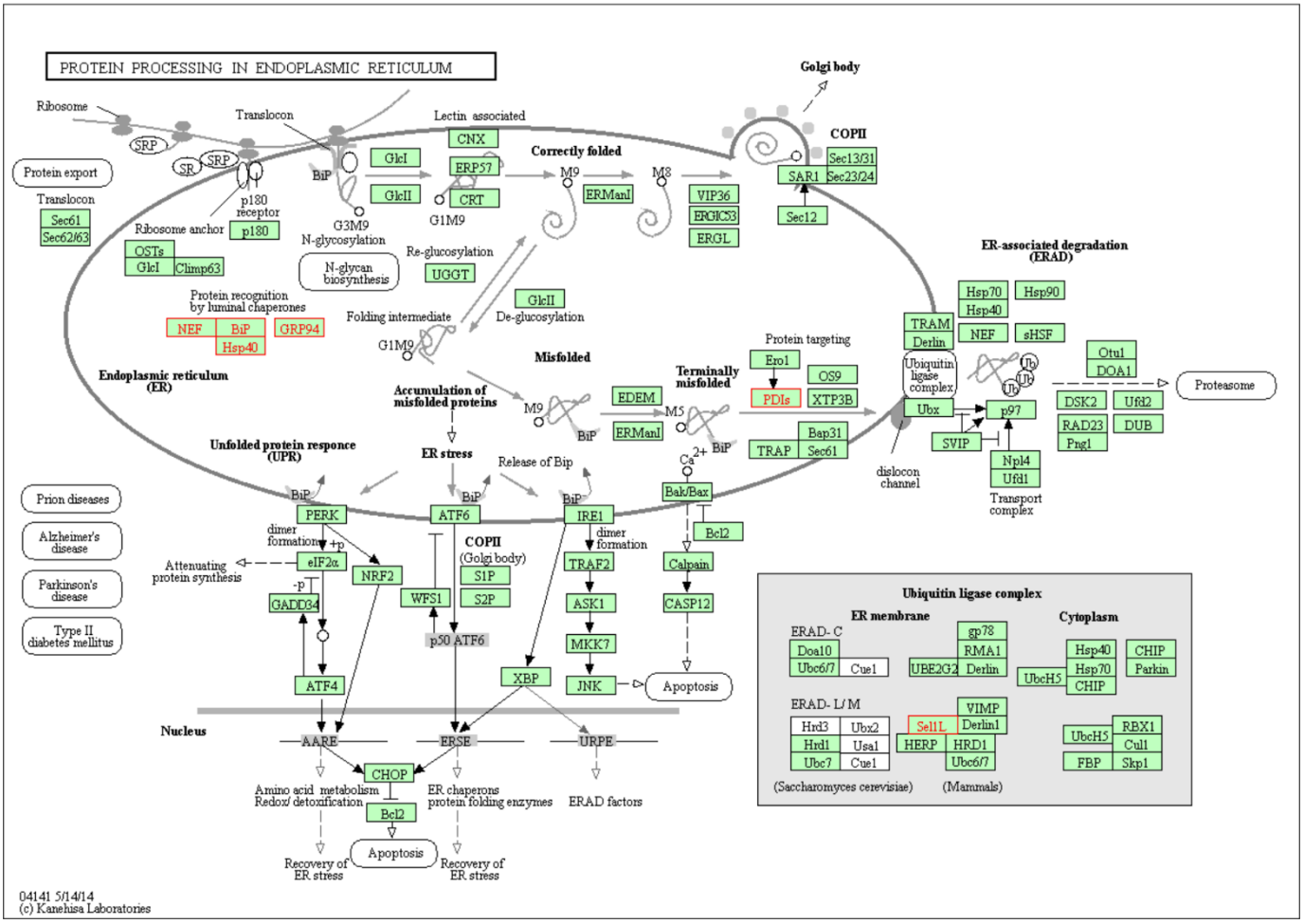

Figure 4.14. KEGG pathway map and SPIA analysis of most relevant altered pathways in VSMC from the non-dilated zone of 3´UTR FBN1 mutation. (A) *KEGG pathway enrichment analysis identified protein processing in the endoplasmic reticulum as the molecular network involving the DEGs of the 3´UTR FBN1 mutation in the non-dilated aortic zone.* ***(B)*** *SPIA visual map of the intracellular molecular network affected by the 3´UTR FBN1 mutation in the non-dilated aortic zone.*

4.3.5. 3'UTR SNP on chr15 48409001 is a predicted target for miR-1252-5p

MicroRNAs (miRNAs) are short, 19-25 basepairs (bp) containing non-coding RNA molecules that can interfere with mRNA stability and translation (182). Given that the 3´UTR is the main target for miRNAs (183), we performed an analysis of target prediction for the 3'UTR SNP target identified in the two MFS patients M031d/nd and M054d/nd using the miRDB online database for target prediction and functional annotations (Available at: www.mirdb.org/miRDB/). *FBN1* was predicted to be targeted by 110 miRNAs of which the highest scoring ones included the family of *miR-2*9 (*miR-29a, miR-29b* and *miR29c*) whose increased expression has previously been described to drive aneurysm formation in MFS (184,185). Furthermore, using a custom prediction with 50 nucleotides flanking the mutation region up- and downstream, we found *miR-1252-5p* (NCBI gene ID: 100302136) to bind to the exact SNP site at chr15 48409001 with a prediction score of 56 of 100. No other information was found in the literature on *miR-1252-5p*.

Discussion

5. Discussion

5.1. The contribution of TGF-β compartmentalization to its increased signalling in MFS

The ECM is a highly heterogenous but at the same time intricately ordered blend of multimolecular compounds, which provides structural integrity, regulates intracellular signalling molecules and transmits mechanical properties to every organ system. Such is the organized nature of interacting structural components, that mutations in ECM proteins impact the higher order tissue structures in a deleterious way, as is reflected by the vast spectrum of pathological phenotypes (22). Not surprisingly, the clinical features seen in MFS due to mutated *FBN1* are wide ranging as well as the fragmentation of elastic fibres causes yet another cascade of molecular consequences due to increased TGF-β availability in the extracellular environment (53). Moreover, the contribution of TGF-β molecular behaviour is thus far largely unexplored in MFS even though many steps, from its activation to signalling, potentially serve as control stations (87). Studies in a murine model of MFS have shown that both canonical and non-canonical signalling are involved in the disease progression as well as aortic risk phenotype and the inactivation of one can be compensated for by the other (53,151). In addition, our lab has previously shown that pSMAD2 and pSMAD3 levels are increased in MFS patients and that the pharmacological inhibition of TBRI reverts both proteins to control levels (127), strongly indicating that the canonical TGF-β signalling plays a pivotal role in MFS disease development. Nonetheless, as the TGF-β receptor complex can internalise through both clathrin- and CAV-1 dependent pathways with opposing signalling qualities (101), the role of TGF-β compartmentalization in MFS remains elusive. To assess whether increased TGF-β signalling in human VSMC from MFS patients is contributed to by altered TGF-β compartmentalization, we here examined TGF-β endocytosis through the clathrin- and CAV-1 dependent intracellular pathways and their associated signal mediators.

5.1.1. Increase of signal mediators and receptor complex interaction at endomembranes in MFS

The TGF-β signalling mediators SARA and SMAD2 are tightly associated with the clathrin-dependent endocytic pathway whose signalling characteristics localize to early endosomes. On the contrary, the inhibitory SMAD7 and its signal antagonising function localizes primarily to CAV-1 positive vesicles (101). As these signalling molecules are found in the cytosol as well as at intracellular membranes and their recruitment to endomembranes upon stimulus is crucial for signal transduction, we analysed their enrichment at cell membranes relative to their presence in the cytosol. We found increased enrichment of TGF-β signal promoting mediators at membranes in MFS patients, demonstrating that

the proteins responsible for signal transduction are, in fact, more recruited to their location of action in MFS patients. The increased TGF-β-dependent signal mediation was supported by immunoprecipitation experiments showing the heightened interaction of both SARA and SMAD2 with TBRII. In contrast, in both instances the CAV-1 associated signal mediator SMAD7 was unaffected, strongly suggesting that the increased signal promotion in MFS is attributed to a heightened activation of the clathrin-pathway associated signalling in MFS patients. Furthermore supporting the suggested increase of TGF-β signal mediators associated with the early endosomal pathway, is the observation that SARA is strictly associated with early endosomes and is recruited to the early endosomal membrane by means of a single mode interaction of the SARA FYVE domain with early endosomal PtdIns(3)P (116,186). Importantly, although SMAD1 and SMAD5 share about 80% sequence homology with SMAD2, SARA does not interact with either of them and is therefore exclusively associated with SMAD2 mediated signalling through the early endosomal pathway (115). The FYVE domain controls the subcellular localisation of SARA whilst its C-terminal domain interacts with the TGF-β receptor complex, where its 85-residue Smad-binding domain (SBD) interacts with the MH2 SMAD domain (115,172). In order to establish whether the TGF-β signal propagating key players are in fact localized to early endosomes as previously established, we performed colocalization experiments of SARA with the early endosome marker EEA1 and of SMAD7 with CAV-1. After TGF-β stimulation we observed an increased colocalization of SARA and EEA1 in VSMC from MFS patients, whereas CAV-1-associated SMAD7 was unaffected. This strongly supports that the previously seen increase of signalling mediators in membrane fractions as well as their TBRII interaction is localized to early endosomes, therefore indicating an over-activation of the clathrin-dependent signalling pathway in MFS. This is in accordance with previous results demonstrating that SARA localization at early endosomes is crucial for downstream signalling (186). Meanwhile, SMAD7, which has the ability to interfere with the signal transduction by competing with the regulatory SMADs for receptor binding, does not seem to be able to compensate for the increased binding of SMAD2 and SARA by augmenting its own receptor interaction.

5.1.2. Subcellular compartmentalisation of TGF-β and its signal mediators

The increased localization of signal promoting mediators at early endosomal membranes suggests an imbalance in the TGF-β pathway segregation in favour of the clathrin-dependent pathway. We therefore assessed whether b-TGF-β localizes more to early endosomes than CAV-1-positive vesicles after ligand internalisation. We found no alterations of TGF-β endocytosis through either pathway. Also at the transcriptional level we did not observe any alteration of key players associated with either pathway. This was unexpected, considering the increased signal promotion at early endosomes.

Despite having validated the b-TGF-β bioactivity, we cannot exclude the possibility that the addition of the biotinylated ligand saturated the receptor system in both VSMC from MFS patients and controls, therefore masking alterations that are potentially evident under basal conditions. Considering the increased concentration of extracellular bioactive TGF-β in MFS patients due to mutated FBN1 (53), the addition of equal b-TGF-β concentrations to MFS and control VSMC could induce biased results. However, when analysing colocalization of SARA and EEA1 after the addition of recombinant TGF-β, we observed a clear increase of the signal mediator at early endosomes, indicating that in MFS the endogenous signalling machinery is, in fact, altered and that this alteration is evident and unmasked, even after the induced TGF-β internalisation. Therefore, we are challenged with the question of just how the TGF-β signalling associated with the endosomal pathway is increased in MFS, despite equal levels of TGF-β trafficking into early endosomes. Paradoxically increased TGF-β signalling is perhaps one of the biggest challenges in MFS and related diseases. Augmented TGF-β signalling has been reported in syndromic presentations of MFS and MFS-like diseases, whilst loss-of-function mutations in those cases affected either of the TGF-β receptors or even TGF-β itself (187,188). This suggests additional intracellular mechanisms that facilitate the TGF-β signalling cascade by other means such as chronic compensatory events or epigenetic modifications of the SMAD2 promoter (171,187). Nonetheless, the absence of endocytic alterations we observed with respect to the clathrin-dependent early endosomal pathway could furthermore be attributed to the fact that TGF-β internalises through two distinct heterodimer combinations with disparate signalling responses. In both scenarios TBRII remains the initial ligand binding receptor. However, TBRI/ALK5 can be replaced by a second type I receptor named ALK1. The TBRII/ALK1 receptor complex induces downstream signalling though SMAD1/5 whilst SMAD2/3 signalling is specific to TBRII/ALK5. Thereby, TBRII/ALK1 creates a dissimilar signalling profile to TBRII/ALK5 (189,190). It has even been suggested that the TBRII/ALK1 signalling profile not only induces a contrasting response to TBRII/ALK5, but that it actively antagonizes SMAD2/3 signalling (189). Therefore, as we visualized the ligand itself instead of TBRI/ALK5, we need to consider the possibility that the b-TGF-β which localised to EEA1 positive early endosomes is not necessarily entirely associated with SARA and SMAD2. To address this issue and to analyse only those TGF-β containing endosomes that also show signalling activity, we performed triple-colocalization studies of b-TGF-β, EEA1 and SARA. We found an increase in triple-colocalizing structures in VSMC from MFS patients, strongly suggesting that, although TGF-β does not show increased internalization to early endosomes, its SARA-dependent signalling efficiency at early endosomes is increased in MFS. In addition, TGF-β receptor activation, and in particular TBRI GS domain phosphorylation, requires a multitude of steps in order to efficiently transduce signal. Signal inhibitory proteins such as FKBP12 have been shown to interact physically with the TBRI GS domain

and to prevent TBRI phosphorylation, but not heterodimer formation (191,192). Another essential inhibitory protein is the so called BAMBI which can interfere with the TGF-β receptor heterocomplex formation at the plasma membrane level but, more interestingly, can also form a complex with SMAD7 to prevent R-SMAD binding and signal propagation at the endosomal level (193). Upon ligand binding, TGF-β receptor heterodimer might internalize through the early endosomal pathway without leading to a signal response due to control mechanisms such as BAMBI, which could explain the pool of b-TGF-β containing early endosomes that is negative for SARA. An alteration of such intracellular control mechanisms could lead to the increased signalling at early endosomes in MFS. Furthermore, the recruitment of SARA to early endosomal membranes is a pivotal facilitator of TGF-β signal transduction by virtue of its SMAD2 and TGF-β receptor complex binding ability as well as its control over SMAD2 subcellular distribution (115,172). SARA mutants retain the ability to bind SMAD2 but fail to induce its correct subcellular localization which, as a consequence, leads to TGF-β signal abrogation (115). Through its FYVE domain, SARA furthermore binds to RAB5 positive early endosomes (116,117). Mutant FYVE domains fail to induce membrane localization and are mainly found in the cytosol (115). The endosomal distribution of SARA depends on its FYVE domain interaction with Ptdlns(3)P, whose enrichment at early endosomal membranes is stimulated by RAB5 (116,117,194), indicating that RAB5 is a crucial control point of SARA localization and subsequent downstream events. We therefore assessed *RAB5* transcriptional expression as well as RAB5 enrichment at membranes, where the small GTPase is found in its active and GTP-bound conformation (173). We found that RAB5 is increased at the transcriptional level as well as it shows heightened membrane enrichment in Marfan VSMC. Considering that RAB5 is an essential regulator of its effector SARA, which on the other hand controls the subsequent SMAD2 signalling cascade, our results strongly suggest that the dysregulation of RAB5 is a major inducer of the increased signalling efficacy at early endosomes in MFS. Taking into account that at the transcriptional level no changes were seen for SARA, its increased localization to early endosome residing TGF-β receptors in MFS VSCM is strongly suggested to be dependent on an upstream control mechanism such as RAB5. The relationship of RAB5 and SARA has been thoroughly examined as well as the localization of the SARA FYVE domain-dependent recruitment to early endosomes and its SMAD2 recruiting functions (116,117). It has been suggested in previous reports that SARA, in addition to its signal transducing role, furthermore plays a crucial part in the morphology and dynamics of early endosome function, thereby providing a link between membrane trafficking and signal transduction (117). The importance of SARA as a RAB5 effector, its TGF-β signal induction, and the possibility of it being a therapeutic target in MFS propose interesting topics for future research.

5.1.3. TGF-β trafficking into CAV-1/EEA1 positive vesicles

Even though the TGF-β receptor compartmentalization in association with the disparate signalling responses is a refined cellular mechanism to account for TGF-β signal homeostasis, controversial debate about whether CAV-1-positive vesicles fuse with early endosomal membranes to induce lysosomal cargo degradation challenges the segregation rule. This is supported by studies involving viral infection which was demonstrated to be exchanged between early endosomes and caveolae, showing pathway interdependence (133). As such, caveolar vesicles have been shown to follow a RAB5-dependent pathway, leading to their fusion with early endosomes (133,145). The low pH within early endosomes allows the caveolar vesicle cargo to diffuse into the surrounding membrane whilst remaining trapped within the limiting endosomal membrane, suggesting a transient but stable formation of subdomains (133). We showed that these CAV-1 and EEA1 positive vesicles form in VSMC, therefore supporting the view that the CAV-1 and endosomal pathways merge. We furthermore showed that b-TGF-β induces the formation of these vesicles, whose ability to do so is decreased in MFS. Interestingly, it has been demonstrated that TGF-β receptors internalised through CAV-1/EEA1 positive vesicles are subjected to lysosomal degradation through the endosomal pathway by inclusion into MVBs (146). A receptor degradative mechanism has been proposed by which the endosomal sorting complex required for transport (ESCRT) recognizes cargo in early endosomes and delivers the it to MVBs for degradation (147). Apart from the central role in TGF-β signal propagation, these results suggest that early endosomes are key components of signal termination as well. Interestingly, some cargo destined for lysosomal degradation through the endosomal pathway has been shown to be ubiquitinated, which is a quality that has conventionally been associated with the CAV-1-dependent pathway for TGF-β receptor complex degradation by the proteasome (101,147). Nonetheless, the question remains of why CAV-1-positive and EEA1-positive vesicles merge. Possibly, the fusion of these vesicles is a mechanism to adapt to bursts of TGF-β as often seen in peak times of inflammation when TGF-β effects are most prominent and cells experience an increased load of TGF-β signal (146). By utilizing either pathway for receptor complex degradation and signal abrogation, this cell mechanism might prevent proteasome overload, which has been shown to have detrimental effects on cell stress and induces apoptosis (195). In MFS, this compensatory intracellular mechanism seems to be affected, which potentially prevents the cell from maintaining homeostasis by losing the ability to avert an excessive proteasome workload. Even though CAV-1/EEA1-double positive vesicles have been well characterized, we must consider their signalling properties as well as their endocytic stage. It has been demonstrated that caveolae and clathrin-coated vesicles fuse immediately after budding off the plasma membrane, leading to the formation of CAV-1/EEA1 double positive vesicles which share signal properties of either pathways and show colocalization of SMAD7 and SMURF2 as well as

SARA and SMAD3, leaving room for debate about the cargo fate (145). Downstream of the endosomal pathways, CAV-1/EEA1-double positive vesicles have furthermore been described to form MVBs, subsequently and necessarily leading to cargo lysis (146). As MVBs have been described as large multi-vesicles carrying fusion cargo (146), we analysed structures resembling this morphological observation and found, in accordance with previous results, significantly less CAV-1/EEA1 large structures colocalizing with b-TGF-β. Although we cannot conclusively suggest that the lysosomal pathway is indeed affected in MFS, we can confidently propose that multi-vesicular sorting stations exist in VSCM upon TGF-β internalization. These see themselves negatively affected in MFS, thereby indirectly providing a platform for EEA1-single positive signalling vesicles. As a matter of fact, the RAB5-dependent nature of endocytic vesicle fusion poses an interesting challenge, as we showed an increase in RAB5 transcriptional expression as well as membrane bound state. However, based on our results, we can deduce that in MFS the increased RAB5 seems to boost the signalling efficacy rather than the vesicular fusion. RAB GTPases are proving to be interesting targets for future research in MFS. Actin cytoskeleton rearrangements have been observed in VSMC from MFS and elements of the actin cytoskeleton are major transport routes for RAB proteins (127,173). A disruption or reorganization of this major transport pathway possibly induces a deviation of RAB protein delivery and an aberration of their functions as they fail to perform their regulatory task, with conceivably pathophysiological consequences. Finally, the overexpression of SMAD2 signalling itself has been shown to induce the long-term reorganization of the actin cytoskeleton, thereby possibly enabling a permanent change of the RAB protein transport and sorting route in MFS (127,196). Taken together, we propose a model in which the the increased endosomal pathway associated signaling in MFS is due to an increase in RAB5-mediated SARA recruitment to early endosomes, which facilitates the subsequent SMAD2/TGF-β receptor complex binding. The increased signaling at early endosomes is aided by a reduced trafficking of TGF-β into EEA1/CAV-1-double positive endocytic structures reported to be associated with signal attenuation. Both endocytic trafficking alterations converge to provide a signaling platform that consequently leads to the chronic TGF-β signal promotion.

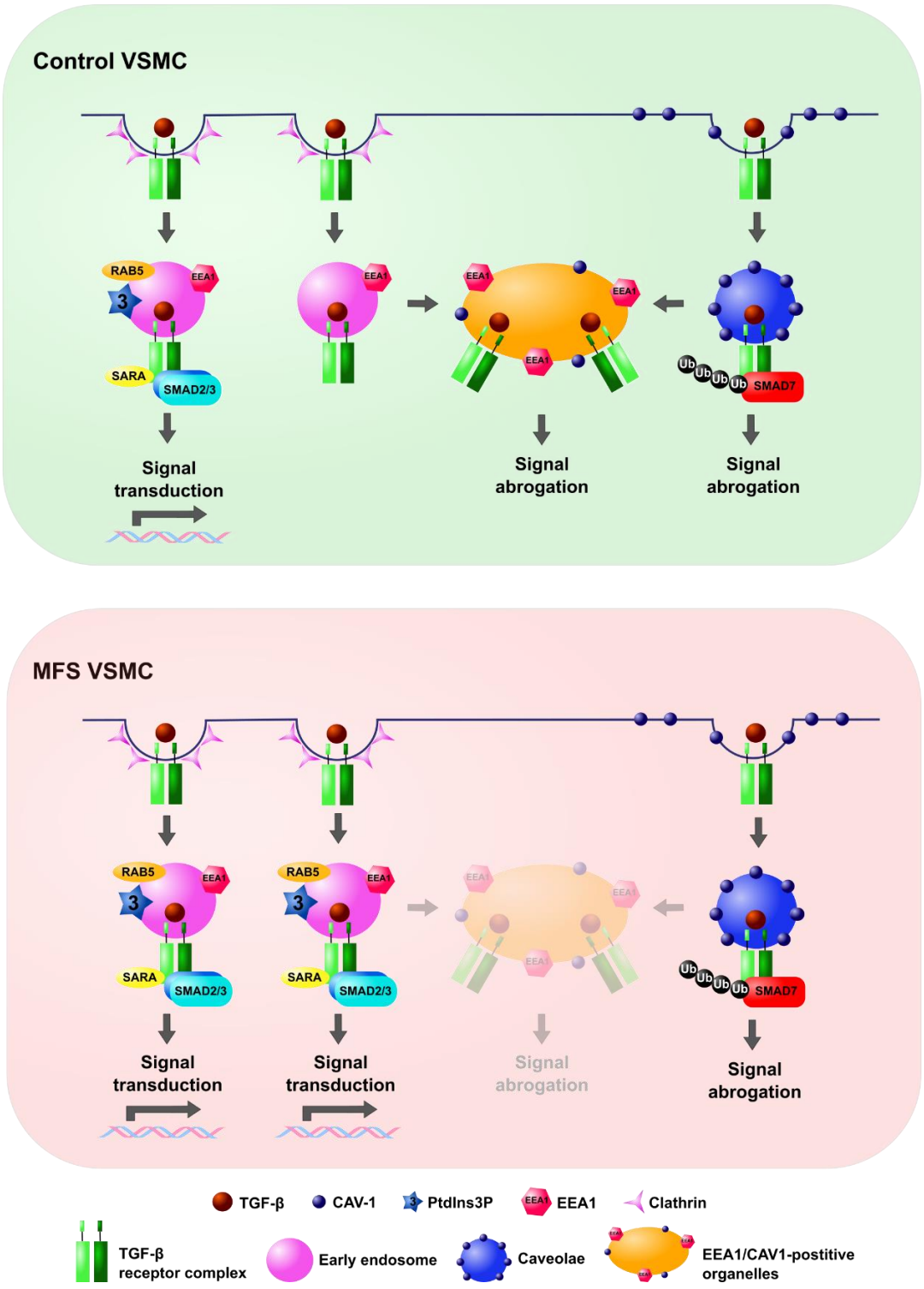

Figure 5.1. Proposed model of increased early endosome-associated TGF-β signalling in MFS. *Despite equal levels of internalization through either endocytic pathway, the early endosomal pathway-associated TGF-β signalling is increased in MFS through a heightened recruitment of SARA to early endosomes in a RAB5-mediated manner, facilitating the SMAD2 signalling cascade. The simultaneously decreased TGF-β trafficking into EEA1/CAV-1-double positive endocytic structures associated with signal abrogation assists the already facilitated TGF-β signal mediation by providing a platform for TGF-β signal promotion.*

5.2. Integrins and the ECM

Integrins are receptors found in the ECM that mediate numerous processes such as cell adhesion and cell signalling (197). Integrins are crucial for matrix assembly and fibrillogenesis: the subunit β1 for example has been shown to be able to form heterodimeric receptors with at least 10 α subunits, of which the α5β1 integrin is indispensable for ECM organization and ECM sensing qualities (198). Although integrins are overall assumed not to have any enzymatic activity themselves, their quality lies in their ability to accumulate in integrin-based cell adhesion zones and the recruitment of other components to these specialized extracellular areas (89). Due to the lack of integrin signalling, they rely heavily on interactions with other molecules whose signalling has been described to induce integrin activation in an "inside-out" fashion (89). Conversely, integrins aid in ligand presentation to their receptors through spatial proximity, which is strengthened by the accumulation of integrins in cell adhesion zones (95). However, this interplay of ECM sensing mechanisms has thus far remained vastly unexplored in MFS, which is a particularly intriguing topic due to the remodelling of the ECM. We here assessed the expression levels of FBN1- and TGF-β-binding integrins in the dilated zone of aortic tissue of MFS patients, in order to establish whether this TGF-β-activating mechanism facilitates the increased TGF-β signalling associated with MFS.

5.2.1. Downregulation of TGF-β binding integrins

Integrin-dependent activation is one of the mechanisms by which cells can control TGF-β signalling at the extracellular level. The reciprocal relationship between integrins and TGF-β is hereby of central importance. TGF-β induces the upregulation of a variety of integrins whereas on the other hand integrins regulate TGF-β through their shared spatial distribution, thereby inducing a positive feedback loop, which ultimately leads to increased TGF-β signalling (89,98). Considering the increased TGF-β signalling by means of pSMAD signal transduction as well as augmented circulating TGF-β levels in MFS (69,127), increased levels of signal facilitating factors at the extracellular TGF-β regulatory level are expected. Interestingly, of the α5, β5, and β1 integrin subunits examined, we found a downregulation at the transcriptional level. Out of the three subunits analysed on the transcriptional level, *ITGB1* is the most compelling due to its upregulation playing a vital part in fibrosis by mediating TGF-β activation (98). Therefore, we assessed ITGB at the protein level and, in contradiction to previous findings, we found ITGB1 to be less active in MFS than in control aortae. As integrin β subunits have been described to be the inducers of integrin heterocomplex activation (174), we can conclude that the whole complex that ITGB1 is part of remains more inactive in MFS patients than in control. Interestingly, *ITGB1* as well as *FBN1* and other ECM components are all targets of *miR-29b*, which, strikingly, we found to be upregulated in aortic tissue of MFS patients. In addition, *miR-29b* has

recently attracted a lot of attention due to its regulatory role in ECM synthesis and deposition as well as its involvement in the development of aortic aneurysms in MFS (175). Evolutionarily, miRNAs are quality mechanisms to inhibit protein translation as well as they induce mRNA degradation. Furthermore they are involved in most biological processes ranging from immune response regulation to tissue differentiation during development (183). miRNAs are part of an ample mRNA surveillance mechanism which exists to ensure that the gene product contains no errors and is suitable for protein translation (199). Mutations in *FBN1* might provoke an intracellular alert state, which induces the degradation of mutated gene transcripts and simultaneously of other targets, causing collateral damage. This assumption is supported by the finding that increased TGF-β signalling in MFS reduces the activity of an *miR-29b* repressor, thereby increasing its expression and facilitating the subsequent and possibly random degradation of target genes (175). On the other hand, seen that miRNAs are a quality control that functions not only in diseased states but also under normal conditions, it is debatable whether an evolutionary control mechanism this precise binds in such unspecific manners, that collateral damage is induced. Another explanation for the downregulation of TGF-β activating integrins is that despite the proposed model of increased contractility enhancing the shear forces applied by integrins (95), it has been shown that their pulling force requires an ECM threshold resistance (96). In MFS, the ECM of aortic tissue from the dilated zone might already be too damaged and degraded to provide the necessary mechanoresistance. Without mechanoresistance, integrins might lack the ability to properly bind their targets and perform their TGF-β controlling function. From this point of view, it would be interesting to assess integrin activity in non-dilated aortic tissue of MFS patients, which does not show signs of a compromised ECM structure yet. On the other hand, little is known about the integrin distribution with respect to lipid-rafts and non-lipid rafts. Rab1a for example, has been demonstrated to regulate β1 localization to lipid rafts, where their TGF-β presentation to its receptor complex induces TGF-β signal abrogation (200). These findings are supported by further studies showing that inactive integrins are tethered away from lipid rafts by cytoskeletal restraints (201). Therefore, the downregulation of TGF-β-activating integrins could be a cellular mechanism to compensate for the increased extracellular TGF-β. However, with respect to the TGF-β receptor compartmentalization, it could also be a pathological mechanism to withdraw TGF-β signal abrogation and turnover from the cell by means of preventing CAV-1 pathway-associated internalization. Further research into this field might be a promising contribution to elucidating the extracellular TGF-β-enabling mechanisms in MFS.

5.3. Transcriptome analysis in MFS

MFS is an astonishingly heterogeneous connective tissue disease with multi-organ affection. The recurrence of each individual *FBN1* mutation is so low, that large-scale studies have attempted to correlate disease phenotype with mutations clustered by type (8). A further problem is, that conventional sequencing methods analyse only the most commonly affected exons, which in itself carries the bias of neglecting to explore less commonly mutated gene regions. Furthermore, gene testing is not always available and the patient diagnosis is challenging due to the overlapping phenotype with other MFS-like diseases (36,188). Furthermore, most large-scale studies address the association between *FBN1* mutation type and severity of organ involvement as well as the specificity of organ involvement in relation with mutation type, but do not focus on aortic risk within-group correlations (8,49). For instance nonsense, frameshift, splice site mutations and gene deletions have been classified as haploinsufficient phenotype causative, whereas missense mutations have been classified as dominant negative mutations (202). As haploinsufficient mutations of *FBN1* are predicted to lead to reduced levels of FBN1, they have been associated with more severe phenotypes as dominant-negative mutations, which in turn are predicted to result in more phenotypic variability, qualitative defects of FBN1 and disorganization of the ECM (39,202,203). Despite this classification, studies are still too underpowered to conclusively evaluate differential risk of aortic dissection or need for clinical intervention between these groups (202). As our focus lies on the aortic risk assessment rather than on the overall multisystemic nature of the disease, we here assessed differential gene expression and GO enrichment analysis of 5 male patients who have undergone aortic reparatory surgery. Furthermore, in order to assess any differential expressions in genes that may facilitate the development of aortic aneurysms in the course of their formation, here we assessed the transcriptomic profile of the dilated zone of aneurysms which had undergone reparatory surgery and furthermore a more distal area of aortic tissue which did not show loss of structural integrity.

5.3.1. Genetic heterogeneity of aortic risk phenotype in MFS

Due to the limited genotype-phenotype correlation and low prediction of aortic risk, we analysed RNA extracted from VSMC from 5 male patients with a similar clinical history - all having undergone surgical aortic repair - by RNA sequencing. Despite the homogeneousness in terms of clinical outcome, we surprisingly found a large heterogeneity of *FBN1* mutations, including the absence of an *FBN1* mutation in any exonic region of the gene. This emphasizes even more so the immense variety of mutation types and the poor correlation of mutation type and aortic risk. As a matter of fact, even with a technique as powerful as RNA sequencing, we cannot exclude the possibility of intronic mutations in our samples. Furthermore, due to the challenging nature of MFS and the scoring system

for diagnosis which does not necessarily require gene analysis, it is possible that the two patients lacking a *FBN1* mutation were misdiagnosed. This is particularly likely as MFS-like systemic features such as familial thoracic aneurysms can also be caused by mutations in the TGF-β encoding genes as well as its receptors, independently of *FBN1* (187,188,204). Therefore, we cannot entirely exclude the possibility that our sample group contained two patients who did not have MFS. However, we were able to detect mutations in the other three patients. Furthermore, two out of three showed to have two different mutations in the *FBN1* gene at the same time, which has been rarely described. Thus far, compound heterozygous mutations have been identified in isolated case studies, predicting a particularly severe phenotype and lethality at a young age due to both *FBN1* alleles being affected, each at a particular gene locus (205). Here, we cannot be sure that in these two cases mutations are found only on one allele or are compound heterozygous. However, the number of mutations within the same gene, be it heterozygous or compound heterozygous may possibly be an indicator of disease severity and aortic risk. As we found in total three distinct mutant variants and therefore a vast genetic heterogeneity, we decided to cluster the MFS patients by their mutation type, in order to control for downstream molecular consequences that are potentially mutation type-dependent. However, we were unable to cluster the intronic mutation chr15 48416186 as our sample group did not provide another similar mutation. As pure intronic mutations cannot be detected by mRNA sequencing, this particular variation was associated with an intron-exon junction and an RNA splicing error leading to a missense mutation. The patient furthermore had a cysteine-substituting missense mutation, which allowed us to cluster him in a group with the second patient who had a cysteine substitution. However, we were unable to find a common gene profile between these two patients, even though both mutations are of the same dominant negative missense type. This is particularly interesting as in a normal clinical setting these two mutations would be the only ones detected by conventional molecular tests. Yet, they shared no other features but the mutation type and the aortic phenotype. This is supported by studies showing vast localized structural effects in terms of cbEGF-domain affected by a cysteine substitution (43,206). Furthermore, the cysteine substituting missense mutation chr15 48456714 had previously been described to not cause aortic risk in MFS (179), indicating that this particular gene loci is unlikely to be the principal driver of aneurysm formation. Nonetheless, using conventional molecular tests, this specific mutation would have been clustered into the same group as alternative aortic risk inducing missense mutations. Biases in analysis techniques as well as grouping errors could help explain the poor correlation found between mutation type and associated phenotype. Especially, as the patient with the mutation described as non-aortic risk cysteine substitution had a second mutation in an overall much more obscure gene region which thus far has not quite received the attention it deserves: the 3´UTR. The regulation of gene expression is not only

dependent on the pure mRNA containing the nucleotide sequences, but on numerous RNA-binding proteins which bind to domains all across the whole sequence. However, these are usually found in the 3´UTR region (207). In addition, the 3´UTR provides ample binding regions for miRNAs, which have been proposed to have co-evolved with their target genes (183). 3´UTR mutations, albeit scarcely studied in MFS, have been shown to be of importance in congenital heart diseases through their regulatory and controlling functions such as subcellular targeting as well as the control over the rate of mRNA translation and degradation (208). Surprisingly, considering the attention that *miR29b* has received in the past, the 3´UTR as MFS causative mutation region has been given little to no importance. Even more compellingly, taking into account the low recurrence of identical mutations in MFS, it is startling that a second patient of our MFS samples had the exact same mutation in the 3´UTR region. As 3´UTRs do not translate into a protein product, in the case of MFS this type of mutation cannot be clustered into any of the two major groups of either a haploinsufficient or a dominant negative phenotype. However, considering the patient with the double mutation of (1) a cysteine substitution in a domain that has been associated with low aortic risk and (2) the 3´UTR point mutation, and given his clinical history of aortic reparatory surgery, the driving force behind the aortic phenotype is likely to be the 3´UTR mutation. This is supported by the second patient who has also undergone aortic reparatory surgery and who only had this identical 3´UTR mutation. Based on the patient mutation type we therefore obtained three different patient clusters: 1) two patients with cysteine substitution, 2) two patients without *FBN1* mutation 3) two patients with 3´UTR mutation. With this design, the patient who had a cysteine substitution *and* a 3´UTR mutation was clustered once in group 1 and once in group 3. We then assessed any differential transcriptomic expression of the nondilated as well as the dilated zone in comparison with controls.

5.3.2. 3´UTR point mutation induces a distinct and transient transcriptomic profile

Our analysis revealed that in comparison to control mRNA, only mRNA extracted from VSCM from the non-dilated aortic zone of 3´UTR MFS patients showed differentially expressed genes. Possibly, in the case of the patient group with a cysteine substitution missense mutation, the molecular consequences based on the localized structural effects of this mutation type were to heterogeneous to find a common profile. The same would be true for the patients who did not have any mutation in the *FBN1* gene and might therefore not actually belong to the same mutation type as we cannot exclude other gene mutations. However, gene ontological analysis for the non-dilated aortic zone of 3´UTR mutations furthermore revealed a strong response to unfolded protein in the ER, which included the increased expression of cell stress-associated chaperones and the activation of endoplasmic reticulum-associated protein degradation (ERAD). The unfolded protein response (UPR) and ERAD are

primarily adaptive mechanisms to restore homeostasis when misfolded proteins are present, but, if unresolved, lead to pathophysiological changes in gene expression patterns (209). Classically, UPR and ERAD have been thought of as responses to the accumulation of misfolded protein, whereas a mutation in the 3´UTR is not predicted to be translated into a protein product at all (210). However, due to the many regulatory functions attributed to the 3´UTR, it is likely to be the cause of the ER stress itself by inducing a disequilibrium of ER homeostasis. Surprisingly, the differential gene expression as well as the compelling ER stress pathway association were only found in mRNA from the non-dilated aortic zone, whereas one might expect differences to be more prominent the more the disease develops. However, ER stress in response to unfolded protein has previously been shown to be transient and to appear before the onset of persistent and deleterious remodelling effects in cardiac tissue in a murine model of cardiac fibrosis. Even more compellingly, in the same model, pharmacologic inhibition of the stress response at the critical stage and before subsidence, prevented cardiac fibrosis and preserved heart function (211). This indicates, that the UPR coping mechanism in response to ER homeostasis disruption eventually manifests itself in the aortic phenotype. In addition, prolonged UPR has been shown to induce cardiac remodelling and fibrosis through pathogenic consequences such as cellular apoptosis and alterations in signalling pathways (212–214). Interestingly, these pathogenic consequences might well be attributed to the simultaneous implication of ER stress key players in the TGF-β signalling cascade by stabilizing the SMAD2-dependent signalling and inducing collagen deposition and cardiac remodelling (215,216). HSP90 is one of the most crucial candidates as it directly interacts with both TBRI and TBRII, regulates SMAD2 localization, and its inhibition leads to increased TGF-β receptor complex ubiquitination and degradation (191,217). However, other ER stress key players have also been shown to induce similar TGF-β stabilizing effects such as SEL1L and HSPA5 (218,219). Interestingly, it has recently been demonstrated that the effect of Losartan on fibrosis is attributed to the attenuation of ER stress, and, in particular, the inhibition of HSPA5 in chronic renal diseases (218). Targeted ER stress induction by a *cog* mutant of thyroglobulin is even able to promote the same phenotype as a mutation in *Col10a1*, as was demonstrated in a mouse model of the connective tissue disease metaphyseal chondrodysplasia type Schmid (MCDS). In addition, in the same study, ER stress levels have been shown to correlate with severity of MCDS, providing compelling evidence for the impact of ER stress on connective tissue disease outcome (220). Furthermore, the phenotype driving potential of the identified 3´UTR mutation in MFS is supported by its binding site for the novel and scarcely studied *miR-1252-5p*. As mRNAs mainly target 3´UTR sequences and act as mRNA degradation inducer, they are considered to be an evolutionary conserved quality control (183). Lacking the binding through mutation may lead to insufficient *FBN1* degradation, accumulation in the ER and consequentially ER

stress. The deregulation of miRNAs is a scarcely studied but intriguing new field in MFS, not at last due to the aforementioned *miR-29b*. Future research towards the involvement of miRNAs and their deregulation through 3´UTR mutation could be and interesting tool to further elucidate the disease development of MFS. Considering the previous results we therefore propose the following model of this novel identified *FBN1* 3´UTR mutation.

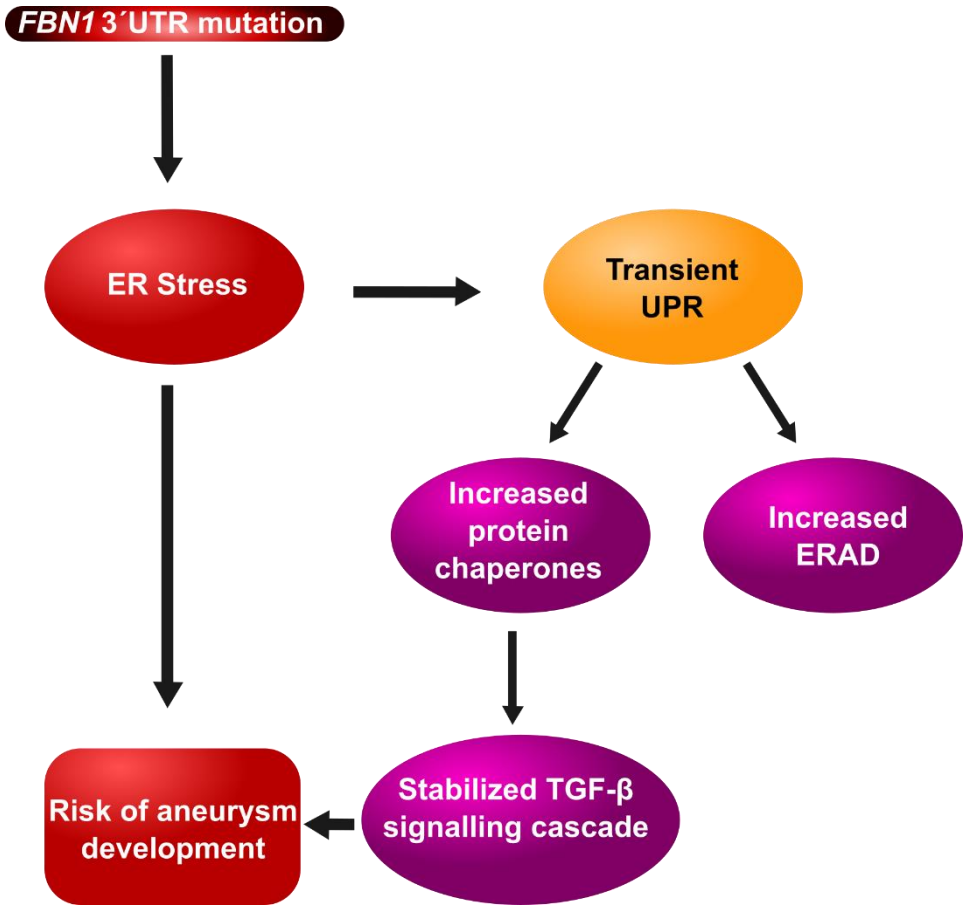

Figure 5.2. Proposed model of a novel FBN1 3' UTR mutation that drives the formation of aortic aneurysms through transient development of ER stress. *The 3' UTR mutation in the FBN1 gene drives aneurysm formation by increasing ER stress, possibly due to a homeostatic imbalance, and increasing transient UPR-associated target proteins, which simultaneously stabilize the TGF-β signalling cascade.*

Conclusions

6. Conclusions

1) The increased TGF-β signalling in VSMC form MFS patients is associated with the clathrin-dependent pathway.

2) The heightened TGF-β signalling at early endosomes is RAB5-dependent through the increased recruitment of the RAB5 effector SARA to early endosomes, thereby facilitating the SMAD2/TGF-β receptor complex binding, and enhancing the TGF-β signalling efficiency at early endosomes.

3) The increased signalling at early endosomes is accompanied by a reduced trafficking of TGF-β into EEA1/CAV-1-double positive endocytic structures, providing a signalling platform for EEA1 single-positive endosomes that facilitates the chronic TGF-β signal promotion in MFS.

4) The downregulation of TGF-β- and FBN1-binding integrins suggests a compensatory mechanism at the extracellular level.

5) A novel mutation in the 3´UTR is a potential driving force in MFS aneurysm formation through the induction of transient ER stress, the loss of cellular homeostasis, and the simultaneous stabilization of TGF-β signalling.

6) The inclusion of non-coding regions such as UTRs as a diagnostic criterion might provide new insights into thus far unknown patient clusters and could allow for a better assessment of aortic risk prediction in MFS patients.

References

7. References

1. Kodolitsch Y Von, De Backer J, Schüler H, Bannas P, Behzadi C, Bernhardt AM, et al. Perspectives on the revised ghent criteria for the diagnosis of marfan syndrome. Appl Clin Genet. 2015;8:137–55.

2. Dietz HC, Cutting GR, Pyeritz RE, Maslen CL, Sakai LY, Corson GM, et al. Marfan syndrome caused by a recurrent de novo missense mutation in the fibrillin gene. Nature. 1991 Jul;352(6333):337–9.

3. Perrucci GL, Rurali E, Gowran A, Pini A, Antona C, Chiesa R, et al. Vascular smooth muscle cells in Marfan syndrome aneurysm : the broken bricks in the aortic wall. Cell Mol Life Sci. 2016;

4. Collod-Beroud G, Le Bourdelles S, Ades L, Ala-Kokko L, Booms P, Boxer M, et al. Update of the UMD-FBN1 mutation database and creation of an FBN1 polymorphism database. Hum Mutat. 2003 Sep;22(3):199–208.

5. Sakai LY, Keene DR, Renard M, De Backer J. FBN1: The disease-causing gene for Marfan syndrome and other genetic disorders. Gene. 2016;591(1):279–91.

6. Milewicz DM. Treatment of Aortic Disease in Patients With Marfan Syndrome. Circulation. 2005;111(11):e150–7.

7. Karnebeek CDM Van, Naeff MSJ, Mulder BJM, Hennekam RCM, Offringa M. Natural history of cardiovascular manifestations in Marfan syndrome Natural history of cardiovascular manifestations in Marfan syndrome. 2001;(June 2008):129–37.

8. Faivre L, Collod-Beroud G, Loeys BL, Child A, Binquet C, Gautier E, et al. Effect of mutation type and location on clinical outcome in 1,013 probands with Marfan syndrome or related phenotypes and FBN1 mutations: an international study. Am J Hum Genet. 2007;81(3):454–66.

9. Attenhofer Jost CH, Greutmann M, Connolly HM, Weber R, Rohrbach M, Oxenius A, et al. Medical Treatment of Aortic Aneurysms in Marfan Syndrome and Other Heritable Conditions. Curr Cardiol Rev. 2014;161–71.

10. Finkbohner R, Johnston D, Crawford ES, Coselli J, Milewicz DM. Marfan syndrome. Long-term survival and complications after aortic aneurysm repair. Circulation. 1995 Feb;91(3):728–33.

11. Scherer LR, Arn PH, Dressel DA, Pyeritz RM, Haller JAJ. Surgical management of children and young adults with Marfan syndrome and pectus excavatum. J Pediatr Surg. 1988 Dec;23(12):1169–72.

12. Loeys BL, Dietz HC, Braverman AC, Callewaert BL, De Backer J, Devereux RB, et al. The revised Ghent nosology for the Marfan syndrome. J Med Genet. 2010 Jul;47(7):476–85.

13. Sponseller PD, Hobbs W, Riley LH 3rd, Pyeritz RE. The thoracolumbar spine in Marfan syndrome. J Bone Joint Surg Am. 1995 Jun;77(6):867–76.

14. Cohn RD, van Erp C, Habashi JP, Soleimani A a, Klein EC, Lisi MT, et al. Angiotensin II type 1 receptor blockade attenuates TGF-β-induced failure of muscle regeneration in multiple myopathic states. Nat Med. 2007;13(2):204–10.

15. Maumenee IH. The eye in the Marfan Syndrome. Trans Am Ophthalmol Soc. 1981;79:684–7337.

16. Karpman C, Aughenbaugh GL, Ryu JH. Pneumothorax and bullae in Marfan syndrome. Respiration. 2011;82(3):219–24.

17. Viveiro C, Rocha P, Carvalho C, Zarcos MM. Spontaneous pneumothorax as manifestation of Marfan syndrome. BMJ Case Rep. 2013;1–3.

18. Mo L, He Q, Wang Y, Dong B, He J. High prevalence of obstructive sleep apnea in Marfan's syndrome. Chin Med J (Engl). 2014;127(17):3150–5.

19. Kohler M, Pitcher A, Blair E, Risby P, Senn O, Forfar C, et al. The impact of obstructive sleep apnea on aortic disease in Marfan's syndrome. Respiration. 2013;86(1):39–44.

20. Colovati ME, da Silva LR, Takeno SS, Mancini TI, N Dutra AR, Guilherme RS, et al. Marfan syndrome with a complex chromosomal rearrangement including deletion of the FBN1 gene. Mol Cytogenet. 2012 Jan;5:5.

21. Robinson PN, Booms P, Katzke S, Ladewig M, Neumann L, Palz M, et al. Mutations of FBN1 and genotype-phenotype correlations in Marfan syndrome and related fibrillinopathies. Hum Mutat. 2002;20(3):153–61.

22. Ramirez F, Sakai LY, Rifkin DB, Dietz HC. Extracellular microfibrils in development and disease. Cell Mol Life Sci. 2007;64(18):2437–46.

23. Sakai LY, Keene DR, Engvall E. Fibrillin, A New 350-kD Glycoprotein, Is a Component ofExtracellular Microfibrils.pdf. 1986;103(6):2499–509.

24. Reinhardt DP, Ono RN, Notbohm H, Müller PK, Bächinger HP, Sakai LY. Mutations in Calcium-binding Epidermal Growth Factor Modules Render Fibrillin-1 Susceptible to Proteolysis A POTENTIAL DISEASE-CAUSING MECHANISM IN MARFAN SYNDROME. J Biol Chem. 2000;275(16):12339–45.

25. Handford P. Fibrillin-1, a calcium binding protein of extracellular matrix. Biochim Biophys Acta - Mol Cell Res. 2000;1498(2):84–90.

26. Whiteman P, Hutchinson S, Handford PA. Fibrillin-1 misfolding and disease. Antioxid Redox Signal. 2006;8(3–4):338–46.

27. Reinhard DP, Mechling DE, Boswell BA, Keene DR, Sakai LY, Bächinger HP. Calcium determines the shape of fibrillin. J Biol Chem. 1997;272(11):7368–73.

28. Jensen S a., Iqbal S, Bulsiewicz A, Handford P a. A microfibril assembly assay identifies different mechanisms of dominance underlying Marfan syndrome, stiff skin syndrome and acromelic dysplasias. Hum Mol Genet. 2015;24(15):4454–63.

29. Yuan X, Downing AK, Knott V, Handford PA. Solution structure of the transforming growth factor β-binding protein-like module, a domain associated with matrix fibrils. EMBO J. 1997 Nov;16(22):6659–66.

30. Isogai Z, Ono RN, Ushiro S, Keene DR, Chen Y, Mazzieri R, et al. Latent transforming growth factor β-binding protein 1 interacts with fibrillin and is a microfibril-associated protein. J Biol Chem. 2003 Jan;278(4):2750–7.

31. Bax D V., Bernard SE, Lomas A, Morgan A, Humphries J, Shuttleworth CA, et al. Cell Adhesion to Fibrillin-1 Molecules and Microfibrils Is Mediated by α5β1 and αvβ3 Integrins. J Biol Chem. 2003;278(36):34605–16.

32. Sakamoto H, Broekelmann T, Cheresh DA, Ramirez F, Mecham RP, Sakamoto H, et al. Cell Biology and Metabolism : Cell-type Specific Recognition of RGD- and Non-RGD-containing Cell Binding Domains in Fibrillin-1 Cell-type Specific Recognition of RGD- and Non-RGD-containing Cell Binding Domains in Fibrillin-1. 1996;271(9):4916–22.

33. Wallis DD, Putnam EA, Cretoiu JS, Carmical SG, Cao S-N, Thomas G, et al. Profibrillin-1 maturation by human dermal fibroblasts: proteolytic processing and molecular chaperones. J Cell Biochem. 2003 Oct;90(3):641–52.

34. Milewicz DM, Grossfield J, Cao SN, Kielty C, Covitz W, Jewett T. A mutation in FBN1 disrupts profibrillin processing and results in isolated skeletal features of the Marian syndrome. J Clin Invest. 1995;95(5):2373–8.

35. Raghunath M, Putnam E a, Ritty T, Hamstra D, Park ES, Tschödrich-Rotter M, et al. Carboxy-terminal conversion of profibrillin to fibrillin at a basic site by PACE/furin-like activity required for incorporation in the matrix. J Cell Sci. 1999;112 (Pt 7(7):1093–100.

36. Gillis E, Kempers M, Salemink S, Timmermans J, Cheriex EC, Bekkers SCAM, et al. An FBN1 Deep Intronic Mutation in a Familial Case of Marfan Syndrome : An Explanation for Genetically Unsolved Cases? 2014;6.

37. Groth K a., Gaustadnes M, Thorsen K, Østergaard JR, Jensen UB, Gravholt CH, et al. Difficulties in diagnosing Marfan syndrome using current FBN1 databases. Genet Med. 2015;18(November 2014):1–5.

38. Robinson PN, Godfrey M. The molecular genetics of Marfan syndrome and related microfibrillopathies. J Med Genet. 2000 Jan;37(1):9–25.

39. Judge DP, Biery NJ, Keene DR, Geubtner J, Myers L, Huso DL, et al. Evidence for a critical contribution of haploinsufficiency in the complex pathogenesis of Marfan syndrome. J Clin Invest. 2004 Jul;114(2):172–81.

40. Downing AK, Knott V, Werner JM, Cardy CM, Campbell ID, Handford PA. Solution structure of a pair of calcium-binding epidermal growth factor-like domains: implications for the Marfan syndrome and other genetic disorders. Cell. 1996 May;85(4):597–605.

41. Whiteman P, Handford PA. Defective secretion of recombinant fragments of fibrillin-1: Implications of protein misfolding for the pathogenesis of Marfan syndrome and related disorders. Hum Mol Genet. 2003;12(7):727–37.

42. Kettle S, Yuan X, Grundy G, Knott V, Downing AK, Handford PA. Defective calcium binding to fibrillin-1: consequence of an N2144S change for fibrillin-1 structure and function. J Mol Biol. 1999 Jan;285(3):1277–87.

43. Ji YS, Jensen S, McGettrick A, Willis AC, Whiteman P, Redfield C, et al. Structural consequences of cysteine substitutions C1977Y and C1977R in calcium-binding epidermal growth factor-like domain 30 of human fibrillin-1. J Biol Chem. 2004;279(49):51258–65.

44. Vollbrandt T, Tiedemann K, El-Hallous E, Lin G, Brinckmann J, John H, et al. Consequences of cysteine mutations in calcium-binding epidermal growth factor modules of fibrillin-1. J Biol Chem. 2004;279(31):32924–31.

45. Ng DK, Chau KW, Black C, Thomas TM, Mak KL, Boxer M. Neonatal Marfan syndrome: a case report. J Paediatr Child Health. 1999 Jun;35(3):321–3.

46. Schrijver I, Liu W, Odom R, Brenn T, Oefner P, Furthmayr H, et al. Premature termination mutations in FBN1: distinct effects on differential allelic expression and on protein and clinical phenotypes. Am J Hum Genet. 2002;71(2):223–37.

47. Baudhuin LM, Kotzer KE, Lagerstedt S a. Increased frequency of FBN1 truncating and splicing variants in Marfan syndrome patients with aortic events. Genet Med. 2014;17(November 2014):1–12.

48. Rommel K, Karck M, Haverich A, von Kodolitsch Y, Rybczynski M, Muller G, et al. Identification of 29 novel and nine recurrent fibrillin-1 (FBN1) mutations and genotype-phenotype correlations in 76 patients with Marfan syndrome. Hum Mutat. 2005 Dec;26(6):529–39.

49. Collod-Béroud G, Le Bourdelles S, Ades L, Ala-Kokko L, Booms P, Boxer M, et al. Update of the UMD-FBN1 mutation database and creation of an FBN1 polymorphism database. Hum Mutat. 2003;22(3):199–208.

50. Liu W, Schrijver I, Brenn T, Furthmayr H, Francke U. Multi-exon deletions of the FBN1 gene in Marfan syndrome. BMC Med Genet. 2001;2(1):11.

51. Hilhorst-Hofstee Y, Hamel BCJ, Verheij JBGM, Rijlaarsdam MEB, Mancini GMS, Cobben JM, et al. The clinical spectrum of complete FBN1 allele deletions. Eur J Hum Genet. 2011 Mar;19(3):247–52.

52. Liu W, Qian C, Comeau K, Brenn T, Furthmayr H, Francke U. Mutant fibrillin-1 monomers lacking EGF-like domains disrupt microfibril assembly and cause severe marfan syndrome. Hum Mol Genet. 1996 Oct;5(10):1581–7.

53. Neptune ER, Frischmeyer P a, Arking DE, Myers L, Bunton TE, Gayraud B, et al. Dysregulation of TGF-β activation contributes to pathogenesis in Marfan syndrome. Nat Genet. 2003;33(3):407–11.

54. Chaudhry SS, Cain S a., Morgan A, Dallas SL, Shuttleworth CA, Kielty CM. Fibrillin-1 regulates the bioavailability of TGF β1. J Cell Biol. 2007;176(3):355–67.

55. Dijke P, Arthur HM. Extracellular control of TGFβ signalling in vascular development and disease. 2007;8(november).

56. Isogai Z. Latent Transforming Growth Factor β-binding Protein 1 Interacts with Fibrillin and Is a Microfibril-associated Protein. J Biol Chem. 2003;278(4):2750–7.

57. Gordon KJ, Blobe GC. Role of transforming growth factor-β superfamily signaling pathways in human disease. Biochim Biophys Acta. 2008;1782(4):197–228.

58. Branton MH, Kopp JB. TGF-β and fibrosis. Microbes Infect. 1999 Dec;1(15):1349–65.

59. Varga J, Jimenez SA. Stimulation of normal human fibroblast collagen production and processing by transforming growth factor-β. Biochem Biophys Res Commun. 1986 Jul;138(2):974–80.

60. Overall CM, Wrana JL, Sodek J. Independent regulation of collagenase, 72-kDa progelatinase, and metalloendoproteinase inhibitor expression in human fibroblasts by transforming growth factor-β. J Biol Chem. 1989 Jan;264(3):1860–9.

61. Leask A, Abraham J. TGF- signaling and the fibrotic response. FASEB J. 2004;18(7):816–27.

62. Mori R, Kondo T, Ohshima T, Ishida Y, Mukaida N. Accelerated wound healing in tumor necrosis factor receptor p55-deficient mice with reduced leukocyte infiltration. FASEB J Off Publ Fed Am Soc Exp Biol. 2002 Jul;16(9):963–74.

63. Gillery P, Serpier H, Polette M, Bellon G, Clavel C, Wegrowski Y, et al. Gamma-interferon inhibits extracellular matrix synthesis and remodeling in collagen lattice cultures of normal and scleroderma skin fibroblasts. Eur J Cell Biol. 1992 Apr;57(2):244–53.

64. Bottinger EP, Letterio JJ, Roberts AB. Biology of TGF-β in knockout and transgenic mouse models. Kidney Int. 1997 May;51(5):1355–60.

65. Kulkarni AB, Karlsson S. Transforming growth factor-β 1 knockout mice. A mutation in one cytokine gene causes a dramatic inflammatory disease. Am J Pathol. 1993 Jul;143(1):3–9.

66. Habashi JP, Doyle JJ, Holm TM, Aziz H, Schoenhoff F, Bedja D, et al. Angiotensin II type 2 receptor signaling attenuates aortic aneurysm in mice through ERK antagonism. Science. 2011 Apr;332(6027):361–5.

67. Habashi JP, Judge DP, Holm TM, Cohn RD, Loeys BL, Cooper TK, et al. Losartan, an AT1 antagonist, prevents aortic aneurysm in a mouse model of Marfan syndrome. Science. 2006 Apr;312(5770):117–21.

68. Lavoie P, Robitaille G, Agharazii M, Ledbetter S, Lebel M, Larivière R. Neutralization of transforming growth factor-β attenuates hypertension and prevents renal injury in uremic rats. J Hypertens. 2005;23(10):1895–903.

69. Matt P, Schoenhoff F, Habashi J, Holm T, Van Erp C, Loch D, et al. Circulating transforming growth factor-β in Marfan syndrome. Circulation. 2009 Aug;120(6):526–32.

70. Nataatmadja M, West J, West M. Overexpression of transforming growth factor-?? is associated with increased hyaluronan content and impairment of repair in Marfan syndrome aortic aneurysm. Circulation. 2006;114:371–8.

71. Meng X, Nikolic-Paterson DJ, Lan HY. TGF-β: the master regulator of fibrosis. Nat Rev Nephrol. 2016;12(6):325–38.

72. Yu L, Border WA, Huang Y, Noble NA. TGF-β isoforms in renal fibrogenesis. Kidney Int. 2003 Sep;64(3):844–56.

73. Massague J. TGF-β signal transduction. Annu Rev Biochem. 1998;67:753–91.

74. Rifkin DB. Latent transforming growth factor-β (TGF-β) binding proteins: Orchestrators of TGF-β availability. J Biol Chem. 2005;280(9):7409–12.

75. Saharinen J, Keski-Oja J. Specific sequence motif of 8-Cys repeats of TGF-β binding proteins, LTBPs, creates a hydrophobic interaction surface for binding of small latent TGF-β. Mol Biol Cell. 2000 Aug;11(8):2691–704.

76. Annes JP, Munger JS, Rifkin DB. Making sense of latent TGFβ activation. J Cell Sci. 2003 Jan;116(Pt 2):217–24.

77. Ge G, Greenspan DS. BMP1 controls TGFβ1 activation via cleavage of latent TGFβ-binding protein. J Cell Biol. 2006 Oct;175(1):111–20.

78. Yu Q, Stamenkovic I. Cell surface-localized matrix metalloproteinase-9 proteolytically activates TGF-β and promotes tumor invasion and angiogenesis. Genes Dev. 2000 Jan;14(2):163–76.

79. Lu P, Takai K, Weaver VM, Werb Z. Extracellular matrix degradation and remodeling in development and disease. Cold Spring Harb Perspect Biol. 2011;1–25.

80. Krstic J, Santibanez JF. Transforming growth factor-β and matrix metalloproteinases: functional interactions in tumor stroma-infiltrating myeloid cells. ScientificWorldJournal. 2014;2014:521754.

81. Lyons RM, Keski-Oja J, Moses HL. Proteolytic activation of latent transforming growth factor-β from fibroblast-conditioned medium. J Cell Biol. 1988 May;106(5):1659–65.

82. Liu R-M, Desai LP. Reciprocal regulation of TGF-β and reactive oxygen species: A perverse cycle for fibrosis. Redox Biol. 2015 Dec;6:565–77.

83. Barcellos-Hoff MH, Dix TA. Redox-mediated activation of latent transforming growth factor-β1. Mol Endocrinol. 1996 Sep;10(9):1077–83.

84. Schultz-Cherry S, Murphy-Ullrich JE. Thrombospondin causes activation of latent transforming growth factor-β secreted by endothelial cells by a novel mechanism. J Cell Biol. 1993;122(4):923–32.

85. Chen Y. Controlling TGF-β signaling. 2000;627–44.

86. Ribeiro SM, Poczatek M, Schultz-Cherry S, Villain M, Murphy-Ullrich JE. The activation sequence of thrombospondin-1 interacts with the latency-associated peptide to regulate activation of latent transforming growth factor-β. J Biol Chem. 1999 May;274(19):13586–93.

87. Daniel C, Wiede J, Krutzsch HC, Ribeiro SMF, Roberts DD, Murphy-Ullrich JE, et al. Thrombospondin-1 is a major activator of TGF-β in fibrotic renal disease in the rat in vivo. Kidney Int. 2004 Feb;65(2):459–68.

88. Liu Z, Morgan S, Ren J, Wang Q, Annis DS, Mosher DF, et al. Thrombospondin-1 (TSP1) contributes to the development of vascular inflammation by regulating monocytic cell motility in mouse models of abdominal aortic aneurysm. Circ Res. 2015 Jul;117(2):129–41.

89. Munger JS, Sheppard D. Integrins , and the Extracellular Matrix. 2011;1–17.

90. Hynes RO. Integrins: Bidirectional, allosteric signaling machines. Cell. 2002;110(6):673–87.

91. Jovanovic J, Iqbal S, Jensen S, Mardon H, Handford P. Fibrillin-integrin interactions in health and disease. Biochem Soc Trans. 2008 Apr;36(Pt 2):257–62.

92. Streuli CH, Akhtar N. Signal co-operation between integrins and other receptor systems. Biochem J. 2009;418(3):491–506.

93. Ignotz RA, Heino J, Massagué J. Regulation of cell adhesion receptors by transforming growth factor-β. Regulation of vitronectin receptor and LFA-1. J Biol Chem. 1989;264(1):389–92.

94. Ignotz RA, Massague J. Cell adhesion protein receptors as targets for transforming growth factor-β action. Cell. 1987 Oct;51(2):189–97.

95. Worthington JJ, Klementowicz JE, Travis MA. TGF β: A sleeping giant awoken by integrins. Trends Biochem Sci. 2011;36(1):47–54.

96. Wipff P-J, Rifkin DB, Meister J-J, Hinz B. Myofibroblast contraction activates latent TGF-β1 from the extracellular matrix. J Cell Biol. 2007 Dec;179(6):1311–23.

97. Honda E, Yoshida K, Munakata H. Transforming growth factor-β upregulates the expression of integrin and related proteins in MRC-5 human myofibroblasts. Tohoku J Exp Med. 2010;220(4):319–27.

98. Reed NI, Jo H, Chen C, Tsujino K, Arnold TD, DeGrado WF, et al. The αvβ1 integrin plays a critical in vivo role in tissue fibrosis. Sci Transl Med. 2015 May;7(288):288ra79.

99. Manning G, Whyte DB, Martinez R, Hunter T, Sudarsanam S. The protein kinase complement of the human genome. Science. 2002 Dec;298(5600):1912–34.

100. Shi Y, Massagué J. Mechanisms of TGF-β signaling from cell membrane to the nucleus. Cell. 2003;113(6):685–700.

101. Di Guglielmo GM, Le Roy C, Goodfellow AF, Wrana JL. Distinct endocytic pathways regulate TGF-β receptor signalling and turnover. Nat Cell Biol. 2003;5(5):410–21.

102. Sankar S, Mahooti-Brooks N, Centrella M, McCarthy TL, Madri JA. Expression of transforming growth factor type III receptor in vascular endothelial cells increases their responsiveness to transforming growth factorβ2. J Biol Chem. 1995 Jun;270(22):13567–72.

103. Hart PJ, Deep S, Taylor AB, Shu Z, Hinck CS, Hinck AP. Crystal structure of the human TβR2 ectodomain–TGF-β3 complex. Nat Struct Biol. 2002;(26587):203–8.

104. Huse M, Chen YG, Massague J, Kuriyan J. Crystal structure of the cytoplasmic domain of the type I TGF β receptor in complex with FKBP12. Cell. 1999 Feb;96(3):425–36.

105. Zhao B, Wang Q, Du J, Luo S, Xia J, Chen Y-G. PICK1 promotes caveolin-dependent degradation of TGF-β type I receptor. Cell Res. 2012;22(10):1467–78.

106. McMahon HT, Boucrot E. Molecular mechanism and physiological functions of clathrin-mediated endocytosis. Nat Rev Mol Cell Biol. 2011;12(8):517–33.

107. Doherty GJ, McMahon HT. Mechanisms of endocytosis. Annu Rev Biochem. 2009;78:857–902.

108. Grant BD, Donaldson JG. Pathways and mechanisms of endocytotic recycling. Mol Cell Biol. 2009;10(9):597–604.

109. Derynck R, Zhang Y, Feng XH. Smads: transcriptional activators of TGF-β responses. Cell. 1998 Dec;95(6):737–40.

110. Derynck R, Gelbart WM, Harland RM, Heldin CH, Kern SE, Massague J, et al. Nomenclature: vertebrate mediators of TGFβ family signals. Vol. 87, Cell. United States; 1996. p. 173.

111. Savage C, Das P, Finelli AL, Townsend SR, Sun CY, Baird SE, et al. Caenorhabditis elegans genes sma-2, sma-3, and sma-4 define a conserved family of transforming growth factor β pathway components. Proc Natl Acad Sci U S A. 1996 Jan;93(2):790–4.

112. Feng X-H, Derynck R. Specificity and Versatility in Tgf-B Signaling Through Smads. Annu Rev Cell Dev Biol. 2005;21(1):659–93.

113. Persson U, Izumi H, Souchelnytskyi S, Itoh S, Grimsby S, Engstrom U, et al. The L45 loop in type I receptors for TGF-β family members is a critical determinant in specifying Smad isoform activation. FEBS Lett. 1998 Aug;434(1–2):83–7.

114. Chen YG, Hata a, Lo RS, Wotton D, Shi Y, Pavletich N, et al. Determinants of specificity in TGF-β signal transduction. Genes Dev. 1998;12(14):2144–52.

115. Tsukazaki T, Chiang TA, Davison AF, Attisano L, Wrana JL. SARA, a FYVE domain protein that recruits Smad2 to the TGFβ receptor. Cell. 1998 Dec;95(6):779–91.

116. Itoh F, Divecha N, Brocks L, Oomen L, Janssen H, Calafat J, et al. The FYVE domain in Smad anchor for receptor activation (SARA) is sufficient for localization of SARA in early endosomes and regulates TGF-β/Smad signalling. Genes Cells. 2002 Mar;7(3):321–31.

117. Hu Y. SARA, a FYVE domain protein, affects Rab5-mediated endocytosis. J Cell Sci. 2002;115(24):4755–63.

118. Attisano L, Wrana JL. Smads as transcriptional co-modulators. Curr Opin Cell Biol. 2000 Apr;12(2):235–43.

119. Runyan CE, Schnaper HW, Poncelet AC. The role of internalization in transforming growth factor β1-induced Smad2 association with Smad anchor for receptor activation (SARA) and Smad2-dependent signaling in human mesangial cells. J Biol Chem. 2005;280(9):8300–8.

120. Xu L, Chen YG, Massagué J. The nuclear import function of Smad2 is masked by SARA and unmasked by TGFβ-dependent phosphorylation. Nat Cell Biol. 2000;2(8):559–62.

121. Jonk LJ, Itoh S, Heldin CH, ten Dijke P, Kruijer W. Identification and functional characterization of a Smad binding element (SBE) in the JunB promoter that acts as a transforming growth factor-β, activin, and bone morphogenetic protein-inducible enhancer. J Biol Chem. 1998 Aug;273(33):21145–52.

122. Dennler S, Itoh S, Vivien D, Dijke P, Gauthier J. Direct binding of Smad3 and Smad4 to critical TGFb inducible elements in the promoter of human plasminogen activator inhibitor type 1 gene. 1998;17(11):1–10.

123. Kang Y, Chen C-R, Massague J. A self-enabling TGFβ response coupled to stress signaling: Smad engages stress response factor ATF3 for Id1 repression in epithelial cells. Mol Cell. 2003 Apr;11(4):915–26.

124. Pan X, Chen Z, Huang R, Yao Y, Ma G. Transforming growth factor β1 induces the expression of collagen type I by DNA methylation in cardiac fibroblasts. PLoS One. 2013;8(4):e60335.

125. McGowan SE, McNamer R. Transforming growth factor-β increases elastin production by neonatal rat lung fibroblasts. Am J Respir Cell Mol Biol. 1990 Oct;3(4):369–76.

126. Yuan S-M, Ma H-H, Zhang R-S, Jing H. Transforming growth factor-β signaling pathway in Marfan's syndrome: a preliminary histopathological study. Vasa. 2011 Sep;40(5):369–74.

127. Crosas-Molist E, Meirelles T, Lopez-Luque J, Serra-Peinado C, Selva J, Caja L, et al. Vascular Smooth Muscle Cell Phenotypic Changes in Patients With Marfan Syndrome. Arterioscler Thromb Vasc Biol. 2015;960–72.

128. Mitchell H, Choudhry A, Pagano RE, Loef EB. Ligand-dependent and -independent Transforming Growth Factor- β Receptor Recycling Regulated by Clathrin-mediated Endocytosis and Rab11. Mol Biol Cell. 2004;15:4166–78.

129. Zhao B, Chen Y. Regulation of TGF- β Signal Transduction. 2014;2014.

130. Nabi IR, Le PU. Caveolae/raft-dependent endocytosis. J Cell Biol. 2003;161(4):673–7.

131. Thomsen P, Roepstorff K, Stahlhut M, van Deurs B. Caveolae Are Highly Immobile Plasma Membrane Microdomains, Which Are not Involved in Constitutive Endocytic Trafficking. Mol Biol Cell. 2002;13(1):238–50.

132. Le Roy C, Wrana JL. Clathrin- and non-clathrin-mediated endocytic regulation of cell signalling. Nat Rev Mol Cell Biol. 2005;6(2):112–26.

133. Pelkmans L, Bürli T, Zerial M, Helenius A. Caveolin-stabilized membrane domains as multifunctional transport and sorting devices in endocytic membrane traffic. Cell. 2004;118(6):767–80.

134. Bizet AA, Liu K, Tran-Khanh N, Saksena A, Vorstenbosch J, Finnson KW, et al. The TGF-β co-receptor, CD109, promotes internalization and degradation of TGF-β receptors. Biochim Biophys Acta - Mol Cell Res. 2011;1813(5):742–53.

135. Hayashi H, Abdollah S, Qiu Y, Cai J, Xu YY, Grinnell BW, et al. The MAD-related protein Smad7 associates with the TGFβ receptor and functions as an antagonist of TGFβ signaling. Cell. 1997 Jun;89(7):1165–73.

136. Afrakhte M, Moren A, Jossan S, Itoh S, Sampath K, Westermark B, et al. Induction of inhibitory Smad6 and Smad7 mRNA by TGF-β family members. Biochem Biophys Res Commun. 1998 Aug;249(2):505–11.

137. Ruiz-Ortega M, Rodríguez-Vita J, Sanchez-Lopez E, Carvajal G, Egido J. TGF-β signaling in vascular fibrosis. Cardiovasc Res. 2007;74(2):196–206.

138. Finnson KW, Tam BYY, Liu K, Marcoux A, Lepage P, Roy S, et al. Identification of CD109 as part of the TGF-β receptor system in human keratinocytes. FASEB J Off Publ Fed Am Soc Exp Biol. 2006 Jul;20(9):1525–7.

139. Ito T, Williams JD, Fraser DJ, Phillips AO. Hyaluronan regulates transforming growth factor-β1 receptor compartmentalization. J Biol Chem. 2004;279(24):25326–32.

140. Ito T, Williams JD, Fraser D, Phillips AO. Hyaluronan attenuates transforming growth factor-β1-mediated signaling in renal proximal tubular epithelial cells. Am J Pathol. 2004 Jun;164(6):1979–88.

141. Xiao LZ, Topley N, Ito T, Phillips A. Interleukin-6 regulation of transforming growth factor (TGF)-β receptor compartmentalization and turnover enhances TGF-β1 signaling. J Biol Chem. 2005;280(13):12239–45.

142. Atfi A, Dumont E, Colland F, Bonnier D, L'helgoualc'h A, Prunier C, et al. The disintegrin and metalloproteinase ADAM12 contributes to TGF-β signaling through interaction with the type II receptor. J Cell Biol. 2007 Jul;178(2):201–8.

143. Yan X, Liao H, Cheng M, Shi X, Lin X, Feng X, et al. Smad7 Protein Interacts with Receptor-regulated Smads (R-Smads) to Inhibit Transforming Growth Factor-β (TGF-β)/Smad Signaling. 2016;291(1):382–92.

144. Zhang S, Fei T, Zhang L, Zhang R, Chen F, Ning Y, et al. Smad7 antagonizes transforming growth factor β signaling in the nucleus by interfering with functional Smad-DNA complex formation. Mol Cell Biol. 2007 Jun;27(12):4488–99.

145. He K, Yan X, Li N, Dang S, Xu L, Zhao B, et al. Internalization of the TGF-β type I receptor into caveolin-1 and EEA1 double-positive early endosomes. Cell Res. 2015;738–52.

146. Balogh P, Magyar M, Szabó A, Müllner N, Likó I, Patócs A, et al. The subcellular compartmentalization of TGFβ-RII and the dynamics of endosomal formation during the signaling events: An in vivo study on rat mesothelial cells. Eur J Cell Biol. 2015;94(5):204–13.

147. Katzmann DJ, Babst M, Emr SD. Ubiquitin-dependent sorting into the multivesicular body pathway requires the function of a conserved endosomal protein sorting complex, ESCRT-I. Cell. 2001 Jul;106(2):145–55.

148. Benke K, Bence Á, Szilveszter B, Tarr F, Nagy ZB, Pólos M, et al. The role of transforming growth factor-β in Marfan syndrome. Cardiol J. 2013;20(3):227–34.

149. Qi M, Elion EA. MAP kinase pathways. J Cell Sci. 2005 Aug;118(Pt 16):3569–72.

150. Lee MK, Pardoux C, Hall MC, Lee PS, Warburton D, Qing J, et al. TGF-β activates Erk MAP kinase signalling through direct phosphorylation of ShcA. EMBO J. 2007;26(17):3957–67.

151. Holm TM, Habashi JP, Doyle JJ, Bedja D, Chen Y, van Erp C, et al. Noncanonical TGFβ signaling contributes to aortic aneurysm progression in Marfan syndrome mice. Science. 2011 Apr;332(6027):358–61.

152. Yamashita M, Fatyol K, Jin C, Wang X, Liu Z, Zhang YE. TRAF6 mediates Smad-independent activation of JNK and p38 by TGF-β. 2009;31(6):918–24.

153. Yu JSL, Ramasamy TS, Murphy N, Holt MK, Czapiewski R, Wei S-K, et al. PI3K/mTORC2 regulates TGF-β/Activin signalling by modulating Smad2/3 activity via linker phosphorylation. Nat Commun. 2015 May;6:7212.

154. Javelaud D, Mauviel A. Crosstalk mechanisms between the mitogen-activated protein kinase pathways and Smad signaling downstream of TGF-β: implications for carcinogenesis. Oncogene. 2005 Aug;24(37):5742–50.

155. Rodriguez-Vita J, Sanchez-Lopez E, Esteban V, Ruperez M, Egido J, Ruiz-Ortega M. Angiotensin II activates the Smad pathway in vascular smooth muscle cells by a transforming growth factor-β-independent mechanism. Circulation. 2005 May;111(19):2509–17.

156. Kupfahl C, Pink D, Friedrich K, Zurbrugg HR, Neuss M, Warnecke C, et al. Angiotensin II directly increases transforming growth factor β1 and osteopontin and indirectly affects collagen mRNA expression in the human heart. Cardiovasc Res. 2000 Jun;46(3):463–75.

157. Gray MO, Long CS, Kalinyak JE, Li HT, Karliner JS. Angiotensin II stimulates cardiac myocyte hypertrophy via paracrine release of TGF-β 1 and endothelin-1 from fibroblasts. Cardiovasc Res. 1998 Nov;40(2):352–63.

158. Wenzel S, Taimor G, Piper HM, Schluter KD. Redox-sensitive intermediates mediate angiotensin II-induced p38 MAP kinase activation, AP-1 binding activity, and TGF-β expression in adult ventricular cardiomyocytes. FASEB J Off Publ Fed Am Soc Exp Biol. 2001 Oct;15(12):2291–3.

159. Rosenkranz S. TGF-β1 and angiotensin networking in cardiac remodeling. Cardiovasc Res. 2004;63(3):423–32.

160. Jiang F, Liu GS, Dusting GJ, Chan EC. NADPH oxidase-dependent redox signaling in TGF-β-mediated fibrotic responses. Redox Biol. 2014;2(1):267–72.

161. Murillo MM, Carmona-Cuenca I, Del Castillo G, Ortiz C, Roncero C, Sanchez A, et al. Activation of NADPH oxidase by transforming growth factor-β in hepatocytes mediates up-regulation of epidermal growth factor receptor ligands through a nuclear factor-kappaB-dependent mechanism. Biochem J. 2007 Jul;405(2):251–9.

162. Loeys BL, Chen J, Neptune ER, Judge DP, Podowski M, Holm T, et al. A syndrome of altered cardiovascular, craniofacial, neurocognitive and skeletal development caused by mutations in TGFBR1 or TGFBR2. Nat Genet. 2005 Mar;37(3):275–81.

163. Loeys BL, Dietz HC, Braverman AC, Callewaert BL, Backer J De, Devereux RB, et al. The revised Ghent nosology for the Marfan syndrome. J Med Genet. 2010;47(7):476–85.

164. Liao Y, Smyth GK, Shi W. The Subread aligner: Fast, accurate and scalable read mapping by seed-and-vote. Nucleic Acids Res. 2013;41(10).

165. Liao Y, Smyth GK, Shi W. featureCounts: an efficient general purpose program for assigning sequence reads to genomic features. Bioinformatics. 2014 Apr;30(7):923–30.

166. Law CW, Chen Y, Shi W, Smyth GK. voom: precision weights unlock linear model analysis tools for RNA-seq read counts. Genome Biol. 2014;15(2):R29.

167. Ritchie ME, Phipson B, Wu D, Hu Y, Law CW, Shi W, et al. limma powers differential expression analyses for RNA-sequencing and microarray studies. Nucleic Acids Res. 2015 Apr;43(7):e47.

168. Carmona-Saez P, Chagoyen M, Tirado F, Carazo JM, Pascual-Montano A. GENECODIS: a web-based tool for finding significant concurrent annotations in gene lists. Genome Biol. 2007;8(1):R3.

169. Tarca AL, Draghici S, Khatri P, Hassan SS, Mittal P, Kim J-S, et al. A novel signaling pathway impact analysis. Bioinformatics. 2009 Jan;25(1):75–82.

170. Cook JR, Clayton NP, Carta L, Galatioto J, Chiu E, Smaldone S, et al. Dimorphic Effects of Transforming Growth Factor-β Signaling During Aortic Aneurysm Progression in Mice Suggest a Combinatorial Therapy for Marfan Syndrome. Arterioscler Thromb Vasc Biol. 2015.

171. Gomez D, Kessler K, Michel JB, Vranckx R. Modifications of chromatin dynamics control smad2 pathway activation in aneurysmal smooth muscle cells. Circ Res. 2013;113(7):881–90.

172. Wu G, Chen YG, Ozdamar B, Gyuricza C a, Chong P a, Wrana JL, et al. Structural basis of Smad2 recognition by the Smad anchor for receptor activation. Science. 2000;287(5450):92–7.

173. Bhuin T, Roy JK. Rab proteins: The key regulators of intracellular vesicle transport. Exp Cell Res. 2014;328(1):1–19.

174. Geiger B, Spatz JP, Bershadsky AD. Environmental sensing through focal adhesions. Nat Rev Mol Cell Biol. 2009 Jan;10(1):21–33.

175. Merk DR, Chin JT, Dake BA, Maegdefessel L, Miller MO, Kimura N, et al. MiR-29b participates in early aneurysm development in Marfan syndrome. Circ Res. 2012;110(2):312–24.

176. Chou J, Lin JH, Brenot A, Kim J, Provot S, Werb Z. GATA3 suppresses metastasis and modulates the tumour microenvironment by regulating microRNA-29b expression. Nat Cell Biol. 2013 Feb;15(2):201–13.

177. Cushing L, Kuang PP, Qian J, Shao F, Wu J, Little F, et al. miR-29 is a major regulator of genes associated with pulmonary fibrosis. Am J Respir Cell Mol Biol. 2011;45(2):287–94.

178. Aalberts J, Schuurman AG, Pals G, Hamel BCJ, Bosman G, Hilhorst-Hofstee Y, et al. Recurrent and founder mutations in the netherlands: Extensive clinical variability in Marfan syndrome patients with a single novel recurrent fibrillin-1 missense mutation. 2010;18(2):85–9.

179. Ades LC, Holman KJ, Brett MS, Edwards MJ, Bennetts B. Ectopia lentis phenotypes and the FBN1 gene. Am J Med Genet A. 2004;126A(3):284–9.

180. Tabas-Madrid D, Nogales-Cadenas R, Pascual-Montano A. GeneCodis3: a non-redundant and modular enrichment analysis tool for functional genomics. Nucleic Acids Res. 2012 Jul;40(Web Server issue):W478-83.

181. Nogales-Cadenas R, Carmona-Saez P, Vazquez M, Vicente C, Yang X, Tirado F, et al. GeneCodis: interpreting gene lists through enrichment analysis and integration of diverse biological information. Nucleic Acids Res. 2009 Jul;37(Web Server issue):W317-22.

182. Morin RD, Connor MDO, Griffith M, Kuchenbauer F, Delaney A, Prabhu A, et al. Application of massively parallel sequencing to microRNA profiling and discovery in human embryonic stem cells. Genome Res. 2008;610–21.

183. Meunier J, Lemoine F, Soumillon M, Liechti A, Weier M, Guschanski K, Hu H, Khaitovich P KH. Birth and expression evolution of mammalian microRNA genes. Genome Res. 2013;1–12.

184. Merk DR, Chin JT, Dake BA, Maegdefessel L, Miller MO, Kimura N, et al. miR-29b Participates in Early Aneurysm Development in Marfan Syndrome. 2012;

185. Ott CE, Grünhagen J, Jäger M, Horbelt D, Schwill S, Kallenbach K, et al. MicroRNAs differentially expressed in postnatal aortic development downregulate elastin via 3' UTR and coding-sequence binding sites. PLoS One. 2011;6(1).

186. Panopoulou E, Gillooly DJ, Wrana JL, Zerial M, Stenmark H, Murphy C, et al. Early endosomal regulation of Smad-dependent signaling in endothelial cells. J Biol Chem. 2002;277(20):18046–52.

187. Gallo EM, Loch DC, Habashi JP, Calderon JF, Chen Y, Bedja D, et al. Angiotensin II-dependent TGF-β signaling contributes to Loeys-Dietz syndrome vascular pathogenesis. J Clin Invest. 2014;124(1):448–60.

188. Boileau C, Guo D-C, Hanna N, Regalado ES, Detaint D, Gong L, et al. TGFB2 mutations cause familial thoracic aortic aneurysms and dissections associated with mild systemic features of Marfan syndrome. Nat Genet. 2012 Jul;44(8):916–21.

189. Goumans MJ, Valdimarsdottir G, Itoh S, Lebrin F. Activin receptor-like kinase (ALK) 1 is an antagonistic mediator of lateral TGF [β]/ALK5 signaling. Mol Cell. 2003;12:817–28.

190. González-Núñez M, Muñoz-Félix JM, López-Novoa JM. The ALK-1/Smad1 pathway in cardiovascular physiopathology. A new target for therapy? Biochim Biophys Acta - Mol Basis Dis. 2013;1832(10):1492–510.

191. Huang F, Chen Y-G. Regulation of TGF-β receptor activity. Cell Biosci. 2012;2(1):9.

192. Fortini ME, Bilder D. Endocytic regulation of Notch signaling. Curr Opin Genet Dev. 2009;19(4):323–8.

193. Yan X, Lin Z, Chen F, Zhao X, Chen H, Ning Y, et al. Human BAMBI cooperates with Smad7 to inhibit transforming growth factor-β signaling. J Biol Chem. 2009 Oct;284(44):30097–104.

194. Lawe DC, Patki V, Heller-harrison R, Lambright D, Corvera S. The FYVE Domain of Early Endosome Antigen 1 Is Required for Both Phosphatidylinositol 3-Phosphate and Rab5 Binding. 2000;275(5):3699–705.

195. Lobanova ES, Finkelstein S, Skiba NP, Arshavsky VY. Proteasome overload is a common stress factor in multiple forms of inherited retinal degeneration. Proc Natl Acad Sci U S A. 2013 Jun;110(24):9986–91.

196. Vardouli L, Vasilaki E, Papadimitriou E, Kardassis D, Stournaras C. A novel mechanism of TGFβ-induced actin reorganization mediated by Smad proteins and Rho GTPases. FEBS J. 2008;275(16):4074–87.

197. Bhowmick NA, Zent R, Ghiassi M, McDonnell M, Moses HL. Integrin b1 Signaling is Necessary for Transforming Growtn Factor-b Activation of p38MAPK and Epithelial Plasticity. J Biol Chem. 2001;276(50):46707–13.

198. Pankov R, Cukierman E, Katz BZ, Matsumoto K, Lin DC, Lin S, et al. Integrin dynamics and matrix assembly: Tensin-dependent translocation of alpha5β1 integrins promotes early fibronectin fibrillogenesis. J Cell Biol. 2000;148(5):1075–90.

199. Moraes K. RNA Surveillance: Molecular Approaches in Transcript Quality Control and their Implications in Clinical Diseases. Mol Med. 2010;16(1–2):1.

200. Wang C, Yoo Y, Fan H, Kim E, Guan KL, Guan JL. Regulation of integrin β1 recycling to lipid rafts by Rab1a to promote cell migration. J Biol Chem. 2010;285(38):29398–405.

201. Leitinger B, Hogg N. The involvement of lipid rafts in the regulation of integrin function. J Cell Sci. 2002 Mar;115(Pt 5):963–72.

202. Landis BJ, Veldtman GR, Ware SM. Genotype – phenotype correlations in Marfan syndrome. 2017;8–11.

203. Franken R, Teixido-Tura G, Brion M, Forteza A, Rodriguez-Palomares J, Gutierrez L, et al. Relationship between fibrillin-1 genotype and severity of cardiovascular involvement in Marfan syndrome. Heart. 2017;heartjnl-2016-310631.

204. Lindsay ME, Schepers D, Bolar NA, Doyle JJ, Gallo E, Fert-Bober J, et al. Loss-of-function mutations in TGFB2 cause a syndromic presentation of thoracic aortic aneurysm. Nat Genet. 2012 Jul;44(8):922–7.

205. Karttunen L, Raghunath M, Lönnqvist L, Peltonen L. A compound-heterozygous Marfan patient: two defective fibrillin alleles result in a lethal phenotype. Am J Hum Genet. 1994;55(6):1083–91.

206. Schrijver I, Liu W, Brenn T, Furthmayr H, Francke U. Cysteine substitutions in epidermal growth factor-like domains of fibrillin-1: distinct effects on biochemical and clinical phenotypes. Am J Hum Genet. 1999;65(4):1007–20.

207. Szostak E, Gebauer F. Translational control by 3'-UTR-binding proteins. Brief Funct Genomics. 2013;12(1):58–65.

208. Reamon-Buettner SM, Cho S-H, Borlak J. Mutations in the 3'-untranslated region of GATA4 as molecular hotspots for congenital heart disease (CHD). BMC Med Genet. 2007;8:38.

209. Bateman JF, Boot-Handford RP, Lamandé SR. Genetic diseases of connective tissues: cellular and extracellular effects of ECM mutations. Nat Rev Genet. 2009;10(3):173–83.

210. Boot-Handford RP, Briggs MD. The unfolded protein response and its relevance to connective tissue diseases. Cell Tissue Res. 2010;339(1):197–211.

211. Groenendyk J, Lee D, Jung J, Dyck JRB, Lopaschuk GD, Agellon LB, et al. Inhibition of the unfolded protein response mechanism prevents cardiac fibrosis. PLoS One. 2016;11(7):1–15.

212. Szegezdi E, Logue SE, Gorman AM, Samali A. Mediators of endoplasmic reticulum stress-induced apoptosis. EMBO Rep. 2006;7(9):880–5.

213. Zhang K, Kaufman RJ. Signaling the unfolded protein response from the endoplasmic reticulum. J Biol Chem. 2004;279(25):25935–8.

214. Ayala P, Montenegro J, Vivar R, Letelier A, Urroz PA, Copaja M, et al. Attenuation of endoplasmic reticulum stress using the chemical chaperone 4-phenylbutyric acid prevents cardiac fibrosis induced by isoproterenol. Exp Mol Pathol. 2012 Feb;92(1):97–104.

215. García R, Merino D, Gómez JM, Nistal JF, Hurlé MA, Cortajarena AL, et al. Extracellular heat shock protein 90 binding to TGFβ receptor I participates in TGFβ-mediated collagen production in myocardial fibroblasts. Cell Signal. 2016;28(10):1563–79.

216. Lee S Bin, Lim A, Rah DK, Kim KS, Min HJ. Modulation of heat shock protein 90 affects TGF-β-induced collagen synthesis in human dermal fibroblast cells. Tissue Cell. 2016;48(6):616–23.

217. Lönn P, Morén A, Raja E, Dahl M, Moustakas A. Regulating the stability of TGFβ receptors and Smads. 2009;21–35.

218. Kim H, Baek CH, Lee RB, Chang JW, Yang WS, Lee SK. Anti-fibrotic effect of losartan, an angiotensin II receptor blocker, is mediated through inhibition of ER stress via up-regulation of SIRT1, followed by induction of HO-1 and thioredoxin. Int J Mol Sci. 2017;18(2):1–17.

219. Cattaneo M, Orlandini S, Beghelli S, Moore PS, Sorio C, Bonora A, et al. SEL1L expression in pancreatic adenocarcinoma parallels SMAD4 expression and delays tumor growth in vitro and in vivo. Oncogene. 2003;22(41):6359–68.

220. Rajpar MH, McDermott B, Kung L, Eardley R, Knowles L, Heeran M, et al. Targeted induction of endoplasmic reticulum stress induces cartilage pathology. PLoS Genet. 2009 Oct;5(10):e1000691.

Appendix

8. Appendix

Altered TGF-β endocytic trafficking contributes to the increased signaling in Marfan syndrome

Anna-Maria Siegert[a,*], Carla Serra-Peinado[a,*], Enric Gutiérrez-Martínez[a], Fernando Rodríguez-Pascual[b], Isabel Fabregat[c] and Gustavo Egea[a,d,e,**]

[a]Departamento de Biomedicina, Facultad de Medicina y Ciencias de la Salud, C/Casanova 143, Universidad de Barcelona, 08036 Barcelona, Spain

[b]Centro de Biología Molecular Severo Ochoa, CSIC-UAM, Calle Nicolás Cabrera 1, 28049, Madrid, Spain

[c]Institut d'Investigacions Biomèdiques de Bellvitge (IDIBELL), Avinguda de la Granvia 199, 08908, L'Hospitalet de Llobregat, Barcelona, Spain

[d]Institut d'Investigacions Biomèdiques August Pi I Sunyer, IDIBAPS, Carrer del Rosselló 149, 08036 Barcelona, Spain

[e]Institut de Nanociència I Nanotecnologia, IN2UB, Universitat de Barcelona, Barcelona, Spain

*Contributed equally to this work

** Corresponding author:

Gustavo Egea

Dept. Biomedicina

Facultad de Medicina y Ciencias de la Salud

Universidad de Barcelona

c/ Casanova 143,

08036 Barcelona (Spain)

Tel. (+34) 934021909

E-mail: gegea@ub.edu

Abstract

The main cardiovascular alteration in Marfan syndrome (MFS) is the formation of aortic aneurysms in which augmented TGF-β signaling is a molecular link between the genetic mutation of fibrillin-1 and the disease onset. The compartmentalization of TGF-β endocytic trafficking has been shown to determine the signaling response in which clathrin-dependent internalization leads to TGF-β signal propagation and caveolin-1 (CAV-1) associated internalization leads to signal abrogation. We here studied the contribution of the endocytic trafficking compartmentalization to the increased TGF-β signaling in vascular smooth muscle cells (VSMC) from MFS patients. We examined molecular components involved in the clathrin- (SARA, SMAD2, RAB5) and caveolin-1- (SMAD7, SMURF2 and RAB7) dependent endocytosis. Marfan VSMC showed higher recruitment of SARA and SMAD2 to membranes and their increased interaction with TGF-β receptor II as well as higher colocalization of SARA with the early endosome marker EEA1. We assessed TGF-β internalization using a biotinylated ligand (b-TGF-β). Internalized b-TGF-β colocalized equally with either EEA1 and CAV-1 in VSMC from Marfan patients and controls. However, in Marfan cells, colocalization of b-TGF-β with structures positive for SARA and EEA1 was increased and accompanied by a decreased colocalization with CAV-1 at EEA1-positive endosomes. Moreover, Marfan VSMC showed higher transcriptional levels and protein recruitment to membrane fractions of RAB5. Our results indicate that increased RAB5-dependent SARA localization to early endosomes facilitates its TGF-β receptor binding and phosphorylation of signaling mediator SMAD2 in Marfan VSMC. This is accompanied by a reduction of TGF-β sorting into multi-functional vesicles containing cargo from both internalization pathways.

Keywords: Marfan syndrome, human vascular smooth muscle cells, membrane trafficking, TGF-β signaling.

1. INTRODUCTION

Marfan syndrome (MFS) is a multisystemic connective tissue disorder with autosomal dominant inheritance that affects between 1.5 and 17.2 in 100,000 births [1]. The disease is characterized by skeletal, ocular and cardiovascular manifestations and is caused by a mutation of the gene encoding for the extracellular matrix (ECM) protein fibrillin-1 (FBN1) [2]. FBN1 is the principal component of microfibrils, which, together with elastin, constitute the elastic fibers of the ECM in connective tissues throughout the body. Approximately 2000 *FBN1* mutations with variable dysfunctionality have been found to date, and the progress of the disease is difficult to predict through its mutation [3,4]. The most severe problems arise from abnormalities of the cardiovascular system, such as decreased integrity of the tunica media of the ascending aorta, which consists of vascular smooth muscle cells (VSMCs) and elastic fibers [5]. These aortic abnormalities are due to elastic fiber fragmentation and increased collagen deposition [6]. The severe effects of the mutation are often asymptomatic until a life-threatening aortic aneurysm or dissection occurs.

Transforming growth factor-β (TGF-β) has been suggested to be the molecular link between genetic mutation and disease onset, and has been used as a predictive marker of aneurysm progression [7,8]. TGF-β is secreted into the extracellular environment as a large latent complex (LLC) which is covalently attached to the latent TGF-β binding protein (LTBP). LTBPs interact with FBN1 through their characteristic 8-Cys module which is uniquely shared between the two proteins [9]. The result is a regulatory linkage of mature TGF-β to microfibrils, which prevents the uncontrolled activation of TGF-β. Under physiological conditions, TGF-β is maintained in an inactive state by controlled binding of LTBP to FBN1. In MFS, the fragmentation of microfibrils caused by insufficient or dysfunctional FBN1 leads to the reduced binding capacity of LTBP and increased active TGF-β in the extracellular environment [10]. TGF-β induces collagen production, tightly regulates ECM remodeling and leads to tissue fibrosis which compromises the organ structure as well as its function [11,12].

TGF-β receptor internalization takes place through both clathrin-coated pits and lipid raft-associated caveolin-1- (CAV-1) positive vesicles which have opposite effects on TGF-β signal transduction [13]. The ligand binds the constitutively active TGF-β receptor II (TBRII) which leads to TGF-β receptor I (TBRI; also named ALK5) recruitment and phosphorylation [14]. Receptor/ligand complexes internalized through clathrin-coated pits are targeted to early endosome associated protein-1- (EEA1) positive early endosomes, and initiate regulatory SMAD (R-SMAD) signaling through phosphorylation of SMAD2 and SMAD3. SMAD2/3 phosphorylation is dependent on the SMAD anchor for receptor activation (SARA), which is a bridging factor with binding sites for the TGF-β-receptor, SMAD2 and early endosomes, and is associated with TGF-β signal activation [15–17]. A third SMAD protein, the

inhibitory SMAD7, can compete with SMAD2/3, target the receptor for degradation, and abrogate signaling. In contrast to clathrin-dependent endocytosis, receptor internalization through caveolae destines receptors for proteasome degradation by binding of SMAD7 and E3 ubiquitin ligase poly-ubiquitination, which terminates the signaling cascade [13,18].

The role of TGF-β in MFS has thus far mostly been investigated in murine models. To date, the importance of TGF-β in MFS patients is supported by evidence of increased signaling partly associated with epigenetic modification of the SMAD2 promotor, as well as by the beneficial effects of TGF-β-receptor blockers and neutralizing TGF-β antibodies on the progress of aortic aneurysms in murine models [19–21]. However, in MFS, altered TGF-β endocytic trafficking in human VSMCs is still to be elucidated. Here we examine the significance of TGF-β signal regulation by its endocytic compartmentalization at endogenous levels in primary human VSMC from aortic aneurysm tissue of Marfan patients. We show, that TGF-β internalizes through the clathrin- and CAV-1-associated pathways at equal levels in VSMC from MFS and controls. However, increased RAB5-dependent SARA recruitment to early endosomes favours the spatial interaction of the TGF-β receptor complex with SMAD2, thus facilitating the increased TGF-β signalling in MFS.

2. MATERIAL AND METHODS

2.1. Antibodies and reagents

Rabbit polyclonal antibodies to SARA (ref. sc-9135), RhoGDI (sc-359), RAB5 (sc-309) and mouse monoclonal antibody to SMAD7 (ref. sc-101152) were from Santa Cruz Biotechnology (Santa Cruz, CA, USA). Goat polyclonal anti-TBRII (AF-241-NA) was from R&D Systems (Minneapolis, MN). Mouse monoclonal antibody to SMAD2 (ref. 3103S) and rabbit monoclonal antibody to pSMAD3 (Ser423/425) (ref. 9520) were from Cell Signaling Technology (Danvers, MA, USA). Mouse monoclonal antibody to EEA1 (ref. 610456) was from BD Biosciences (Franklin Lakes, NJ, USA). Mouse monoclonal antibody to the transferrin receptor (ref. 13-6800) was from Invitrogen (Carlsbad, CA, USA). Secondary peroxidase-conjugated antibodies to IgG mouse, rabbit and goat (refs. W402B, W401B and V805A respectively) were from Promega (Madison, WI, USA). Alexa Fluor 647-conjugated goat anti-rabbit IgG (ref. A21245) and Alexa Fluor 488-conjugated goat anti-rabbit (ref. A-11070) were from Invitrogen, Cy3-conjugated goat anti-mouse IgG (ref. 115.167.003) and goat anti-human IgG (ref. 109.005.088) were from Jackson ImmunoResearch (West Grove, PA, USA). Recombinant human TGF-β was from Merck Millipore (Darmstadt, Germany). Human TGF-β 1 Biotinylated Fluorokine Kit (ref. NFTG0) was from R&D

Systems. Protein A-coated Dynabeads (ref. 10001D) were from Invitrogen. Water-soluble mounting medium DAPI-Fluoromount G (ref. 0100-20) was from Southern Biotech (Birmingham, AL, USA).

2.2. Membrane and cytosol fractionation of VSMCs

Tissue from the dilated region of Marfan patient and healthy donor ascending aortae were obtained and VSMC were cultured as indicated previously [19]. VSMC were grown on 100 mm cell culture plates until confluency. Cells were rinsed twice in PBS and scraped into lysis buffer (250 mM saccharose, 10 mM HEPES, 1 mM EDTA, pH 7.5) supplemented with protease inhibitors. Extracts were mechanically lysed with 30 strokes of a 30G syringe, and subjected to 90 min of ultracentrifugation at 45,000 rpm using an S140-AT rotor (Thermo Fisher Scientific, Waltham, MA, USA) at 4°C. The resulting supernatant was the cytosolic fraction. The membrane fraction containing pellet was resuspended in 100 µl radioimmunoprecipitation assay buffer (10 mM Tris-HCl, pH 7.5, 1 mM EDTA, 0.5 mM EGTA, 1% Triton X-100, 0.1% sodium deoxycholate, 0.1% SDS 140 mM NaCl) supplemented with protease inhibitors. Twenty µg of each subcellular fraction were analyzed by 12% (v/v) SDS-PAGE and blotted as described previously [19]. Cytosol and membrane protein bands were quantified and relativized against their respective fraction markers RhoGDI and transferrin receptor. Membrane enrichment was calculated by normalization with the corresponding cytosolic fraction, and membrane enrichment in Marfan patients was normalized against controls. Statistical analysis was performed by one-sample t-test or Wilcoxon signed-rank test. The immunoblots shown are representative of at least four independent experiments.

2.3. Immunoprecipitation experiments

Membrane fractions were obtained as described above and protein concentrations were adjusted using immunoprecipitation buffer (10 mM Tris-HCl, pH 7.5, 50 mM NaCl, 1% Triton X-100, 5mM EDTA), supplemented with protease inhibitors. Equal amounts of membrane fractions (100 µg) were incubated overnight at 4°C with 30 µg of goat anti-TBRII or goat IgG. The following day, lysate and antibody were precipitated with 25 µl of magnetic beads conjugated with protein A for 1 h at 4°C. The beads were rinsed 4 times with immunoprecipitation buffer and proteins were eluted from them by adding 20 µl of loading buffer 5X containing 10% β-mercaptoethanol. Samples were analyzed by 7.5-9% (v/v) SDS-PAGE and blotted as described above. Western blot bands were quantified relative to the precipitated TRBII, and Marfan relative band intensities were normalized against controls. Statistical analysis was performed by one-sample t-test or Wilcoxon signed-rank test. The immunoblots shown are representative of at least three independent experiments.

2.4. Immunofluorescence

VSMC were grown on coverslips to 70-80% confluency and starved in serum-free 231 culture medium for 18 h. Signaling was induced by adding 2ng/µl of recombinant human TGF-β to the cell medium and allowing its internalization for 30 min at 37°C. Cells were rinsed with PBS, fixed in 4% paraformaldehyde in PBS for 15 min at room temperature, rinsed three times with PBS and incubated for 20 min with 50 mM ammonium chloride/PBS pH 7.4. Cells were permeabilized for 10 min with 0.1% saponin, 1% BSA in PBS. Antibody combinations of SARA (1:100)/EEA1 (1:200) and SMAD7 (1:100)/CAV-1 (1:100) were incubated for 1 h at room temperature, followed by 45 min of secondary antibody incubation (Alexa Fluor 488-conjugated goat anti-rabbit: 1:250, Cy3-conjugated goat anti-mouse IgG: 1:250). Coverslips were mounted onto microscope slides using DAPI-Fluoromount water soluble mounting agent. Images were taken using a Leica TSC SL confocal microscope with a 63x oil objective, and analyzed using CellProfiler image analysis software, Carpenter Lab, Broad Institute of Harvard and MIT (pipelines available on request). Statistical analysis was performed using two-tailed paired t-tests. The images shown are representative of four independent experiments.

For pSMAD3 nuclear translocation experiments, VSMC were grown on coverslips to 70-80% confluency and starved in serum-free 231 culture medium for 18 h. VSMCs were either washed and fixed in 4% paraformaldehyde in PBS for 15 min or signaling was induced by incubating cells for 30 min with recombinant TGF-β (2 µg/ml) or b-TGF-β at 37°C. Immunostaining was performed as indicated. pSMAD3 was diluted 1:100. Alexa Fluor 488-conjugated goat anti-rabbit were diluted 1:250. Images were taken using an Olympus BX60 fluorescence microscope with a 60x oil objective, and analyzed using CellProfiler image analysis software (pipelines available on request). The translocation index (TI) was defined as the ratio of the pSMAD3 mean fluorescence intensity in the nucleus in comparison with the pSMAD3 mean fluorescence intensity in the cytosol, relativized by the area of each separate cell. Statistical analysis was performed using repeated measures ANOVA, followed by uncorrected Fisher´s LSD multiple comparison. The images shown are representative of three independent experiments.

2.5. Biotinylated-TGF-β endocytic transport

VSMC were grown on coverslips to 70-80% confluency and starved in serum-free 231 culture medium for 18 h. Internalization experiments were performed as follows: starved cells were incubated with b-TGF-β for 60 min at 4°C, followed by incubation of avidin-fluorescein for 2 h at 4°C, according to the manufacturer's instructions. Cells were either rinsed with cold PBS (0 min) and fixed in 4% paraformaldehyde in PBS for 15 min, or the b-TGF-β/avidin-fluorescein complex was allowed to internalize for 30 minutes at 37°C and cells were subsequently fixed. Immunostaining was performed

as indicated above. Primary antibody dilutions were: EEA1 (1:200), SARA (1:100) and CAV-1 (1:100). Secondary antibody dilutions were: Cy3-conjugated goat anti-mouse IgG: 1:250, Alexa Fluor 647-conjugated goat anti-rabbit IgG: 1:250. Coverslips were mounted onto microscope slides using DAPI-Fluoromount water soluble mounting agent. Images were taken using a Leica TSC SP5 confocal microscope with a 63x oil objective, and analyzed using CellProfiler image analysis software (pipelines available on request). Large EEA1 positive ring-like structures were defined by the Euler number; e ≤ 0.5 was considered a ring-like structure. The ratio of a colocalizing large ring-like structure relative to a non-colocalizing ring-like structure, relative to the entire EEA1 positive pool was calculated as follows:

$$Ratio\ of\ colocalization = \left(\frac{Colocalization\ X}{Total\ large\ structures}\right) * \left(\frac{Total\ large\ structures}{Total\ EEA1}\right)$$

Statistical analysis was performed using repeated measures ANOVA followed by uncorrected Fisher´s LSD multiple comparison. The images shown are representative of at least four independent experiments.

2.6. Gene expression

RNeasy Mini Kit (Qiagen, Valencia, CA) was used for total RNA isolation. Reverse transcription (RT) was carried out using the High Capacity Reverse Transcriptase kit (Applied Biosystems, Foster City, CA, USA). One µg of total RNA from each sample was used for complementary DNA synthesis. Expression levels were determined in triplicate in a C1000 Thermal Cycler CFX384 Real-Time System (BioRad, Hercules, CA, USA) using SYBR® Green JumpStart™ *Taq* ReadyMix™ (Sigma-Aldrich, St. Louis, MO) and primers as stated in table S1. The expression of *RPS28* was used as a house-keeping control. Transcriptional expression of Marfan patients was normalized to controls. Statistical analysis was performed using the one-sample t-test

Table 1: Real-time PCR primer sets used for gene expression experiments

	Primer sequences (5´-3´)	
Gene	**Sense**	**Antisense**
CLTC	CTTTCCAAAGAAGGCAGTGG	TCAAGAACACCACATCATGC
CAV1	GCGACCCTAAACACCTCAAC	GTGAAGCTGGCCTTCCAAAT
AP2B1	CAGATGGGAGCAGTGGATCT	AGGTGAAGGAGCAAAGGTTG
SMURF2	TCCTCGGCTGTCTGCTAACT	TCAGGCATTCTGTGTCATCA
SARA	CTGTGTCACACGACCCAGTC	TTCCAACAGGACTTCCAACC
RAB5A	CAAGGCCGACCTAGCAAATA	TGTTTTAGCGGATGTCTCCA
RAB5C	CCAACATCGTCATTGCACTC	AGCAAACTGTTGTCGTCTGC
RPS28	GCTCGTGTCGTCCATGAAT	CCGTGTGCAGCCTATCAAG

3. RESULTS

3.1. TGF-β signaling mediators SARA and SMAD2 are enriched in membrane fractions and show increased receptor interaction in human Marfan VSMC

To study the contribution of TGF-β signaling mediators associated with the clathrin-dependent signal activation (SARA and SMAD2) and the CAV-1-dependent signal abrogating (SMAD7) endocytic pathways at basal levels, VSMC were cultured from the tunica media of aortic explants from MFS patients (Marfan) and heart donors (control). Confluent VSMC were lysed, cytosolic and membrane fractions were isolated, and subsequently analyzed by Western blot. Results showed significantly increased recruitment of SMAD2 and its anchoring factor SARA to cell membranes in Marfan VSMC (Fig. 1A). However, recruitment to cell membranes was not altered for SMAD7 (Fig. 1B). Next, we assessed the interaction of the TGF-β receptor II (TBRII) with downstream signaling molecules associated with the clathrin- and CAV-1-dependent internalization pathway at basal levels. As indicated above, cultured VSMC from Marfan and control samples were lysed and the respective membrane fractions were isolated. TBRII was immunoprecipitated from membrane fractions and the receptor interaction with SARA, SMAD2, and SMAD7 was analyzed by Western blot. Interaction of

SMAD2 and SARA with endogenous TBRII was significantly higher in Marfan VSMC membranes than in control cells (Fig. 1C). No alterations were observed for SMAD7 (Fig. 1D).

3.2. Localization of SARA at early endosomes is increased in TGF-β-stimulated human Marfan VSMC

To further address the pathway association of the increased TGF-β signaling mediators in Marfan cells, colocalization experiments of SARA/EEA1 and SMAD7/CAV-1 were performed. SARA is a crucial player in the control of TGF-β receptor complex signal promotion through its phosphatidylinositol 3-phosphate (Ptdlns(3)*P*) binding FYVE domain that directly recruits SMAD2 to the receptor complex at early endosomal membranes [15–17]. Cultured Marfan and control VSMC were starved overnight and treated with TGF-β for 30 min. Cells were co-stained with either anti-SARA/anti-EEA1 or anti-SMAD7/anti-CAV-1 antibodies. After TGF-β internalization, Marfan cells showed increased colocalization of SARA and EEA1 (Fig. 2A), whereas SMAD7 and CAV-1 remained unaltered (Fig. 2B).

3.3. TGF-β internalizes equally through the clathrin- and CAV-1-dependent endocytic pathways in human Marfan VSMC

To assess the internalization and endocytic pathway segregation of endogenous TGF-β in Marfan VSMCs, cells were treated with biotinylated TGF-β (b-TGF-β), which was subsequently visualized with FITC-conjugated streptavidin. We first examined b-TGF-β bioactivity by assessing its ability to induce the nuclear translocation of pSMAD3. For comparative purposes, non-biotinylated TGF-β was used in parallel. Results showed that pSMAD3 nuclear translocation induced by TGF-β and b-TGF-β was significantly higher than in untreated cells (Supplemental Figure 1), validating b-TGF-β as a representative molecular tool to explore the internalization routes of TGF-β at endogenous levels in VSMC.

To furthermore identify the endocytic pathways through which b-TGF-β internalizes, immunostainings were performed using specific antibodies to EEA1 as a marker of the clathrin-dependent pathway, and to CAV-1 to reveal the lipid raft/caveolin-1-dependent route. Cells were treated with b-TGF-β, either immediately fixed or allowed to internalize for 30 min prior to fixation, and co-stained with either anti-EEA1 or anti-CAV-1 antibodies. The percentage of colocalizing b-TGF-β with the respective endocytic markers for either pathway was evaluated. As expected, 30 min after internalization of b-TGF-β, both control and Marfan VSMC showed a significant increase in colocalization of b-TGF-β in either EEA1- or CAV-1-positive endomembrane structures (Fig. 3A and 3B, respectively). In contrast to the increased signal propagating mediators associated with the early endosomal pathway, no differences were found between control and Marfan b-TGF-β internalization through either endocytic pathway.

Furthermore, we examined key molecules involved in the two internalization pathways by quantitative RT-PCR. For the clathrin-dependent pathway we assessed transcriptional expression levels of clathrin (*CLTC)* and the catalytic subunit of its adaptor protein (*AP2B1*). CAV1-pathway associated genes were caveolin-1 (*CAV-1*) and the E3 ubiquitin protein ligase which tags the receptor for degradation (*SMURF2*). We did not observe any changes at the transcriptional level in any of the aforementioned genes (Supplementary Fig. 2).

3.4. SARA is increased at TGF-β containing early endosomes in human Marfan VSMC

With respect to the clathrin-dependent early endosomal pathway, TGF-β can internalize through two distinct receptor heterodimer combinations with different signaling responses: TBRII remains the initial ligand binding receptor, but TBRI/ALK5 can be replaced by ALK1. The TBRII/ALK1 receptor complex recruits SMAD1/5 instead of SMAD2/3, thereby creating a different signaling profile to TBRII/ALK5 [22,23]. To exclude the possibility of detecting a TGF-β complex pool containing ALK1 instead of TBRI/ALK5, and to determine whether TBRI/ALK5 specific signaling is altered at early endosomes, we performed b-TGF-β internalization studies as aforementioned and co-stained with EEA1 and SARA. Colocalization of both markers with b-TGF-β was significantly higher after internalization in both Marfan and control VSMC. Importantly, after internalization, Marfan cells showed higher colocalization of SARA with b-TGF-β and EEA1 compared to control cells, indicating an increased signaling activity at early endosomes in Marfan VSMC (Fig. 4A).

3.5. TGF-β is targeted less to EEA1- and CAV-1-positive endosomes in human Marfan cells

Experimental evidence indicates that the clathrin- and the CAV-1-associated endocytic pathways are not entirely separate entities, but that both pathways merge to form multifunctional signaling organelles that are associated with cargo sorting and degradation [24,25]. Therefore, we performed b-TGF-β internalization studies and co-stained VSMC with EEA1 and CAV-1. An increase in triple-colocalization was observed after b-TGF-β internalization in both Marfan and control VSMC (Fig. 4B). In addition, triple-colocalization was significantly lower in Marfan than in control cells after ligand internalization, demonstrating decreased trafficking of TGF-β into these endocytic multifunctional sorting stations (Fig. 4B). Furthermore, the EEA1/CAV-1 double-positive endosomes have been shown to be enlarged structures described as maturing multivesicular bodies (MVBs), which are responsible for sorting of receptors destined for degradation [24]. We indeed observed large, ring-like EEA1-positive structures in VSMC, and quantitative analysis showed a significant increase in both Marfan and control VSMC after b-TGF-β internalization (Fig. 5A). The colocalization before and after b-TGF-β internalization with CAV-1 in these large, ring-like EEA1-positive structures was then assessed, which

significantly increased in control VSMC only (Fig. 5B). However, after b-TGF-β internalization, significantly less colocalization was seen in Marfan than in control cells (Fig. 5B).

3.6. The small GTPase RAB5 is overexpressed in human Marfan VSMC

Like EEA1, SARA is recruited to early endosomes through its FYVE domain by the small GTPase RAB5 and acts as its effector [26]. We therefore assessed the transcriptional level of *SARA*, *RAB5A* and *RAB5C* in Marfan and control VSMC. Marfan cells showed an upregulation of *RAB5A* and *RAB5C*, but not of *SARA* (Fig. 6A). Furthermore, we assessed the ratio of active membrane bound RAB5 to inactive cytosolic RAB5 by membrane cytosol fractionation as described above. In Marfan VSMC, RAB5 was significantly enriched in membrane fractions (Fig. 6B). These results strongly suggest that in Marfan VSMC the increased localization of SARA at endo membranes is mediated by higher expression levels of RAB5.

4. DISCUSSION

To assess potential molecular mechanisms that contribute to the known chronic overactivation of TGF-β signaling in MFS, we examined its endocytic trafficking routes in human VSMC at endogenous levels. We observed that in human Marfan VSMC (i) downstream effectors associated with the clathrin-dependent pathway such as SARA and SMAD2 are recruited more to endomembranes and interact more with TGF-β receptors; (ii) TGF-β internalizes at equal levels through the clathrin- and the CAV-1-dependent endocytic pathways, however, it colocalizes more with SARA and less with CAV-1 at early endosomes, and (iii) the small GTPase RAB5 is overexpressed at transcriptional level and enriched at (endo)membrane fractions.

TGF-β has previously been associated with MFS as a molecular element of disease onset and progression [7]. This was, in part, explained by TGF-β-associated signaling events both in mice and humans, as well as by epigenetic modifications of the SMAD2 promoter region [19,21,27,28]. However, the subcellular compartmentalization of receptor-mediated TGF-β internalization, which is directly related to opposing signaling responses, has not been examined in Marfan VSMC. TGF-β receptor compartmentalization is a molecular mechanism that may contribute to the increased TGF-β signaling seen in MFS [29]. This is based on previous observations in clonal cell lines in which TGF-β signal activation and abrogation are respectively caused by its receptors segregation into clathrin- or caveolin/lipid raft-associated endocytic pathways [13]. We hypothesized that the chronic hyperactivation of TGF-β signaling in MFS is favored by an imbalance between both endocytic pathways. To address this hypothesis, we avoided transfecting cultured VSMC with tagged forms of

TGF-β receptors, but assessed TGF-β internalization and the subsequent signaling response at endogenous levels.

We here show that in VSMC from Marfan patients downstream signaling mediators of the clathrin-associated pathway are enriched in membrane fractions and interact more with TBRII. Furthermore, TGF-β induces an increased localization of SARA at early endosomes. SARA controls the subcellular localization of SMAD2, and the increased recruitment of SARA and SMAD2 to endomembranes is indicative for the propagation of TGF-β signaling [30,31]. In fact, the increased localization of SARA at EEA-1-labeled early endosomes upon TGF-β addition in Marfan VSMC demonstrates that the recruitment to membrane fractions as well as the receptor interaction of SMAD2 occurs in the endosomal pathway.

To assess whether an imbalance of the endocytic pathway compartmentalization contributes to the MFS-associated increased TGF-β signaling, we functionally characterized a biotinylated TGF-β and assessed its internalization through the clathrin- and CAV-1-dependent pathways. We observed that in control and Marfan VSMC, b-TGF-β localizes equally with either endocytic route marker EEA1 or CAV-1. Additionally, at the transcriptional level, we did not show any alteration of essential molecular elements involved in either pathway. However, analysis of triple-colocalization of b-TGF-β with EEA1 and SARA showed an increase of the signaling mediator SARA at b-TGF-β-containing early endosomes. Our results illustrate that the essential molecular machinery associated with activated TGF-β signaling is increased at early endosomes in Marfan VSMC. The endosomal membrane distribution of SARA depends on its FYVE domain interaction with phosphoinositides (Ptdlns(3)*P)* and it has been shown that Ptdlns(3)*P* enrichment at early endosomal membranes is stimulated by the small GTPase RAB5 [15,26][32]. In Marfan VSMC, RAB5 was increased at the transcriptional level and at cell membranes, where RAB5 is found in its GTP-bound active form. We therefore propose that in MFS, RAB5 controls the increased recruitment of SARA to early endosomes, due to its spatial and temporal control over Ptdlns(3)*P* levels [26,33]. This then results in an increased interaction of SARA with the TGF-β receptor complex, SMAD2/3 recruitment and phosphorylation, and subsequent increased TGF-β signaling.

In contrast to the classical view of TGF-β endocytic route segregation in which early endosomes are invariably associated with signal promotion [13], experimental evidence shows that the early endosomal pathway is also involved in TGF-β signal attenuation by merging with CAV-1-positive vesicles [24,25,34]. This subpopulation of EEA1/CAV-1-double positive endocytic structures has been shown to destine cargo for a second round of sorting and to attenuate signaling by maturing into MVBs [24,25]. This reinforces the idea that TGF-β receptors not only segregate into different plasma membrane domains for their subsequent internalization [13], but that their final subcellular fate is

determined at various stages, possibly mediated by different molecular checkpoints. In accordance with this idea, we observed that internalized b-TGF-β is delivered in part to an integrated endocytic compartment containing markers of both pathways. Interestingly, we found a decrease in localization of b-TGF-β with such EEA1/CAV-1 double-positive vesicles in Marfan cells, suggesting that internalized TGF-β is delivered less to this specialized pathway associated with receptor re-sorting and signal attenuation. These merged vesicles have morphologically been observed to be enlarged structures, which are demonstrative for the formation of MVBs [24]. We showed that the number of these enlarged endocytic structures augmented in VSMC from controls and Marfan after TGF-β internalization. However, less EEA1/CAV-1-double positive enlarged endocytic structures containing TGF-β were observed in Marfan cells.

In conclusion, our study demonstrates that in MFS the increased endosomal pathway associated signaling is due to an increase in RAB5-mediated SARA recruitment to early endosomes, which facilitates the subsequent SMAD2/TGF-β receptor complex binding. The increased signaling at early endosomes is aided by a reduced trafficking of TGF-β into EEA1/CAV-1-double positive endocytic structures reported to be associated with signal attenuation. Both endocytic trafficking alterations converge to provide a signaling platform that consequently leads to the chronic TGF-β signal promotion.

ACKNOWLEDGEMENTS

We thank Laura Barberà and Maite Muñoz for technical assistance. This study was funded through the National Marfan Foundation (NMF), in part by the Spanish *Ministerio de Economia y Competitividad* grants BFU2012-33932 and SAF2015-64136R, the *Fundación Ramón Areces* and the Government of Catalonia grant 2014SGR-334.

REFERENCES

[1] Y. Von Kodolitsch, J. De Backer, H. Schüler, P. Bannas, C. Behzadi, A.M. Bernhardt, M. Hillebrand, B. Fuisting, S. Sheikhzadeh, M. Rybczynski, T. Kölbel, K. Püschel, S. Blankenberg, P.N. Robinson, Perspectives on the revised ghent criteria for the diagnosis of marfan syndrome, Appl. Clin. Genet. 8 (2015) 137–155. doi:10.2147/TACG.S60472.

[2] H.C. Dietz, G.R. Cutting, R.E. Pyeritz, C.L. Maslen, L.Y. Sakai, G.M. Corson, E.G. Puffenberger, A. Hamosh, E.J. Nanthakumar, S.M. Curristin, Marfan syndrome caused by a recurrent de novo missense mutation in the fibrillin gene., Nature. 352 (1991) 337–339. doi:10.1038/352337a0.

[3] G.L. Perrucci, E. Rurali, A. Gowran, A. Pini, C. Antona, R. Chiesa, G. Pompilio, P. Nigro, Vascular smooth muscle cells in Marfan syndrome aneurysm: the broken bricks in the aortic wall, Cell. Mol. Life Sci. (2016). doi:10.1007/s00018-016-2324-9.

[4] G. Collod-Béroud, S. Le Bourdelles, L. Ades, L. Ala-Kokko, P. Booms, M. Boxer, A. Child, P. Comeglio, A. De Paepe, J.C. Hyland, K. Holman, I. Kaitila, B. Loeys, G. Matyas, L. Nuytinck, L. Peltonen, T. Rantamaki, P. Robinson, B. Steinmann, C. Junien, C. Béroud, C. Boileau, Update of the UMD-FBN1 mutation database and creation of an FBN1 polymorphism database, Hum. Mutat. 22 (2003) 199–208. doi:10.1002/humu.10249.

[5] K. Hirata, F. Triposkiadis, E. Sparks, J. Bowen, C.F. Wooley, H. Boudoulas, The Marfan syndrome: abnormal aortic elastic properties., J. Am. Coll. Cardiol. 18 (1991) 57–63.

[6] S.-M. Yuan, H.-H. Ma, R.-S. Zhang, H. Jing. Transforming growth factor-β signaling pathway in Marfan's syndrome: a preliminary histopathological study., Vasa. 40 (2011) 369–374. doi:10.1024/0301-1526/a000133.

[7] P.N. Robinson, E. Arteaga-Solis, C. Baldock, G. Collod-Béroud, P. Booms, a De Paepe, H.C. Dietz, G. Guo, P. a Handford, D.P. Judge, C.M. Kielty, B. Loeys, D.M. Milewicz, a Ney, F. Ramirez, D.P. Reinhardt, K. Tiedemann, P. Whiteman, M. Godfrey, The molecular genetics of Marfan syndrome and related disorders., J. Med. Genet. 43 (2006) 769–787. doi:10.1136/jmg.2005.039669.

[8] P. Matt, F. Schoenhoff, J. Habashi, T. Holm, C. Van Erp, D. Loch, O.D. Carlson, B.F. Griswold, Q. Fu, J. De Backer, B. Loeys, D.L. Huso, N.B. McDonnell, J.E. Van Eyk, H.C. Dietz, Circulating transforming growth factor-β in Marfan syndrome., Circulation. 120 (2009) 526–532. doi:10.1161/CIRCULATIONAHA.108.841981.

[9] P. Dijke, H.M. Arthur, Extracellular control of TGF β signalling in vascular development and disease, 8 (2007). doi:10.1038/nrm2262.

[10] S.S. Chaudhry, S. a. Cain, A. Morgan, S.L. Dallas, C.A. Shuttleworth, C.M. Kielty, Fibrillin-1 regulates the bioavailability of TGF β1, J. Cell Biol. 176 (2007) 355–367. doi:10.1083/jcb.200608167.

[11] A. Leask, J. Abraham, TGF-β signaling and the fibrotic response, FASEB J. 18 (2004) 816–827. doi:10.1096/fj.03-1273rev.

[12] M. Ruiz-Ortega, J. Rodríguez-Vita, E. Sanchez-Lopez, G. Carvajal, J. Egido, TGF-β signaling in vascular fibrosis, Cardiovasc. Res. 74 (2007) 196–206. doi:10.1016/j.cardiores.2007.02.008.

[13] G.M. Di Guglielmo, C. Le Roy, A.F. Goodfellow, J.L. Wrana, Distinct endocytic pathways regulate TGF-β receptor signalling and turnover., Nat. Cell Biol. 5 (2003) 410–421. doi:10.1038/ncb975.

[14] Y. Shi, J. Massagué, Mechanisms of TGF-β signaling from cell membrane to the nucleus., Cell. 113 (2003) 685–700. doi:10.1016/S0092-8674(03)00432-X.

[15] F. Itoh, N. Divecha, L. Brocks, L. Oomen, H. Janssen, J. Calafat, S. Itoh, P. ten Dijke Pt, The FYVE domain in Smad anchor for receptor activation (SARA) is sufficient for localization of SARA in early endosomes and regulates TGF-β/Smad signalling., Genes Cells. 7 (2002) 321–331.

[16] T. Tsukazaki, T.A. Chiang, A.F. Davison, L. Attisano, J.L. Wrana, SARA, a FYVE domain protein that recruits Smad2 to the TGF-β receptor., Cell. 95 (1998) 779–791.

[17] G. Wu, Y.G. Chen, B. Ozdamar, C. a Gyuricza, P. a Chong, J.L. Wrana, J. Massagué, Y. Shi, Structural basis of Smad2 recognition by the Smad anchor for receptor activation., Science. 287 (2000) 92–97. doi:10.1126/science.287.5450.92.

[18] X. Yan, H. Liao, M. Cheng, X. Shi, X. Lin, X. Feng, Y. Chen, Smad7 Protein Interacts with Receptor-regulated Smads (R-Smads) to Inhibit Transforming Growth Factor-β (TGF-β)/Smad Signaling, 291 (2016) 382–392. doi:10.1074/jbc.M115.694281.

[19] E. Crosas-Molist, T. Meirelles, J. López-Luque, C. Serra-Peinado, J. Selva, L. Caja, D. Gorbenko Del Blanco, J.J. Uriarte, E. Bertran, Y. Mendizábal, V. Hernández, C. García-Calero, O. Busnadiego, E. Condom, D. Toral, M. Castellà, A. Forteza, D. Navajas, E. Sarri, F. Rodríguez-Pascual, H.C. Dietz, I. Fabregat, G. Egea, Vascular smooth muscle cell phenotypic changes in patients with marfan syndrome, Arterioscler. Thromb. Vasc. Biol. 35 (2015) 960–972. doi:10.1161/ATVBAHA.114.304412.

[20] J.R. Cook, N.P. Clayton, L. Carta, J. Galatioto, E. Chiu, S. Smaldone, C. a. Nelson, S.H. Cheng, B.M. Wentworth, F. Ramirez, Dimorphic Effects of Transforming Growth Factor- Signaling During Aortic Aneurysm Progression in Mice Suggest a Combinatorial Therapy for Marfan Syndrome, Arterioscler. Thromb. Vasc. Biol. (2015). doi:10.1161/ATVBAHA.114.305150.

[21] D. Gomez, K. Kessler, J.B. Michel, R. Vranckx, Modifications of chromatin dynamics control smad2 pathway activation in aneurysmal smooth muscle cells, Circ. Res. 113 (2013) 881–890. doi:10.1161/CIRCRESAHA.113.301989.

[22] M. González-Núñez, J.M. Muñoz-Félix, J.M. López-Novoa, The ALK-1/Smad1 pathway in cardiovascular physiopathology. A new target for therapy?, Biochim. Biophys. Acta - Mol. Basis Dis. 1832 (2013) 1492–1510. doi:10.1016/j.bbadis.2013.05.016.

[23] M.J. Goumans, G. Valdimarsdottir, S. Itoh, F. Lebrin, Activin receptor-like kinase (ALK) 1 is an antagonistic mediator of lateral TGF-β/ALK5 signaling, Mol. Cell. 12 (2003) 817–828. doi:10.1016/S1097-2765(03)00386-1.

[24] P. Balogh, M. Magyar, A. Szabó, N. Müllner, I. Likó, A. Patócs, A.L. Kiss. The subcellular compartmentalization of TGF-β-RII and the dynamics of endosomal formation during the signaling events: An in vivo study on rat mesothelial cells, Eur. J. Cell Biol. 94 (2015) 204–213. doi:10.1016/j.ejcb.2015.03.001.

[25] K. He, X. Yan, N. Li, S. Dang, L. Xu, B. Zhao, Z. Li, Z. Lv, X. Fang, Y. Zhang, Y.-G. Chen, Internalization of the TGF-β type I receptor into caveolin-1 and EEA1 double-positive early endosomes, Cell Res. (2015) 738–752. doi:10.1038/cr.2015.60.

[26] Y. Hu, SARA, a FYVE domain protein, affects Rab5-mediated endocytosis, J. Cell Sci. 115 (2002) 4755–4763. doi:10.1242/jcs.00177.

[27] T.M. Holm, J.P. Habashi, J.J. Doyle, D. Bedja, Y. Chen, C. van Erp, M.E. Lindsay, D. Kim, F. Schoenhoff, R.D. Cohn, B.L. Loeys, C.J. Thomas, S. Patnaik, J.J. Marugan, D.P. Judge, H.C. Dietz, Noncanonical TGF-β signaling contributes to aortic aneurysm progression in Marfan syndrome mice, Science 332 (2011) 358–361. doi:332/6027/358 [pii]\r10.1126/science.1192149.

[28] J.P. Habashi, J.J. Doyle, T.M. Holm, H. Aziz, F. Schoenhoff, D. Bedja, Y. Chen, A.N. Modiri, D.P. Judge, H.C. Dietz, Angiotensin II type 2 receptor signaling attenuates aortic aneurysm in mice through ERK antagonism., Science. 332 (2011) 361–365. doi:10.1126/science.1192152.

[29] E.R. Neptune, P. a Frischmeyer, D.E. Arking, L. Myers, T.E. Bunton, B. Gayraud, F. Ramirez, L.Y. Sakai, H.C. Dietz, Dysregulation of TGF-β activation contributes to pathogenesis in Marfan syndrome., Nat. Genet. 33 (2003) 407–11. doi:10.1038/ng1116.

[30] S. Hayes, A. Chawla, S. Corvera, TGF-β receptor internalization into EEA1-enriched early endosomes: Role in signaling to Smad2, J. Cell Biol. 158 (2002) 1239–1249. doi:10.1083/jcb.200204088.

[31] T. Tsukazaki, T. a. Chiang, A.F. Davison, L. Attisano, J.L. Wrana, SARA, a FYVE domain protein that recruits Smad2 to the TGF-β receptor, Cell. 95 (1998) 779–791. doi:10.1016/S0092-8674(00)81701-8.

[32] D.C. Lawe, V. Patki, R. Heller-harrison, D. Lambright, S. Corvera, The FYVE Domain of Early Endosome Antigen 1 Is Required for Both Phosphatidylinositol 3-Phosphate and Rab5 Binding, 275 (2000) 3699–3705.

[33] T. Bhuin, J.K. Roy, Rab proteins: The key regulators of intracellular vesicle transport, Exp. Cell Res. 328 (2014) 1–19. doi:10.1016/j.yexcr.2014.07.027.

[34] L. Pelkmans, T. Bürli, M. Zerial, A. Helenius, Caveolin-stabilized membrane domains as multifunctional transport and sorting devices in endocytic membrane traffic, Cell. 118 (2004) 767–780. doi:10.1016/j.cell.2004.09.003.

FIGURE LEGENDS

Figure 1. SARA and SMAD2 are enriched in membrane fractions and show increased interaction with TGF-β receptor II in Marfan VSMC. Membrane enrichment analysis of (A) SARA (N=7, *p<0.05) and SMAD2 (N=7, *p<0.05) and (B) Smad7 (N=4, p=0.4392). VSMC of Marfan and controls were lysed and membrane and cytosol were fractionated and analyzed by Western blot. Cytosol and membrane protein bands were quantified and relativized against their respective fraction markers RhoGDI and transferrin receptor (TrfR). Membrane enrichment was calculated by normalization with the corresponding cytosolic fraction, and membrane enrichment in Marfan patients was normalized against controls. (C) TBRII was immunoprecipitated from the membrane fraction only. Immunoprecipitates were subjected to Western blotting, and receptor interaction of SARA (N=7, *p<0.05) and SMAD2 (N=4, **p<0.01), and (D) SMAD7 (N=3, p=0.7514) was analyzed by quantifying protein bands relative to the precipitated TRBII. Marfan relative band intensities were normalized against controls. Results are represented as mean ± SEM.

Figure 2. SARA localizes more to early endosomes in TGF-β stimulated Marfan VSMC. Cultured VSMC were starved and treated with recombinant TGF-β for 30 min and subsequently fixed and immunolabeled. Colocalization of (A) SARA with EEA1 (N=4, **p<0.01) and (B) SMAD7 with CAV-1 (N=4, p=0.5179) was analyzed. The percentage of colocalization was calculated relative to non-colocalizing SARA and SMAD7, respectively. Results are represented as mean ± SEM. Bar, 20 µm.

Figure 3. The clathrin- and CAV-1-dependent endocytic pathways are unaltered in VSMC from MFS patients. VSMC were starved and incubated with b-TGF-β followed by fluorescein-conjugated avidin. The complex was internalized for 0 or 30 min. Colocalization of b-TGF-β with (A) EEA1 (N=9, RM ANOVA ****p<0.0001, LSD Control 0 min vs. Marfan 0 min p=0.1949; Control 30 min vs. Marfan 30 min p=0.5157) (B) or CAV-1 (N=5, RM ANOVA **p<0.01, LSD Control 0 min vs. Marfan 0 min p= 0.5279; Control 30 min vs. Marfan 30 min p=0.1795) was analyzed. The percentage of colocalization was calculated relative to non-colocalizing b-TGF-β. Results are represented as mean ± SEM. White arrows in A show colocalization of b-TGF-β (green) with EEA1 (red) in endocytic vesicular structures. Bar, 20 µm.

Figure 4. TGF-β internalizes more through SARA/EEA1- and less through EEA1/CAV-1-positive early endosomes in Marfan VSCM. VSMC were starved and incubated with b-TGF-β followed by fluorescein-conjugated avidin. The complex was internalized for 0 and 30 min. Colocalization of b-TGF-β with (A) EEA1/SARA (N=4, RM ANOVA **p<0.01, LSD Control 0 min vs Marfan 0 min p=0.8486; LSD Control 30 min vs Marfan 30 min *p<0.05) and (B) EEA1/CAV-1 (N=5, RM ANOVA **p<0.01, LSD Control 0 min vs. Marfan 0 min, p=0.3899; Control 30 min vs. Marfan 30 min, *p<0.05) was analyzed.

The percentage of colocalization was calculated relative to non-colocalizing b-TGF-β. Results are represented as mean ± SEM. White arrows show triple colocalization of internalized b-TGF-β with EEA1/SARA or EEA1/CAV-1 in endocytic vesicular structures, respectively. Bar, 20 μm.

Figure 5. Internalized b-TGF-β is destined less to EEA1/CAV-1 double-positive large endosomal structures in Marfan VSMC. VSMC were starved and incubated with b-TGF-β followed by fluorescein-conjugated avidin. The complex was internalized for 0 or 30 min. (A) The percentage of EEA1-positive large ring-like cytoplasmic vesicular structures was analyzed relative to total EEA1-positive structures (N=5, RM ANOVA *p<0.05, LSD C 0 min vs. C 30 min, *p<0.05, Marfan 0 min vs. Marfan 30 min, *p<0.05). (B) Colocalization of b-TGF-β with CAV-1- and EEA1-positive large ring-like structures was analyzed (N=5, RM ANOVA p=0.0977, LSD Control 0 min vs. Marfan 0 min, p=0.7343; Control 30 min vs. Marfan 30 min, *p<0.05). The ratio of colocalizing large ring-like endosomal structures to non-colocalizing ones was calculated relative to total EEA1 positive endosomes. Results are represented as mean ± SEM. White arrows show colocalization of internalized b-TGF-β with double-positive large ring-like early endosomes. Bar, 20 μm.

Figure 6. RAB5 is upregulated and recruited more to cell membranes in Marfan VSMC. (A) RNA from VSMC was extracted and transcriptional expression of RAB5A (Control N=6; Marfan N=8, *p<0.05), RAB5C (N=7, *p<0.05) and SARA (Control N=6; Marfan N=8, p=0.3125) was assessed. Gene expression in Marfan patients was normalized to controls. Results are represented as box and whiskers from min to max. (B) Membrane enrichment analysis by Western blotting of RAB5 (N=5, *p<0.05). Membrane and cytosol fractions from Marfan and control VSMC were obtained and analyzed by Western blot. Membrane and cytosol bands were relativized against their respective fraction marker, and membrane fractions were normalized against their corresponding cytosolic fraction. Marfan membrane bands were normalized against controls. Results are represented as mean ± SEM.

Figure 1

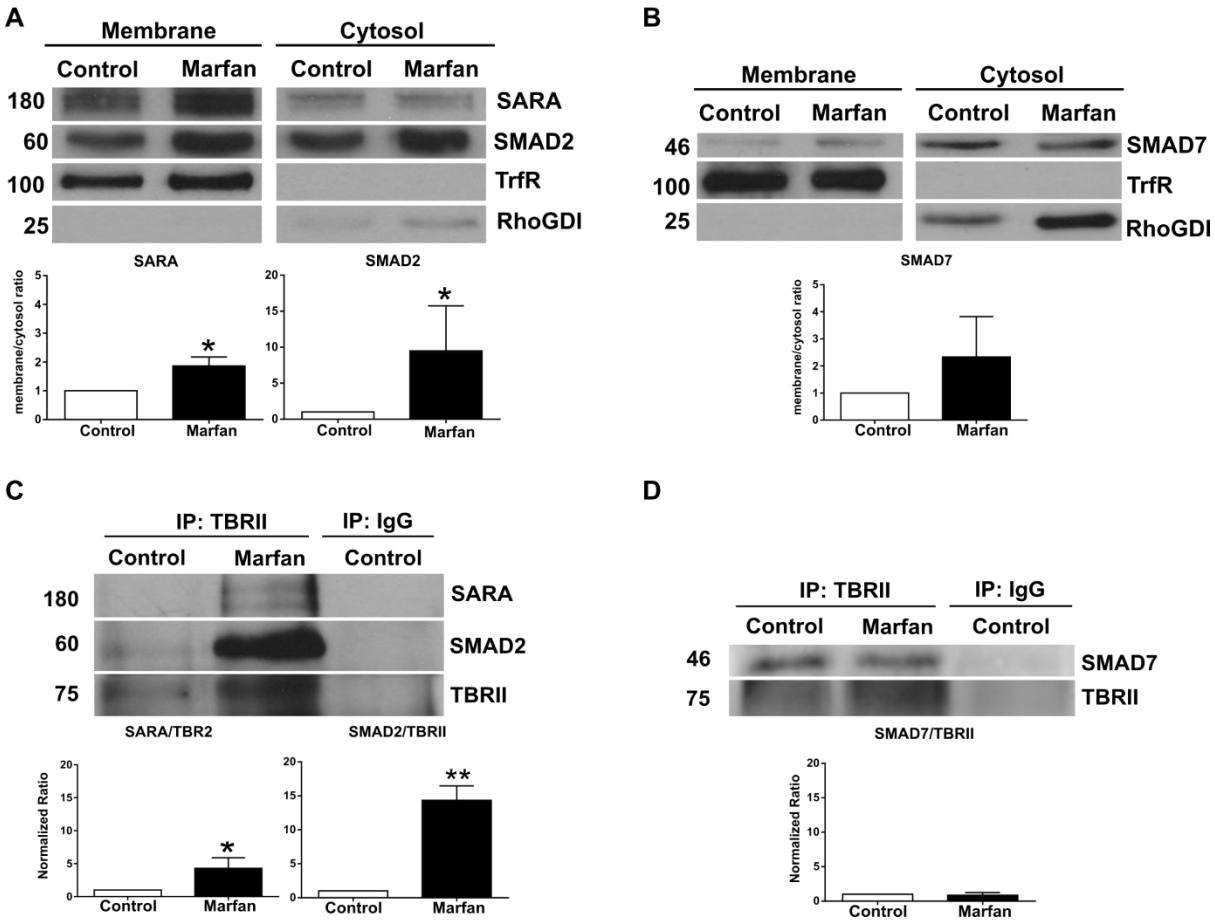
A
Membrane
Cytosol
Control
Marfan
Control
Marfan
180
60
100
25
SARA
SMAD2
TrfR
RhoGDI
SARA
SMAD2
membrane/cytosol ratio
Control
Marfan
Control
Marfan
B
Membrane
Cytosol
Control
Marfan
Control
Marfan
46
100
25
SMAD7
TrfR
RhoGDI
SMAD7
membrane/cytosol ratio
Control
Marfan
C
IP: TBRII
IP: IgG
Control
Marfan
Control
180
60
75
SARA
SMAD2
TBRII
SARA/TBR2
SMAD2/TBRII
Normalized Ratio
Control
Marfan
Control
Marfan
D
IP: TBRII
IP: IgG
Control
Marfan
Control
46
75
SMAD7
TBRII
SMAD7/TBRII
Normalized Ratio
Control
Marfan

Figure 2

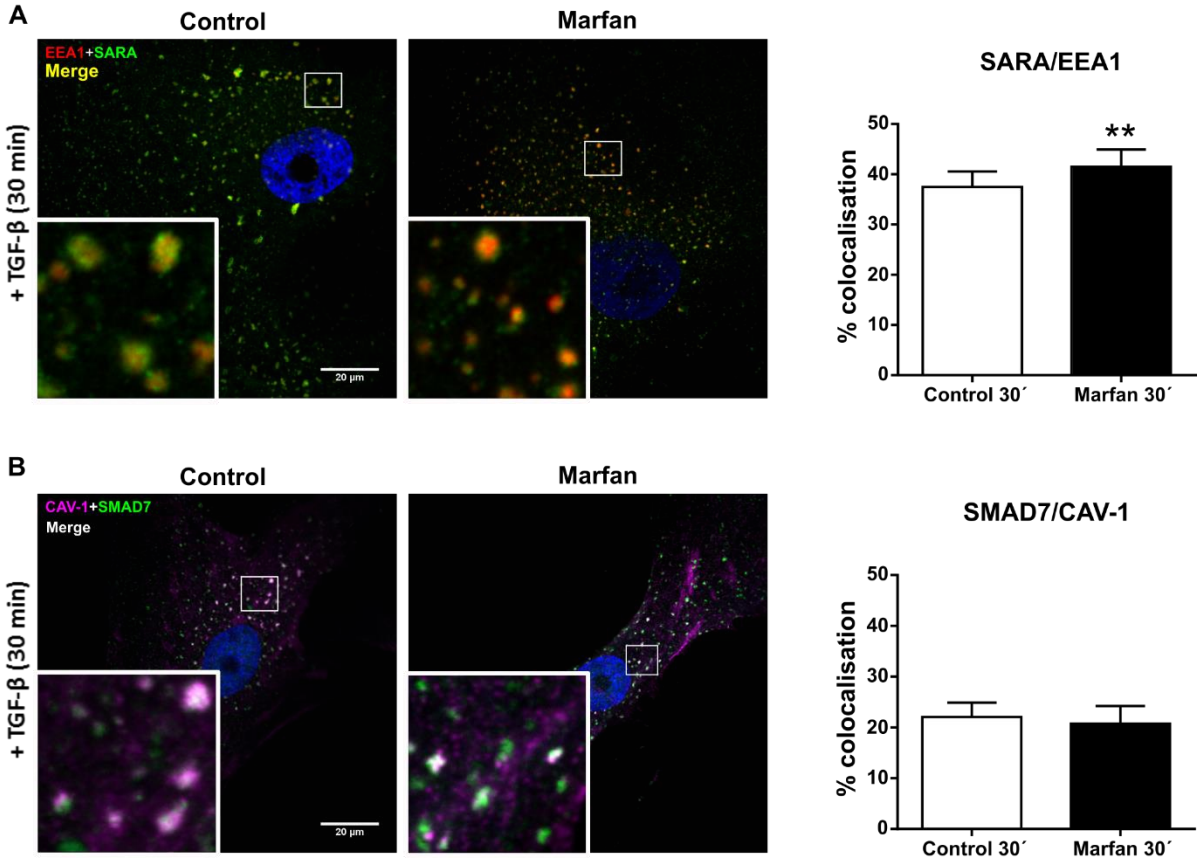
A
Control
Marfan
EEA1+SARA
Merge
+ TGF-β (30 min)
20 µm
SARA/EEA1
% colocalisation
50
40
30
20
10
0
**
Control 30´
Marfan 30´
B
Control
Marfan
CAV-1+SMAD7
Merge
+ TGF-β (30 min)
20 µm
SMAD7/CAV-1
% colocalisation
50
40
30
20
10
0
Control 30´
Marfan 30´

Figure 3

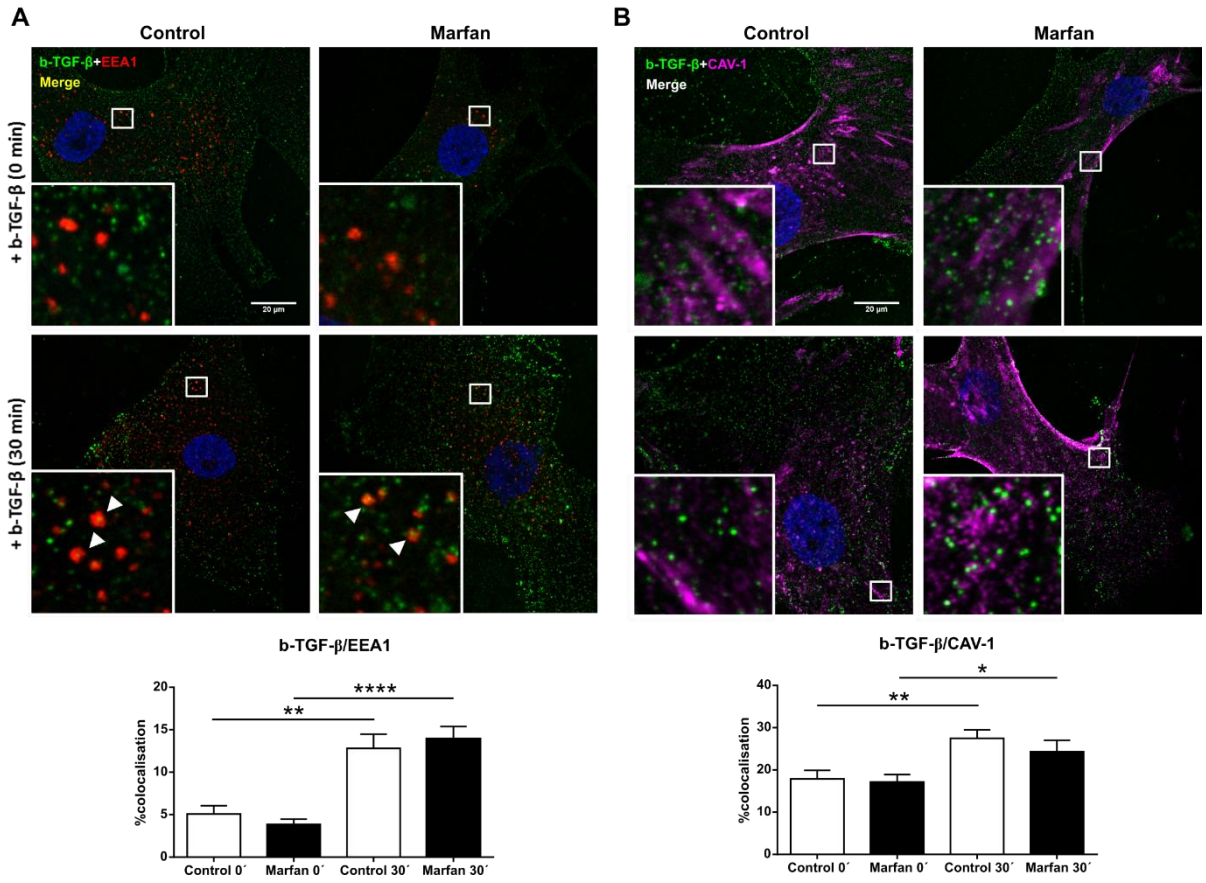
A
Control
Marfan
b-TGF-β+EEA1
Merge
+ b-TGF-β (0 min)
+ b-TGF-β (30 min)
20 µm
B
Control
Marfan
b-TGF-β+CAV-1
Merge
20 µm
b-TGF-β/EEA1
%colocalisation
20
15
10
5
0
****
**
Control 0´
Marfan 0´
Control 30´
Marfan 30´
b-TGF-β/CAV-1
%colocalisation
40
30
20
10
0
*
**
Control 0´
Marfan 0´
Control 30´
Marfan 30´

Figure 4

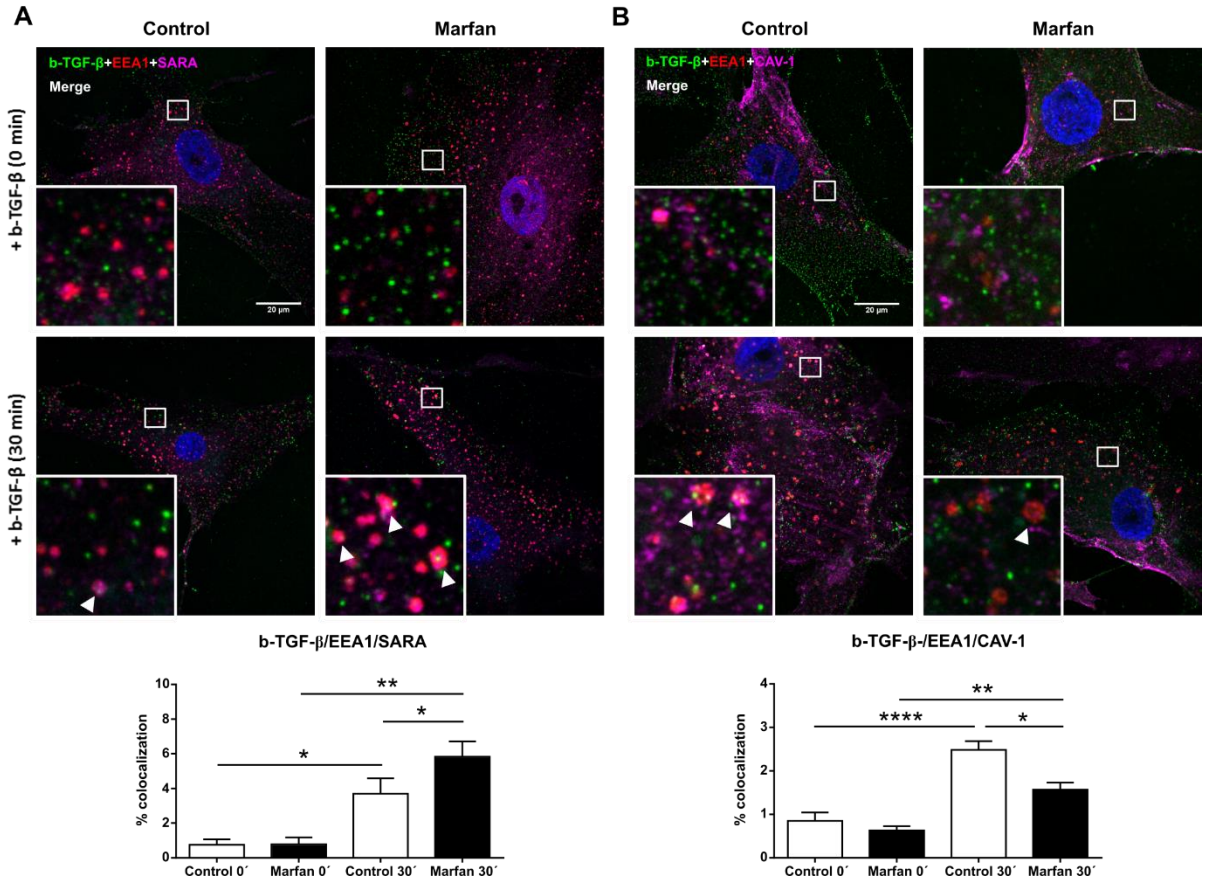
A
Control
Marfan
b-TGF-β+EEA1+SARA
Merge
+ b-TGF-β (0 min)
+ b-TGF-β (30 min)
20 µm
B
Control
Marfan
b-TGF-β+EEA1+CAV-1
Merge
20 µm
b-TGF-β/EEA1/SARA
% colocalization
Control 0´
Marfan 0´
Control 30´
Marfan 30´
b-TGF-β-/EEA1/CAV-1
% colocalization
Control 0´
Marfan 0´
Control 30´
Marfan 30´

Figure 5

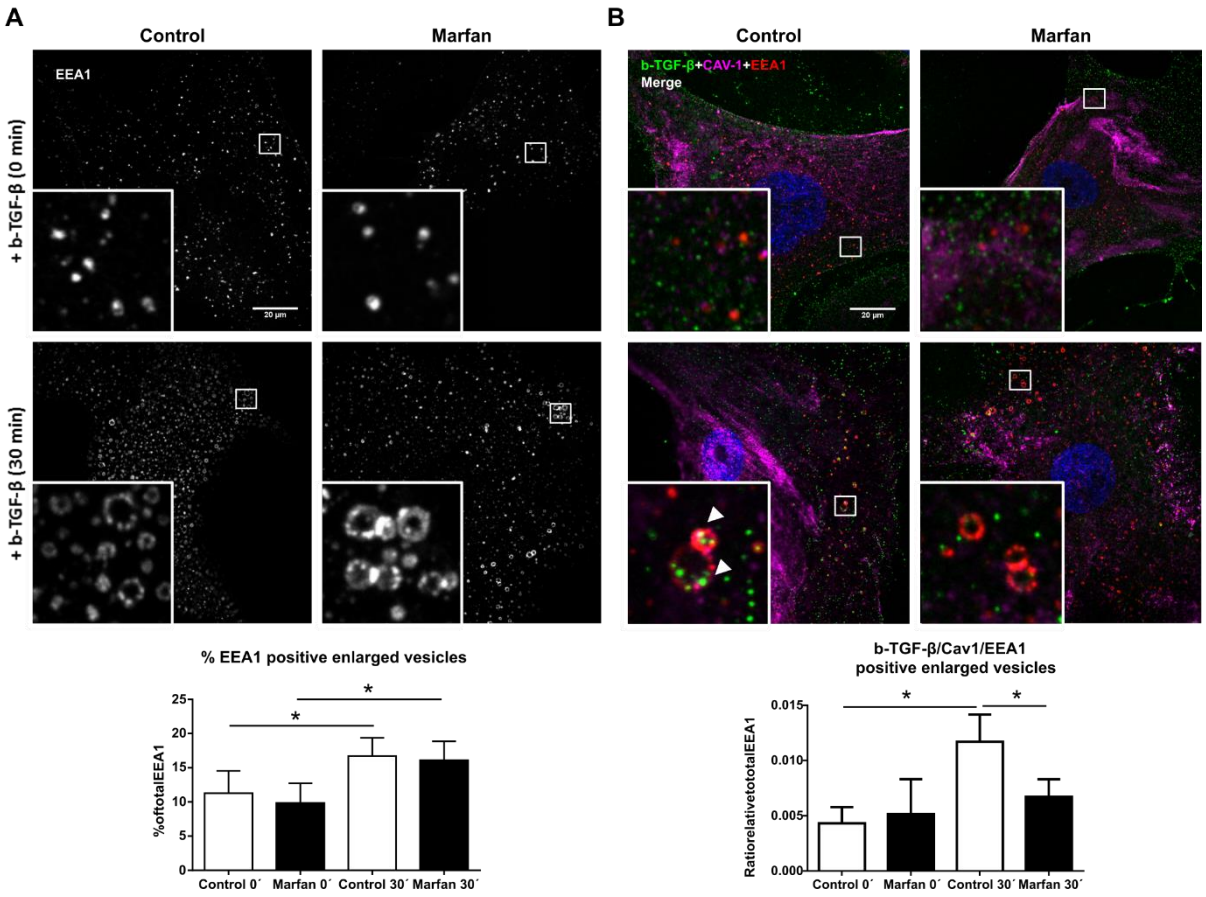
A
Control
Marfan
EEA1
+ b-TGF-β (0 min)
+ b-TGF-β (30 min)
20 µm
B
Control
Marfan
b-TGF-β+CAV-1+EEA1
Merge
20 µm
% EEA1 positive enlarged vesicles
%oftotalEEA1
25
20
15
10
5
0
Control 0´
Marfan 0´
Control 30´
Marfan 30´
b-TGF-β/Cav1/EEA1
positive enlarged vesicles
RatiorelativetototalEEA1
0.015
0.010
0.005
0.000
Control 0´
Marfan 0´
Control 30´
Marfan 30´

Figure 6

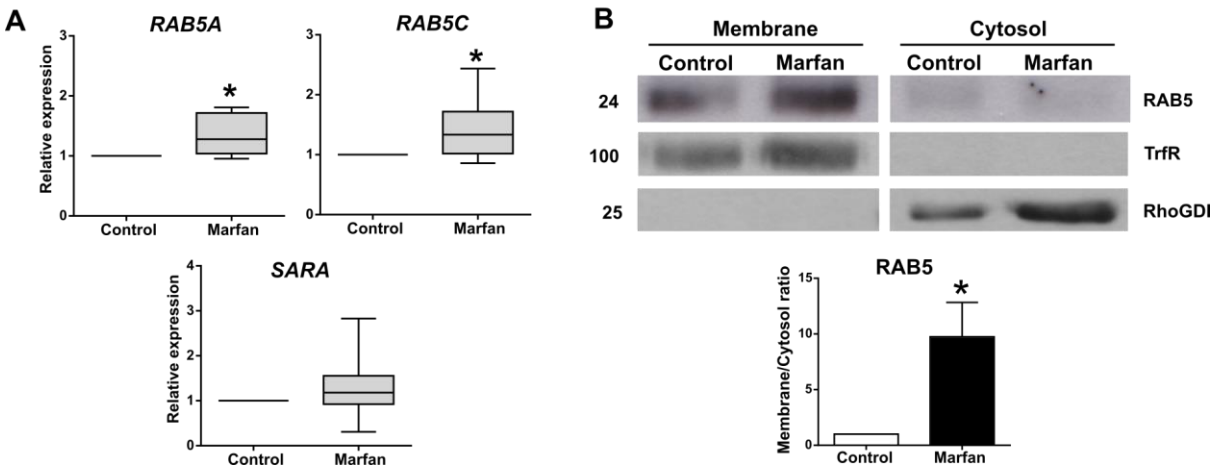
A
RAB5A
RAB5C
SARA
Relative expression
Control
Marfan
B
Membrane
Cytosol
Control
Marfan
24
100
25
RAB5
TrfR
RhoGDI
RAB5
Membrane/Cytosol ratio

SUPPLEMENTARY INFORMATION

Figure S1. Biotin-tagged TGF-β is bioactive. VSMC were starved and either fixed or TGF-β and b-TGF-β were allowed to internalize for 30 min. Nuclear translocation of pSMAD3 was analyzed (N=3, RM ANOVA *p<0.05, LSD Control vs. +TGF-β *p<0.05, Control vs. +b-TGF-β *p<0.05). Results are represented as mean ± SEM. Bar, 50 μm.

Figure S2. Clathrin- and caveolin-1-dependent downstream effectors are not transcriptionally altered in Marfan VSMC. RNA from VSMC was extracted and transcriptional expression of CLTC (Clathrin; N=6, p=0.2624), CAV1 (Caveolin-1; N=6, p=0.118), AP2B1 (Clathrin-adaptor protein complex 2 subunit B1; N=6, p=0.0598) and SMURF2 (SMAD Ubiquitination Regulatory Factor 2; N=6, p=0.3532) was analyzed. Expression results in Marfan patients were normalized to Control. Results are represented as box and whiskers from min to max.

Supplemental Figure 1

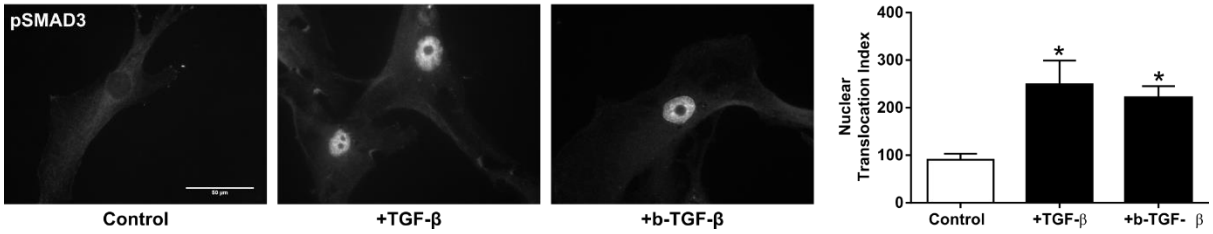

Supplemental Figure 2

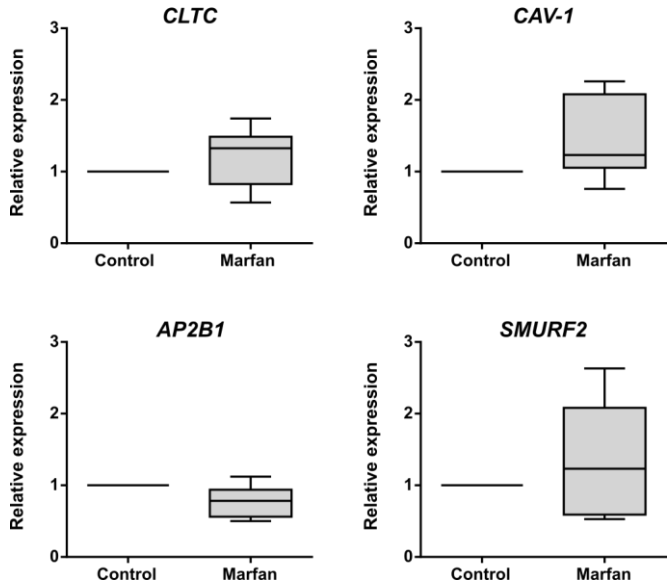

3'UTR mutations in *FBN1* are a molecular signature for aortic aneurysm in Marfan syndrome: involvement of the ER stress response and ERAD pathways

Anna-Maria Siegert,[1,8] Gerardo García Díaz-Barriga,[1, 4, 6, 7, 8] Anna Esteve-Codina,[2, 3] Darya Gorbenko del Blanco,[1] Jordi Alberch,[1,4, 6, 7] Simon Heath[2, 3] and Gustavo Egea[1,4,5]*

[1]Departament de Biomedicina, Facultat de Medicina i Ciències de la Salut, Universitat de Barcelona, Barcelona, 08036, Spain

[2]CNAG-CRG. Centre for Genomic Regulation (CRG), Barcelona Institue of Science and Technology (BIST), Barcelona, 08028, Spain

[3]Universitat Pompeu Fabra (UPF), Barcelona, 08002, Spain

[4]Institut d'Investigacions Biomèdiques August Pi I Sunyer, IDIBAPS, Barcelona, 08036, Spain

[5]Institut de Nanociència I Nanotecnologia, IN2UB, Universitat de Barcelona, Barcelona, 08036, Spain

[6]Institut de Neurociencias, UBNeuro, Universitat de Barcelona, Barcelona, 08036, Spain

[7]Centro de Investigaciones Biomédica en Red en Enfermedades Neurodegenerativas (CIBERNED), Instituto Carlos III, Madrid, 28031, Spain

[8]These authors contributed equally to this work

* Correspondence: gegea@ub.edu

Abstract

Marfan Syndrome (MFS) is an autosomal dominant mulitsystemic disease caused by mutations in the ECM protein fibrillin-1 (FBN1), which affects the formation of connective tissue elastic fibres. The most severe clinical outcome is the loss of aortic integrity leading to aneurysm formation. FBN1 is responsible for the structural integrity of the ECM as well as the regulation of TGF-β and its controlled release in the extracellular environment. However, the phenotype-genotype correlation is low and the prediction of disease outcome and organ involvement is challenging through conventional exonic sequencing only. Here we show that mutations in the non-coding 3´UTR region are sufficient to drive the aortic aneurysm. By sequencing of vascular smooth muscle cell mRNA derived from the dilated and non-dilated aortic medial layer from MFS patients, we identified a 3´UTR mutation thus far not annotated as MFS causative. We found 21 genes differentially expressed in the non-dilated zone with a clear gene ontological ER stress response with UPR, indicating a transient molecular profile in the aneurysm formation. Non-coding regions are often overlooked when sequencing MFS patients for diagnosis and ER stress induced by mutations in these regions have been linked to other connective tissue and cardiovascular diseases. We suggest that our results are of relevance for the future diagnosis of MFS and emphasise the importance of mutations in non-coding regions in the development of connective tissue diseases with impact on the cardiovascular system.

Marfan Syndrome (MFS [MIM: 154700]) is an autosomal dominant inherited disease that affects between 1.5 and 17.2 in 100,000 live births and has been associated with mutations in the protein Fibrillin-1 (FBN1 [MIM: 134797]) (1,2). MFS is characterised by skeletal, ocular and cardiovascular manifestations with the most severe problems arising from abnormalities of the cardiovascular system. Progressive aortic root enlargement and ascending aortic aneurysms are the primary cause of death and an estimated 5-7.5% of all ascending aortic aneurysms in the general population are attributed to MFS (3–7).

FBN1 is a large extracellular (ECM) glycoprotein which is a crucial component of connective tissue elastic fibres and an important extracellular regulator of the profibrotic Transforming Growth Factor-β (TGF-β) (8,9). Excessive release of TGF-β through mutated FBN1 leads to ECM remodelling, tissue fibrosis and compromised organ integrity (10). Mutations in *FBN1* are found throughout the entire length of the gene with only 12% of all variants being recurrent while the actual number of mutations might be significantly higher due to failure to report mutations or correctly diagnose MFS (11,12). Large-scale studies have addressed the association between *FBN1* mutation type and severity of disease as well as the specificity of organ involvement (7,11). In fact, several attempts have been made to classify mutations in the FBN1 gene to provide predictive power to phenotypic associations. For instance, nonsense, frameshift, splice site mutations and gene deletions have been classified as haploinsufficient (HI) phenotype causing, whereas missense mutations have been classified as dominant negative (DN) mutations (13). Despite this classification, studies are still underpowered to conclusively evaluate differential risk of aortic dissection or need for clinical intervention between this groups (14). Evidently, the large variability of variant mutations is not easily interpreted and variant databases have been found to contain confounding information (15). Furthermore, a significant portion of unresolved cases shows that conventional exon analysis might be insufficient to detect and phenotypically associate all disease-causing variants (16).

We here report a novel non-exonic *FBN1* 3'UTR mutation in vascular smooth muscle cells (VSMC) from the non-dilated aortic zone of MFS patients. We show distinct gene ontology enrichment and pathway enrichment from the differentially expressed genes (DEGs) indicating a transient endoplasmic reticulum (ER) stress response with intracellular consequences sufficient to drive aortic aneurysm formation. Thus, we show that non-exonic 3'UTR *FBN1* mutations are relevant in the prediction of MFS disease outcome.

Normal ascending aortic tissue was collected from heart donors through the organ donation organization at Hospital Clínic i Provincial (Barcelona, Spain). Ascending aortic samples were collected from MFS patients undergoing aortic aneurysm repair surgery. All patients fulfilled

diagnostic criteria according to Ghent nosology (17). Human tissues were collected with the required approval from the Institutional

Clinical Review Board of the clinical centers (Hospital Clínic i Provincial and the Marfan Unit at the Hospital 12 de Octubre in Madrid) and the patient's written consent conformed to the ethical guidelines of the 1975 Declaration of Helsinki. VSMC from five male MFS patients and four male control donors were extracted and cultured from the dilated (MFSd) and non-dilated (MFSnd) zone of aortic medial explants as stated previously (18). All patients had suffered aortic dilatation and had undergone surgical repair. VSMC were collected in sterile PBS and RNA was extracted using RNeasy® Mini Kit (Quiagen, Hilden, Germany). Total RNA was assayed for quantity and quality using Qubit® RNA HS Assay (Life Technologies) and RNA 6000 Nano Assay on a Bioanalyzer 2100. The RNASeq libraries were prepared from total RNA using the TruSeq®Stranded mRNA LT Sample Prep Kit. The libraries were sequenced on HiSeq2000 (Illumina, Inc) in paired-end mode with a read length of 2x76bp using TruSeq SBS Kit v4. In total, four different *FBN1* mutations were found in MFS samples of which one mutation was identical in patients M031d/nd and M054d/nd (Table 1). Two MFS patients did not have any mutation in the *FBN1* gene despite showing a clinical MFS phenotype. Patients M057d/nd and M054d/nd had a predicted missense variant on chr15 48446711 and chr15 48456714, respectively. The mutation on chr15 48446711 is a common mutation type found in MFS which substitutes a cysteine in the FBN1 calcium-binding EGF-like domain 32 (19). The second missense variant of patient M054d/nd on chr15 48456714 is predicted to cause another cysteine substitution, but at amino acid position 1782. However, this particular protein position has been described to show little cardiac effect (20). Furthermore, a second mutation was identified in patient M057d/nd on chr15 48416186. This mutation is an intron variant at rs76155368 SNP site as annotated (National Institute of Biotechnology Information, Available at: www.ncbi.nlm.nih.gov/SNP/, Accessed on May 5, 2017), which has not been previously associated with MFS. A second mutation was also identified in patient M054d/nd at chr15 48409001. Interestingly, this was the exact same mutation which was identified in patient M031d/nd. Given that of all reported *FBN1* mutations only 12% are recurrent, two out of five unrelated patients sharing the exact same mutation is an intriguing finding (11). The mutation is located at the SNP site rs56194244 within the 3´UTR of *FBN1* and has been associated with a sole case of MFS, with no citation available (National Institute of Biotechnology Information, Available at: www.ncbi.nlm.nih.gov/variation/view/, Accessed on May 5, 2017).

We proceeded to analyse the samples, using reads mapped to the GRCh38 (NCBI) version of the human genome, while gene quantification was obtained after feature summarization with the RSubread package in R. Raw counts were normalized with *voom* quantile normalization and CPM

values were log transformed to perform Principal Component Analysis (PCA) on all samples (Fig. 1A). Due to the high

variability within the MFSd and MFSnd groups and the heterogeneity of mutation types, principal components 1 to 3 accounted for a low cumulative amount of the variance (Fig. 1B). As a result of the high heterogeneity of mutations in our samples and the low genotype to phenotype correlation in MFS (7), patients were clustered by mutation to control for molecular consequences that could be mutation type-dependent. Thus, six groups were obtained from the MFS diagnosed patients: MFS 3´UTR (M031 and M054), MFS no mutation (M035 and M052) and MFS cysteine substitution (M054 and M057); the groups were further divided into dilated and non-dilated zone samples. We accounted for the fact that samples from patient M054 had both a 3'UTR mutation and a cysteine substitution by analysing the data twice, once clustering them in the 3'UTR group and once in the cysteine group in the experimental design.

For each clustered group, expression levels from the dilated zone and the non-dilated zone were compared with control expression levels. After using the *voom/limma*21 pipeline in the R environment*,* DEGs were selected based on the following criteria: log fold change >2, and adjusted p-value < 0.05 with Benjamini-Hochberg correction. Neither MFS patients with cysteine mutation nor MFS patients without *FBN1* mutation showed any significant changes in gene expression in either zone. However, 21 genes were differentially expressed in the non-dilated zone of MFS patients with 3´UTR mutation, of which 20 were upregulated and 1 was downregulated in comparison with control levels (Table 2 and Fig. 2). Intriguingly, no differences in gene expression were observed in the dilated zone from the same patients in comparison to control levels.

Amongst the upregulated targets were transcripts for proteins involved in the ER stress response to unfolded protein such as *SEL1L* (MIM: 602329), *MANF* (MIM: 601916) and *CRELD2* (MIM: 607171). Furthermore, the transcripts for molecular chaperones *HSP90B1* (MIM: 191175)*, HSPA5* (MIM: 138120)*, HSP90B3P, HSP90B2P*, *SDF2L1* (MIM: 607551) and the hypoxia-induced *HYOU1* (MIM: 601746) were also found to be upregulated. Further differentially expressed chaperones were DnaJ Heat Shock Protein Family Member B11, C3 and B9 (*DNAJB11* [MIM: 611341]*, DNAJC3* [MIM: 601184]*, DNAJB9* [MIM: 602634]*)*. Other targets resident in the ER and associated with protein processing were the Protein Disulfide Isomerase (PDI) Family A members PDIA4 and PDIA6 (MIM: 611099). Given the increased TGF-β release from the ECM in MFS, an interesting finding is the upregulation of TGF-β signal inhibitor *MTMR4* (MIM: 603559) and the downregulation of the TGF-β activator *ADAMTS1* (MIM: 605174). Further upregulations were observed for the novel protein coding sequence *ISOC2* (MIM:

612928), the multi-pass transmembrane protein *TMEM50B*, the Cyclin-dependent-Kinase associated protein *CDK2AP2* and the two pseudogenes *AL354702.7* and *RP11-39C10.1*.

Gene ontology analysis was performed using the GeneCodis tool for modular and singular enrichment analysis (22–24). Out of the 21 differentially expressed genes, 4 genes did not show any annotations: *HSP90B3P, HSP90B2P, AL354702.7* and *RP11-39C10.1*. Enrichment analysis clearly identified a specific cluster of Biological Processes (BP) associated with the catabolic cellular mechanisms involved with glycoprotein misfolding in the ER. Amongst the most significant processes were *protein folding* (GO: 0006457)*, ER-associated protein catabolic processes* (GO: 0030433) and *glycerol ether metabolic processes* (GO: 0006662) (Fig. 3A). The upregulated genes associated with these, amongst others, belong to the family of molecular chaperones such as *HSP90B1, HSPA5,* the *DNAJ* members and the ER resident *PDIA6* and *PDIA4*. The elemental activities as defined by Molecular Functions (MF) of the gene products were found to be *misfolded protein binding* (GO: 0051787) and *unfolded protein binding* (GO: 0051082) as well as *heat shock protein binding* (GO: 0031072), *chaperone binding* (GO: 0051087), *protein disulphide isomerase* and *oxireductase* activity (GO: 003756 and GO: 0015035 respectively) (Fig. 3B). In line with the previous results, enrichment analysis identified the *endoplasmic reticulum* (GO: 005783), the *endoplasmic reticulum-Golgi intermediate compartment* (GO: 005793) and the *melanosome* (GO: 0042470) as cellular compartments (CC) of gene product activity (Fig. 3C). Besides chaperone family members and protein isomerases, gene products of *SDF2L1, SEL1L, TMEM50B, MANF, HYOU1* and *CRELD2* were also associated with the CC identified, which strongly supports the ER as the main subcellular localization of the affected DEGs.

In addition, the Kyoto Encyclopedia of Genes and Genomes (KEGG) pathway maps identified genes involved in *protein processing in the endoplasmic reticulum* as a molecular network (Fig. 4A). We then performed Signalling Pathway Impact Analysis (SPIA) (25) to identify the most relevant altered cellular pathways due to 3´UTR *FBN1* mutation. We found a significant alteration of *protein processing at the endoplasmic reticulum* (Fig. 4B) which was shown to be activated on the 3'UTR MFS samples with respect to controls (p-value=1.10×10^{-7}). More specifically, our identified differentially expressed genes were shown to be involved in protein recognition by luminal chaperones and protein targeting of terminally misfolded and accumulated proteins leading to ER-associated protein degradation (ERAD) of ubiquitin-tagged proteins by the proteasome.

Finally, given that the 3´ UTR is the main target for microRNAs (miR) regulation (26), we performed an analysis of target prediction for the 3' UTR SNP target identified in the two MFS patients M031d/nd and M054d/nd using the miRDB online database for target prediction and functional annotations (Available at: www.mirdb.org/miRDB/, Accessed on May 5, 2017). *FBN1* was predicted to be targeted

by 110 miRNAs of which the highest scoring ones were the family of miR-29 (miR-29a, miR-29b and miR29c) whose overexpression has previously been described to drive aneurysm formation in MFS.27,28 Furthermore, using a custom prediction with 50 nucleotides flanking the mutation region up- and downstream, we found miR-1252-5p (NCBI gene ID: 100302136) to bind to the exact SNP site at chr15 48409001 with a prediction score of 56 of 100. Very little further information is currently available on miR-1252-5p.

Due to the limited genotype-phenotype correlation and low prediction of disease outcome in MFS, many attempts are made to correlate mutation types with disease progression and organ involvement. It has recently been argued that the detection of non-exonic mutation variants is compromised due to conventional molecular testing, which omits deep-intronic mutations, pseudo-exons and untranslated regions (16). In addition, few studies exist that directly address the genetic alterations posing a risk of aneurysm formation and dissection. Here we focused on a group of 5 male patients who shared the clinical history of aortic aneurysm, dilatation, and reparatory surgery and therefore represented a homogenous group with respect to organ involvement. Despite the shared clinical outcome between patients, we found large heterogeneity of *FBN1* mutations including their absence, emphasizing the tremendous variety of mutation types. As a matter of fact, even with a technique as powerful as RNA sequencing, we cannot exclude the possibility of other intronic mutations in our samples. Strikingly, we found a novel mutation in two patients in the *FBN1* 3´UTR, which, given the small percentage of recurrence in *FBN1* mutation, highlights the potential importance of this particular gene loci**.** Interestingly, 3´UTR mutations have in fact been demonstrated to be critical gene locations in congenital heart diseases (29,30). This is attributable to their regulatory and controlling functions such as subcellular targeting as well as rate of translation and degradation (29). However, in MFS, 3´UTR mutations are rarely studied. Compellingly, based on the genetic mutations found in our studied samples only two of our patients (M054 and M057) would have been classified under the prevailing paradigm of mutation analysis under the DN category. Of those, at least M054 would have been misclassified, presenting a DN described as non-aortic risk causative and having a second mutation that is not routinely screened for, which in this case might be the driving force of aneurysm formation.

RNA sequencing analysis predicted a strong response to unfolded protein in the ER in VSCM from the non-dilated aortic zone in patients carrying the 3´UTR mutation. This included the increased expression of cell stress-associated chaperones and the activation of ERAD. The unfolded protein response (UPR) and ERAD are primarily adaptive mechanisms to restore homeostasis when misfolded proteins are present, but, if unresolved, lead to pathophysiological changes in gene expression patterns (31). The fact that no DEGs were found in the dilated zone of VSMC with 3´UTR mutation

indicates a transient response as seen previously in a model of cardiac fibrosis, indicating that the UPR coping mechanism in response to ER homeostasis disruption eventually manifesting itself in the aortic phenotype (32). Accordingly, in connective tissue diseases, it was widely believed that the mutant gene product is the primary cause of disease phenotype. However, it is becoming clear that UPR and ER stress, which are induced by the mutant gene product, are key mediators of disease outcome (33). In addition, prolonged UPR has been shown to induce cardiac remodelling and fibrosis through pathogenic consequences such as cellular apoptosis and alterations in signalling pathways (34–36). This might well be attributed to the implication of ER stress key players such as HSP90, which simultaneously are stabilizer of the TGF-β signalling cascade, inducing collagen deposition and fibrosis (37). Compellingly, it has recently been shown that the fibrosis reducing effect of Losartan, the pharmacological standard for MFS treatment, is due to the attenuation of ER stress, and in particular to the inhibition of HSPA5 in chronic renal diseases (38,39). ER stress can even induce the same phenotype as a mutation in *Col10a1* (MIM: 120110) in a mouse model of the connective tissue disease metaphyseal chondrodysplasia type Schmid (MCDS [MIM: 156500]). Additionally, ER stress levels correlate with severity of MCDS, providing compelling evidence for the impact of ER stress on connective tissue disease outcome (40).

The phenotype driving potential of the identified 3´UTR mutation in MFS is supported by its binding site for the novel and scarcely studied miR-1252-5p. As mRNAs mainly target 3´UTR sequences and act as mRNA degradation inducer, they are considered to be an evolutionary conserved quality control (26). Lacking the binding site through mutation may lead to insufficient *FBN1* degradation, accumulation in the ER and consequentially ER stress. Deregulation of miRNAs is a scarcely studied but intriguing new field in MFS due to the recently discovered miR-29 which specifically targets ECM genes such as collagens (*COL1A1* [MIM: 120150]*, COL1A2* [MIM: 120160]*, COL3A1* [MIM: 120180]), elastin (*ELN* [MIM: 130160]) and *FBN1* (27). Further research towards the involvement of miRNAs and their deregulation through 3´UTR mutation could be an interesting tool to further elucidate the disease development of MFS.

In conclusion, we describe for the first time a 3'UTR mutation of *FBN1* in patients with aortic rupture. Additionally, our results strongly suggest that *FBN1* 3'UTR mutations are sufficient to drive aortic aneurysm formation in MFS patients. Pathway analysis of DEGs strongly converged on processes that produce ER stress, which in turn is capable of inducing downstream pathogenic effects since ER homeostasis mediators simultaneously stabilise fibrotic signals (37,41). Due to conventional exonic testing, non-coding regions are often omitted in the genetic diagnosis of MFS, leading to genetically unresolved cases and an incomplete view of genotype-phenotype correlation. The inclusion of non-

coding *FBN1* 3'UTR regions as a diagnostic criterion could provide new insights into thus far unknown patient cluster and might allow for a better aortic risk prediction.

REFERENCES

1. Kodolitsch, Y. Von, De Backer, J., Schüler, H., Bannas, P., Behzadi, C., Bernhardt, A.M., Hillebrand, M., Fuisting, B., Sheikhzadeh, S., Rybczynski, M., et al. (2015). Perspectives on the revised ghent criteria for the diagnosis of marfan syndrome. Appl. Clin. Genet. *8*, 137–155.

2. Dietz, H.C., Cutting, G.R., Pyeritz, R.E., Maslen, C.L., Sakai, L.Y., Corson, G.M., Puffenberger, E.G., Hamosh, A., Nanthakumar, E.J., and Curristin, S.M. (1991). Marfan syndrome caused by a recurrent de novo missense mutation in the fibrillin gene. Nature *352*, 337–339.

3. Januzzi, J., Marayati, F., Mehta, R., Cooper, J., O'Gara, P., Sechtem, U., Bossone, E., Evangelista, A., Oh, J., Nienaber, C., et al. (2004). Comparison of aortic dissection in patients with and without Marfan's syndrome (results from the International Registry of Aortic Dissection). Am. J. Cardiol. *94*, 400–402.

4. Yao, Z., Jaeger, J.C., Ruzzo, W.L., Morale, C.Z., Emond, M., Francke, U., Milewicz, D.M., Schwartz, S.M., and Mulvihill, E.R. (2007). A Marfan syndrome gene expression phenotype in cultured skin fibroblasts. BMC Genomics *8*, 319.

5. Milewicz, D.M. (2005). Treatment of Aortic Disease in Patients With Marfan Syndrome. Circulation *111*, e150–e157.

6. Karnebeek, C.D.M. Van, Naeff, M.S.J., Mulder, B.J.M., Hennekam, R.C.M., and Offringa, M. (2001). Natural history of cardiovascular manifestations in Marfan syndrome Natural history of cardiovascular manifestations in Marfan syndrome. 129–137.

7. Faivre, L., Collod-Beroud, G., Loeys, B.L., Child, A., Binquet, C., Gautier, E., Callewaert, B., Arbustini, E., Mayer, K., Arslan-Kirchner, M., et al. (2007). Effect of mutation type and location on clinical outcome in 1,013 probands with Marfan syndrome or related phenotypes and FBN1 mutations: an international study. Am. J. Hum. Genet. *81*, 454–466.

8. Dijke, P., and Arthur, H.M. (2007). Extracellular control of TGF β signalling in vascular development and disease. *8*.

9. Neptune, E.R., Frischmeyer, P. a, Arking, D.E., Myers, L., Bunton, T.E., Gayraud, B., Ramirez, F., Sakai, L.Y., and Dietz, H.C. (2003). Dysregulation of TGF-β activation contributes to pathogenesis in Marfan syndrome. Nat. Genet. *33*, 407–411.

10. Ruiz-Ortega, M., Rodríguez-Vita, J., Sanchez-Lopez, E., Carvajal, G., and Egido, J. (2007). TGF-β signaling in vascular fibrosis. Cardiovasc. Res. *74*, 196–206.

11. Collod-Beroud, G., Le Bourdelles, S., Ades, L., Ala-Kokko, L., Booms, P., Boxer, M., Child, A., Comeglio, P., De Paepe, A., Hyland, J.C., et al. (2003). Update of the UMD-FBN1 mutation database and creation of an FBN1 polymorphism database. Hum. Mutat. *22*, 199–208.

12. Sakai, L.Y., Keene, D.R., Renard, M., and De Backer, J. (2016). FBN1: The disease-causing gene for Marfan syndrome and other genetic disorders. Gene *591*, 279–291.

13. Landis, B.J., Veldtman, G.R., and Ware, S.M. (2017). Genotype – phenotype correlations in Marfan syndrome. Heart 8–11.

14. Franken, R., Teixido-Tura, G., Brion, M., Forteza, A., Rodriguez-Palomares, J., Gutierrez, L., Garcia Dorado, D., Pals, G., Mulder, B.J., and Evangelista, A. (2017). Relationship between fibrillin-1 genotype and severity of cardiovascular involvement in Marfan syndrome. Heart heartjnl-2016-310631.

15. Groth, K. a., Gaustadnes, M., Thorsen, K., Østergaard, J.R., Jensen, U.B., Gravholt, C.H., and Andersen, N.H. (2015). Difficulties in diagnosing Marfan syndrome using current FBN1 databases. Genet. Med. *18*, 1–5.

16. Gillis, E., Kempers, M., Salemink, S., Timmermans, J., Cheriex, E.C., Bekkers, S.C.A.M., Fransen, E., Die-smulders, C.E.M. De, Loeys, B.L., and Laer, L. Van (2014). An FBN1 Deep Intronic Mutation in a Familial Case of Marfan Syndrome: An Explanation for Genetically Unsolved Cases? Hum Mutat. 35, 571-4.

17. Loeys, B.L., Dietz, H.C., Braverman, A.C., Callewaert, B.L., Backer, J. De, Devereux, R.B., Hilhorst-Hofstee, Y., Jondeau, G., Faivre, L., Milewicz, D.M., et al. (2010). The revised Ghent nosology for the Marfan syndrome. J. Med. Genet. *47*, 476–485.

18. Crosas-Molist, E., Meirelles, T., Lopez-Luque, J., Serra-Peinado, C., Selva, J., Caja, L., del Blanco, D.G., Uriarte, J.J., Bertran, E., Mendizabal, Y., et al. (2015). Vascular Smooth Muscle Cell Phenotypic Changes in Patients With Marfan Syndrome. Arterioscler. Thromb. Vasc. Biol. 960–972.

19. Rommel, K., Karck, M., Haverich, A., von Kodolitsch, Y., Rybczynski, M., Muller, G., Singh, K.K., Schmidtke, J., and Arslan-Kirchner, M. (2005). Identification of 29 novel and nine recurrent fibrillin-1 (FBN1) mutations and genotype-phenotype correlations in 76 patients with Marfan syndrome. Hum. Mutat. *26*, 529–539.

20. Ades, L.C., Holman, K.J., Brett, M.S., Edwards, M.J., and Bennetts, B. (2004). Ectopia lentis phenotypes and the FBN1 gene. Am J Med Genet A *126A*, 284–289.

21. Ritchie, M.E., Phipson, B., Wu, D., Hu, Y., Law, C.W., Shi, W., and Smyth, G.K. (2015). limma powers differential expression analyses for RNA-sequencing and microarray studies. Nucleic Acids Res. *43*, e47.

22. Carmona-Saez, P., Chagoyen, M., Tirado, F., Carazo, J.M., and Pascual-Montano, A. (2007). GENECODIS: a web-based tool for finding significant concurrent annotations in gene lists. Genome Biol. *8*, R3.

23. Nogales-Cadenas, R., Carmona-Saez, P., Vazquez, M., Vicente, C., Yang, X., Tirado, F., Carazo, J.M., and Pascual-Montano, A. (2009). GeneCodis: interpreting gene lists through enrichment analysis and integration of diverse biological information. Nucleic Acids Res. *37*, W317-22.

24. Tabas-Madrid, D., Nogales-Cadenas, R., and Pascual-Montano, A. (2012). GeneCodis3: a non-redundant and modular enrichment analysis tool for functional genomics. Nucleic Acids Res. *40*, W478-83.

25. Tarca, A.L., Draghici, S., Khatri, P., Hassan, S.S., Mittal, P., Kim, J.-S., Kim, C.J., Kusanovic, J.P., and Romero, R. (2009). A novel signaling pathway impact analysis. Bioinformatics *25*, 75–82.

26. Meunier J, Lemoine F, Soumillon M, Liechti A, Weier M, Guschanski K, Hu H, Khaitovich P, K.H. (2013). Birth and expression evolution of mammalian microRNA genes. Genome Res. 1–12.

27. Merk, D.R., Chin, J.T., Dake, B.A., Maegdefessel, L., Miller, M.O., Kimura, N., Tsao, P.S., Iosef, C., Berry, G.J., Mohr, F.W., et al. (2012). miR-29b Participates in Early Aneurysm Development in Marfan Syndrome.

28. Ott, C.E., Grünhagen, J., Jäger, M., Horbelt, D., Schwill, S., Kallenbach, K., Guo, G., Manke, T., Knaus, P., Mundlos, S., et al. (2011). MicroRNAs differentially expressed in postnatal aortic development downregulate elastin via 3′ UTR and coding-sequence binding sites. PLoS One *6*.

29. Reamon-Buettner, S.M., Cho, S.-H., and Borlak, J. (2007). Mutations in the 3'-untranslated region of GATA4 as molecular hotspots for congenital heart disease (CHD). BMC Med. Genet. *8*, 38.

30. Spengler, R.M., Zhang, X., Cheng, C., McLendon, J.M., Skeie, J.M., Johnson, F.L., Davidson, B.L., and Boudreau, R.L. (2016). Elucidation of transcriptome-wide microRNA binding sites in human cardiac tissues by Ago2 HITS-CLIP. Nucleic Acids Res. *44*, 7120–7131.

31. Bateman, J.F., Boot-Handford, R.P., and Lamandé, S.R. (2009). Genetic diseases of connective tissues: cellular and extracellular effects of ECM mutations. Nat. Rev. Genet. *10*, 173–183.

32. Groenendyk, J., Lee, D., Jung, J., Dyck, J.R.B., Lopaschuk, G.D., Agellon, L.B., and Michalak, M. (2016). Inhibition of the unfolded protein response mechanism prevents cardiac fibrosis. PLoS One *11*, 1–15.

33. Boot-Handford, R.P., and Briggs, M.D. (2010). The unfolded protein response and its relevance to connective tissue diseases. Cell Tissue Res. *339*, 197–211.

34. Szegezdi, E., Logue, S.E., Gorman, A.M., and Samali, A. (2006). Mediators of endoplasmic reticulum stress-induced apoptosis. EMBO Rep. *7*, 880–885.

35. Zhang, K., and Kaufman, R.J. (2004). Signaling the unfolded protein response from the endoplasmic reticulum. J. Biol. Chem. *279*, 25935–25938.

36. Ayala, P., Montenegro, J., Vivar, R., Letelier, A., Urroz, P.A., Copaja, M., Pivet, D., Humeres, C., Troncoso, R., Vicencio, J.M., et al. (2012). Attenuation of endoplasmic reticulum stress using the chemical chaperone 4-phenylbutyric acid prevents cardiac fibrosis induced by isoproterenol. Exp. Mol. Pathol. *92*, 97–104.

37. García, R., Merino, D., Gómez, J.M., Nistal, J.F., Hurlé, M.A., Cortajarena, A.L., and Villar, A. V. (2016). Extracellular heat shock protein 90 binding to TGF?? receptor I participates in TGF-β-mediated collagen production in myocardial fibroblasts. Cell. Signal. *28*, 1563–1579.

38. Habashi, J.P., Judge, D.P., Holm, T.M., Cohn, R.D., Loeys, B.L., Cooper, T.K., Myers, L., Klein, E.C., Liu, G., Calvi, C., et al. (2006). Losartan, an AT1 antagonist, prevents aortic aneurysm in a mouse model of Marfan syndrome. Science *312*, 117–121.

39. Kim, H., Baek, C.H., Lee, R.B., Chang, J.W., Yang, W.S., and Lee, S.K. (2017). Anti-fibrotic effect of losartan, an angiotensin II receptor blocker, is mediated through inhibition of ER stress via up-regulation of SIRT1, followed by induction of HO-1 and thioredoxin. Int. J. Mol. Sci. *18*, 1–17.

40. Rajpar, M.H., McDermott, B., Kung, L., Eardley, R., Knowles, L., Heeran, M., Thornton, D.J., Wilson, R., Bateman, J.F., Poulsom, R., et al. (2009). Targeted induction of endoplasmic reticulum stress induces cartilage pathology. PLoS Genet. *5*, e1000691.

41. Lee, J., An, Y.S., Kim, M.-R., Kim, Y.-A., Lee, J.K., Hwang, C.S., Chung, E., Park, I.-C., and Yi, J.Y. (2016). Heat Shock Protein 90 Regulates Subcellular Localization of Smads in Mv1Lu Cells. J. Cell. Biochem. *117*, 230–238.

FIGURE LEGENDS

Figure 1. Principal Component Analysis of DE genes. Raw counts were normalized and log transformed and Principal Component Analysis (PCA) was performed on all samples. (A) Linear combination of components 1 to 3 are shown. Control samples are shown in green, the non-dilated aortic zone of MFS patients in red and the dilated zone in yellow. (B) Standard deviation, Proportion of variance and cumulative proportion of principal components 1 to 3.

Figure 2. Genes from the non-dilated aortic zone of 3´UTR FBN1 mutations are differentially expressed. A heat map of the 21 differentially expressed genes is shown. MFSnd 3´UTR (red box) expression levels were compared with control (green box) expression levels. Differentially expressed genes were selected based on the following criteria: adjusted p-value < 0.05 with Benjamini-Hochberg correction, and LFC > 2. Colour codes are representative for log2 RPKM (reads per kilobase million). Counts range from low (black) to high (yellow).

Figure 3. Gene ontology enrichment analysis of VSMC from the non-dilated aortic zone of MFS patients vs controls. GO was identified by GeneCodis. (A) GO Biological Processes identified a distinct profile of ER-associated processes in response to protein misfolding. (B) The Molecular Functions associated with the differentially expressed genes were grouped into unfolded protein binding. (C) The Cellular Components involved in the misfolded protein binding processes were shown to be the ER and the ER-Golgi intermediates.

Figure 4. KEGG pathway Map and SPIA analysis of most relevant altered pathways in VSMC from the non-dilated zone of 3´UTR FBN1 mutation. (A) KEGG pathway enrichment analysis identifies protein processing in the endoplasmic reticulum as the molecular network involving the DEG of the 3´UTR FBN1 mutation in the non-dilated aortic zone. (B) SPIA visual map of the intracellular molecular network affected by the 3´UTR FBN1 mutation in the non-dilated aortic zone.

FBN1 mutation VSMC extracted from the dilated aortic medial zone								
		Mutation type		M031d	M035d	M052d	M054d	M057d
chr15	48409001	3´UTR	G>A	*DP2=2,49*	DP2=51,0	DP2=191,0	*DP2=66,60*	DP2=129,0
chr15	48416186	intron	C>T	DP2=9,0	DP2=8,0	DP2=8,0	DP2=7,0	*DP2=9,12*
chr15	48446711	missense	C>T	DP2=1422,0	DP2=1091,0	DP2=4060,1	DP2=3455,1	*DP2=2025,1467*
chr15	48456714	missense	C>T	DP2=721,0	DP2=546,0	DP2=1994,0	*DP2=807,845*	DP2=1693,1
FBN1 mutation VSMC extracted from the non-dilated aortic medial zone								
		Mutation type		M031	M035	M052	M054	M057
chr15	48409001	3´UTR	G>A	*DP2=4,21*	DP2=73,0	DP2=73,0	*DP2=36,39*	DP2=58,0
chr15	48416186	intron	C>T	DP2=2,0	DP2=15,0	DP2=10,0	DP2=8,0	*DP2=8,3*
chr15	48446711	missense	C>T	DP2=1140,0	DP2=1691,1	DP2=1805,0	DP2=1818,0	*DP2=817,694*
chr15	48456714	missense	C>T	DP2=551,0	DP2=796,0	DP2=843,0	*DP2=496,503*	DP2=839,0

Table 1. FBN1 mutations of MFS patients. FBN1 was screened for mutations in all five male MFS diagnosed patients. In total four different mutations were found of which one was shared between two patients (chr15 48409001). Cysteine substitutions (chr15 48446711 and 48456714) were both predicted to cause missense mutations of the gene. One novel intronic mutation (chr15 48416186) with unknown outcome was found as a compound mutation in one patient. Upper panel: mutation type and chromosomal location identified in VSMC from the dilated aortic medial zone. Lower panel: mutation type and chromosomal location identified in VSMC from the non-dilated aortic medial zone. Italic font indicates the number of an alternative allele to the reference sequence e.g. a FBN1 variant different from the unmutated allele

Differentially expressed genes MFS non-dilated zone 3´UTR mutation vs. Control						
Ensembl_ID	Chr	P.Value	adj.P.Val	Entrez_ID	Gene_Symbol	logFC
ENSG00000145050	3	1.51E-07	0.000881447	7873	MANF	2.218700236
ENSG00000203914	1	2.26E-07	0.000881447	343477	HSP90B3P	1.401730176
ENSG00000259706	15	2.66E-07	0.000881447	7190	HSP90B2P	1.512506073
ENSG00000184164	22	1.90E-06	0.00308846	79174	CRELD2	2.106644862
ENSG00000090520	3	2.04E-06	0.00308846	51726	DNAJB11	1.809949117
ENSG00000102580	13	2.17E-06	0.00308846	5611	DNAJC3	1.477015156
ENSG00000149428	11	2.07E-06	0.00308846	10525	HYOU1	2.271583263
ENSG00000215895	1	1.42E-05	0.014096289	400750	AL354702.7	2.101273797
ENSG00000128228	22	4.88E-06	0.00606918	23753	SDF2L1	2.452464154
ENSG00000142188	21	2.21E-05	0.018290602	757	TMEM50B	1.413483265
ENSG00000166598	12	9.41E-06	0.010390831	7184	HSP90B1	1.447354609
ENSG00000167797	11	3.81E-05	0.027051472	10263	CDK2AP2	1.472378972
ENSG00000108389	17	4.59E-05	0.03040555	9110	MTMR4	1.117620691
ENSG00000154734	21	1.94E-05	0.017550027	9510	ADAMTS1	-2.405840232
ENSG00000250746	4	6.38E-05	0.036255719	100288073	RP11-39C10.1	1.920543762
ENSG00000071537	14	5.47E-05	0.033970467	6400	SEL1L	1.313808596
ENSG00000044574	9	3.80E-05	0.027051472	3309	HSPA5	1.990675005
ENSG00000063241	19	8.97E-05	0.044360615	79763	ISOC2	1.046034128
ENSG00000128590	7	0.000103118	0.044578343	4189	DNAJB9	1.738096843
ENSG00000143870	2	9.37E-05	0.044360615	10130	PDIA6	1.044457326
ENSG00000155660	7	9.82E-05	0.044364931	9601	PDIA4	1.91095168

Table 2. Differentially expressed genes identified in FBN1 MFSnd 3'UTR mutation vs Control. 21 genes were identified to be differentially expressed in VSMC from the non-dilated zone of MFS patients with 3´UTR mutation in FBN1. All genes but ADAMTS1 were upregulated in comparison with control.

Figure 1

A

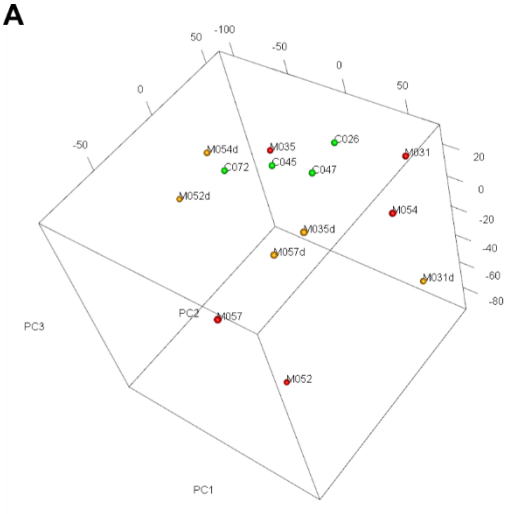

B

	PC1	PC2	PC3
Standard deviation	53.47	40.29	35.24
Proportion of Variance	0.29	0.16	0.12
Cumulative Proportion	0.29	0.45	0.58

Figure 2

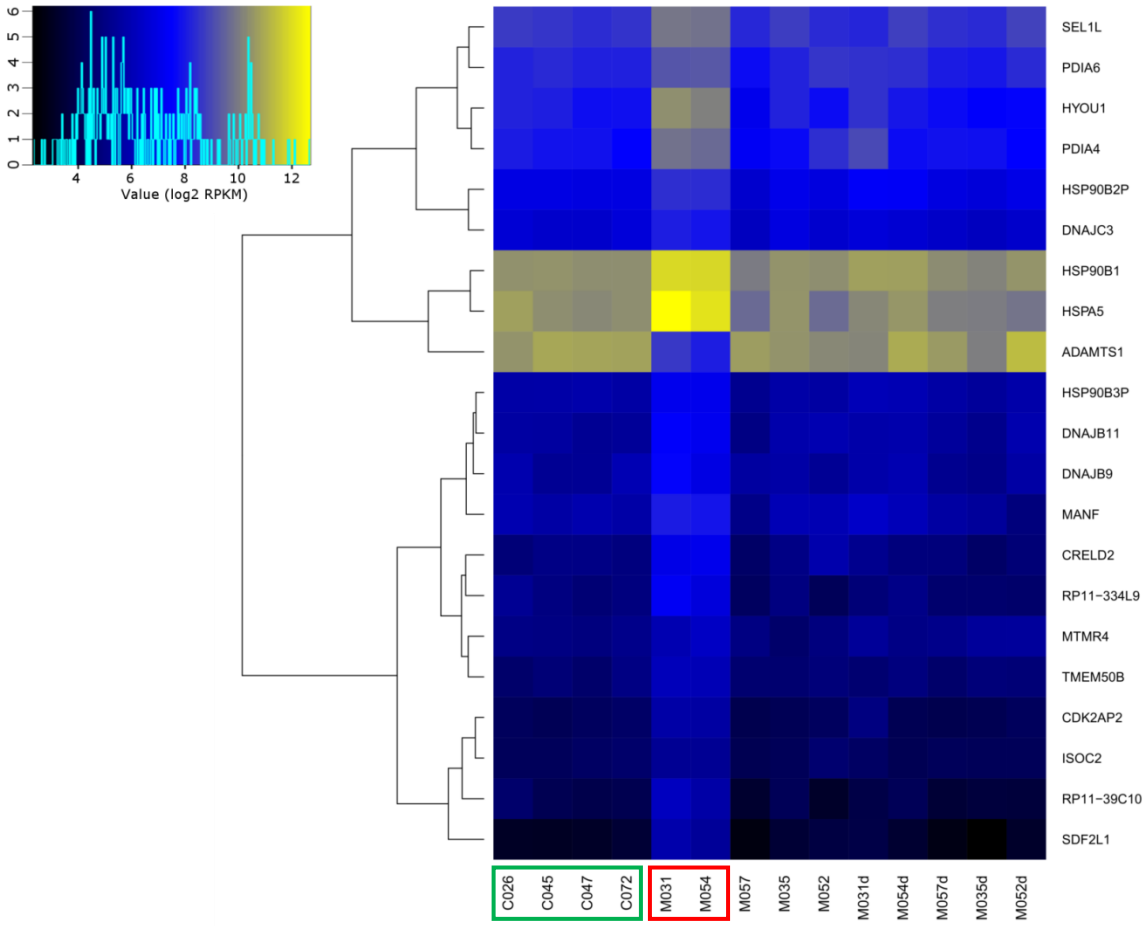
0 1 2 3 4 5 6
4 6 8 10 12
Value (log2 RPKM)
SEL1L
PDIA6
HYOU1
PDIA4
HSP90B2P
DNAJC3
HSP90B1
HSPA5
ADAMTS1
HSP90B3P
DNAJB11
DNAJB9
MANF
CRELD2
RP11−334L9
MTMR4
TMEM50B
CDK2AP2
ISOC2
RP11−39C10
SDF2L1
C026
C045
C047
C072
M031
M054
M057
M035
M052
M031d
M054d
M057d
M035d
M052d

Figure 3

A

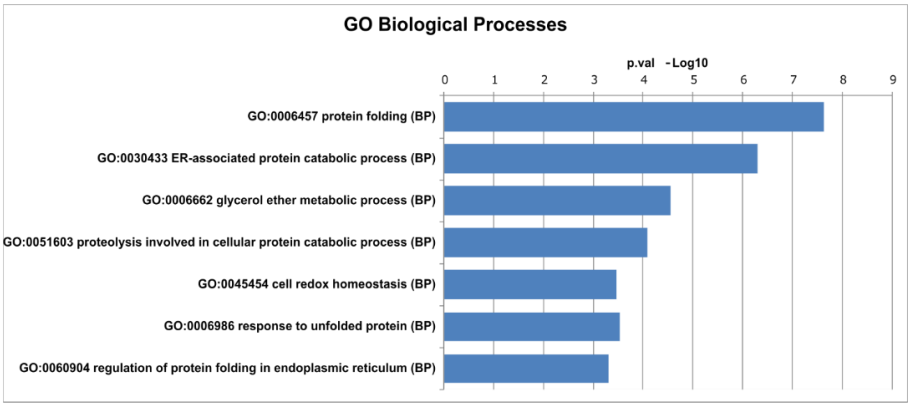
GO Biological Processes
p.val -Log10
0
1
2
3
4
5
6
7
8
9
GO:0006457 protein folding (BP)
GO:0030433 ER-associated protein catabolic process (BP)
GO:0006662 glycerol ether metabolic process (BP)
GO:0051603 proteolysis involved in cellular protein catabolic process (BP)
GO:0045454 cell redox homeostasis (BP)
GO:0006986 response to unfolded protein (BP)
GO:0060904 regulation of protein folding in endoplasmic reticulum (BP)

B

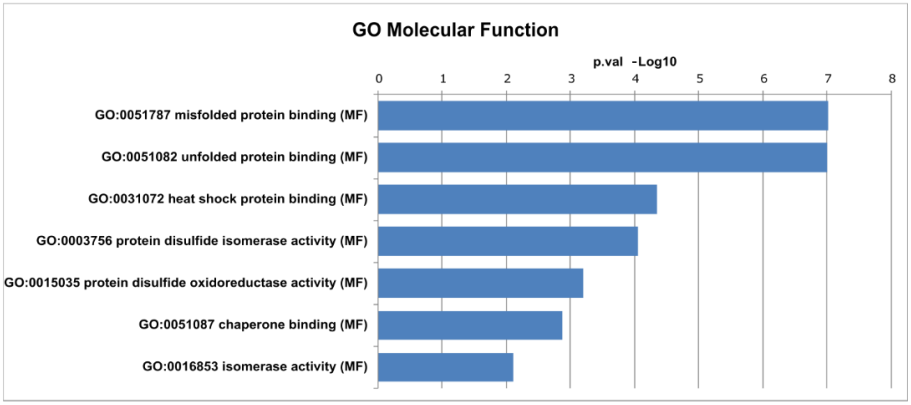
GO Molecular Function
p.val -Log10
0
1
2
3
4
5
6
7
8
GO:0051787 misfolded protein binding (MF)
GO:0051082 unfolded protein binding (MF)
GO:0031072 heat shock protein binding (MF)
GO:0003756 protein disulfide isomerase activity (MF)
GO:0015035 protein disulfide oxidoreductase activity (MF)
GO:0051087 chaperone binding (MF)
GO:0016853 isomerase activity (MF)

C

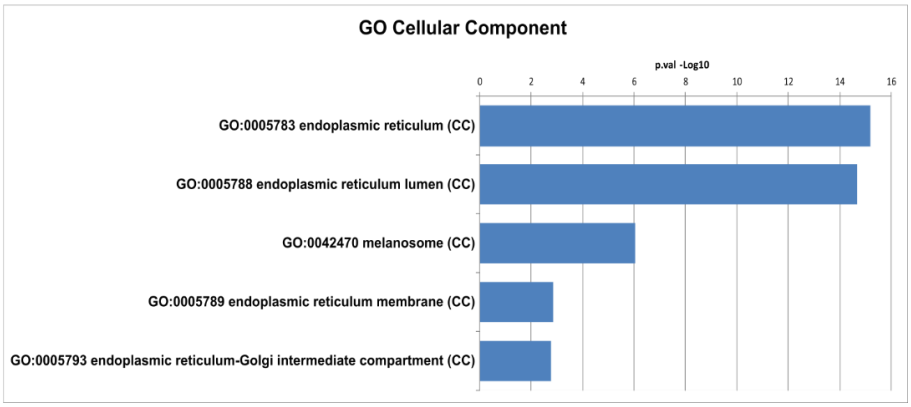
GO Cellular Component
p.val -Log10
0
2
4
6
8
10
12
14
16
GO:0005783 endoplasmic reticulum (CC)
GO:0005788 endoplasmic reticulum lumen (CC)
GO:0042470 melanosome (CC)
GO:0005789 endoplasmic reticulum membrane (CC)
GO:0005793 endoplasmic reticulum-Golgi intermediate compartment (CC)

Figure 4

A

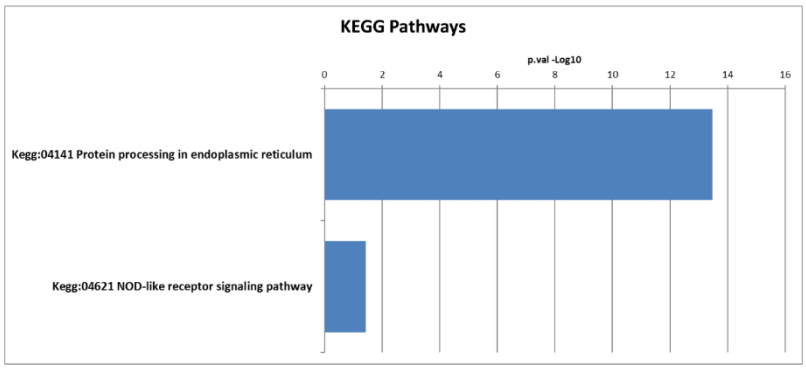
KEGG Pathways
p.val -Log10
0
2
4
6
8
10
12
14
16
Kegg:04141 Protein processing in endoplasmic reticulum
Kegg:04621 NOD-like receptor signaling pathway

B

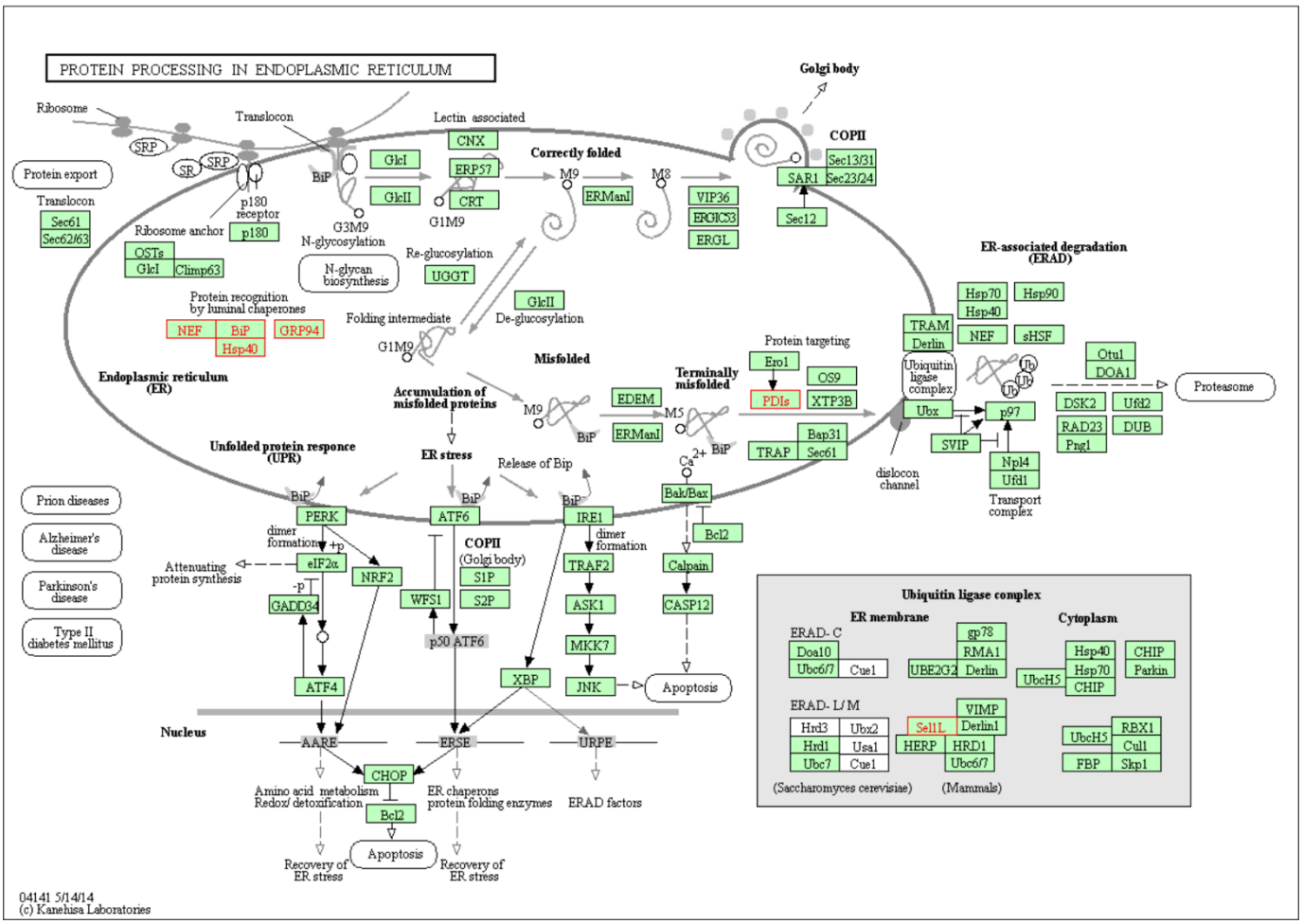
PROTEIN PROCESSING IN ENDOPLASMIC RETICULUM
Golgi body
Ribosome
Translocon
Lectin associated
CNX
COPII
Sec13/31
Sec23/24
SAR1
Sec12
Protein export
Translocon
Sec61
Sec62/63
Ribosome anchor
p180
p180 receptor
OSTs
Glcl
Clmp63
GlcI
GlcII
CRT
ERP57
Correctly folded
M9
M8
ERManI
VIP36
ERGIC53
ERGL
G3M9
N-glycosylation
G1M9
N-glycan biosynthesis
Re-glucosylation
UGGT
GlcII
De-glucosylation
Protein recognition by luminal chaperones
NEF
BiP
Hsp40
GRP94
Folding intermediate
G1M9
Endoplasmic reticulum (ER)
Misfolded
Accumulation of misfolded proteins
EDEM
M9
M5
ERManI
Terminally misfolded
Protein targeting
Ero1
OS9
PDIs
XTP3B
Bap31
TRAP
Sec61
ER-associated degradation (ERAD)
TRAM
Derlin
Ubiquitin ligase complex
Ubx
SVIP
p97
Npl4
Ufd1
Transport complex
dislocon channel
Hsp70
Hsp90
Hsp40
NEF
sHSF
Otu1
DOA1
DSK2
Ufd2
RAD23
DUB
Png1
Proteasome
Unfolded protein responce (UPR)
ER stress
Release of Bip
Ca2+
BiP
PERK
ATF6
IRE1
Bak/Bax
Bcl2
dimer formation
+p
eIF2α
-p
Attenuating protein synthesis
NRF2
GADD34
ATF4
WFS1
p50 ATF6
COPII
(Golgi body)
S1P
S2P
TRAF2
ASK1
MKK7
JNK
Calpain
CASP12
Apoptosis
XBP
Nucleus
AARE
ERSE
URPE
CHOP
Bcl2
Amino acid metabolism
Redox/ detoxification
ER chaperons
protein folding enzymes
ERAD factors
Apoptosis
Recovery of ER stress
Recovery of ER stress
Prion diseases
Alzheimer's disease
Parkinson's disease
Type II diabetes mellitus
Ubiquitin ligase complex
ER membrane
Cytoplasm
ERAD- C
Doa10
Ubc6/7
Cue1
gp78
RMA1
UBE2G2
Derlin
UbcH5
Hsp40
Hsp70
CHIP
CHIP
Parkin
ERAD- L/M
Hrd3
Ubx2
Hrd1
Usa1
Ubc7
Cue1
Sel1L
Derlin1
HERP
HRD1
Ubc6/7
VIMP
UbcH5
RBX1
Cul1
FBP
Skp1
(Saccharomyces cerevisiae)
(Mammals)
04141 5/14/14
(c) Kanehisa Laboratories

Cardiovascular benefits of moderate exercise training in Marfan syndrome: insights from an animal model

Aleksandra Mas-Stachurskaa,#, MD, MSc; Anna-Maria Siegertb,#, MSc; Monsterrat Batllec, PhD; Darya Gorbenko del Blancob, PhD; Thayna Meirellesb, PhD; Carla Serra-Peinadob, PhD; Bart Bijnensd,e, PhD; Julio Baudinc, BSc; Cira Rubiesc, PhD; Marta Sitgesa,c, MD, PhD; Lluís Monta,c, MD, PhD; Eduard Guasch, MD,PhDa,c,*; Gustavo Egea, PhDb,c,f,*

aInstitut Cardiovascular, Hospital Clínic de Barcelona, Universitat de Barcelona, 08036 Barcelona, (Spain).

bDepartament de Biomedicina, Facultat de Medicina, Universitat de Barcelona, 08036 Barcelona (Spain).

cInstitut d'Investigacions Biomédiques August Pi i Sunyer (IDIBAPS), Barcelona (Spain).

dICREA, Barcelona (Spain)

eUniversitat Pompeu Fabra, Barcelona (Spain)

fInstitut de Nanociències i Nanotecnologia (IN2UB), Universitat de Barcelona, Barcelona (Spain)

# AM-S and A-M.S. contributed equally and share first authorship.

* EG and GE contributed equally and share senior authorship.

Short title: Cardiovascular impact of exercise in Marfan syndrome

Keywords: aorta, aneurysm, myocardiopathy, endurance exercise, aortic stiffness, fibrosis

Address for correspondence:

Gustavo Egea, PhD, Dept. Biomedical Sciences, University of Barcelona School of Medicine, C/Casanova 136, 08036 Barcelona (Spain) E-mail: gegea@ub.edu; phone (+34) 934021909

Eduard Guasch MD, PhD, Cardiovascular Institute, Hospital Clínic, C/ Villarroel 170, 08036 Barcelona (Spain). E-mail: eguasch@clinic.cat; phone (+34) 932275551

ABSTRACT

Marfan syndrome (MF) leads to aortic root dilatation and a predisposition to aortic dissection, mitral valve prolapse, and primary and secondary cardiomyopathy. Overall, regular physical exercise is recommended for a healthy life style, but dynamic sports are strongly discouraged in MF patients. Nonetheless, evidence supporting this recommendation is lacking. Therefore, we study the role of long-term dynamic exercise of moderate intensity on the MF cardiovascular phenotype. In a transgenic mouse model of MF (Fbn1C1039G/+), 4-month-old wild-type (WT) and MF mice were subjected to training on a treadmill for 5 months; sedentary littermates served as controls for each group. Aortic and cardiac remodeling was assessed by echocardiography and histology. The 4-month-old MF mice showed aortic root dilatation, elastic lamina rupture, and tunica media fibrosis, as well as cardiac hypertrophy, left ventricular fibrosis, and intramyocardial vessel remodeling. Over the 5-month experimental period, aortic root dilation rate was significantly greater in the sedentary MF group, compared to the WT group (Δmm, 0.27±0.07 vs 0.13±0.02, respectively). Exercise significantly blunted the aortic root dilation rate in MF mice compared to sedentary MF littermates (Δmm, 0.10±0.04 vs 0.27±0.07, respectively). However, these two groups were indistinguishable by aortic root stiffness, tunica media fibrosis, and elastic lamina ruptures. In MF mice, exercise also produced cardiac hypertrophy regression without changes in left ventricular fibrosis. Our results indicate that moderate dynamic exercise mitigates the progression of the MF cardiovascular phenotype.

SIGNIFICANCE STATEMENT

Whereas regular moderate physical exercise is highly recommended for a healthy life style, dynamic sports are strongly discouraged in Marfan syndrome patients on the basis of potential deleterious effects in aortic size. Nevertheless, this recommendation lacks supporting evidence. Our study in a murine model of Marfan syndrome is the first to address this issue showing partial cardioprotective effects, suggesting that moderate regular physical activity in Marfan patients could reduce aortic dilation and Marfan-associated cardiomyopathy.

INTRODUCTION

Marfan syndrome (MF) is a connective tissue disorder caused by mutations in the gene encoding fibrilin-1 (FBN1), a connective tissue protein (1). FBN1 provides structural and elastic support to a variety of tissues by modulating the biogenesis and homeostasis of elastic fibers as well as the availability and activity of TGF-β family members (2). Important insights on the molecular mechanisms involved in the pathogenesis of MF have been reported (3). Major efforts have focused on uncovering the mechanisms of aortic root dilation leading to dissection and rupture, a hallmark of MF that critically determines survival. Advances in basic research have recently been translated into clinical trials with the aim of pharmacological interference, predominantly testing β-blockers and angiotensin II receptor antagonists, with the progression of aneurysm (4). Unfortunately, most trials have failed to demonstrate improvement in the progression of aortic dilation, and prophylactic and timely surgical intervention remains the only life-saving measure (5). Mitral valve prolapse often accompanies MF and could evolve into a secondary cardiomyopathy. However, recent reports suggest that cardiomyopathy could also be a primary manifestation of MF (6,7) Other well-known systemic manifestations of MF include bone overgrowth, pulmonary emphysema, and evident myopathy, the latter being a consequence of the inability to repair muscle tissue injury and to increase skeletal muscle mass despite physical exercise (8).

Regular physical activity is an efficient therapeutic approach to reduce the burden of cardiovascular (CV) diseases in the general population. Among other benefits, it improves left ventricular (LV) function and tissue perfusion, lowers blood pressure (BP), and reduces chronic low-grade inflammation (9). To meet the higher metabolic demands that exercise entails, the CV system develops remarkable structural and functional changes in a remodeling process termed athlete's heart, whose features are markedly influenced by which sport is practiced. Exercise can be categorized as static (e.g., weightlifting) and dynamic (e.g., distance running), with very different physiological responses to each type of exercise. Although most sports include a mixture of both components, static exercise is characterized by increased BP and concentric LV hypertrophy, while volume overload and eccentric LV hypertrophy is typical in dynamic exercise (10). Importantly, the exercise-induced remodeling process also affects the ascending aorta. In this respect, regular physical activity prompts a mild but significant aortic root dilatation, which is greater for practitioners of more dynamic sports, compared to static sports (11).

Since dynamic physical training promotes cardiovascular extracellular matrix (ECM) remodeling, changes in the aforementioned exercise-induced CV parameters will have a special impact on patients with inherited diseases, such as MF, that lead to abnormal ECM remodeling. Consequently, it is

assumed that exercise-induced ECM remodeling is adverse in these patients and worsens the progression of the aortic dilatation and cardiomyopathy. On the basis of this reasoning, dynamic physical activity has been strongly discouraged in MF patients (12). However, no evidence is available to support this recommendation (13).

Our aim was to evaluate the impact of dynamic exercise on the ascending aortic dilation and the cardiomyopathy in MF. We implemented a modest-to-moderate endurance exercise model, as this is the level of exercise most widely practiced by the general population. The experimental working model we selected was a heterozygous mouse line carrying a targeted mutation (C1039G) in exon 25 of the Fbn1 gene, (14) representative of the most common class of mutations causing human MF. This murine model captures many of the clinical manifestations of MF, including aortic dilatation, cardiomyopathy, lung abnormalities, and skeletal deformations and myopathy.

METHODS

An extended description of the Methods is provided in Supplementary material.

Animals and Experimental design

Fbn1C1039G/+ mice, a validated MF animal model, (14) were obtained from Jackson Laboratory (Bar Harbor, ME, USA). Wild-type (WT) and Fbn1C1039G/+ (MF) mice were bred on C57BL/6 background. Comparisons were made between contemporary littermates. Animal care and experimentation conformed to the European Union (Directive 2010/63/UE) and the Spanish guidelines (RD 53/2013) for the use of experimental animals. Ethical approval was obtained from the local animal ethical committee (CEEA).

Training protocol

Experimental groups of WT and MF mice were randomly conditioned to run in a treadmill (Ex groups). After a 2-week adaptation period, Ex mice eventually ran at 20 cm/s, with a 12º positive slope for 60 min/day, for 5 months (from the age of 4 months to 9 months). A metallic grid at the back part of the treadmill delivered a constant intensity (≈2 mA) electric shock upon contact and motivated mice to keep running. In this training protocol, electric shocks were virtually absent in all animals. All training sessions were monitored by an experienced investigator to ensure proper running and lack of stress. Parallel WT and MF groups not undergoing training served as sedentary (Sed) controls. Sample size at the beginning of the experimental protocol was WT-Sed, n=11; MF-Sed n=9; WT-Ex, n= 10; and MF-Ex n=10.

Blood pressure assessment

Systolic (SBP) and diastolic (DBP) BP were non-invasively measured in all mice (tail-cuff; Panlab, Barcelona, Spain) at baseline, and after 1, 2, 3, and 5 months of training. Mean BP was calculated as 1/3*SBP + 2/3*DBP.

Echocardiography

Two-dimensional transthoracic echocardiography was performed in all animals (1.5% inhaled isoflurane) at the 4-month and 9-month time-points. In Ex-groups, recordings were obtained at least 24 hours after the final exercise session. The aortic root and ascending aorta were measured in a parasternal long-axis view. Both the maximum and minimum diameters (inner edge to inner edge) were measured at the aortic sinus level (aortic root) and at 1 cm above the sinotubular junction (ascending aorta). The aortic root dilation rate was calculated as the diastolic aortic root diameter at the 9-month time-point minus the diastolic aortic root diameter at the 4-month time-point.

The M-mode spectrum was traced at the papillary muscle level in a parasternal short-axis view. The LV dimensions were measured at both end-diastole (LVEDD) and end-systole (LVESD), LV ejection fraction (LVEF), and the anterior (AW) and posterior wall (PW) thickness at end-diastole.

The presence of post-systolic motion (PSM) was assessed in M-mode recordings obtained with the cursor positioned in the LV basal septum in a parasternal long-axis view. An animal was considered to have PSM if a “double peak sign” was consistently identified. The “double peak sign” consists of a normal-shaped deformation pattern (first peak) during the ejection period followed by an ongoing deformation (second peak) after aortic valve closure.

Aortic pulsatility and stiffness estimation

Aortic root pulsatility was calculated to assess the relative distension of the aortic root at each beat. Aorta stiffness was estimated with the previously validated β index (15).

Elastic laminae ruptures and aortic collagen deposition

Elastic fiber ruptures were quantified (number/µm) in 5-µm thick paraffin sections of the ascending aorta stained with Verhoeff-Van Gieson; the average was calculated for each animal. Collagen deposition was quantified in the tunica media of picrosirius red-stained ascending aorta.

Left ventricle histological study

Myocardial fibrosis was quantified in 4-µm-thick mid-ventricular paraffin sections stained with picrosirius red. Intramyocardial vessel remodeling was assessed through quantification of perivascular fibrosis (A), tunica media, and lumen area (Supplementary figure 1). Blinded quantification of vascular remodeling and collagen deposit was carried out using ImageJ 1.48v (NIH, Bethesda, MD, USA).

Statistics

Continuous variables are shown as mean ± SEM. Non-paired t-tests and two-way ANOVA with post-hoc pairwise comparisons adjusted for least-significant difference were used to analyze data. Normality of the residuals (Q-Q plot and Shapiro-Wilks) was checked for all analyses. Categorical variables are reported as percentage and analyses were performed with a Fisher exact or McNemar test. Mouse survival is shown on a curve and comparisons were done using a log-rank test. A $p \leq 0.05$ was considered significant.

All echocardiogram and histological measurements were carried out in a blinded manner of genotype and treatment group.

RESULTS

All mice subjected to exercise adequately adapted to the training protocol. Two MF mice allocated to the Sed group died early in the experimental protocol; no other deaths occurred in any other group (Supplementary figure 2). Necropsy was not performed and the cause of death remained unknown for both dead animals. The difference in mortality between groups did not reach significance (p=0.063).

Over the 5-month training period, weight gain was similar in all groups, both for male and female mice (Figure 1A). There were no differences in BP measurements at baseline between WT and MF mice (SBP was 130±2 vs 134±3; DBP was 79±2 vs 79±2; WT vs MF). In Sed animals, BP remained similar throughout the experimental period. In contrast, MF-Ex mice developed a higher SBP compared to WT-Ex, with no changes in DBP or mean BP (Figure 1B).

Moderate exercise slows the progression of aortic root dilation in Marfan mice

All groups were subjected to echocardiographic evaluation of the aortic root (Figure 2). In accordance with clinical data and previous reports, 4-month-old MF mice had an enlarged aortic root at the beginning of the study (Figure 2A). All groups were scanned again at the end of the experimental period (9 months), with representative echocardiographic images shown in Figure 2B. In WT mice, moderate exercise did not induce changes in the size of the aortic root. In MF mice subjected to exercise,

however, aortic root diameter was smaller than in Sed littermates (Figure 2B). To more accurately assess changes in aorta diameter over time, aortic root dilation rate was defined as the change in the aortic root size over the 5-month experimental protocol and was calculated from mouse-by-mouse aortic root size (Supplementary figure 3). Dilation rate in MF-Sed mice was twice that of WT (Δmm, 0.27±0.07 vs 0.13±0.02, respectively; Figure 2D). Remarkably, this parameter was blunted in trained MF mice, becoming comparable to the WT dilation rate (MF-Ex Δmm 0.10±0.04; Figure 2C). Aorta measurements at a more distal level yielded similar results: the ascending aorta was dilated at baseline in MF mice and dilation was blunted in trained mice (Supplementary figure 4).

The aortic root in MF patients is stiffer than in healthy individuals (16). In our mice, aorta mechanic properties were estimated by combining in vivo data obtained from BP measurements and echocardiographic maximum and minimum aorta diameters. At 4 months, we observed significant differences in the aortic root expansibility (pulsatility) between WT and MF mice, which is indicative of a loss of elasticity (Figure 3A, left panel). At 9 months, differences between WT and MF persisted. WT-Ex mice showed a slight increase in pulsatility compared with WT-Sed, but it did not reach statistical significance. MF-Ex mice showed undistinguishable pulsatility from MF-Sed (Figure 3A). Subsequent calculation of the β-index at baseline (4 months) supported increased aortic root stiffness in MF mice compared to WT mice (Figure 3B). After the exercise training, β-index (aortic stiffness) significantly improved in WT but not in MF mice.

Aortic structural abnormalities remain unaltered in trained Marfan mice

The most representative histological damage evaluated in MF mice is the rupture of elastic fibers in the tunica media of the ascending aorta. As expected, we observed a significant increase in the number of elastic lamina ruptures in MF mice, compared to WT animals (Figures 4A/upper panels and 4B for quantitative analysis). Exercise did not increase lamina ruptures, indicating no additional structural damage in the tunica media of MF aorta.

Next, we examined the collagen content as a compensatory mechanism to the elastic fibers ruptures. In Sed mice, the tunica media had more collagen staining in MF than in WT animals (Figure 4A, middle and lower panels). As with elastic fibers, dynamic exercise did not have any impact on these differences between WT and MF mice (Figure 4C, quantitative results).

Exercise improves Marfan-associated cardiac hypertrophy

The potential impact of moderate exercise on the heart was also examined, with LV dilation and hypertrophy observed at baseline in MF mice (Table 1). After the 5-month training protocol, LV hypertrophy evaluated by echocardiography significantly regressed in MF-Ex mice, as shown by

decreased AW and PW wall diameters (Table 2). A nonsignificant decrease in LVDD and LVSD was also observed.

PSM is attributed to differential loading or contractility in neighboring segments and, when perfusion is normal, predominantly reflects pressure overload. More specifically, it occurs when there is an imbalance between local (pressure-induced) wall-stress, contractility and tissue structural properties. (17) PSM was more common in MF than in WT mice at 4 months (14/17 [84%] vs 7/21 [33%], respectively; p≤0.01). While the presence of PSM remained unaltered (71%) at the 9-month time-point in MF-Sed mice, it showed a decreasing trend in MF-Ex mice (PSM 40%, p=0.12, McNemar test) (Figure 5).

As with aortae, LV changes were histologically assessed from collagen content. An evident increase in collagen deposition was observed in 9-month old MF-Sed mice. Moderate training did not modify LV fibrosis in either the WT or MF Ex-groups (Figure 6A).

In the heart, vascular remodeling was also studied in small arteries in the LV (Figure 6B). A prominent vascular remodeling in MF mice included a narrow lumen as well as thickening and increased perivascular fibrosis (Figure 6B). Again, moderate regular exercise showed no effect.

Effects of exercise on Marfan-associated cardiovascular remodeling are independent of sex

We explored potential sex-related impacts of MF- or exercise-promoted CV remodeling. The most representative findings are shown in Supplementary figures 5 and 6 (4-month and 9-month results, respectively). At baseline (4 months), aortic dilatation and LV hypertrophy were similar in male and female MF mice. At the end of the experimental protocol (9 months), the protective effect of moderate exercise on aortic dilation and LV hypertrophy, both examined by echocardiography, were similar in male and female mice (Supplementary figure 6). Altogether, our results discard any sex-related impact on aortic and LV alterations that were attributable to the exercise protocol.

DISCUSSION

We evaluated the effects of exercise in the MF phenotype, particularly focussing on CV remodelling. In a murine MF model, moderate exercise (a) mitigated aortic dilation, (b) did not increase aortic elastic fiber ruptures and collagen deposition, and (c) partially reversed MF-associated cardiac hypertrophy. Overall, our results suggest positive effects of moderate exercise in CV manifestations of MF.

Exercise and the aortic root in MF

Aortic root dilation is a hallmark of the CV phenotype of MF and a main determinant of premature mortality and morbidity. The degree of aortic dilation closely correlates with the risk of aortic dissection (18). Factors such as an increased central pulse pressure (19), obstructive sleep apnea (20), or genetic predisposition based on polymorphisms in genes other than FBN1(21) have been proposed to influence aortic dilation rate in MF. A repetitive, pulsatile increase in aortic stretch during each exercise bout has been claimed to trigger accelerated aortic dilation (11, 12).

Contrary to this hypothesis, we showed that regular, moderate exercise does not accelerate aortic dilation rate, but rather normalizes its progression to values comparable to WT animals. Echocardiographic improvement was not accompanied by a restoration of the histological integrity of elastic fibers. Nevertheless, we cannot rule out the possibility that improvements in microstructural ruptures in MF-Ex mice could precede evident elastic fiber repair evaluated by regular histological approaches.

Exercise and Marfan-associated cardiomyopathy

The most frequent and well-known cardiac manifestation of MF is mitral valve prolapse (5). If severe, mitral prolapse and regurgitation may evolve as progressive LV dilation and dysfunction and, eventually, heart failure. Nevertheless, recent data supports the existence of a primary myocardial affectation in MF patients even in the presence of competent valves (6, 7, 22). Structural abnormalities in the MF cardiomyopathy include LV hypertrophy and, in some series, dilation; these may be accompanied by variable degrees of systolic dysfunction, which occasionally remains subclinical and only detectable through deformation analysis (23). Currently, it is unclear whether this cardiomyopathy is associated with worse clinical outcomes.

Our findings in this animal model of MF concur with most of these cardiac manifestations. We show increased collagen deposition in the LV myocardium of MF mice. A similar trend was previously reported in the same mouse strain, but failed to reach significance, likely because of the limited sample size and large intrinsic variability (22). The clinical and physiological significance of such fibrosis is unknown, but could contribute to some characteristics of MF cardiomyopathy. It is possible that both myocardial fibrosis and hypertrophy underlie the diastolic dysfunction observed in patients with MF (24). Moreover, fibrosis is a hallmark of cardiac arrhythmogenesis and likely contributes to the increased burden of ventricular arrhythmias in these patients (25).

Our results indicate a positive impact of moderate exercise on MF cardiomyopathy as evidenced by an antihypertrophic effect and the absence of deleterious effects on LV myocardial fibrosis (Table 2). This

is consistent with the role of physical activity in other cardiac conditions reported in human and animal models. Moderate exercise improves cardiac remodeling in hypertensive patients (26), and blunts cardiac hypertrophy and fibrosis in a hypertrophic cardiomyopathy mouse model (27).

Clinical implications

Whereas moderate aerobic physical activity in healthy individuals and in patients with some CV disorders is largely acknowledged (9), MF patients are usually excluded or largely limited from obtaining these positive effects by current recommendations. Moderate-to-strenuous dynamic exercise is prohibited for these patients and only low-dynamic sports such as bowling, golf and archery are allowed (12). Nevertheless, this recommendation (level of evidence C) lacks clinical or experimental supporting data (12). Our results suggest not only that moderate physical activity may be safe, but this it might prove beneficial in MF patients by decelerating the aortic dilation rate and improving signs of cardiac hemodynamic overload. If our results were reproduced in humans, physical activity of moderate intensity should not only be allowed, but encouraged in patients with MF. This idea is supported by a case report showing that a CV physical therapy program reversed LV dilatation and hypertrophy in a patient with MF (28). It is important to note that the present results reflect changes promoted by light or moderate endurance training. More intense forms of physical activity or other sorts of exercise may yield opposite results. Current evidence suggests that a U-shaped relationship between exercise and outcomes exists for outcomes such as atrial fibrillation, ventricular arrhythmias, or even atherosclerosis (29). Under this hypothesis, low doses of physical activity should yield beneficial effects, but might turn deleterious at strenuous doses in healthy individuals (30). A U-shaped relationship has also been found in inherited cardiomyopathies. Competitive exercise accelerates the progression of arrhythmogenic right ventricular cardiomyopathy (31), although moderate exercise was shown to be safe (32). Further research is needed to explore the potential benefits of encouraging light or moderate physical activity in patients with MF.

Limitations of the study

First, the Fbn1C1039G/+ mouse strain presents a low risk of aortic dissection and relatively long lifespan. During the 5-month experimental period, only 2 of 22 MF mice died, neither of them in the MF-Ex group. Whether our results would similarly apply to individuals at high risk remains unknown. Second, the translation of results obtained in mouse models to human beings, and interpretation of the exercise intensity in human terms, warrants caution. Reported data suggest that our study assessed moderate exercise intensity (33). Moreover, the lack of a clear phenotype for athlete's heart, including LV hypertrophy and dilation parameters, further supports the characterization of the exercise as moderate. A rigorous measurement of aortic root stiffness requires invasive blood pressure

recordings. We measured the non-invasive blood pressure (tail-cuff) to estimate aortic stiffness, but it remains controversial whether this method provides a robust estimation of central blood pressure in mice. Nevertheless, our findings in sedentary animals recapitulate clinical observations in MF patients.

Conclusion

In a murine model of MF, moderate dynamic exercise prevented aortic root dilation and mitigates cardiac hypertrophy. Our data invite validation in other animal models of MF and eventually in patients.

ACKNOWLEDGEMENTS

The authors thank Laura Barberà and Nadia Castillo for excellent technical assistance, and Elaine Lilly for outstanding editorial assistance. This work was partially supported by grants from the Instituto de Salud Carlos III (PI13/01580, PI16/00703); Sociedad Española de Cardiología; National Marfan Foundation; Ministerio de Economia y Competitividad [SAF2015-64136R, TIN2014-52923-R]; FEDER; 2014 SGR 334; CERCA programme/Generalitat de Catalunya and CIBER 16/11/00354.

REFERENCES

1. Dietz HC, et al. (1991) Marfan syndrome caused by a recurrent de novo missense mutation in the fibrillin gene. Nature 352(6333):337–9.

2. Doyle JJ, Gerber EE, Dietz HC (2012) Matrix-dependent perturbation of TGFβ signaling and disease. FEBS Lett 586(14):2003–15.

3. Perrucci GL, et al. (2016) Vascular smooth muscle cells in Marfan syndrome aneurysm: the broken bricks in the aortic wall. Cell Mol Life Sci:1–11.

4. Singh MN, Lacro R V. (2015) Recent Clinical Drug Trials Evidence in Marfan Syndrome and Clinical Implications. Can J Cardiol 32(1):66–77.

5. Hiratzka LF, et al. (2010) 2010 ACCF/AHA/AATS/ACR/ASA/SCA/SCAI/SIR/STS/SVM guidelines for the diagnosis and management of patients with Thoracic Aortic Disease: a report of the American College of Cardiology Foundation/American Heart Association Task Force on Practice Guidelines, A. Circulation 121(13):e266-369.

6. Campens L, et al. (2015) Intrinsic cardiomyopathy in Marfan syndrome: results from in-vivo and ex-vivo studies of the Fbn1C1039G/+ model and longitudinal findings in humans. Pediatr Res 78(3):256–63.

7. Cook JR, et al. (2014) Abnormal muscle mechanosignaling triggers cardiomyopathy in mice with Marfan syndrome. J Clin Invest 124(3):1329–39.

8. Cohn RD, et al. (2007) Angiotensin II type 1 receptor blockade attenuates TGF-beta-induced failure of muscle regeneration in multiple myopathic states. Nat Med 13(2):204–10.

9. Schuler G, Adams V, Goto Y (2013) Role of exercise in the prevention of cardiovascular disease: results, mechanisms, and new perspectives. Eur Heart J 34(24):1790–9.

10. Volianitis S, Secher NH (2016) Cardiovascular control during whole body exercise. J Appl Physiol 121(2):376–90.

11. Iskandar A, Thompson PD (2013) A meta-analysis of aortic root size in elite athletes. Circulation 127(7):791–8.

12. Braverman AC, Harris KM, Kovacs RJ, Maron BJ (2015) Eligibility and Disqualification Recommendations for Competitive Athletes With Cardiovascular Abnormalities: Task Force 7: Aortic Diseases, Including Marfan Syndrome: A Scientific Statement From the American Heart Association and American College of Cardi. J Am Coll Cardiol 66(21):2398–405.

13. Cheng A, Owens D (2015) Marfan syndrome, inherited aortopathies and exercise: What is the right answer? Heart 101:752–757.

14. Judge DP, et al. (2004) Evidence for a critical contribution of haploinsufficiency in the complex pathogenesis of Marfan syndrome. J Clin Invest 114(2):172–81.

15. Hirai T, Sasayama S, Kawasaki T, Yagi S (1989) Stiffness of systemic arteries in patients with myocardial infarction. A noninvasive method to predict severity of coronary atherosclerosis. Circulation 80(1):78–86.

16. Hirata K, et al. (1991) The Marfan syndrome: abnormal aortic elastic properties. J Am Coll Cardiol 18(1):57–63.

17. Claus P, et al. (2007) Mechanisms of postsystolic thickening in ischemic myocardium: mathematical modelling and comparison with experimental ischemic substrates. Ultrasound Med Biol 33(12):1963–70.

18. Kim EK, et al. (2014) Aortic diameter predicts acute type A aortic dissection in patients with Marfan syndrome but not in patients without Marfan syndrome. J Thorac Cardiovasc Surg 147(5):1505–10.

19. Jondeau G, et al. (1999) Central pulse pressure is a major determinant of ascending aorta dilation in Marfan syndrome. Circulation 99(20):2677–81.

20. Kohler M, et al. (2009) The prevalence of obstructive sleep apnoea and its association with aortic dilatation in Marfan's syndrome. Thorax 64(2):162–166.

21. Benke K, et al. (2015) Gene polymorphisms as risk factors for predicting the cardiovascular manifestations in Marfan syndrome. Role of folic acid metabolism enzyme gene polymorphisms in Marfan syndrome. Thromb Haemost 114(4):748–756.

22. Tae H-J, Petrashevskaya N, Marshall S, Krawczyk M, Talan M (2016) Cardiac remodeling in the mouse model of Marfan syndrome develops into two distinctive phenotypes. Am J Physiol Heart Circ Physiol 310(2):H290-9.

23. Kiotsekoglou A, et al. (2011) Impaired biventricular deformation in marfan syndrome: A strain and strain rate study in adult unoperated patients. Echocardiography 28(4):416–430.

24. De Backer JF, et al. (2006) Primary impairment of left ventricular function in Marfan syndrome. Int J Cardiol 112(3):353–8.

25. Savolainen A, Kupari M, Toivonen L, Kaitila I, Viitasalo M (1997) Abnormal ambulatory electrocardiographic findings in patients with the Marfan syndrome. J Intern Med 241(3):221–6.

26. Kokkinos PF, et al. (1995) Effects of regular exercise on blood pressure and left ventricular hypertrophy in African-American men with severe hypertension. N Engl J Med 333(22):1462–7.

27. Konhilas JP, et al. (2006) Exercise can prevent and reverse the severity of hypertrophic cardiomyopathy. Circ Res 98(4):540–548.

28. Medeiros WM, Peres PA, Carvalho AC, Gun C, De Luca FA (2012) Effect of a physical exercise program in a patient with Marfan syndrome and ventricular dysfunction. Arq Bras Cardiol 98(4):e70-3.

29. Guasch E, Mont L (2017) Diagnosis, pathophysiology, and management of exercise-induced arrhythmias. Nat Rev Cardiol 14(2):88–101.

30. Calvo N, et al. (2016) Emerging risk factors and the dose-response relationship between physical activity and lone atrial fibrillation: a prospective case-control study. Europace 18(1):57–63.

31. James CA, et al. (2013) Exercise increases age-related penetrance and arrhythmic risk in arrhythmogenic right ventricular dysplasia/cardiomyopathy-associated desmosomal mutation carriers. J Am Coll Cardiol 62(14):1290–7.

32. Sawant AC, et al. (2016) Safety of American Heart Association-recommended minimum exercise for desmosomal mutation carriers. Heart Rhythm 13(1):199–207.

33. Wisløff U, Helgerud J, Kemi OJ, Ellingsen O (2001) Intensity-controlled treadmill running in rats: VO(2 max) and cardiac hypertrophy. Am J Physiol Heart Circ Physiol 280(3):H1301-10.

FIGURE LEGENDS

Figure 1: Weight and blood pressure measurements in sedentary and trained WT and MF mice. (A) Weight measurement during the experimental protocol (weeks 1 to 14) in all animals; results are shown separately for male and female mice. Analysis was performed with mixed-effects models; no significant differences were found between groups. (B) Blood pressure was measured in all groups at 1, 2, 4 and 5 months. Analysis was performed with mixed-effects models. No differences were found in Sed animals. In trained mice, a significant genotype effect was observed ($p<0.05$).

Figure 2: Echocardiographic measurements in sedentary and trained WT and MF mice. (A) Average aortic root size at the 4-month time-point in WT and MF mice. Analysis used a non-paired t-test. (B) Aortic root size after the experimental protocol (9 months) in all groups. Representative echocardiographic images of the aortic root size in all groups (left panel). Quantitative analysis (right panel) was done with two-way ANOVA. A significant (genotype x training group) interaction was found ($p<0.05$); pairwise comparisons (training group within genotype and genotype within training group) are shown. (C) Dilation rate in all groups. In two-way ANOVA, genotype x training group interaction was found ($p<0.05$); pairwise comparisons (Sed vs Ex within each genotype) are reported: *$p<0.05$; **$p<0.01$; ***$p<0.001$.

Figure 3: Aortic root pulsatility and stiffness in sedentary and trained WT and MF mice. Aortic root pulsatility (A) and β-index (B) at baseline (4-month-old mice; non-paired t-test) and at the end of the experimental training (9-month-old mice; two-way ANOVA test). *$p<0.05$; **$p<0.01$.

Figure 4: Aorta histological analyses in sedentary and trained WT and MF mice. (A) Representative images of elastic laminae (stained in black by Verhoeff-Van Gieson [VVG] staining, upper panel) and collagen content (stained by picrosirius red [PSR]), visualized under brightfield or polarized light in the middle and low panels, respectively. (B) Quantitative analysis of elastic laminae ruptures. Two-way ANOVA showed no interaction but a genotype (WT vs MF) effect was evident (****$p<0.0001$). (C) Quantitative analysis of fibrosis. Two-way ANOVA showed no interaction but a genotype effect was clear (**$p<0.01$). Bars 100 µm.

Figure 5: Cardiac hemodynamic overload (post-systolic motion [PSM]) in sedentary and trained WT and MF mice. (A) Number of mice with and without PSM for all groups and all time-points. Analysis done with McNemar test. (B) Representative images for each group.

Figure 6: Histological analysis of the left ventricle in sedentary and trained WT and MF mice. (A) Representative picrosirius red-stained myocardial samples of all groups (left panel) and their respective quantitative analysis (right panel). (B) Histological evaluation of intramyocardial vessels

(upper panel) and quantitation of the perivascular fibrosis, tunica media thickness, and lumen area. Two-way ANOVA (all measurements) showed no significant interaction, but a genotype (WT vs MF) was found for all analyses. Bars are 100 µm.

Figure 1

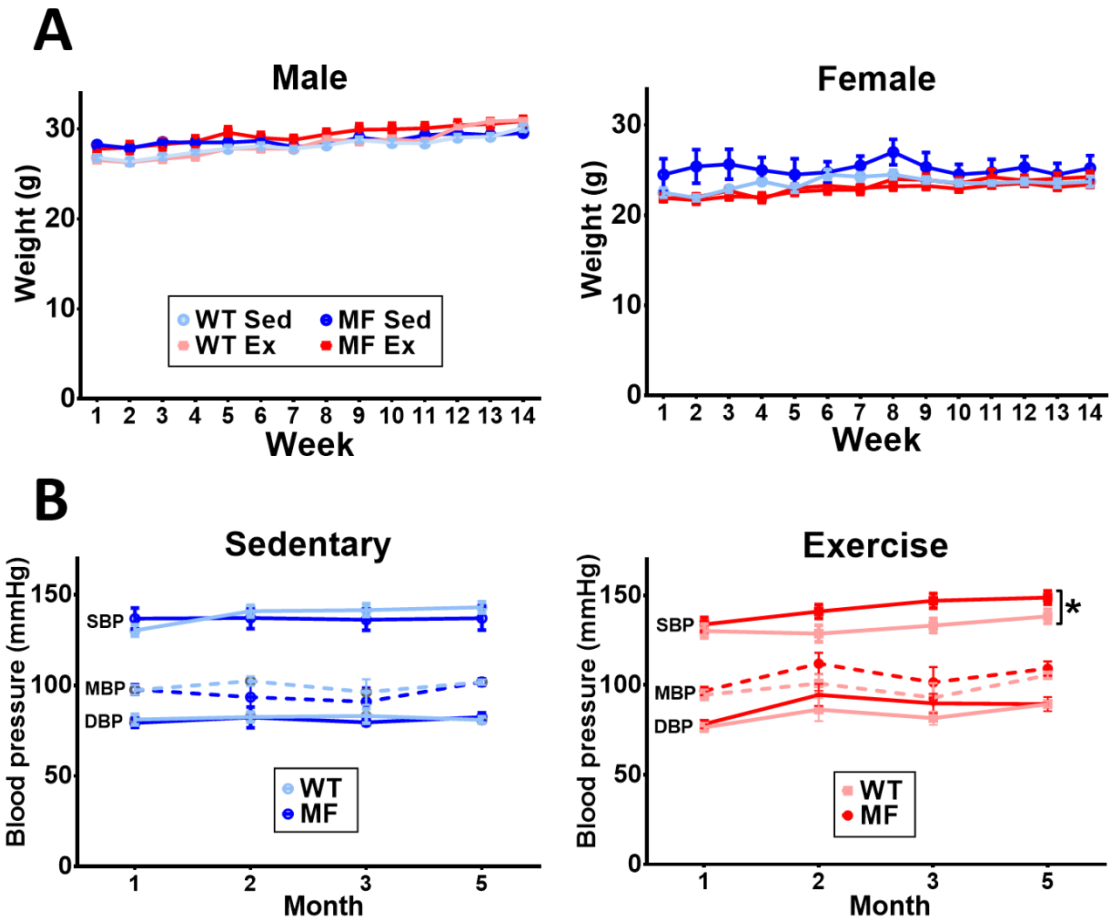
A
Male
Female
Weight (g)
Week
WT Sed
WT Ex
MF Sed
MF Ex
B
Sedentary
Exercise
Blood pressure (mmHg)
SBP
MBP
DBP
WT
MF
Month
*

Figure 2

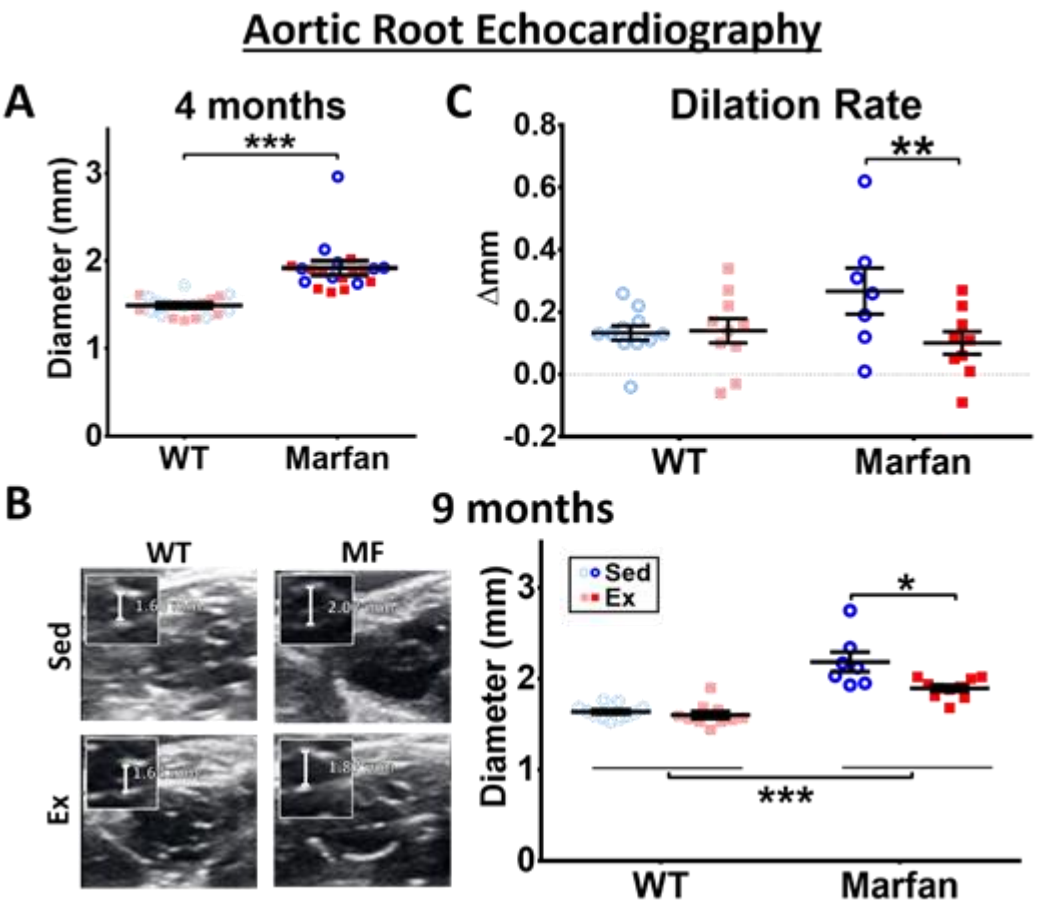
Aortic Root Echocardiography
A
4 months
***
Diameter (mm)
0
1
2
3
WT
Marfan
C
Dilation Rate
**
Δmm
0.8
0.6
0.4
0.2
0.0
-0.2
WT
Marfan
B
9 months
WT
MF
Sed
Ex
Sed
Ex
*
***
Diameter (mm)
0
1
2
3
WT
Marfan

Figure 3

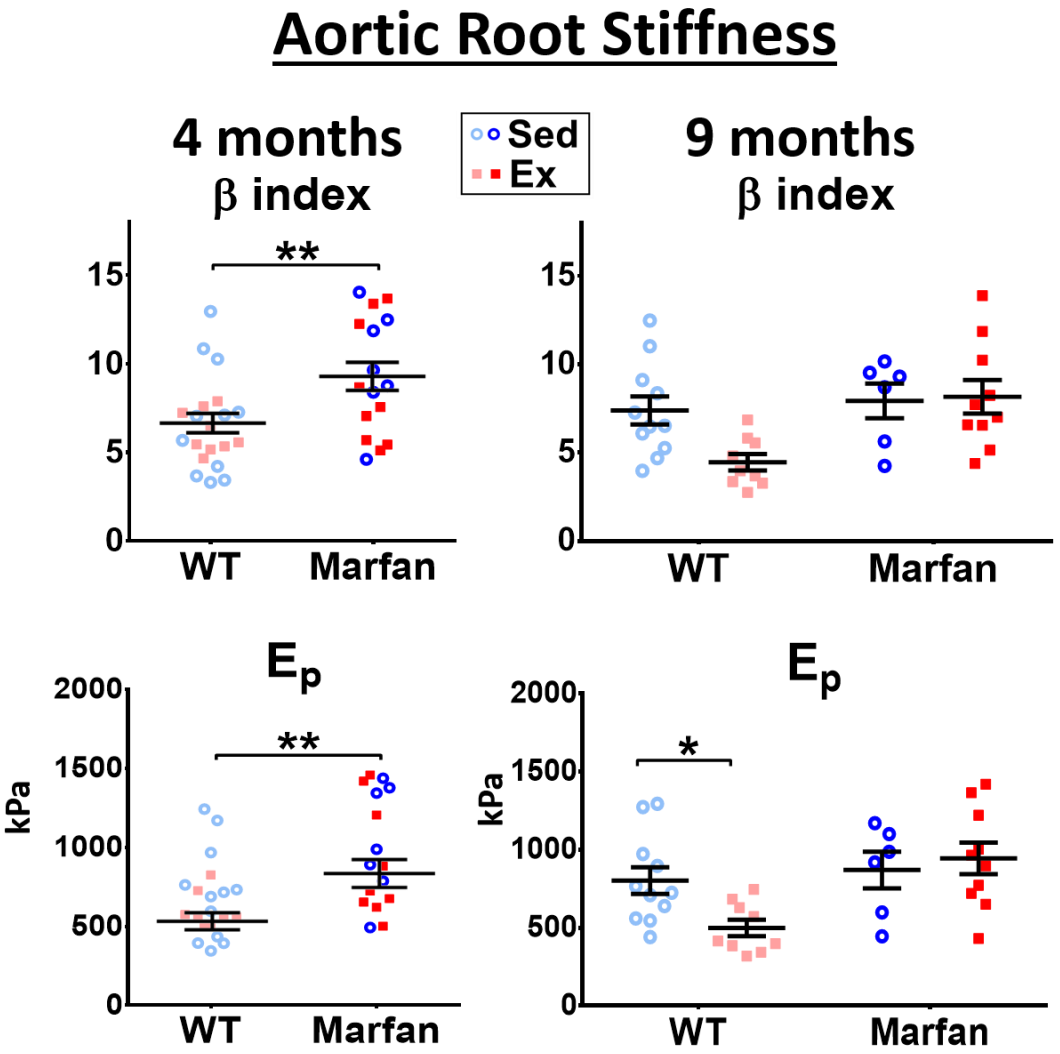
Aortic Root Stiffness
4 months
β index
Sed
Ex
9 months
β index
**
15
10
5
0
WT
Marfan
Ep
kPa
2000
1500
1000
500
*

Figure 4

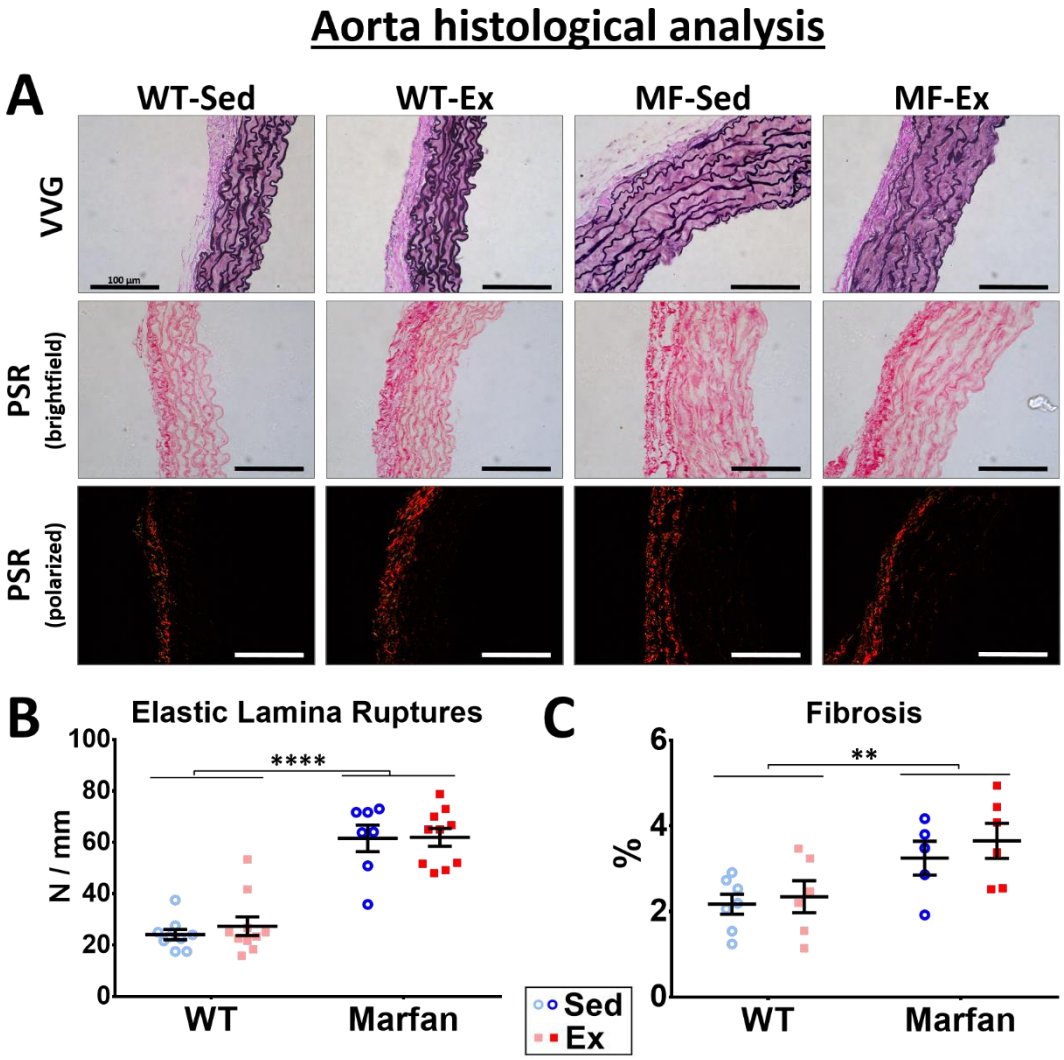
Aorta histological analysis
A
WT-Sed
WT-Ex
MF-Sed
MF-Ex
VVG
PSR (brightfield)
PSR (polarized)
100 µm
B
Elastic Lamina Ruptures
****
N / mm
100
80
60
40
20
0
WT
Marfan
C
Fibrosis
**
%
6
4
2
0
WT
Marfan
Sed
Ex

Figure 5

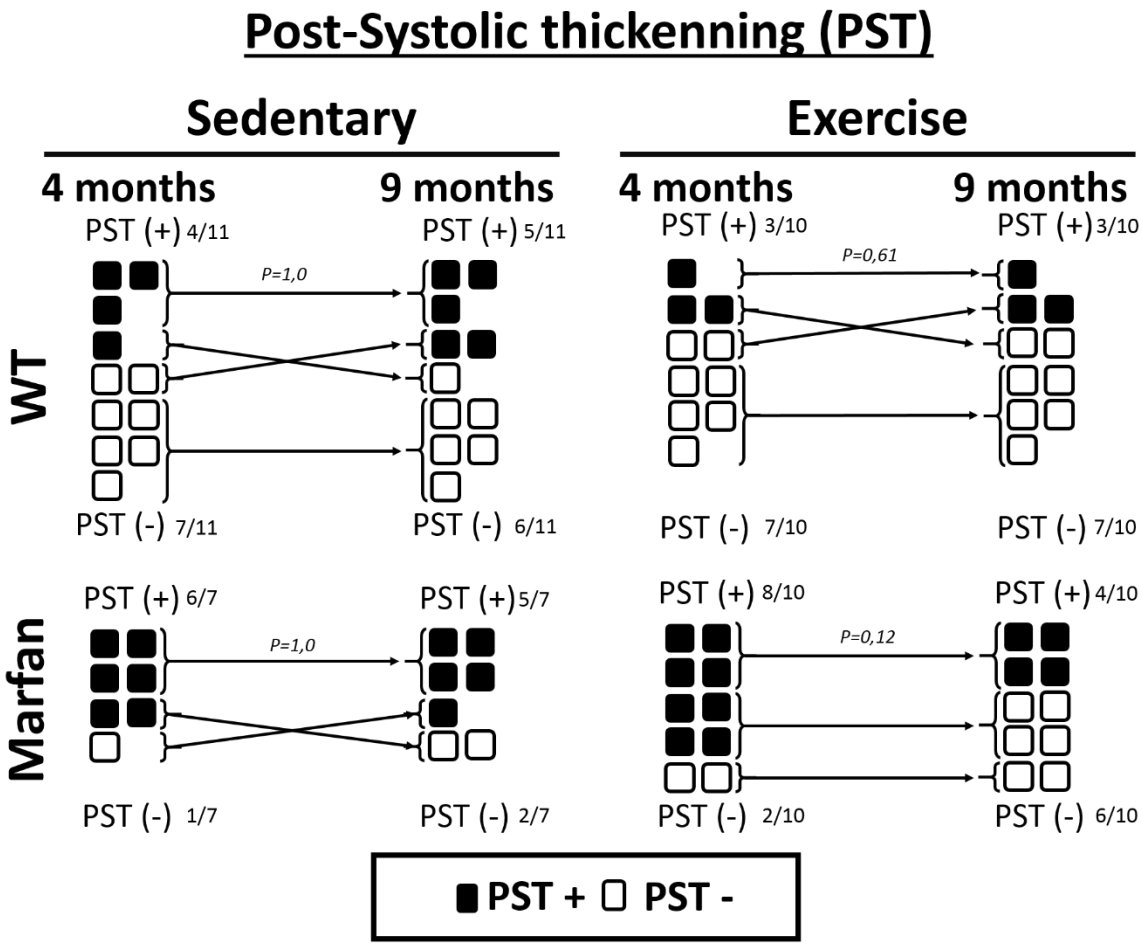
Post-Systolic thickenning (PST)
Sedentary
Exercise
4 months
9 months
4 months
9 months
WT
PST (+) 4/11
PST (+) 5/11
P=1,0
PST (-) 7/11
PST (-) 6/11
PST (+) 3/10
PST (+) 3/10
P=0,61
PST (-) 7/10
PST (-) 7/10
Marfan
PST (+) 6/7
PST (+) 5/7
P=1,0
PST (-) 1/7
PST (-) 2/7
PST (+) 8/10
PST (+) 4/10
P=0,12
PST (-) 2/10
PST (-) 6/10
PST + PST -

Figure 6

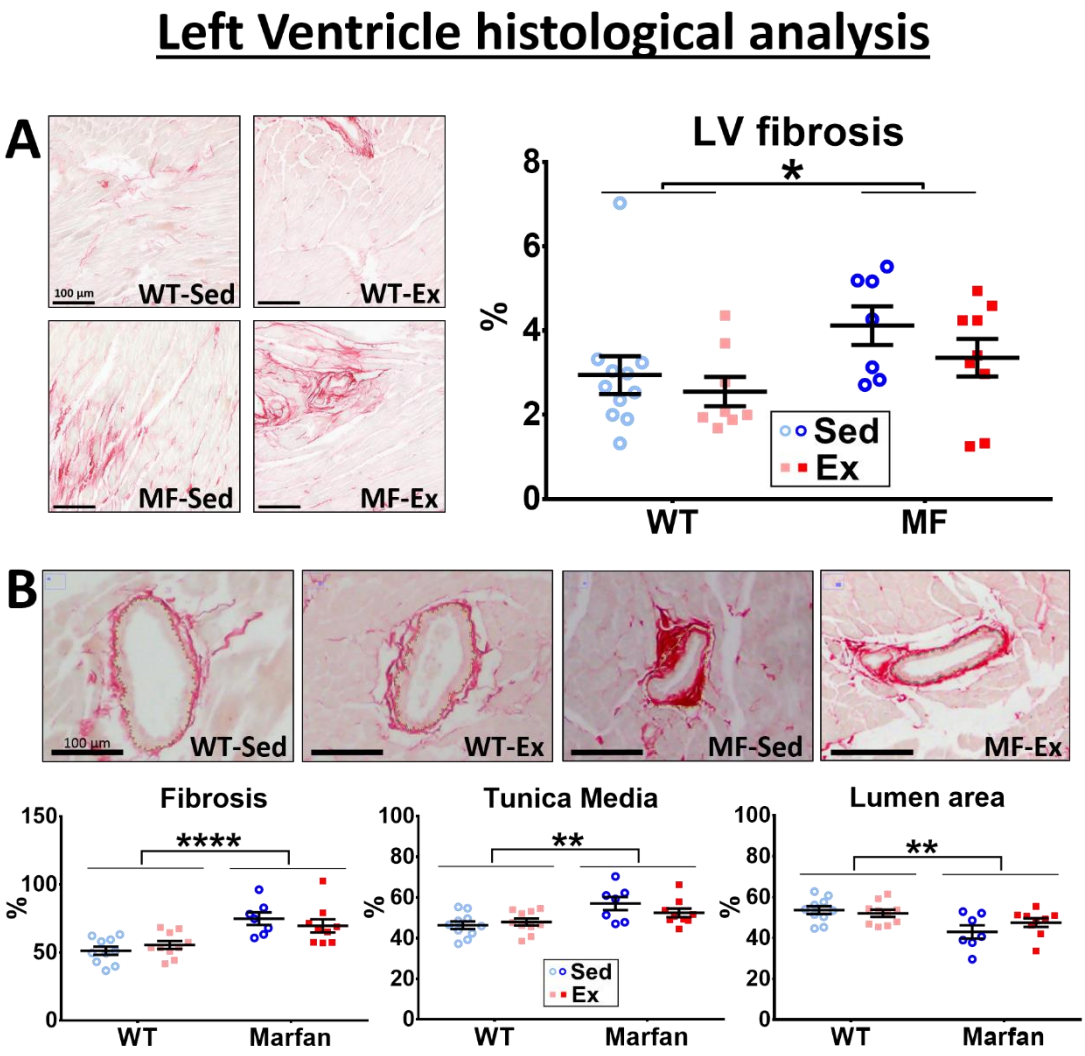
Left Ventricle histological analysis
A
100 µm
WT-Sed
WT-Ex
MF-Sed
MF-Ex
LV fibrosis
*
%
8
6
4
2
0
Sed
Ex
WT
MF
B
100 µm
WT-Sed
WT-Ex
MF-Sed
MF-Ex
Fibrosis
****
%
150
100
50
0
WT
Marfan
Tunica Media
**
%
100
80
60
40
20
0
Sed
Ex
WT
Marfan
Lumen area
**
%
100
80
60
40
20
0
WT
Marfan

TABLES

Table 1. Echocardiographic measurements of LV structural and functional parameters in all groups at 4 months (before training).

	Wild type (n=21)	Marfan (n=17)
AW (mm) *	0.59±0.02	0.65±0.01
LVEDD (mm) *	3.75±0.08	3.98±0.07
PW (mm) *	0.57±0.02	0.63±0.02
LVESD (mm)	2.54±0.08	2.76±0.06
LVEF (%)	69±2	67±1

LVEDD: left ventricle end-diastolic diameter; LVESD: left ventricle end-systolic diameter; AW: anterior wall; PW: posterior wall; LVEF: left ventricular ejection fraction. *p<0.05, **p<0.01; WT vs Marfan.

Table 2. Echocardiographic measurements of LV structural and functional parameters in all groups at the 9-month time point.

	Wild type		Marfan	
	Sedentary	**Trained**	**Sedentary**	**Trained**
LVEDD (mm) **	3.89±0.1	3.79±0.04	4.24±0.19	4.04±0.08
LVESD (mm) *	2.65±0.06	2.61±0.07	2.95±0.18	2.73±0.1
AW (mm) **	0.66±0.02	0.64±0.01	0.72±0.02	0.69±0.02 #
PW (mm) *	0.65±0.02	0.63±0.01	0.73±0.03	0.68±0.02 #
LVEF (%)	67±1	67±2	66±3	69±3

Abbreviations as in Table 1. *p<0.05, **p<0.01 WT vs Marfan; #p<0.05 vs genotype-matched sedentary group.

SUPPLEMENTARY METHODS

Animals and Experimental design

Fbn1C1039G/+ mice were obtained from Jackson Laboratory (Bar Harbor, ME 04609, EE. UU) and used as a validated MFS animal model (1). Both Wild Type (WT) and Fbn1C1039G/+ mice (hereinafter, Marfan [MF] mice) were bred on C57BL/6 background. Comparisons were made between contemporary littermates. All mice were housed in a controlled environment (12/12-hour light/dark cycle) and provided with ad libitum access to food and water. All animals were weighed once a week throughout the duration of the experiment. Animal care and experimentation conformed to the European Union (Directive 2010/63/UE) and Spanish guidelines (RD 53/2013) for the use of experimental animals.

Training protocol

A group of WT and MF mice were randomly conditioned to run in a treadmill (Ex groups). After a 2-week adaptation period in which treadmill speed and slope and training duration were progressively increased, a stable regime was reached. Eventually, Ex mice ran at 20 cm/s, with a 12º positive slope for 60 minutes per day, for 5 months (from the age of 4 months to 9 months). A metallic grid at the back of the treadmill delivered a constant intensity (≈2 mA) electric shock upon contact and motivated mice to keep running. In this training protocol, electric shocks were virtually absent in all animals. All training sessions were monitored by an experienced investigator to ensure proper running and lack of stress. Parallel WT and MF groups not undergoing training served as sedentary (Sed) controls. Sample size at the beginning of the experimental protocol was WT-Sed n=11; MF-Sed n=9; WT-Ex n= 10; MF-Ex n=10.

Blood pressure assessment

Systemic blood pressure was non-invasively measured in all mice by a tail cuff system (Panlab NIPB system, consisting of control unit LE5007 and the automatic heater and scanner for 6 mice, LE56506). Briefly, mice were placed in a warming restrainer (34ºC), with the tail carefully inserted into an inflatable cuff. Systolic blood pressure (SBP) and diastolic blood pressure (DBP) were automatically measured. Mean blood pressure was calculated as 1/3*SBP + 2/3*DBP.

Before initiating the exercise protocol, all mice were placed in the setup as many times as needed until they became adapted, thereby minimizing stress associated with the procedure. Blood pressure was thereafter measured at baseline, and after 1, 2, 3, and 5 months of training.

Echocardiography

Two-dimensional transthoracic echocardiography was performed in all animals under 1.5% inhaled isoflurane. Each animal was scanned twice: at carried out at least 24 hours after the final exercise session. Images were obtained with a 10-13 MHz phased-array linear transducer (IL12i GE Healthcare, Madrid, Spain) in a Vivid Q system (GE Healthcare, Madrid, Spain). Images were all recorded and later analyzed off-line using commercially available software (EchoPac v. 108.1.6, GE Healthcare, Madrid, Spain).

The aortic root and ascending thoracic aorta were measured in a parasternal long-axis view. Both the maximum and minimum diameters (inner edge to inner edge) were measured at the aortic sinus level (for the aortic root) and at 1 cm above the sinotubular junction (for the ascending aorta). The aortic root dilation rate was calculated as the diastolic aortic root diameter at the 9-month time-point minus the diastolic aortic root diameter at the 4-month time-point.

The M-mode spectrum was traced at the papillary muscle level in a parasternal short axis view, where left ventricular (LV) dimensions at both end-diastole (LVDD) and end-systole (LVSD) were measured. The anterior (AW) and posterior wall (PW) thickness at end-cardiac diastole were also measured. LV ejection fraction (LVEF) was subsequently calculated as follows:

$$LVEF = \frac{LVDD^3 - LVSD^3}{LVDD^3} * 100$$

The presence of post-systolic thickening (PST) was assessed in M-mode recordings obtained with the cursor positioned in the LV basal septum in a parasternal long-axis view. An animal was considered to have PST if a “double peak sign” was consistently identified. The “double peak sign” consists of a normal-shaped deformation pattern (first peak) during the ejection period followed by an ongoing deformation (second peak) after aortic valve closure.

Aortic pulsability and aortic stiffness estimation

Aortic pulsatiliy was used as a distensibility estimator, and calculated as follows:

$$Pulsatility = \frac{Aomax - Aomin}{Aomin} * 100$$

where Aomax stands for maximum aortic diameter, and Aomin stands for minimum aortic diameter. The final result is shown as percentage (%).

Aortic stiffness was calculated with a previously validated method (2) using the blood pressure and echocardiographic aorta diameter in vivo. For each animal, the following formula was used to calculate the β-index:

$$\beta = \frac{\log(\frac{SBP}{DBP})}{(\frac{Aomax-Aomin}{Aomin})}$$

where SBP stands for systolic blood pressure, DBP stands for diastolic blood pressure, Aomax stands for maximum aortic diameter, and Aomin stands for minimum aortic diameter. The final result is dimensionless.

Euthanasia and sample collection

Nine-month-old mice were sacrificed with an overdose of isoflurane inhalation and ascending aorta, heart samples were quickly excised, immersed in cold physiological serum, and processed as described below.

Aortic collagen deposition and elastic fiber ruptures

The thoracic aorta was cut just above the aortic valve, and the ascending aorta was subsequently fixed in formaldehyde and embedded in paraffin. Four-µm-thick sections were obtained and stained with Verhoeff-Van Gieson stain. Sections were examined using a Leica DMRB microscope (40x). Two blinded investigators quantified aortic elastic fiber ruptures by fiber discontinuities per longitude in at least four representative images in each animal, and the average was calculated for each animal.

Furthermore, sections were stained with picrosirius red to analyze collagen deposition. Six representative images were taken of each animal using the brightfield and polarized light of a Leica DMRB microscope. The tunica media was delimited using the brightfield images and corresponding polarized light images were used to quantify Picrosirius Red stained collagen deposition.

Left ventricle histological study

The whole heart was fixed in formaldehyde and transversally cut through mid-ventricle in two blocks (basal and apical blocks). Both blocks were embedded in paraffin wax and 4-µm-thick sections were obtained from the basal block and layered in poly-L-lysine–coated glass slides. The slides were stained with picrosirius red as previously described (3). Intramyocardial collagen deposit was quantified, excluding the endomyocardial, epicardial, and perivascular fibrosis. Pictures (40X) of 3 different representative areas of left ventricle (LV) were taken from each sample and the mean percentage of collagen deposition was calculated.

In order to assess intramyocardial vessel remodeling, pictures of both right ventricle (RV) and left ventricle (LV) were taken (100X) whenever a vessel was identified. Around 10 intramyocardial arteries were localized and different measurements were taken: perivascular area (A), limited by perivascular fibrosis; external area (Ae), limited by outer tunica adventitia; and internal area (Ai), limited by internal elastic lamina (Supplementary Figure 1). The area of the lumen, tunica media and perivascular fibrosis were all normalized to the vessel size (Ae) to exclude any bias in selecting vessels. All pictures were taken with an Olympus BX41TF microscope and DP73 camera. Blinded quantification of vascular remodeling and collagen deposition was performed with ImageJ 1.48v.

Statistics

All results for continuous variables are reported as mean ± SEM. Because no mice had yet been trained, only the effect of genotype (i.e., WT vs MF) was analyzed at the 4-month time point; a non-paired t-test was used for comparisons in these cases. When two main factors were present in the study design (e.g., genotype x training), data was modelled in a two-way ANOVA that included the two main factors and their interaction. Data with a repeated measurement factor (e.g., several measurements over time) were analyzed with a linear mixed-effects model. For intramyocardial vascular remodeling, each analyzed vessel was nested within rat and a random effect included in the model. When a significant interaction was found, LSD-adjusted pairwise comparisons are reported. In the absence of a significant interaction, significant main effects, if present, are reported. A normal distribution of the residuals (Q-Q plot and Shapiro-Wilks) was checked for all analyses.

Categorical variables (e.g., PST presence) are reported as percentages. Proportion of mice with PST in all groups at baseline were compared with a Fisher exact test. Change of PST over time (from 4-month to 9-month time-points) in MF was assessed through a McNemar test.

Mouse survival is shown on a survival curve and comparisons carried out with a log-rank test.

A p value ≤ 0.05 was considered significant. Statistical analysis was carried out with Stata v13 (College Station, Texas, USA) and Graphpad Prism v6.0 (GraphPad Software, Inc, USA).

REFERENCES

1. Ng CM, Cheng A, Myers LA, et al. TGF-beta-dependent pathogenesis of mitral valve prolapse in a mouse model of Marfan syndrome. J. Clin. Invest. 2004;114:1586–92.

2. Hirai T, Sasayama S, Kawasaki T, Yagi S. Stiffness of systemic arteries in patients with myocardial infarction. A noninvasive method to predict severity of coronary atherosclerosis. Circulation 1989;80:78–86.

3. Guasch E, Benito B, Qi X, et al. Atrial fibrillation promotion by endurance exercise: demonstration and mechanistic exploration in an animal model. J. Am. Coll. Cardiol. 2013;62:68–77.

SUPPLEMENTARY FIGURE LEGENDS

Supplementary figure 1. Intramyocardial artery assessment. First, the perivascular area (A, limited by perivascular fibrosis), the external area (Ae, limited by outer tunica adventitia) and internal area (Ai, limited by internal elastic lamina) were identified and limits traced (left pannel). Thereafter, the area within each of these limits was automatically quantified. Perivascular fibrosis was then calculated as A – Ae (yellow area in the right panel); tunica media area was calculated as Ae – Ai (green area in the right panel); and luminal area was identified as Ai (red area in the right panel).

Supplementary figure 2. Survival rate during the experimental protocol in all groups. Analysis with Log-rank test.

Supplementary figure 3. Changes of the aortic root size during the experimental protocol examined for each mouse (at 4 months and at 9 months).

Supplementary figure 4. Measurements of the ascending aorta in all groups at the 4-month time-point (left panel; comparison with a t-test) and at the 9-month time-point (right panel; comparison with two-way ANOVA; significant interaction was found). *p<0.05; **p<0.01; ***p<0.001.

Supplementary figure 5. Echocardiographic results according to sex at the 4-month time point. Comparisons were carried out with 2-way ANOVA (genotype [WT, MF], sex and genotype x sex). No significant interaction was found in any comparison.

Supplementary figure 6. Echocardiographic results according to sex at the 9-month time point. Comparisons were carried out with 2-way ANOVA (genotype [WT, MF], sex and genotype x sex). No significant interaction was found in any comparison.

Supplementary figure 1

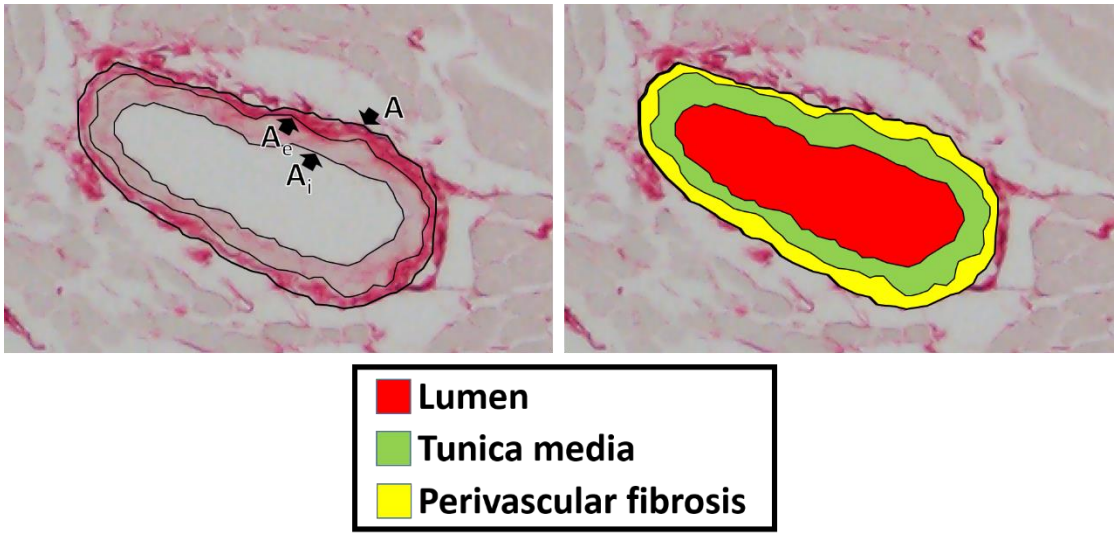

Supplementary figure 2

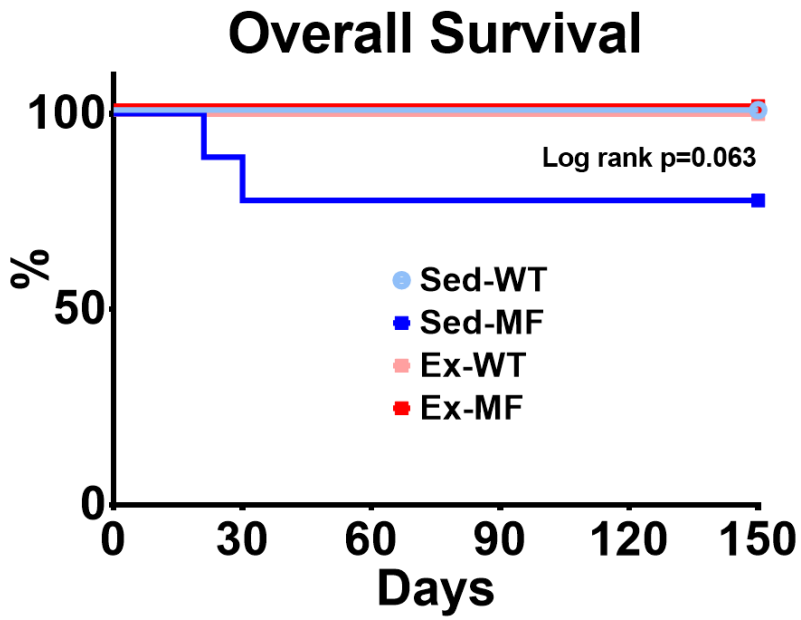

Supplementary figure 3

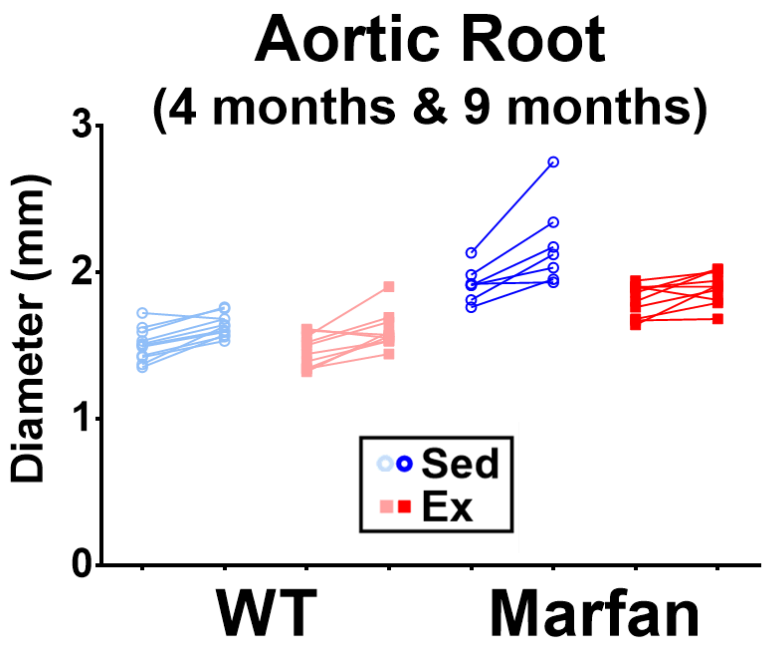

Supplementary figure 4

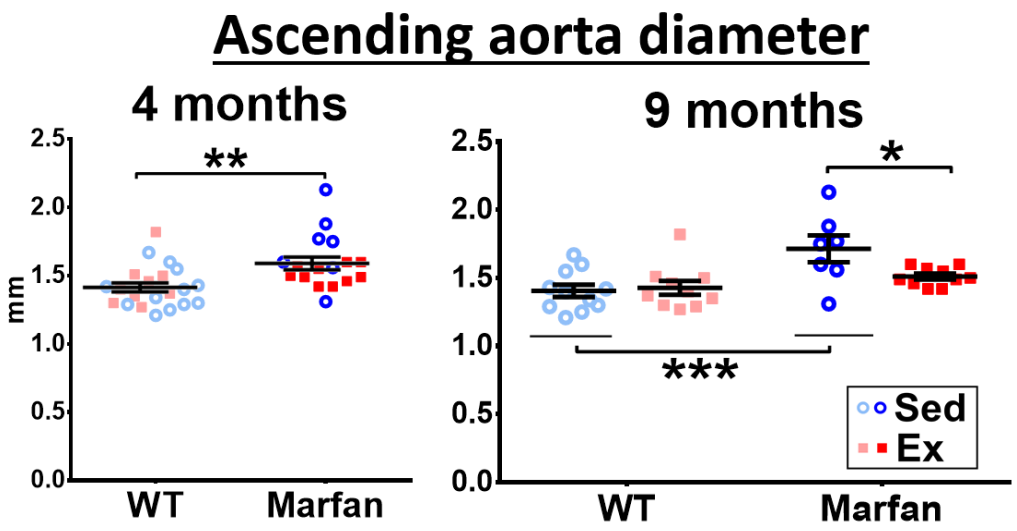

Supplementary figure 5

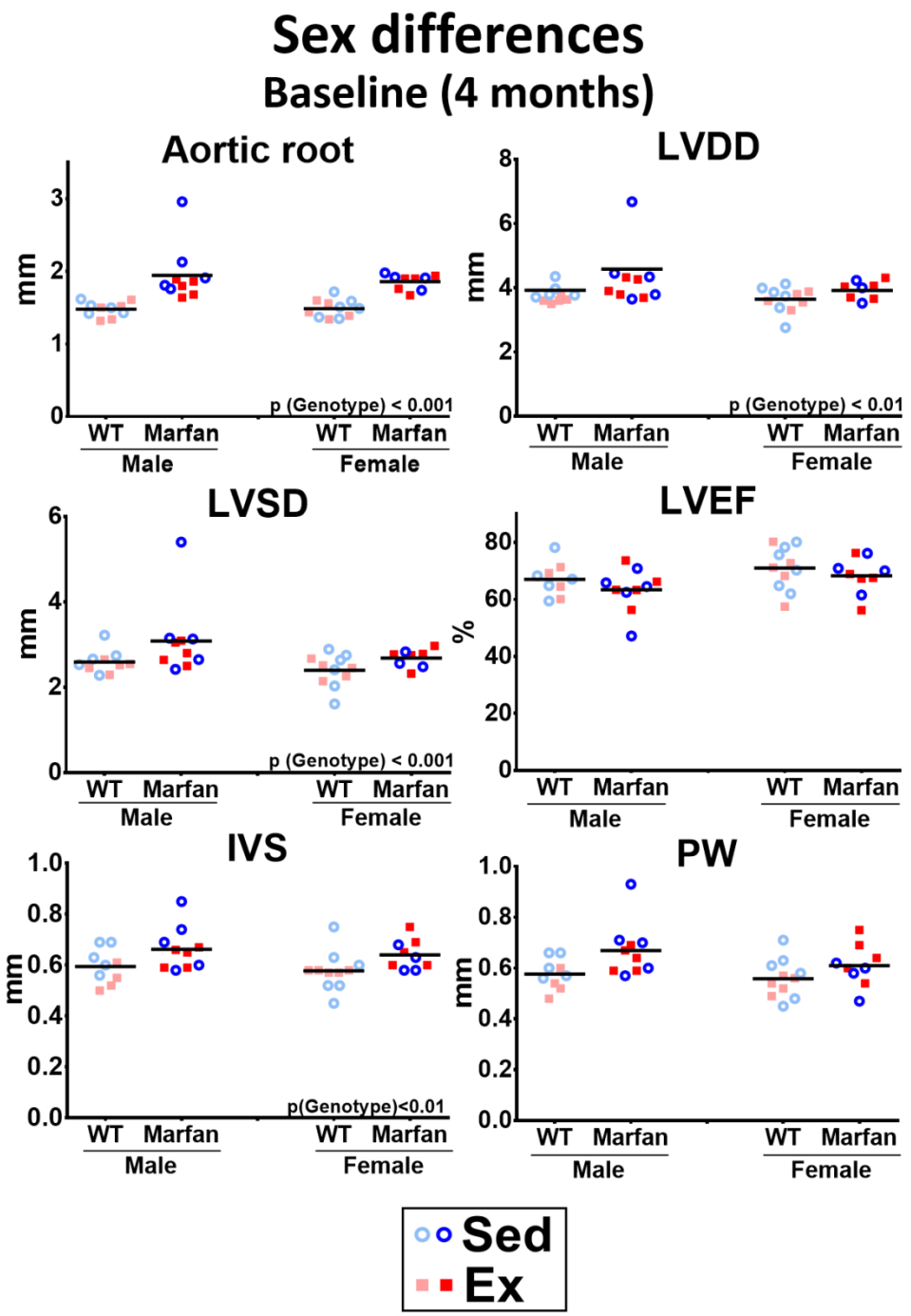

Supplementary figure 6

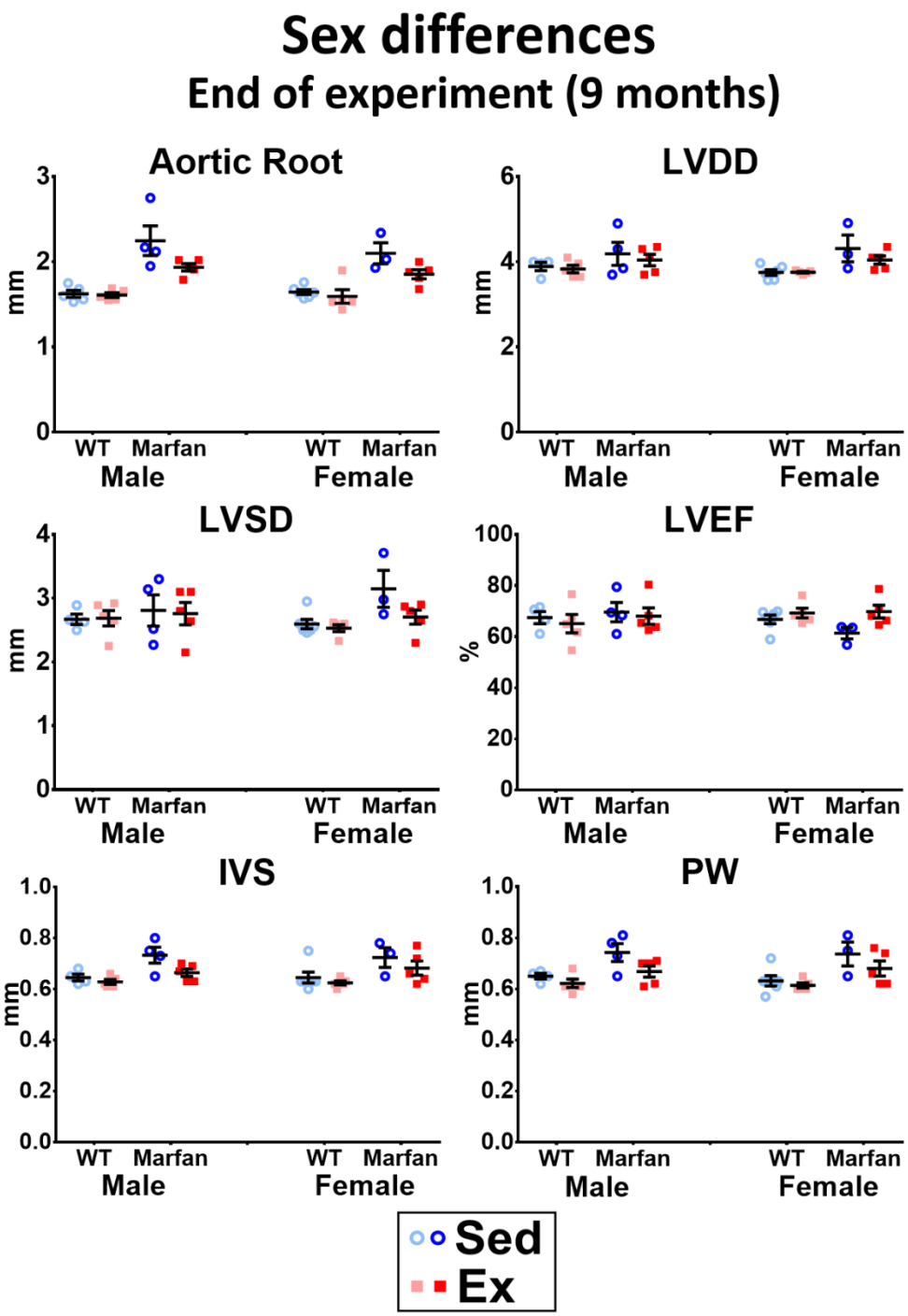

Increased Phenylephrine Contractions in the Ascending Aorta of Males Reveal Regional and Sex Differences in a Murine Model of Marfan Syndrome

Francesc Jiménez-Altayó[1]*, Anna-Maria Siegert[2], Fabio Bonorino[2], Thayna Meirelles[2], Laura Barberà[2], Ana P. Dantas[3], Elisabet Vila[1], Gustavo Egea[2]

[1]Departament de Farmacologia, de Terapèutica i de Toxicologia, Institut de Neurociències, Facultat de Medicina, Universitat Autònoma de Barcelona, Bellaterra, Spain; [2]Departament de Biomedicina, Facultat de Medicina i Ciències de la Salut, Universitat de Barcelona, Barcelona, Spain; Institut d'Investigacions Biomèdiques August Pi i Sunyer, Barcelona, Spain; [3]Institut Clínic del Tòrax, Institut d'Investigacions Biomèdiques August Pi i Sunyer, Barcelona, Spain

Correspondence: Dr F Jiménez-Altayó, Departament de Farmacologia, de Terapèutica i de Toxicologia, Facultat de Medicina, Universitat Autònoma de Barcelona, 08193 Bellaterra (Cerdanyola del Vallès), Spain. E-mail: francesc.jimenez@uab.cat, Tel: (+34) 93 581 1952; Fax: (+34) 93 581 1953

1. Abstract

Marfan syndrome (MFS) is a hereditary disorder of the connective tissue that causes life-threatening aortic aneurysm, which initiates at the aortic root and can progress into the ascending portion. However, analysis of ascending aorta reactivity in animal models of MFS has remained elusive. Epidemiologic evidence suggests that although MFS is equally prevalent in men and women, men are at increased risk for aortic complications than non-pregnant women. Nevertheless, there is no experimental evidence to support this hypothesis. The aim of this work was to explore whether there are regional and sex differences in thoracic aorta function in 6-mo-old mice heterozygous for the fibrillin 1 (*Fbn1*) allele encoding a missense mutation (*Fbn1*$^{C1039G/+}$), the most common class of mutation in MFS. Ascending and descending thoracic aorta reactivity was evaluated by wire myography. Ascending aorta mRNA levels and elastic fiber integrity was assessed by qRT-PCR and Verhoeff-Van Gieson histological staining, respectively. MFS differently altered reactivity in the ascending and descending thoracic aorta by either increasing or decreasing phenylephrine contractions, respectively. When mice were separated by sex, contractions to phenylephrine were higher in MFS ascending aortas of males, whereas contractions in females were unchanged. Endothelium-dependent relaxation was unaltered in the MFS ascending aorta of either sex, an effect related to augmented endothelium dependent hyperpolarization-type dilations. In MFS males, the non-selective cyclooxygenase (COX) inhibitor indomethacin prevented the MFS-induced enhancement of phenylephrine contractions linked to increased COX-1 and COX-2 expression. In MFS females, the non-selective nitric oxide synthase inhibitor L-NAME unrevealed a negative feedback of NO on phenylephrine contractions to counteract increased COX-1 expression. Finally, MFS ascending aortas showed a greater number of elastic fiber ruptures than the wild-types, and males exhibited more fragmentations than females. These results show regional and sex differences in *Fbn1*$^{C1039G/+}$ mice thoracic aorta contractility and aortic media injuries. The presence of more pronounced aortic alterations in male mice provides experimental evidence to support that men MFS patients are at increased risk to suffer aortic complications.

Keywords: Marfan syndrome; sex differences; gender; ascending thoracic aorta; aortic aneurysm; fibrillin-1; arterial reactivity; aortic contraction

2. Introduction

Marfan syndrome is an autosomal dominant hereditary disorder of connective tissue that results from mutations in the gene for fibrillin 1 (*Fbn1*), the major constitutive element of extracellular microfibrils (Dietz et al., 1991). Aortic complications, either severe aortic regurgitation or acute aortic dissection, are potentially life threatening (Murdoch et al., 1972). Prophylactic surgical repair of the ascending aorta has extended life in Marfan syndrome over the past decades, but as a result, new features have emerged including aortic dilatation beyond the aortic root (Pyeritz, 2016). Although both ascending and descending portions of thoracic aorta show mechanical abnormalities in Marfan syndrome (Chung et al., 2007b; Bellini et al., 2016), aneurysmal expansion initiates at the aortic root and progresses into the ascending portion. This sequence of events could be at least partly associated with the more pronounced mechanical alterations of this aortic region (Bellini et al., 2016). Remarkably, exploration of the ascending portion of thoracic aorta reactivity in murine models of Marfan syndrome has remained elusive. As far as we know, all studies have been conducted in the aortic arch or descending thoracic portion, where compromised reactivity is reported (Chung et al., 2007a, 2007b, 2007c; Chung et al., 2008; Yang et al., 2009; Yang et al., 2010a, 2010b; Gibson et al., 2017).

Marfan syndrome is equally prevalent in men and women (Mueller et al., 2013; Dietz, 2017). Epidemiological evidence suggests that male patients with Marfan syndrome have a higher risk of an aortic event (aortic surgery or aortic dissection) than females (Detaint et al., 2010; Franken et al., 2016; Groth et al., 2017). Nevertheless, the mechanisms that promote higher susceptibility to injury in males are not clear. Besides, pregnancy is associated with an increased risk of aortic dissection in Marfan syndrome (Elkayam et al., 1995; Goland and Elkayam, 2009; Wanga et al., 2016). The pregnancy-induced myriad of aortic wall changes triggered by variations in hormone concentrations (Manalo-Estrella and Barker, 1967) and the altered hemodynamic load (Elkayam and Gleicher, 1998) could jointly render the aorta more susceptible to injury. It is unknown, however, whether preexistent aortic alterations may predispose Marfan syndrome females towards injury during pregnancy. Of note, no studies to date have directly attempted to examine the influence of sex on aortic disease in animal models of Marfan syndrome. These studies are fundamental to comprehend the complex pathophysiological mechanisms underlying aortic pathology in Marfan syndrome.

Clinical trials have not produced robust evidence of an effective pharmacological treatment in Marfan syndrome (Dietz, 2017). To date, the only effective approach is the prophylactic surgical repair of the dilated ascending aorta, which involves non-negligible risks. Therefore, it is mandatory to go from bedside to bench for improved understanding of Marfan syndrome pathogenesis to uncover new

potential effective pharmacological strategies, particularity for the management of both aortic root and ascending aorta dilatation. To this aim, the present study sought to examine whether there are regional and sex differences in thoracic aorta reactivity from 6-mo-old mice heterozygous for the *Fbn1* allele encoding a missense mutation (*Fbn1*$^{C1039G/+}$), the most common class of mutation in Marfan syndrome. The *Fbn1*$^{C1039G/+}$ mice develop progressive aortic dilatation starting at about 2 months of age and although mice rarely die from aortic dissection, they recapitulate most of the aortic complications observed in human Marfan syndrome (Judge et al., 2004; Lee et al., 2016).

3. Methods

3.1 Animals

Fbn1$^{C1039G/+}$ (Marfan) male and female mice were obtained from The Jackson Laboratory/Charles River (Lyon, France). All mice were housed according to institutional guidelines (constant room temperature at 22°C, 12h: 12h light-dark cycle, 60% humidity, and had access to food and water ad libitum). Experiments were conducted under the guidelines established by Spanish legislation (RD 1201/2005), were approved by the Ethics Committee of the Universitat de Barcelona, and were carried out in accordance with the recommendations of the European legislation (Directive 2010/63/EU).

3.2 Tissue preparation

Segments of the ascending [vascular reactivity, mRNA levels, elastin breaks] and descending [vascular reactivity] thoracic aorta were dissected (Figure 1A) free of fat and connective tissue in ice-cold physiological salt solution (PSS; composition in mM: NaCl 112.0; KCl 4.7; $CaCl_2$ 2.5; KH_2PO_4 1.1; $MgSO_4$ 1.2; $NaHCO_3$ 25.0 and glucose 11.1) gassed with 95% O_2 and 5% CO_2.

3.3 Vascular reactivity

Six-mo-old wild-type (male n = 11; female n= 11) and Marfan (male n = 12; female n= 10) mice were used. Segments (2 mm) of ascending and descending thoracic aorta were set up on an isometric wire myograph (model 410 A; Danish Myo Technology, Aarhus, Denmark) filled with PSS (37 °C; 95 % O_2 and 5 % CO_2), as previously described (Onetti et al., 2013). The vessels were stretched to 6 mN, as described (Chung et al., 2007a), washed and allowed to equilibrate for 45 min. The tissues were contracted two times with 100 mM KCl every 5 min. After washing, vessels were left to equilibrate for a further 30 min before starting the experiments. Endothelial-dependent vasodilatations to acetylcholine (ACh; 10^{-9} to 10^{-5} M) were performed in 3×10^{-6} M phenylephrine (Phe)-precontracted vessels. Contractile

responses mediated by α_1-adrenoceptor stimulation were studied by evaluating Phe (10^{-9} to 3×10^{-5} M)-induced contraction. The effects of the nonselective nitric oxide synthase (NOS) inhibitor Nω-nitro-l-arginine methyl ester (L-NAME; 3 x 10^{-4} M), the nonselective cyclooxygenase (COX) inhibitor indomethacin (10^{-5} M), the intermediate-conductance K_{Ca} (IK_{Ca}) and large-conductance K_{Ca} (BK_{Ca}) channel blocker charybdotoxin (100 nM), and the small-conductance K_{Ca} (SK_{Ca}) channel blocker apamin (100 nM) were determined by adding each treatment 30 min before Phe- or ACh-induced responses.

3.4 Quantitative real-time PCR

A different set of 6-mo-old wild-type (male n = 15; female n= 14) and Marfan (male n = 15; female n= 13) mice was used. mRNA expression was determined by quantitative real-time PCR (qRT-PCR) using SYBER green detection, as described (Novensa et al., 2010). Amounts of mRNA encoding COX1, COX2, eNOS and iNOS were expressed relative to Ribosomal Protein S28 (Rps28), used as internal control. qRT-PCR reactions were set up following the manufacturer's guidelines to SYBR green master mix (Thermo Fisher Scientific, Waltham, MA USA). Cycle threshold (Ct) values for each gene were referenced to the internal control [comparative Ct (ΔΔCt)] and converted to the linear form relative to corresponding levels in sex-matched wild-type levels ($2^{-\Delta\Delta Ct}$). Primer sequences for murine genes used in this study are shown in Table 1.

3.5 Analysis of elastin breaks

An additional set of 6-mo-old wild-type (male n = 8; female n= 7) and Marfan (male n = 8; female n= 8) mice was used. The ascending thoracic aorta of mice was dissected, rinsed and fixed in buffered formalin for 24 h, and posteriorly embedded in paraffin. Five-micron aortic sections were stained with Verhoeff-van Gienson (VVG) to visualize elastic fibers. Slides were examined using an Olympus BX60 microscope. Four representative VVG images of each mouse aorta were assessed and two blinded observers counted the number of elastin breaks.

3.6 Statistics

All results are expressed as means ± SE of the number (*n*) of mice indicated in the figure legends. Relaxations to ACh are expressed as the percentage change from the Phe precontracted level. Contractions to Phe are expressed as a percentage of the tone generated by 100 mM KCl. Area under the curve was individually calculated from each concentration-response curve to Phe and was expressed as arbitrary units. Differences between concentration-response curves were assessed by two-way repeated measures ANOVA with Tukey's post-test. Differences between area under the curve, mRNA levels, and elastin ruptures were assessed by regular two-way ANOVA with Tukey's post-

test. Data analysis was carried out using GraphPad Prism, version 5 (GraphPad Software, La Jolla, CA). A value of $P < 0.05$ was considered significant.

4. Results

4.1 Influence of Marfan syndrome on mice thoracic aorta reactivity

Contractile responses to KCl (100 mM) were unaffected by Marfan syndrome either in descending (wild-type: 6.10 ± 0.87 mN, n = 10; Marfan: 6.23 ± 0.77 mN, n = 10) or ascending (wild-type: 5.09 ± 0.25 mN, n = 22; Marfan: 4.98 ± 0.31 mN, n = 22) thoracic aortas. The magnitude of the concentration-dependent contractions evoked by Phe was higher in the ascending (Figure 1C) than descending (Figure 1B) aorta. Marfan syndrome differently altered reactivity in descending and ascending aorta by either decreasing ($P < 0.05$; Figure 1B) or increasing (Figure 1C) Phe-induced contractions, respectively. Conversely, endothelium-dependent ACh-induced vasodilatation showed no differences between wild-type and Marfan mice in both thoracic aorta segments (results not shown).

4.2 Influence of sex on Phe-mediated contractions of Marfan thoracic aorta

We next separated mice by sex to examine whether Marfan syndrome affects thoracic aorta reactivity of males and females differently. Marfan syndrome neither altered contractile responses to KCl in descending aortas from males (wild-type: 5.14 ± 0.96 mN, n = 5; Marfan: 5.31 ± 0.70 mN, n = 5) and females (wild-type: 7.05 ± 1.41 mN, n = 5; Marfan: 7.34 ± 1.40 mN, n = 5), nor in ascending aortas from males (wild-type: 4.92 ± 0.43 mN, n = 11; Marfan: 4.54 ± 0.42 mN, n = 12) and females (wild-type: 5.25 ± 0.27 mN, n = 11; Marfan: 5.50 ± 0.42 mN, n = 10). Contractions to Phe were similar in the wild-type mice from either sex (Figures 2A–B). The Marfan descending thoracic aorta showed a trend ($P = 0.059$) toward a decreased contraction in males only (Figure 2A). Remarkably, Marfan syndrome mice showed higher ($P < 0.05$) Phe-induced contractions than wild-type mice in ascending aortas from males, whereas contractions in females were unaffected (Figure 2B).

4.3 Influence of COX on sex differences in Phe contractions of Marfan ascending aorta

Considering that aneurysmal expansion in human Marfan syndrome initiates at the aortic root and progresses into the ascending portion, we subsequently focused on the mechanisms mediating sex differences in Marfan ascending aorta contractions. The non-selective COX inhibitor indomethacin (10^{-5} M) reduced ($P < 0.05$) Phe-induced contractions in mice from both sexes, revealing a physiological COX-derived contractile influence (Figure 2B *versus* 2C). Interestingly, Phe-induced contractions after indomethacin addition were similar in Marfan compared to wild-type mice in either sex (Figure 2C).

We then measured mRNA levels of COX isoforms (Figure 2D). Marfan syndrome significantly increased COX-1 expression in either sex. In contrast, mRNA levels of COX-2 only augmented in Marfan males. These results suggest that COX activation underlies the Marfan-induced contractile alterations in males.

4.4 Influence of NOS on sex differences in Phe contractions of Marfan ascending aorta

We next evaluated the effects of the non-selective NOS inhibitor L-NAME (3×10^{-4} M) that similarly potentiated ($P < 0.001$) Phe-induced contractions in wild-type mice from both sexes (Figure 3A-B). The observed Marfan-induced increase in Phe-induced contractions (Figure 2B) in males was maintained after L-NAME addition (Figure 3A). However, in the presence of L-NAME, the area under the curve was increased ($P < 0.01$) in Marfan compared to wild-type mice (Figure 3B). In Marfan females, L-NAME addition induced higher Phe-induced contractions compared to the wild types (Figure 3A), though the increased area under the curve did not reach statistical significance (Figure 3B). Analysis of mRNA levels of NOS isoforms showed a significant Marfan syndrome-dependent increase in eNOS and iNOS in males and females, respectively (Figure 3C). These results suggest a higher negative influence of NO on Phe-induced contractions in either sex.

4.5 Influence of sex on ACh-mediated relaxations of Marfan ascending aorta

Endothelium-dependent ACh-induced vasodilatation was similar in ascending aortas from all groups of mice (Figure 4A). In addition, indomethacin did not significantly modify ACh-mediated relaxation in either group (results not shown). However, incubation of L-NAME (results not shown) or L-NAME plus indomethacin (Figure 4B) to isolate endothelium-dependent hyperpolarization (EDH)-type dilation, showed higher aortic relaxations in Marfan than in wild-type. Subsequent addition of the IK_{Ca} and BK_{Ca} channel blocker charybdotoxin (100 nM) plus the specific SK_{Ca} channel blocker apamin (100 nM) almost abolished ACh-evoked EDH-type relaxations, and removed differences between Marfan and wild-type mice (Figure 4C).

4.6 Influence of sex on ascending aorta elastin breaks in Marfan syndrome

Fragmentation of elastin is an important component of the aneurysmal progression in Marfan syndrome. As expected, number of elastin breaks was higher ($P < 0.001$) in the ascending aorta of Marfan syndrome mice compared to wild-type mice (Figure 5). Furthermore, sex influenced the occurrence of elastin breaks in Marfan syndrome, since males showed a greater ($P < 0.05$) amount of breaks than females.

5. Discussion

There are two key novel findings in this study. Firstly, Marfan syndrome triggers opposite alterations in the ascending and descending thoracic aorta of mice, as evidenced by increased or decreased Phe-induced contractions, respectively. Secondly, sex differently affects ascending aorta reactivity in Marfan syndrome, since contractions increased only among males. Therefore, these results suggest the presence of regional and sex-related differences in ascending aorta reactivity, which likely have physiological relevance to the management of thoracic aorta disease in Marfan syndrome.

A general paradigm of Marfan syndrome pathophysiology is that aortic smooth muscle cells develop phenotypic alterations leading to aortic wall weakening (Chung et al., 2007b; Crosas-Molist et al., 2015). Previous studies reported that contractions of the aortic arch and descending thoracic aorta are decreased in *Fbn1*$^{C1039G/+}$ mice (Chung et al., 2007a, 2007b, 2007c; Chung et al., 2008; Yang et al., 2009; Yang et al., 2010a, 2010b; Gibson et al., 2017). In the current study, however, we demonstrate that Marfan syndrome heterogeneously affects α_1-adrenergic contractions to Phe in aneurismal (ascending aorta) and non-aneurysmal (descending aorta) tissue. Thus, whilst the descending portion showed impaired Phe-induced responses, we found that the ascending aorta, more prone to developing aneurysm in Marfan syndrome, showed augmented contractility. These findings reveal for the first time the presence of regional differences in thoracic aorta reactivity in a mouse model of Marfan syndrome. The results are in agreement with the more pronounced mechanical abnormalities observed in the ascending than descending aorta from different animal models of this pathology, which could render the ascending segment more susceptible to aneurysmal dilatation/rupture (Chung et al., 2007b; Bellini et al., 2016). The underlying determinants of the regional differences could be multiple, including differential mechanical loading that the pulsatile cardiac cycle transmits to the aortic tree (Prokop et al., 1970) and/or the different embryonic cell lineages of both aortic segments (Ruddy et al., 2013). For instance, a difference on α_1-adrenergic receptor density, as reported in the canine thoracic aorta (Griendling et al., 1984), or on the population of α_1-adrenergic receptor subtypes may create distinct environments in the ascending and descending aorta for the development of divergent functional alterations.

There is still controversy about whether Marfan syndrome affects thoracic aorta of men and women differently. However, epidemiological evidence suggests that Marfan males have a higher risk of aortic complications (Detaint et al., 2010; Franken et al., 2016; Groth et al., 2017). An important point is that the sex of Marfan syndrome mice has only rarely been reported in previous studies of aortic reactivity. In the present study, we demonstrate that Marfan ascending aortas from males show

increased contractions, whereas contractions in females are unaltered. These results provide the first evidence of sexual dimorphism in Marfan syndrome thoracic aorta reactivity. Although we cannot discard a later-stage development of abnormalities in Marfan females, the current findings suggest that at least they may experience a delayed onset compared to males. A potential explanation for our results is that the Marfan syndrome disease-causing mutation could have higher penetrance in male than female ascending aortas. To this end, we evaluated the influence of sex on elastin fragmentation as a measure of aortic disease progression. We found that although all Marfan groups exhibited an augmented number of elastic lamina breaks compared to the wild types, breaks were more numerous in males than in females. These results suggest the presence of a more pronounced aortic disease in 6-mo-old *Fbn1*$^{C1039G/+}$ male mice, correlating with the functional alterations observed. We cannot discard a protective effect by estrogens in female Marfan mice. In fact, this effect has been described in rat abdominal aortic aneurysms, where a male predominance for aneurysm is also reported, and estradiol-treated rats exhibited smaller aneurysms (Ailawadi et al., 2004).

Aorta is a poorly innervated vessel that highly depends on circulating catecholamines to maintain sympathetic activity. We suggest that heightened α_1-adrenergic receptor-dependent contractions of male Marfan ascending aortas might be an orchestrated response against excessive aortic enlargement. However, at this stage, it is unclear if maintenance of these alterations may be beneficial at long-term, as for instance: i) sympathetic overactivity in cardiovascular disorders (i.e. hypertension, myocardial infarction) is life threatening (Grassi, 2010); ii) sympathetic tone is chronically elevated in human aging (Casey et al., 2012); and iii) excessive aortic vasoconstriction increases cardiac afterload, which can be detrimental in Marfan syndrome patients, particularly in the setting of congestive heart failure (Dietz, 2017).

The principal vascular cellular type involved in Marfan syndrome pathogenesis is the smooth muscle cell (Crosas-Molist et al., 2015; Perrucci et al., 2016). However, abnormalities of endothelial function disrupt circulatory homeostasis, which could aggravate Marfan syndrome-induced vascular damage. Impaired endothelium-dependent vasodilation to ACh has been reported in Marfan descending thoracic aortas of 3-and 6-mo-old mice (Chung et al., 2007a). In the current study, relaxations to ACh were unaltered in the ascending aorta of 6-mo-old Marfan mice. Importantly, we noted that EDH-type relaxations augmented in Marfan animals from both sexes. In large conduit arteries such as aorta, agonist-induced endothelium-dependent relaxations involve both NO and prostacyclin, whereas EDH-type relaxations are more potent in smaller vessels (Chataigneau et al., 1999; Brandes et al., 2000; Takaki et al., 2008). Increased EDH-type relaxations in microvessels could compensate for endothelial abnormalities in cardiovascular disease (Shimokawa and Urakami-

Harasawa, 1999). Nevertheless, although much less studied, EDH-type relaxations may also serve as a backup mechanism for endothelial responses of mice thoracic aorta (Shen et al., 2003; Csányi et al., 2012). Therefore, we propose that EDH-dependent preservation of endothelium function in Marfan syndrome ascending aorta could be a plausible adaptive mechanism to maintain endothelium-dependent relaxation.

Previous studies reported that impaired Phe-induced contractions of the Marfan descending thoracic aorta are associated with a shift towards a reduced expression of COX-1 and an enhanced expression of COX-2 (Chung et al., 2007c). However, a different scenario occurs in the Marfan ascending aorta, where COX-dependent increases in Phe-induced contractions in males are coupled to upregulation of both COX isoforms expression. Considering that COX-1 is a major source of thromboxane A2 (Clarke et al., 1991; Ge et al., 1995), we could speculate that increased COX-1-derived thromboxane A2 may participate, at least partly, for enlarged Phe contractions in males. Nevertheless, a contribution of COX-2-derived contractile prostanoids should not be discarded (Alvarez et al., 2005). Besides, COX-2 is a vascular source of the relaxing factor prostacyclin under non-physiological conditions (Kirkby et al., 2012). Increased COX-2-derived prostacyclin might be a compensatory mechanism to attenuate enhanced contractile responses in Marfan males. In addition, elevated COX-2 expression is also associated with increased metalloproteinase activation (Tsujii et al., 1997), which in turn is linked to aortic elastic fiber fragmentation and degradation in Marfan syndrome (Chung et al., 2007b). Consistently, increased COX-2 expression correlated with a larger number of elastin breaks in the ascending aorta of Marfan males compared to females. The underlying driving force for increased COX-2 expression is unclear, but it is proposed could be linked to the loss of vessel elasticity and increase in pulse wave velocity of the Marfan thoracic aorta (Chung et al., 2007c). Notably, COX-1 expression also augmented in Marfan females, an effect that was not accompanied by changes in Phe-induced contractions. There is accumulating evidence connecting excessive basal levels of NO and Marfan syndrome-induced aortic pathology (Yang et al., 2010b; Soto et al., 2016; Oller et al., 2017; Gibson et al., 2017). Consistently, our results reveal an increased participation of NO as a negative modulator of Phe-induced contractions in Marfan mice. Moreover, our findings provide evidence for a sex-dependent different source of altered NO generation in Marfan ascending aortas. Specifically, we suggest that an increased participation of an iNOS-derived NO pool may attenuate an excessive contractile influence derived from COX-1 in females. Thus, a previous study showed that peroxynitrite, a product of the reaction between superoxide anion and NO, is capable to desensitize α_1-adrenoceptors (Takakura et al., 2002). Interestingly, a recent study has shown an important role of dysregulated NO production via iNOS in Marfan syndrome aortic dilatation (Oller et al., 2017).

Altogether, the results of the present study provide evidence of regional and sex-related differences in thoracic aorta reactivity in a representative model of Marfan syndrome. Increased α-adrenergic contractions may render the ascending aorta of males more sensitive to circulating catecholamines, which might be a short-term adaptive functional response against excessive aortic enlargement. Nevertheless, further studies are necessary to verify if these alterations can contribute to increase thoracic aorta vulnerability in male Marfan syndrome patients. The present study suggests that the development of an effective drug treatment against excessive aortic enlargement should take into account these functional divergences, which might open the door to provide safer and more effective personalized therapy in Marfan syndrome.

6. Author Contributions

FJ-A: Conceived the study, designed and executed the experiments, guided the experimental design, analyzed and interpreted the data, wrote and revised the manuscript. GE, EV: Guided the experimental design, data analysis and interpretation, read and revised the manuscript. APD, A-MS, FB, TM, LB: executed the experiments, data analysis and interpretation, read and revised the manuscript. All authors gave final approval of the manuscript to be published.

7. Conflict of Interest Statement

The authors declare that the research was conducted in the absence of any commercial or financial relationships that could be construed as a potential conflict of interest.

8. Funding

This work was supported by grants SAF2005-64136-R (to G.E.) and SAF2014-56111-R (to E.V.) from Ministerio de Ciencia e Innovación (Spain), and 2014SGR574 (to E.V. and F.J-A) from Generalitat de Catalunya (Spain).

9. References

Ailawadi, G., Eliason, J.L., Roelofs, K.J., Sinha, I., Hannawa, K.K., Kaldjian, E.P., et al. (2004). Gender differences in experimental aortic aneurysm formation. *Arterioscler Thromb Vasc Biol*. 24, 2116-2122.

Álvarez, Y., Briones, A.M., Balfagón, G., Alonso, M.J., Salaices, M. (2005). Hypertension increases the participation of vasoconstrictor prostanoids from cyclooxygenase-2 in phenylephrine responses. *J Hypertens*. 23, 767–777.

Bellini, C., Korneva, A., Zilberberg, L., Ramirez, F., Rifkin, D.B., Humphrey, J.D. (2016). Differential ascending and descending aortic mechanics parallel aneurysmal propensity in a mouse model of Marfan syndrome. *J Biomech*. 49: 2383–2389. doi: 10.1016/j.jbiomech.2015.11.059

Brandes, R.P., Schmitz-Winnenthal, F.H., Félétou, M., Gödecke, A., Huang, P.L., Vanhoutte, P.M., et al. (2000). An endothelium-derived hyperpolarizing factor distinct from NO and prostacyclin is a major endothelium-dependent vasodilator in resistance vessels of wild-type and endothelial NO synthase knockout mice. *Proc Natl Acad Sci U S A*. 97, 9747–9752.

Casey, D.P., Padilla, J., Joyner, M.J. (2012). α-Adrenergic vasoconstriction contributes to the age-related increase in conduit artery retrograde and oscillatory shear. *Hypertension*. 60, 1016–1022. doi: 10.1161/HYPERTENSIONAHA.112.200618

Chataigneau, T., Félétou, M., Huang, P.L., Fishman, M.C., Duhault, J., Vanhoutte, P.M. (1999). Acetylcholine-induced relaxation in blood vessels from endothelial nitric oxide synthase knockout mice. *Br J Pharmacol.* 126, 219–226. doi: 10.1038/sj.bjp.0702300

Chung, A.W., Au Yeung, K., Cortes, S.F., Sandor, G.G., Judge, D.P., Dietz, H.C., et al. (2007a). Endothelial dysfunction and compromised eNOS/Akt signaling in the thoracic aorta during the progression of Marfan syndrome. *Br J Pharmacol* 150, 1075–1083. doi: 10.1038/sj.bjp.0707181

Chung, A.W., Au Yeung, K., Sandor, G.G., Judge, D.P., Dietz, H.C., van Breemen, C. (2007b). Loss of elastic fiber integrity and reduction of vascular smooth muscle contraction resulting from the upregulated activities of matrix metalloproteinase-2 and -9 in the thoracic aortic aneurysm in Marfan syndrome. *Circ Res*. 101, 512–522. doi: 10.1161/CIRCRESAHA.107.157776

Chung, A.W., Yang, H.H., van Breemen, C. (2007c). Imbalanced synthesis of cyclooxygenase-derived thromboxane A2 and prostacyclin compromises vasomotor function of the thoracic aorta in Marfan syndrome. *Br J Pharmacol*. 152, 305–312. doi: 10.1038/sj.bjp.0707391

Chung, A.W., Yang, H.H., Radomski, M.W., van Breemen, C. (2008). Long-term doxycycline is more effective than atenolol to prevent thoracic aortic aneurysm in marfan syndrome through the inhibition of matrix metalloproteinase-2 and -9. *Circ Res*. 102, e73–85. doi: 10.1161/CIRCRESAHA.108.174367

Clarke, R.J., Mayo, G., Price, P., FitzGerald, G.A. (1991). Suppression of thromboxane A2 but not of systemic prostacyclin by controlled-release aspirin. *N Engl J Med*. 325, 1137–1141. doi: 10.1056/NEJM199110173251605

Crosas-Molist, E., Meirelles, T., López-Luque, J., Serra-Peinado, C., Selva, J., Caja, L., Gorbenko Del Blanco, D., et al. (2015). Vascular smooth muscle cell phenotypic changes in patients with Marfan syndrome. *Arterioscler Thromb Vasc Biol*. 35, 960–972. doi: 10.1161/ATVBAHA.114.304412

Csányi, G., Gajda, M., Franczyk-Zarow, M., Kostogrys, R., Gwoźdź, P., Mateuszuk, L., et al. (2012). Functional alterations in endothelial NO, PGI_2 and EDHF pathways in aorta in ApoE/LDLR-/- mice. *Prostaglandins Other Lipid Mediat*. 98, 107–115. doi: 10.1016/j.prostaglandins.2012.02.002

Detaint, D., Faivre, L., Collod-Beroud, G., Child, A.H., Loeys, B.L., Binquet, C., et al. (2010). Cardiovascular manifestations in men and women carrying a FBN1 mutation. *European heart journal*. 31, 2223–2229. doi: 10.1093/eurheartj/ehq258

Dietz, H.C. (1993-2017). "Marfan Syndrome". In: Pagon, R.A., Adam, M.P., Ardinger, H.H., Wallace, S.E., Amemiya, A., Bean, L.J.H., et al., editor. *GeneReviews®*. Seattle: University of Washington, Seattle.

Dietz, H.C., Cutting, G.R., Pyeritz, R.E., Maslen, C.L., Sakai, L.Y., Corson, G.M., et al. (1991). Marfan syndrome caused by a recurrent de novo missense mutation in the fibrillin gene. *Nature*. 352, 337–339. doi: 10.1038/352337a0

Elkayam, U., and Gleicher, N. (1998). "Hemodynamics and cardiac function during normal pregnancy and the puerperium." In: Elkayam, U., Gleicher, N., editor. *Cardiac Problems in Pregnancy*. New York: Wiley-Liss. p. 23–32.

Elkayam, U., Ostrzega, E., Shotan, A., Mehra, A. (1995). Cardiovascular problems in pregnant women with Marfan syndrome. *Ann Intern Med*. 123, 117–122.

Franken, R., Groenink, M., de Waard, V., Feenstra, H.M., Scholte, A.J., van den Berg, M.P., et al. (2016). Genotype impacts survival in Marfan syndrome. *European heart journal*. 37, 3285–3290. doi: 10.1093/eurheartj/ehv739

Ge, T., Hughes, H., Junquero, D.C., Wu, K.K., Vanhoutte, P.M., Boulanger, C.M. (1995). Endothelium-dependent contractions are associated with both augmented expression of prostaglandin H synthase-1 and hypersensitivity to prostaglandin H2 in the SHR aorta. *Circ Res*. 76, 1003–1010.

Gibson, C.P., Nielsen, C., Alex, R., Cooper, K., Farney, M., Gaufin, D., et al. (2017). Mild aerobic exercise blocks elastin fiber fragmentation and aortic dilatation in a mouse model of Marfan syndrome associated aortic aneurysm. *J Appl Physiol* (1985). 2017 Apr 6:jap.00132.2017. doi: 10.1152/japplphysiol.00132.2017

Goland, S., and Elkayam, U. (2009). Cardiovascular problems in pregnant women with marfan syndrome. *Circulation*. 119, 619–623. doi: 10.1161/CIRCULATIONAHA.104.493569

Grassi, G. (2010). Sympathetic neural activity in hypertension and related diseases. *Am J Hypertens*. 23, 1052–1060. doi: 10.1038/ajh.2010.154

Griendling, K.K., Sastre, A., Milnor, W.R. (1984). Regional differences in alpha 1-adrenoceptor numbers and responses in canine aorta. *Am J Physiol*. 247, H928–H935.

Groth KA, Stochholm K, Hove H, Kyhl K, Gregersen PA, Vejlstrup N, et al. (2017). Aortic events in a nationwide Marfan syndrome cohort. *Clin Res Cardiol*. 106, 105–112. doi: 10.1007/s00392-016-1028-3

Judge, D.P., Biery, N.J., Keene, D.R., Geubtner, J., Myers, L., Huso, D.L., et al. (2004). Evidence for a critical contribution of haploinsufficiency in the complex pathogenesis of Marfan syndrome. *J Clin Invest*. 114, 172–181. doi: 10.1172/JCI20641

Lee, L., Cui, J.Z., Cua, M., Esfandiarei, M., Sheng, X., Chui, W.A., et al. (2016). Aortic and Cardiac Structure and Function Using High-Resolution Echocardiography and Optical Coherence Tomography in a Mouse Model of Marfan Syndrome. *PLoS One*. 11: e0164778. doi: 10.1371/journal.pone.0164778

Manalo-Estrella, P., and Barker, A.E. (1967). Histopathologic findings in human aortic media associated with pregnancy. *Arch Pathol*. 83, 336–341.

Mueller, G.C., Stark, V., Steiner, K. von Kodolitsch, Y., Rybczynski, M., Weil, J., Mir, T.S. (2013). Impact of age and gender on cardiac pathology in children and adolescents with Marfan syndrome. *Pediatr Cardiol*. 34, 991–998. doi: 10.1007/s00246-012-0593-0

Murdoch, J.L., Walker, B.A., Halpern, B.L., Kuzma, J.W., McKusick, V.A. (1972). Life expectancy and causes of death in the Marfan syndrome. *N Engl J Med*. 286, 804–808. doi: 10.1056/NEJM197204132861502

Novensa, L., Selent, J., Pastor, M., Sandberg, K., Heras, M., Dantas, A.P. (2010). Equine estrogens impair nitric oxide production and endothelial nitric oxide synthase transcription in human endothelial cells compared with the natural 17{beta}-estradiol. *Hypertension*. 56, 405–411. doi: 10.1161/HYPERTENSIONAHA.110.151969

Oller, J., Méndez-Barbero, N., Ruiz, E.J., Villahoz, S., Renard, M., Canelas, L.I., et al. (2017). Nitric oxide mediates aortic disease in mice deficient in the metalloprotease Adamts1 and in a mouse model of Marfan syndrome. *Nat Med*. 23, 200–212. doi: 10.1038/nm.4266

Onetti, Y., Jiménez-Altayó, F., Heras, M., Vila, E., Dantas, A.P. (2013). Western-type diet induces senescence, modifies vascular function in non-senescence mice and triggers adaptive mechanisms in senescent ones. *Exp Gerontol*. 48, 1410–1419. doi: 10.1016/j.exger.2013.09.004

Perrucci, G.L., Rurali, E., Gowran, A., Pini, A., Antona, C., Chiesa, R., et al. (2017). Vascular smooth muscle cells in Marfan syndrome aneurysm: the broken bricks in the aortic wall. *Cell Mol Life Sci*. 74, 267–277. doi: 10.1007/s00018-016-2324-9

Prokop, E.K., Palmer, R.F., Wheat, M.W. Jr. (1970). Hydrodynamic forces in dissecting aneurysms. In-vitro studies in a Tygon model and in dog aortas. *Circ. Res.* 27, 121–127.

Pyeritz, R.E. (2016). Recent progress in understanding the natural and clinical histories of the Marfan syndrome. *Trends Cardiovasc Med*. 26, 423–428. doi: 10.1016/j.tcm.2015.12.003

Ruddy, J.M., Jones, J.A., Ikonomidis, J.S. (2013). Pathophysiology of thoracic aortic aneurysm (TAA): is it not one uniform aorta? Role of embryologic origin. *Prog Cardiovasc Dis*. 56, 68–73. doi: 10.1016/j.pcad.2013.04.002

Shen, B., Ye, C.L., Ye, K.H., Liu, J.J. (2003). Mechanism underlying enhanced endothelium-dependent vasodilatation in thoracic aorta of early stage streptozotocin-induced diabetic mice. *Acta Pharmacol Sin*. 24, 422–428.

Shimokawa, H., and Urakami-Harasawa, L. (1999). "Importance of endothelium-derived hyperpolarizing factor in human arteries." In: Vanhoutte, P.M., editor *Endothelium-derived hyperpolarizing factor*. Amsterdam: Harwood Academic Publishers. p. 391–398.

Soto, M.E., Iturriaga Hernández, A.V., Guarner Lans, V., Zuñiga-Muñoz, A., Aranda Fraustro, A., Velázquez Espejel, R., et al. (2016). Participation of oleic acid in the formation of the aortic aneurysm in Marfan syndrome patients. *Prostaglandins Other Lipid Mediat.* 123, 46–55. doi: 10.1016/j.prostaglandins.2016.05.001

Takaki, A., Morikawa, K., Tsutsui, M., Murayama, Y., Tekes, E., Yamagishi, H., et al. (2008). Crucial role of nitric oxide synthases system in endothelium-dependent hyperpolarization in mice. *J Exp Med*. 205, 2053–2063. doi: 10.1084/jem.20080106

Takakura, K., Taniguchi, T., Muramatsu, I., Takeuchi, K., Fukuda, S. (2002) Modification of alpha1α-adrenoceptors by peroxynitrite as a possible mechanism of systemic hypotension in sepsis. *Crit Care Med*. 30, 894–899.

Tsujii, M., Kawano, S., DuBois, R.N. (1997). Cyclooxygenase-2 expression in human colon cancer cells increases metastatic potential. *Proc Natl Acad Sci USA*. 94, 3336–3340.

Wanga, S., Silversides, C., Dore, A., de Waard, V., Mulder, B. (2016). Pregnancy and thoracic aortic disease: managing the risks. *Can J Cardiol*. 32, 78–85. doi: 10.1016/j.cjca.2015.09.003

Yang, H.H., Kim, J.M., Chum, E., van Breemen, C., Chung, A.W. (2009). Long-term effects of losartan on structure and function of the thoracic aorta in a mouse model of Marfan syndrome. *Br J Pharmacol*. 158,1503–1512. doi: 10.1111/j.1476-5381.2009.00443.x

Yang, H.H., Kim, J.M., Chum, E., van Breemen, C., Chung, A.W. (2010a). Effectiveness of combination of losartan potassium and doxycycline versus single-drug treatments in the secondary prevention of thoracic aortic aneurysm in Marfan syndrome. *J Thorac Cardiovasc Surg*. 140, 305–312.e2. doi: 10.1016/j.jtcvs.2009.10.039

Yang, H.H., van Breemen, C., Chung, A.W. (2010b). Vasomotor dysfunction in the thoracic aorta of Marfan syndrome is associated with accumulation of oxidative stress. *Vascul Pharmacol*. 52, 37–45. doi: 10.1016/j.vph.2009.10.005

10. Figure legends

Figure 1. (A) Diagram illustrating the descending and ascending thoracic aorta segments used in the present study. Concentration-response curves to phenylephrine in descending **(B)** and ascending **(C)** aorta from wild-type and Marfan syndrome mice. Results are the mean ± SE from wild-type (descending *n* = 10; ascending *n* = 10) and Marfan syndrome (descending *n* = 10; ascending *n* = 10) mice. **P* < 0.05, ***P* < 0.01, ****P* < 0.001 by two-way ANOVA.

Figure 2. Concentration-response curves to phenylephrine in descending **(A)** and ascending **(B)** aorta from wild-type and Marfan syndrome male (left panel) and female (right panel) mice. Results are the mean ± SE from wild-type (male descending *n* = 5; male ascending *n* = 5; female descending *n* = 5; female ascending *n* = 5) and Marfan syndrome (male descending *n* = 5; male ascending *n* = 5; female descending *n* = 5; female ascending *n* = 5) mice. **P* < 0.05, ***P* < 0.01, ****P* < 0.001 by two-way ANOVA. **(C)** Concentration-response curves to phenylephrine in the presence of the non-selective cyclooxygenase (COX) inhibitor indomethacin (Indo; 10^{-5} M) in ascending aorta from wild-type and Marfan syndrome male (left panel) and female (right panel) mice. Results are the mean ± SE from wild-type (male *n* = 5; female *n* = 6) and Marfan syndrome (male *n* = 5; female *n* = 5) mice. **(D)** Comparative analysis of ascending aorta mRNA levels of COX isoforms, COX1 and COX2. mRNA levels are expressed as $2^{-\Delta\Delta Ct}$ using Ribosomal Protein S28 as internal control. Results are the mean ± SE from wild-type (male *n* = 13-15; female *n* = 14) and Marfan syndrome (male *n* = 13; female *n* = 12) mice. **P* < 0.05, ***P* < 0.01 by two-way ANOVA.

Figure 3. Concentration-response curves to phenylephrine **(A)** and analysis of area under the curve **(B)** in the presence of the nonselective nitric oxide synthase (NOS) inhibitor L-NAME (3 x 10^{-4} M) in ascending aorta from wild-type and Marfan syndrome male (left panel) and female (right panel) mice. Results are the mean ± SE from wild-type (male *n* = 4; female *n* = 5) and Marfan syndrome (male *n* = 5; female *n* = 6) mice. **(C)** Comparative analysis of ascending aorta mRNA levels of NOS isoforms, endothelial NOS (eNOS) and inducible NOS (iNOS). mRNA levels are expressed as $2^{-\Delta\Delta Ct}$ using Ribosomal Protein S28 as internal control. Results are the mean ± SE from wild-type (male *n* = 15; female *n* = 13-14) and Marfan syndrome (male *n* = 14-15; female *n* = 12-13) mice. **P* < 0.05, ***P* < 0.01, ****P* < 0.001 by two-way ANOVA.

Figure 4. Concentration-response curves to acetylcholine in the absence **(A)** or presence of L-NAME (3 x 10^{-4} M) plus Indo (10^{-5} M) **(B)** or L-NAME plus Indo plus the IK_{Ca} and BK_{Ca} channel blocker

charybdotoxin (Charybd; 100 nM) plus the specific SK_{Ca} channel blocker apamin (Apa; 100 nM) **(C)** in ascending aorta from wild-type and Marfan syndrome male (left panel) and female (right panel) mice. Results are the mean ± SE from wild-type (male *n* = 4-6; female *n* = 5-6) and Marfan syndrome (male *n* = 5-6; female *n* = 5-6) mice. **P* < 0.05, ***P* < 0.01, ****P* < 0.001 by two-way ANOVA.

Figure 5. Analysis of elastic fiber breaks in the tunica media of the ascending aorta from wild-type and Marfan syndrome male and female mice. Results are the mean ± SE from wild-type (male *n* = 8; female *n* = 8) and Marfan syndrome (male *n* = 7; female *n* = 8) mice. **P* < 0.05, ****P* < 0.001 by two-way ANOVA.

Table 1 Primer sequences for quantitative real-time PCR

Gene	Sequence (5'→ 3')
COX-1 (NM_008969.3)	*F: GAGCCGTGAGATGGGTGGGAGGG* *R: TGGATGTGCAATGCCAACGGCT*
COX-2 (NM_011198.3)	*F: GTCAGGACTCTGCTCACGAAGGAAC* *R: ACAGCTCGGAAGAGCATCGCAG*
eNOS (NM_008713.4)	*F: TGTCACTATGGCAACCAGCGT* *R: GCGCAATGTGAGTCCGAAAA*
iNOS (NM_010927.3)	*F: TCAGCCACCTTGGTGAAGGGAC* *R: TAGGCTACTCCGTGGAGTGAACA*
Rps28 (NM_016844)	*F: TAGGGTAACCAAAGTGCTGGGC* *R: GACATTTCGGATGATAGAGCGG*

Figure 1

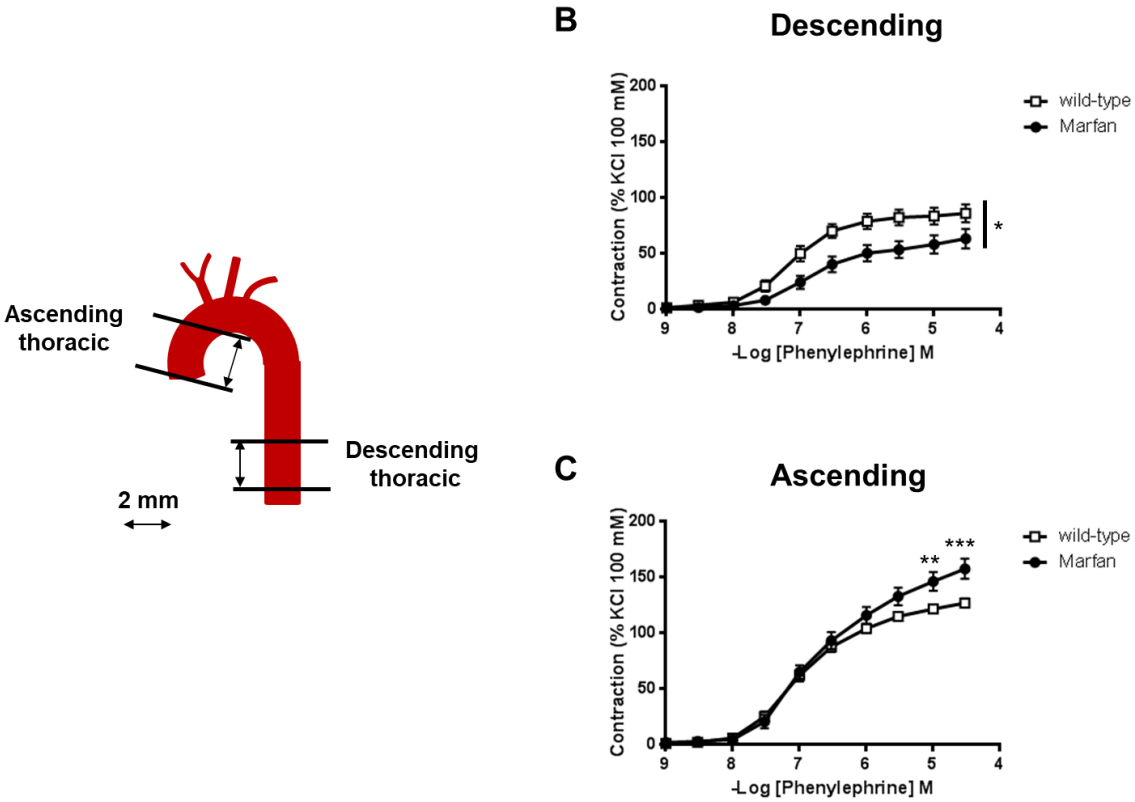
Ascending thoracic
Descending thoracic
2 mm
B
Descending
Contraction (% KCl 100 mM)
-Log [Phenylephrine] M
wild-type
Marfan
*
C
Ascending
**
***

Figure 2

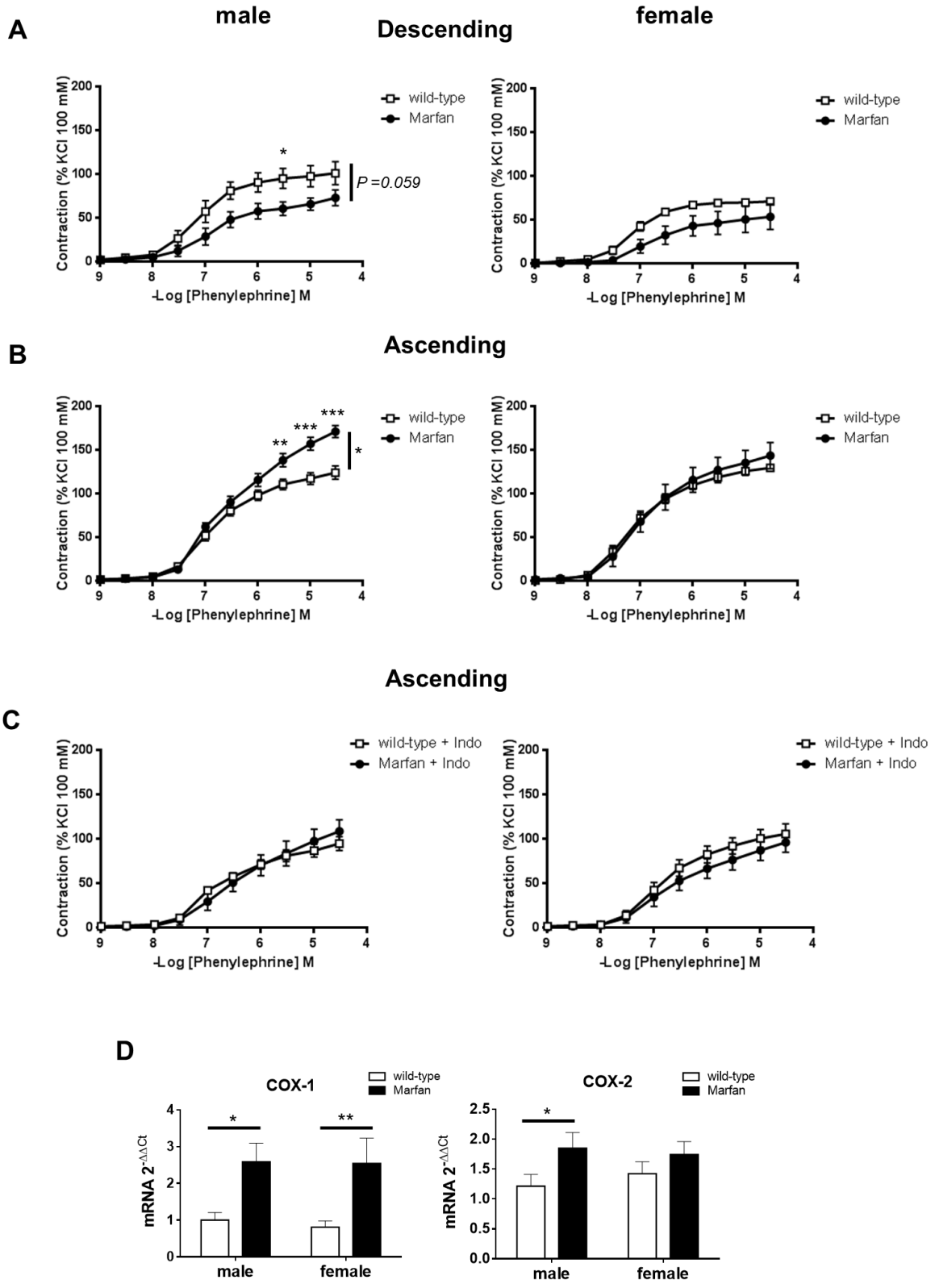
A
male
Descending
female
wild-type
Marfan
Contraction (% KCl 100 mM)
-Log [Phenylephrine] M
*
P =0.059
B
Ascending
**
***
***
*
C
Ascending
wild-type + Indo
Marfan + Indo
D
COX-1
COX-2
mRNA 2-ΔΔCt
male
female
*
**

Figure 3

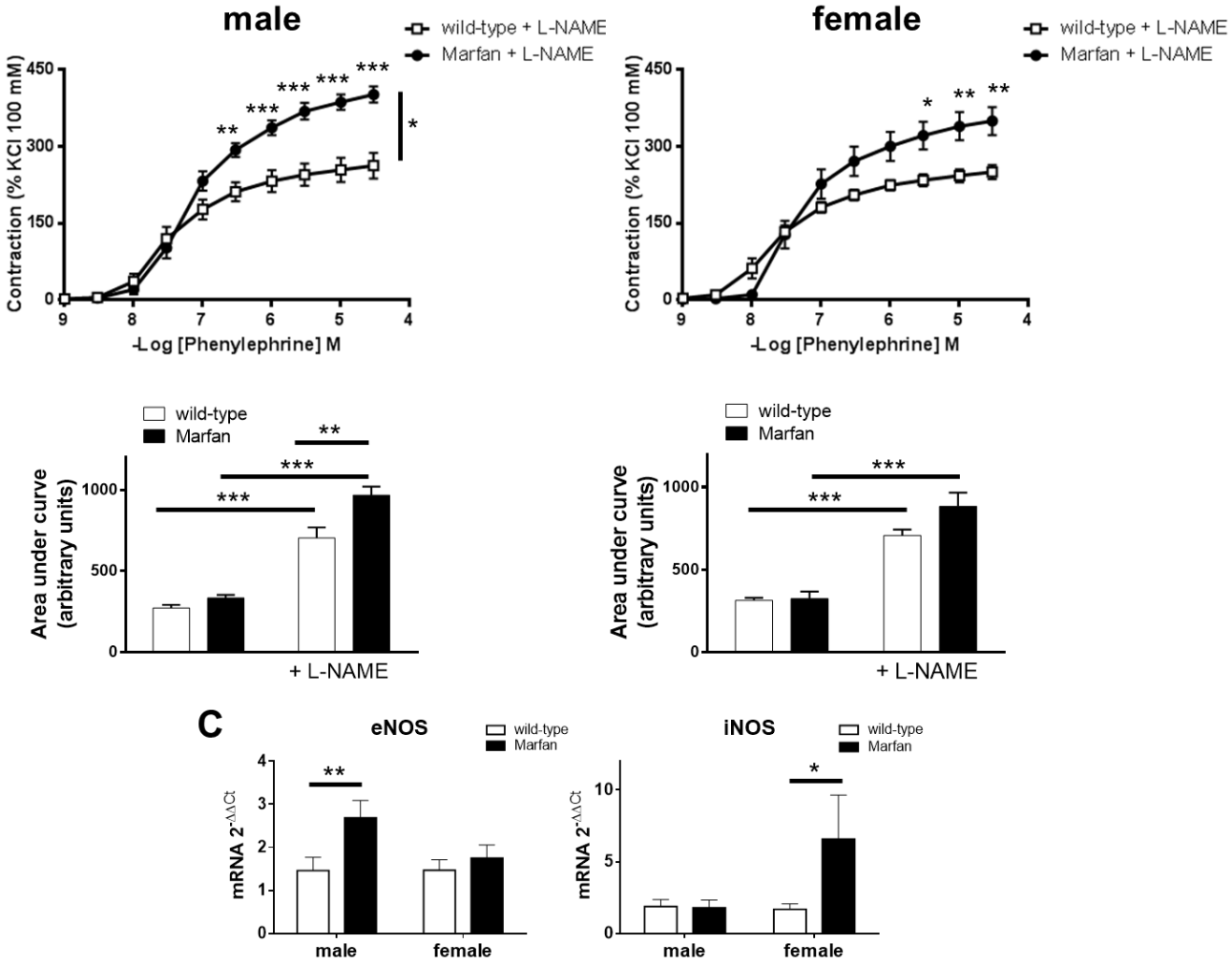
male
wild-type + L-NAME
Marfan + L-NAME
Contraction (% KCl 100 mM)
-Log [Phenylephrine] M
female
wild-type + L-NAME
Marfan + L-NAME
Contraction (% KCl 100 mM)
-Log [Phenylephrine] M
wild-type
Marfan
Area under curve (arbitrary units)
+ L-NAME
wild-type
Marfan
Area under curve (arbitrary units)
+ L-NAME
C
eNOS
wild-type
Marfan
mRNA 2^-ΔΔCt
male
female
iNOS
wild-type
Marfan
mRNA 2^-ΔΔCt
male
female

Figure 4

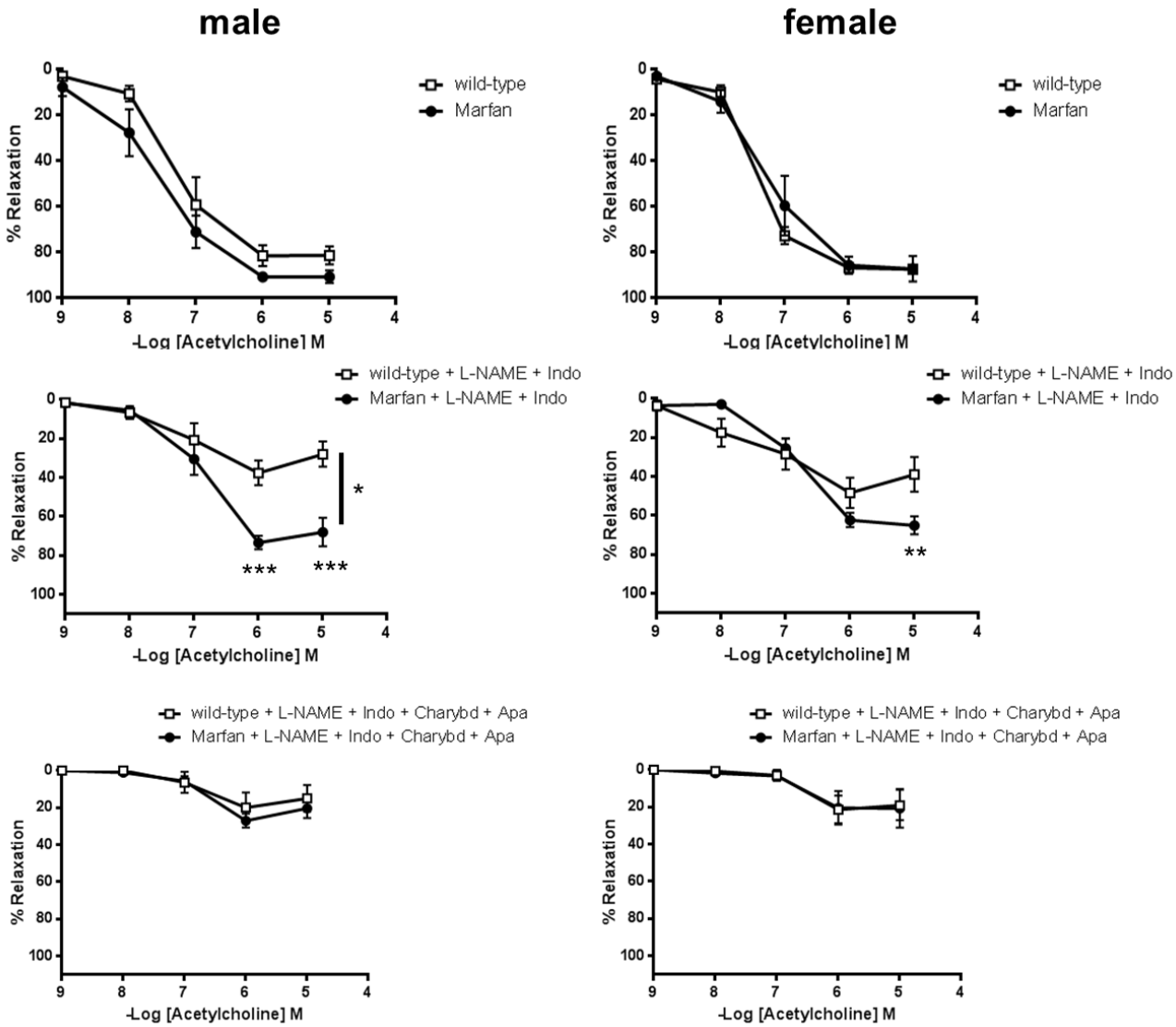
male
female
wild-type
Marfan
wild-type + L-NAME + Indo
Marfan + L-NAME + Indo
wild-type + L-NAME + Indo + Charybd + Apa
Marfan + L-NAME + Indo + Charybd + Apa
% Relaxation
-Log [Acetylcholine] M
*
**
***

Figure 5

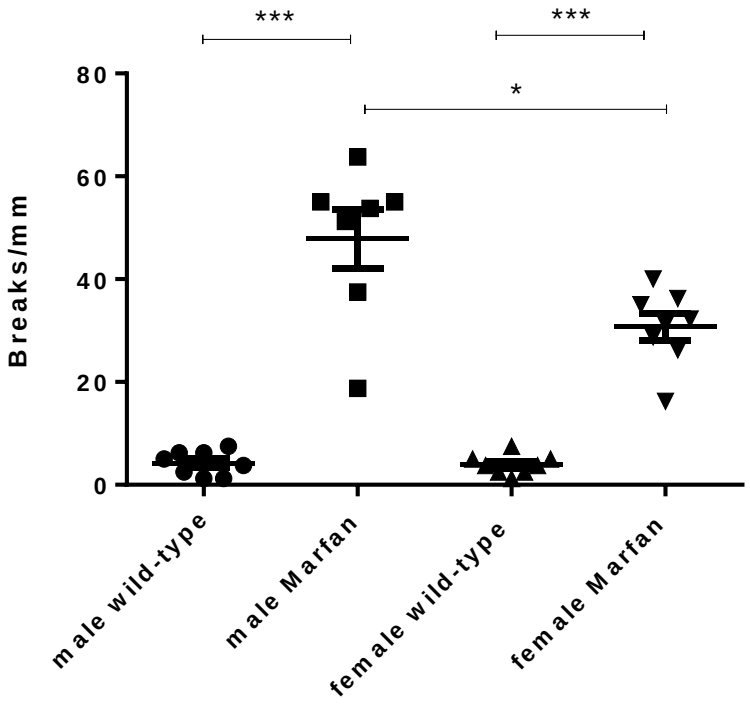
***
***
*
80
60
40
20
0
Breaks/mm
male wild-type
male Marfan
female wild-type
female Marfan